JOURNAL OF THE AERONAUTICAL SCIENCES

VOLUME 19 JANUARY, 1952 NUMBER 1

CONTENTS

Published by the

INSTITUTE OF THE AERONAUTICAL SCIENCES, INC.

JOURNAL OF THE AERONAUTICAL SCIENCES

VOLUME 19 JANUARY, 1952 NUMBER 1

Recent Investigation of Temperature Recovery and Heat Transmission on Cones and Cylinders in Axial Flow in the N.O.L. Aeroballistics Wind Tunnel

G. R. EBER*

U.S. Ordnance Laboratory

ABSTRACT

The Naval Ordnance Laboratory research program on the investigation of aerodynamic heating effects at supersonic velocities is outlined briefly. Results of recent experimental investigations on temperature recovery and heat transmission along the surface of cones and cylindrical bodies in axial flow are presented. The experiments were conducted in the N.O.L. 40 by 40 cm. Aeroballistics Tunnel at Mach Numbers between 1.5 and 5.0, inclusive, and cover the regions of laminar, transition, and fully developed turbulent boundary-layer flow. The experimental results are compared with analytical solutions for temperature recovery and heat transfer with laminar and turbulent boundary layer. The qualitative effect of the direction of the heat flow and the surface temperature on the limits of the transition region is discussed in detail.

INTRODUCTION

THE NEED FOR ACCURATE HEAT-TRANSFER DATA is apparent if one considers that the surface of a supersonic vehicle flying in the atmosphere with 2,500 m.p.h. or a Mach Number of about 3.4 will adopt an equilibrium temperature of about 540°C. above that of the ambient air. This rise in temperature is caused by conversion of kinetic energy of the flying body into heat by compression and friction in the boundary layer, which increases the temperature of the air in proportion to the square of the speed of the flying body.

How much of the heat produced will be transferred to the surface depends greatly on the surface coefficient of heat transfer. This coefficient in turn depends on the flow conditions in the boundary layer. Our knowledge of the aerothermodynamic characteristics in supersonic flow is rather incomplete. It is, therefore, of great importance to investigate surface temperatures ann heat transfer in this range in order to provide the designer with the data that are needed so urgently.

Considerable theoretical and experimental work has been expended in recent years on the solution of the supersonic heat-transfer problem. Despite many valuable results that have been obtained, however, we are still far from a solution of this problem, especially in the region of turbulent-flow boundary layers. More theoretical and experimental work must be done before we will be able to predict supersonic heat transfer reasonably accurately.

Accordingly, the Naval Ordnance Laboratory (N.O.L.) has started a comprehensive experimental and theoretical research program on supersonic heat transfer. The experimental program is being conducted in the White Oak Aeroballistic Research Facility; it consists of the following phases: (1) temperature recovery factors, (2) heat-transfer correlations, and (3) boundary-layer transition.

Although this program is far from completion, some significant results have already been obtained and are presented here.

EXPERIMENTAL FACILITIES AND INSTRUMENTATION

The principal experimental facility is a 40 by 40 cm. aeroballistics wind tunnel. The wind tunnel operates with atmospheric supply pressure. A range of Mach Numbers between 1.2 and 6.5 can be covered in this tunnel by a set of fixed nozzles. (The tunnel, at present intermittent, is described in detail in reference 1.)

Different models have been employed to produce laminar, transitional, and turbulent boundary-layer

Presented at the Hypersonic Aerodynamics Session, Nineteenth Annual Meeting, I.A.S., New York, January 29–February 1, 1951.

* Chief of Aeroballistic Division.

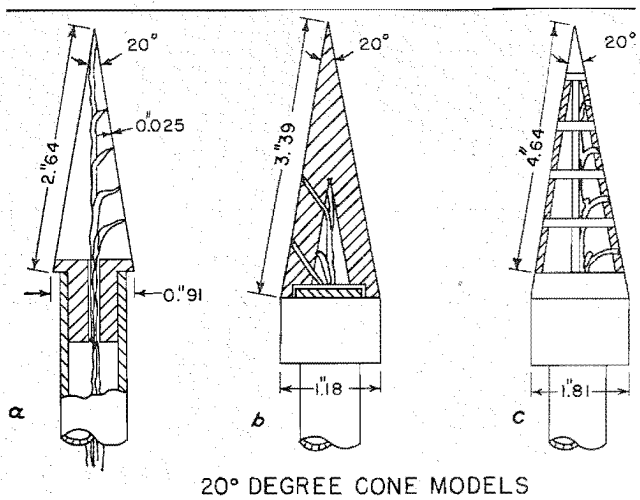

20° DEGREE CONE MODELS

FIG. 1. Three 20° cone models for recovery-factor and heat-transfer measurements: (a) thin-walled cone, (b) thick-walled cone, and (c) cone with insulated frustra.

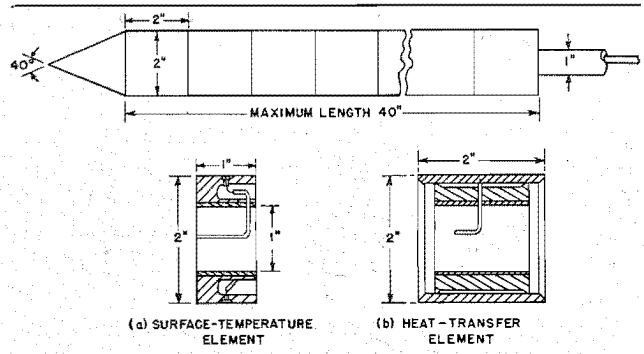

CONE-CYLINDER MODEL

FIG. 2. Cone-cylinder model.

flow. For laminar boundary-layer flow, small cones have been used. Three typical 20° cone-models are presented in Fig. 1. The first cone (a) is a thin-walled copper cone of 0.025-in. wall thickness with several thermocouples inserted along the skin of the cone for surface temperature measurements. The second cone (b) has a thick wall of copper, the heat capacity of which is used for the determination of the average heat-transfer coefficients. The third cone (c) is a copper cone subdivided into frustra. The latter are thermally insulated from each other to avoid heat flow in the axial direction and to allow the determination of local heat-transfer coefficients. Except for the subdivided cone, cones with 10, 40, 60, and 80 deg. total angle were used throughout the investigation.

For transitional and turbulent boundary-layer flow, there were employed cone-cylinder models, as shown in Fig. 2. These models are composed of a 40° cone and a number of cylindrical sections 2 in. in diameter, up to 2 in. longest. The cylinder can be built up to about 40 in. total length. For insulated surface-temperature measurements, the sections are made of thermally insulating material; a surface temperature element as shown in Fig. 2a can be inserted at any desired position of the cylinder. Four cu-const. thermocouples of low heat capacity are inserted equally spaced around the circumference of the measuring element.

For heat-transfer measurements 2-in. sections of copper rings of $^1/_8$-in. wall thickness are used, as shown in Fig. 2b. These sections are mounted on a heat-insulating body. One to four thermocouples are inserted in the copper rings; the heat capacity of the copper ring is used for the determination of the heat-transfer coefficients in the same way as done with the cones.

TEMPERATURE RECOVERY FACTORS

The surface of a body in supersonic flight will assume its highest temperature after it has been heated up to the temperature of the inner edge of the boundary layer. Then the transfer of heat has become zero. This maximum temperature depends on the energy distribution in the compressible boundary layer and is usually expressed in terms of the temperature recovery factor r. This factor is defined as the ratio of the actual temperature rise across the boundary layer to the adiabatic temperature rise. The recovery factor, in general, is a function of the similarity parameters, Reynolds Number Re, Prandtl Number Pr, and Mach Number M. Thus,

$$r = \frac{T_e - T_1}{T_0 - T_1} = f(Re, Pr, M)$$

where T_e is the temperature of the insulated surface, T_1 is the ambient air temperature outside of the boundary layer, and T_0 is the stagnation temperature.

According to the different energy distribution, we must expect different recovery factors on bodies with laminar, transitional, and turbulent boundary layer.

(A) *Laminar Boundary-Layer Flow*

The results of the temperature measurements with the thin-walled cones are presented in Fig. 3. The local recovery factor determined with the local temperature at the inner edge of the boundary layer is plotted versus local Mach Number M_L for the various cones. The local Mach Number was determined from the M.I.T. Tables[2] by disregarding the existence of the boundary layer itself, which was considered immaterial for the small cones. The measurements show that the temperature-recovery factor is 0.845 ± 1 per cent independent of the Mach Number in the entire range and within the measurement accuracy in agreement with the theoretical value $r = \sqrt{Pr}$, provided that the Prandtl Number is evaluated with the physical properties of the air at equilibrium temperature, T_e.

The obvious independence of Mach Number leads to the conclusion that the compressibility effect is the same at all Mach Numbers in the investigated range. It appears, therefore, that the above simple relation

can be applied with confidence in predicting insulated surface temperatures for laminar-flow boundary layer at least up to $M = 5$. It must be considered, however, that the recovery factors are determined at low temperatures. It will be necessary to verify the results for actual flight temperatures.

The Reynolds Numbers, encountered in the cone measurements with laminar boundary layer, presented in Fig. 4, are ranging from 6,000 to 500,000. The Reynolds Numbers are evaluated on T_e basis—i.e., from the physical properties of the air at equilibrium temperature, the velocity v outside of the boundary layer, and the length of the cone along an edge. The investigations with the cones are reported in more detail in reference 3.

(*B*) *Transitional and Turbulent Boundary Layer*

For higher Reynolds Numbers, surface temperatures were measured along the cylindrical part of the cone-cylinder model. The local flow conditions along the cylinder outside of a boundary layer were taken from computations provided by the Ballistic Research Laboratories, Aberdeen, according to a method developed by Clippinger.[4] Static pressure taken along the cylinder was found to be within 2 per cent in agreement with the data given by Clippinger's method.

The temperature recovery factors determined from the surface temperature measurements for Mach Numbers 2.87 and 4.25 are presented as a function of the cylinder length in Fig. 5. The experiments show (a) that there is a separation of the data according to Mach Number for a cylinder length larger than 7 in. and (b) that for each Mach Number there are generally two distinct regions—one in which a rather large variation of the recovery factor occurs and one in which the recovery factor is essentially constant. Schlieren photographs, taken with 0.5 microsec. flashlight (Fig. 6), show that the boundary layer is fully turbulent in the region of constant recovery factors. Hence, the front portion of the cylinder can be considered as having transitional flow in the boundary layer and the rear portion as having turbulent flow. No means of determining precisely the beginning of the transition region on wind-tunnel models has yet been found. The value of the recovery factor 1 in. behind the leading edge of the cylinder is 0.89. This is about 4.5 per cent higher than the laminar value for the cones. This high value indicates that some turbulent motion exists already at this point. As the air moves along the cylinder, the turbulent motion becomes more and more pronounced, and the recovery factor increases until it reaches a distinct maximum in the rear portion of the transition zone. The highest measured values are 0.96 at Mach Number 2.87 and 0.98 at Mach Number 4.25. The recovery factor then drops to its turbulent values of 0.92 at $M = 2.87$ and 0.97 at $M = 4.25$. The data plotted against Reynolds Number are presented in Fig. 7. The Reynolds Numbers are determined on T_e basis in the same way as defined above. The characteristic length is the length of the model along the surface from the tip of the cone to the respective measuring point. The recovery factor results from the measurements on the cylinder may be summarized as follows:

(a) In the transition region the recovery factor increases to a value that is above that of the turbulent recovery factor (an observation that was also made recently by Stalder[5]).

(b) The recovery factor is essentially constant once turbulent flow in the boundary layer is established.

(c) The turbulent recovery factor at $M = 4.25$ is 5 per cent higher than at $M = 2.87$.

(d) The Reynolds Number of transition to turbulent boundary-layer flow is lower for the higher Mach Number.

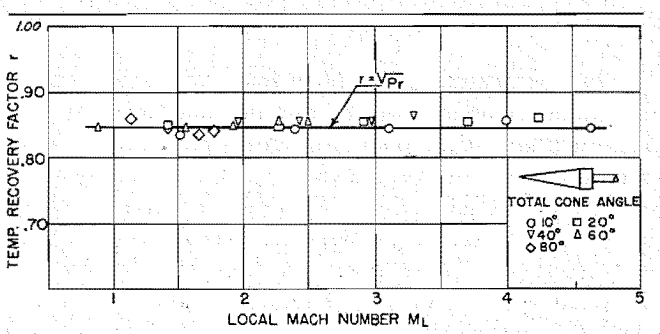

FIG. 3. Recovery factor for laminar boundary-layer flow vs. local Mach Number.

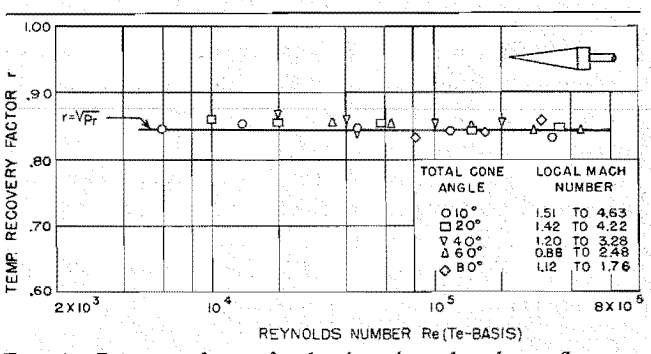

FIG. 4. Recovery factor for laminar boundary-layer flow vs. Reynolds Number.

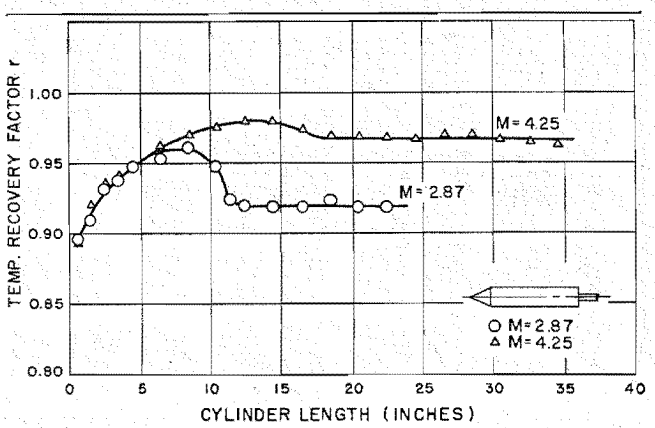

FIG. 5. Recovery factor along a 40° cone-cylinder.

These experimental results differ from the usual concept of turbulent recovery factors deduced from approximate analyses. These analyses give the recovery factor either as a function of the Prandtl Number—i.e., $r = Pr^{1/3}$ (as, for instance, Ackermann[6] and Squire[7])—or as a function of Prandtl Number and Reynolds Number (as, for instance, Seban[8]) but not as a function including the Mach Number. More data at low and high stagnation temperatures are needed to evaluate precisely the influence of the similarity parameters Re, Pr, and M. However, it appears that the recovery factor is considerably higher than widely accepted from various analyses and the few experimental data from cones with artificially induced turbulence. The insulated surface temperature of supersonic vehicles with turbulent boundary layer must be expected to be near the stagnation temperature.

Heat Transmission

The next question is: How much of the heat produced in a boundary layer will be transferred to the solid surface of a body at supersonic speed? The measured temperature recovery factors were used to determine the surface coefficient of heat transfer h and the nondimensional heat-transfer coefficient Nusselt Number Nu. The Nusselt Number is, in general, a function of the Reynolds Number, Prandtl Number, and Mach Number; thus,

$$Nu = hl/k = f(Re, Pr, M)$$

where h is the surface coefficient of heat transfer, l is the characteristic length, and k is the thermal conductivity of the air. However, in compressible flow the similarity parameters referred to free-stream conditions are not adequate for boundary-layer phenomena. The dependence of viscosity, thermal conductivity, and specific heat on the temperature suggests new variables that make the experimental investigations complicated and the comparison of the available data difficult.

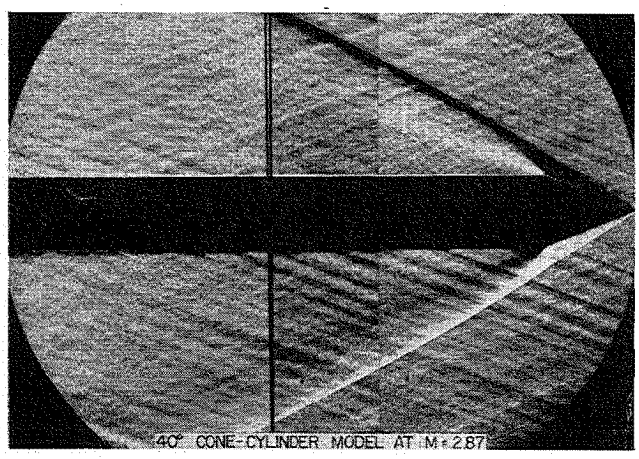

Fig. 6. 40° cone-cylinder model at $M = 2.87$ in the N.O.L. 40- by 40-cm. Aeroballistics Tunnel.

(A) *Laminar Boundary-Layer Flow*

Two sets of experiments have been made with laminar boundary-layer flow on cones: In one set, the average heat transfer over the entire cone was determined with thick-walled copper cones; in the other set, the local heat transfer for each section was determined with the subdivided 20° cone.

Fig. 8 shows the heat-transfer data from the thick-walled copper cones in nondimensional form as Nusselt Number versus Reynolds Number. The physical properties of the air are again evaluated at equilibrium temperature and the velocity at the outer edge of the boundary layer. The data are obtained for heat flow in both directions—that is, into and out of the wall of the cone. The wall temperature, on the average, was either 25°C. below or above the equilibrium temperature. Local Mach Numbers at these measurements ranged from 0.88 to 4.65, inclusive. The data show that the difference between heating and cooling is small. As in the case of the recovery factor, no influence of Mach Number was found. The data can be well represented by the analytical solution for average heat transfer over cones, as given in reference 9,

$$Nu_{av.} = 0.767\, Re^{0.5} Pr^{1/3}$$

In a similar way, the local values of the heat transfer, shown in Fig. 9, have been determined for the subdivided cone in a range of local Mach Numbers from 1.42 to 4.22. These data show even less evidence of a separation with respect to heat-flow direction. Again, the data can be well represented by the corresponding analytical solution for local heat transfer—viz.,

$$Nu = 0.575\, Re^{0.5} Pr^{1/3}$$

From these measurements we may conclude that application of the above heat-transfer correlations to predict supersonic heat transfer in laminar boundary-layer flow with reasonable accuracy is justified up to Mach Numbers of about 5. However, data at higher wall temperatures and higher supply air temperatures are still needed to verify the result in the high temperature range.

(B) *Transitional and Turbulent Boundary Layer*

The heat transfer for transitional and turbulent boundary layer was determined with the cone-cylinder models. The recovery factor for each location along the cylinder observed under identical flow conditions was applied for computing the local heat-transfer coefficients from the wall-temperature measurements. These heat-transfer coefficients were converted into Nusselt Numbers, in the same way as for the laminar boundary layer, by use of the equilibrium temperature as reference temperature for the thermal conductivity. The data, at $M = 2.87$, were taken with a model made up of 2-in. copper sections, thermally insulated from each other. With this arrangement heat transfer occurs

over the full model length, the surface being at uniform temperature within ±5°C. Again the heat transfer is measured for heat flow into and out of the cylinder wall at a wall temperature about 25°C. below and above equilibrium temperature, respectively. Fig. 10 shows the relation between Nusselt Number and Reynolds Number. Contrary to the result for cones with laminar boundary-layer flow, the change in the direction of the heat flow produces roughly 100 per cent change in the amount of heat transferred in the transitional, as well as in the turbulent, flow region. The question whether the separation of the data is due to the direction of heat flow or due to the difference in wall temperature cannot be answered from these experiments. Data in a larger range of wall temperatures are necessary to answer this question.

The data from the starting section of the cylinder for the cold model seem to follow the equation for laminar flow over a flat plate as given by Crocco.[10] Taking into account the ratio of wall temperature and ambient temperature for the flow conditions prevailing on the model in the wind tunnel, the equation reads

$$Nu = 0.295\, Re^{0.5} Pr^{1/3}$$

The data for the heated wall indicate an appreciable amount of turbulent motion in the boundary layer. In the turbulent-flow region, the heat transfer for heat flow from the wall to the air follows closely the turbulent correlation of heat transfer as derived from the momentum-heat transfer analogy by Colburn[11] for subsonic velocities—viz.,

$$Nu = 0.029\, Re^{0.8} Pr^{1/3}$$

The data compiled so far are not sufficient to make any final conclusions. The data, however, indicate that small changes of temperature distributions in the boundary layer near the wall are likely to cause large changes in heat transfer. This is one reason for the nonuniformity of the available heat-transfer data. From the data that we have we must conclude that we cannot expect a high accuracy in predicting turbulent heat transfer. The application of the well-known Colburn correlation for practical design purposes will give fairly accurate data up to Mach Numbers of about 5, as was found at free-flight tests by Fischer and Norris.[12] In the higher Mach Number region, however, predictions are uncertain, as recently pointed out by Kaye,[13] who attempted to determine temperature distributions in a wing flying at supersonic speeds.

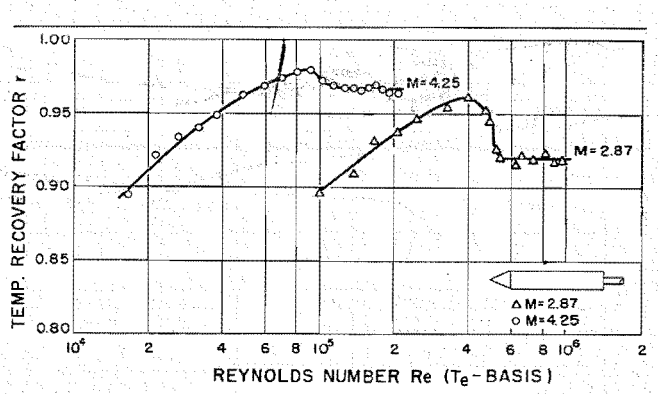

FIG. 7. Recovery factor for a cone-cylinder model vs. Reynolds Number.

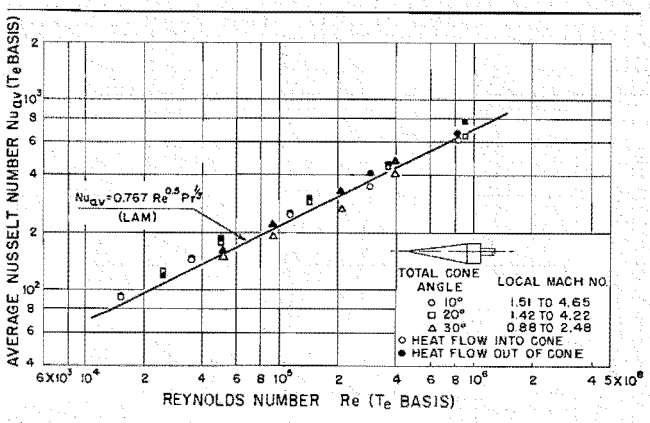

FIG. 8. Average heat transfer for cones with laminar boundary layer vs. Reynolds Number.

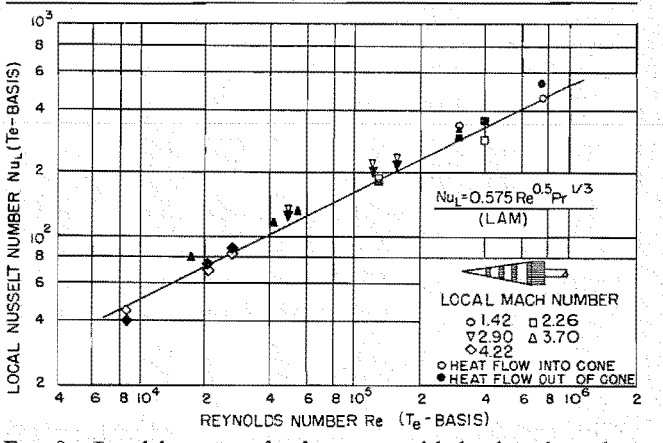

FIG. 9. Local heat transfer for cones with laminar boundary layer vs. Reynolds Number.

TRANSITION OF THE BOUNDARY LAYER

Considerations of the stability of a laminar boundary layer are of considerable practical interest because of the large change in equilibrium temperature, as well as in heat transfer, associated with the change of boundary-layer flow. Boundary-layer theory shows that there is a principal difference between subsonic and supersonic flow. Whereas in subsonic flow instability of a boundary layer will occur in all cases for sufficiently high Reynolds Numbers, in supersonic flow there exists a critical Reynolds Number above which a boundary layer will stay laminar. If the prediction as given in a theory by Lees and Lin[14, 15] is correct, radiative cooling might be sufficient in particular cases to keep a boundary layer laminar.

In Fig. 11, the Reynolds Number of transition which can be observed in a wind-tunnel test is plotted as a function of the ratio of wall temperature, T_w, to ambient

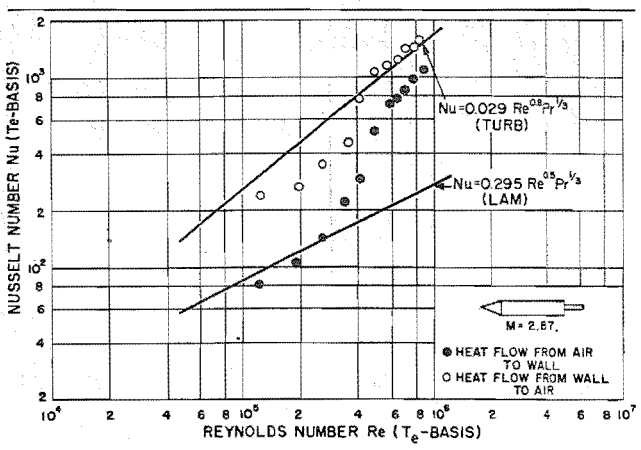

FIG. 10. Heat transfer for a cone-cylinder model vs. Reynolds Number.

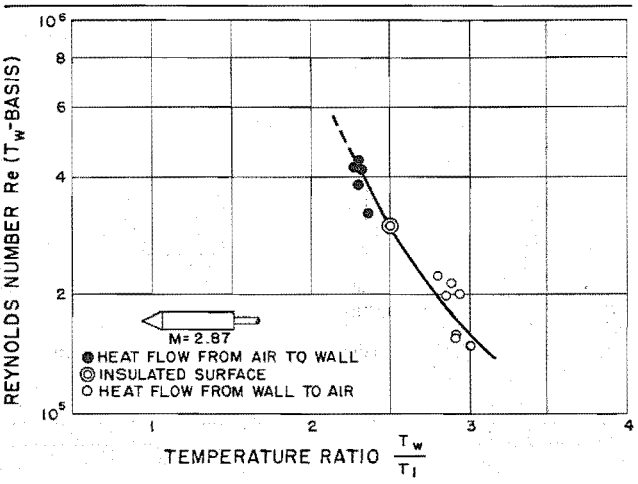

FIG. 11. Reynolds Number of transition vs. wall temperature.

air temperature, T_1, for ratios T_w/T_1 between 2.3 and 3.0. The transition Reynolds Number increases by a factor of about 3 when the wall temperature is lowered over about 100°C. A wall temperature for which a boundary layer stays laminar over the entire length of the body has not yet been established.

CONCLUSIONS

The experimental investigations of temperature recovery, heat transmission, and boundary-layer transition in the N.O.L. Aeroballistics Wind Tunnel have shown the following:

(1) Temperature-recovery factors in a laminar-flow boundary layer, measured on small cones with total angles between 10° and 80°, have been found to be independent of Reynolds Number and Mach Number in a range between $M = 0.88$ and 4.65 and can be represented by the square root of the Prandtl Number for a Prandtl Number evaluated at wall conditions.

(2) The transitional recovery factor rises with Reynolds Number to a maximum that is higher than the turbulent recovery factor for the same Mach Number.

(3) The turbulent recovery factor obtained from temperature measurements on cylinders at $M = 2.87$ and 4.25 is found to be independent of Reynolds Number but 5 per cent higher for $M = 4.25$ than it is for $M = 2.87$.

(4) The Nusselt-Reynolds relation for heat transfer with laminar boundary layers, determined from cones at Mach Numbers between 0.88 and 4.25, can be represented by known correlations. No influence of Mach Number and little influence of the direction of heat flow has been found.

(5) Transitional and turbulent heat transfer for a cone-cylinder model at $M = 2.87$ shows separation of the data according to the direction of the heat flow. There are not sufficient data yet to approve or disapprove existing approximate analyses.

(6) All the experimental data on temperature recovery and heat transfer are taken between −50° and +50°C. Verification of the data at higher temperatures will be indispensable for practical applications.

(7) The Reynolds Number for transition to turbulent boundary-layer flow becomes lower for higher Mach Numbers. For a constant Mach Number, this Reynolds Number increases as the model wall becomes cooler.

REFERENCES

[1] Lightfoot, J. R., *The Naval Ordnance Laboratory Aeroballistic Research Facility*, Naval Ordnance Laboratory Report (N.O.L.R.) No. 1079, 1950.

[2] *Tables of Supersonic Flow Around Cones*, Massachusetts Institute of Technology, Technical Report No. 1, 1947.

[3] Eber, G. R., *Determination of Temperature Recovery Factors on Cones in the NOL 40 × 40 cm Supersonic Wind Tunnel No. 2*, Naval Ordnance Laboratory Memorandum (N.O.L.M.) 10107, 1950.

[4] Personal communication with R. F. Clippinger and J. H. Giese of the Ballistic Research Laboratories, Aberdeen, Md., 1950.

[5] Stalder, J. R., Rubesin, M. W., and Tendeland, T., *A Determination of the Laminar-, Transitional-, and Turbulent-Boundary-Layer Temperature-Recovery Factors on a Flat Plate in Supersonic Flow*, N.A.C.A. T.N. No. 2077, 1950.

[6] Ackermann, G., *Plattenthermometer in Stroemung mit grosser Geschwindigkeit und turbulenter Grenzschicht*, Forschung auf dem Gebiete des Ingenieurwesens, Band 13, p. 226, 1942.

[7] Squire, H. B., *Heat Transfer Calculations for Airfoils*, British Air Ministry R. & M. No. 1986, 1942.

[8] Seban, R. A., *Analysis for the Heat Transfer to Turbulent Boundary Layers in High Velocity Flow*, Ph.D. Thesis, University of California, Berkeley, Calif., 1948.

[9] Johnson, H. A., and Rubesin, M. W., *Aerodynamic Heating and Convective Heat Transfer—Summary of Literature Survey*, Trans. A.S.M.E., Vol. 71, p. 447, 1949.

[10] Crocco, L., *Laminar Boundary Layer in Gases*, Translation, North American Aviation, Inc., Report CF-1038, 1948.

[11] Colburn, A. P., *A Method of Correlating Forced Convection Heat Transfer Data and Comparison with Fluid Friction*, Trans. A.I.C.E., Vol. 29, p. 174, 1933.

(*Continued on page 14*)

The Lift, Rolling Moment, and Pitching Moment on Wings in Nonuniform Supersonic Flow*

HENRY L. ALDEN† AND LEON H. SCHINDEL†
Massachusetts Institute of Technology

SUMMARY

A method is developed for computing aerodynamic coefficients of wings in arbitrary nonuniform supersonic flows. It is shown that lift, pitching moments, and rolling moments can be obtained by single integrations without calculation of pressure distributions as an intermediate stage. Application of the method to wings with supersonic leading and trailing edges is formally similar to conventional strip methods but gives results that are correct within the limits of three-dimensional linearized theory.

NOMENCLATURE

a	=	tangent of sweepback angle of leading edge
b	=	wing span
c	=	wing chord at root
d	=	tangent of sweepforward angle of trailing edge
e, f	=	intersection of Mach line and leading edge
l	=	rolling moment
m	=	pitching moment
q	=	dynamic pressure (free stream)
t	=	parameter locating spanwise position of upwash pulse
u	=	velocity perturbation in x-direction
v	=	velocity perturbation in y-direction
w	=	upwash velocity perturbation in z-direction
w_p	=	upwash due to pulse
x	=	chordwise coordinate on wing
y	=	spanwise coordinate on wing
z	=	vertical coordinate
A.R.	=	aspect ratio
C_L	=	lift coefficient
C_p	=	pressure coefficient
$F(t)$	=	influence function for lift
L	=	lift
M	=	Mach Number (free stream)
$P(t)$	=	pitching moment influence function
$R(t)$	=	rolling moment influence function
U	=	free-stream velocity
α_T	=	local stream angle at wing tip
β	=	$\sqrt{M^2 - 1}$
η	=	spanwise coordinate on wing
ξ	=	chordwise coordinate on wing
φ	=	perturbation velocity potential

INTRODUCTION

THE COEFFICIENTS OF LIFT AND PITCHING MOMENT of supersonic aircraft are known to be affected appreciably by downwash flows over tails and aft wings. In cases where there are stringent requirements on control and stability of the air frame, these effects must be included in any accurate performance estimate of wing-tail combinations. Much work, both theoretical and experimental, has been carried out on various phases of the problem, including studies of pressure interference between wings and bodies and between vertical and horizontal surfaces of cruciforms, and investigations into the structure of flow fields behind lifting surfaces.[1] If a flow field is known, the problem of downwash effects is resolved into the calculation of aerodynamic coefficients of tail surfaces that operate within the nonuniform supersonic flow. In principle, this calculation can be carried out by integrating fundamental solutions of the wave equation[2] to obtain pressure distributions and, hence, the aerodynamic coefficients; in practice, the labor required is enormous. This report deals with the problem by developing a simple method for the direct computation of lift, pitching moment, and rolling moment without recourse to the intermediate stage of pressure distributions. The general approach employs the idea of lifting strips, as presented by Lagerstrom and Van Dyke[3] for the case of straight trailing edges.

BASIC EQUATIONS

The theoretical derivation is subject to the restrictions of nonviscous linearized theory and is based on the

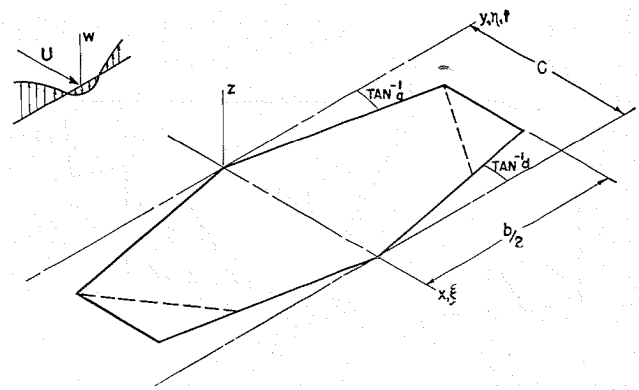

FIG. 1.

Received July 19, 1951.
* This work was carried out as part of the Guided Missiles Program (Project Meteor) at the Massachusetts Institute of Technology and was sponsored by the Bureau of Ordnance of the Navy Department.
† Naval Supersonic Laboratory.

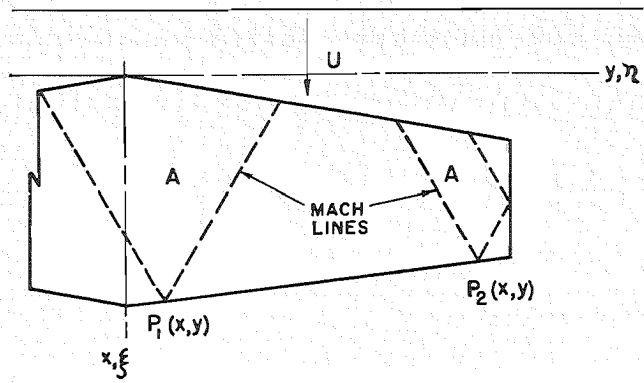

FIG. 2. Areas of integration for determining velocity potential.

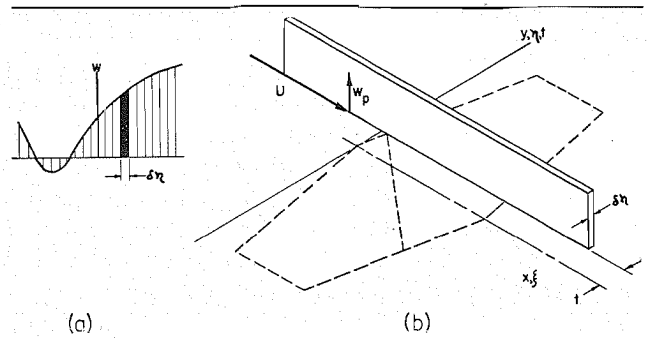

FIG. 3. Upwash pulse on trapezoidal wing.

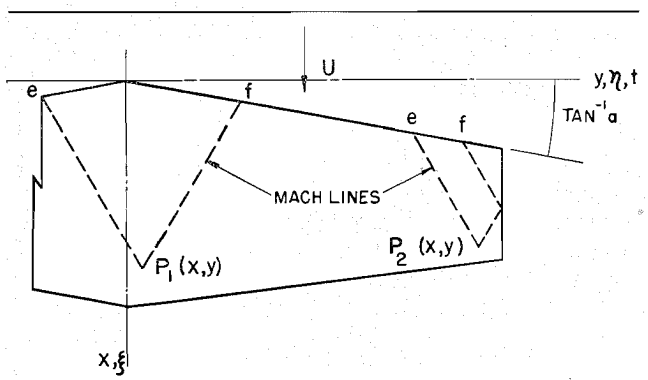

FIG. 4. Limits of integration for pressure coefficient at points $P_1(x,y)$ and $P_2(x,y)$.

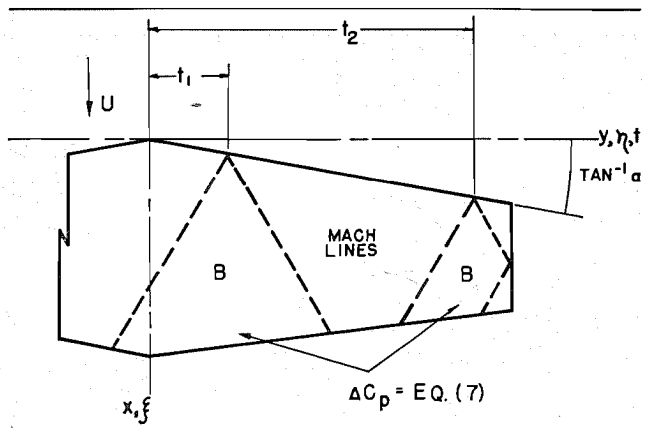

FIG. 5. Areas of integration for determining $F(t)$ at t_1 and t_2.

standard form of the wave equation for the velocity potential of small disturbances,

$$\beta^2 \frac{\partial^2\varphi}{\partial x^2} - \frac{\partial^2\varphi}{\partial y^2} - \frac{\partial^2\varphi}{\partial z^2} = 0 \qquad (1)$$

where $\partial\varphi/\partial x = u$, $\partial\varphi/\partial y = v$, and $\partial\varphi/\partial z = w$. The flow is represented as a stream of velocity U in the x-direction (see Fig. 1) with perturbations v and w. The absence of a perturbation in the x-direction (u) implies a constant-pressure field and no variation of v or w in the flow direction, a situation that physically corresponds to a downwash field several chord lengths behind a wing or at least far enough downstream for the flow pattern to have stabilized. Associated with the field is a velocity potential that satisfies Eq. (1). In this field is placed a thin airfoil that will disturb the field in a manner determined mathematically by a second potential also satisfying Eq. (1). It is this second potential that will describe the pressures and aerodynamic behavior of the airfoil and which will be termed the wing potential φ for the purpose of theoretical development.

The airfoil surfaces under consideration are taken as flat planar surfaces with supersonic leading and trailing edges, as well as tip edges that are aligned with the stream. Within these limitations the wing may have arbitrary angles of leading-edge sweep, trailing-edge sweep, and aspect ratio.

The boundary conditions are thus set up for flat plates, since the increments due to thickness are additive and can be treated independently. In the plane of the wing, the flow field has an upward velocity $w(y)$ and a lateral velocity $v(y)$ which are constant in the chordwise direction; to ensure that flow over the wing is tangent to the surface, it is sufficient to specify that the vertical velocity of the wing potential cancels the vertical stream velocity or

$$w(y) + (\partial\varphi/\partial z) = 0 \qquad (2)$$

on the wing in the plane $z = 0$. Off the wing in the $z = 0$ plane, the pressure will be zero.[2,4] Since $C_p = -2u/U = 0$,

$$u = \partial\varphi/\partial x = 0 \qquad (3)$$

off the wing in the plane $z = 0$. Provided there are no subsonic edges, Eq. (1), with the boundary conditions expressed in Eqs. (2) and (3), determines a wing potential that will vanish at an infinite distance from the plane of the wing. For the present purpose, the argument is carried through for wings with supersonic leading and trailing edges, as indicated in the typical plan form in Fig. 1. The problem, as stated here, is completely equivalent to a warped wing in a uniform flow if small chordwise strips are inclined to the stream at various angles equal to $w(y)/U$.

By superimposing fundamental source solutions to Eq. (1), several authors have been able to demonstrate that full solutions to the above problem can be expressed

formally as integrals. The lift, for example, can be written as a triple integral with variable limits. The wing potential, a double integral over the fore-cones of Mach lines, is given as[2]

$$\varphi(x, y) = \frac{1}{\pi} \int \int_A \frac{g(\xi, \eta) d\xi d\eta}{\sqrt{(x - \xi)^2 - \beta^2 (y - \eta)^2}} \quad (4)$$

where $g(\xi, \eta)$ = upwash distribution function. Sample areas of integration which would give the potential on the trailing edge are indicated in Fig. 2, showing that, for points (x, y) not influenced by tip Mach lines, the region A is the Mach fore-cone, whereas in tip zones the region is modified as shown. To evaluate the lift in a field of arbitrary vertical velocities by pursuing this method is generally impractical. A different approach is desirable.

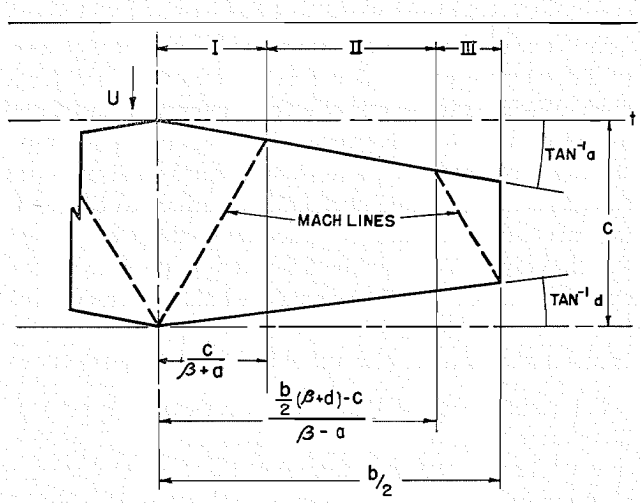

FIG. 6.

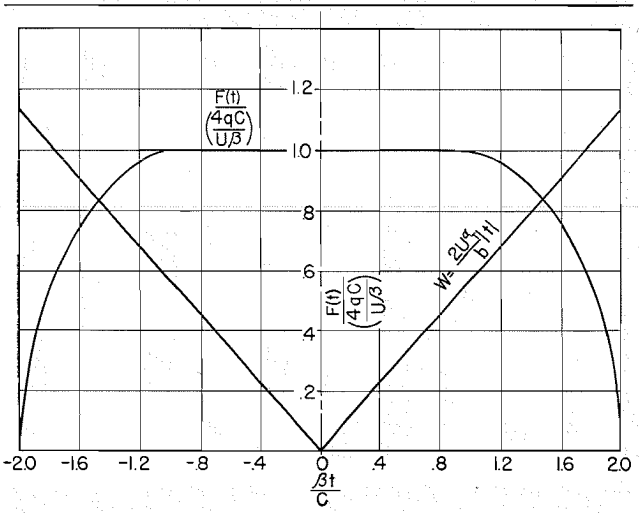

FIG. 7. Linear symmetric upwash distribution $w(t)$ and influence function $F(t)$ for rectangular wing of effective aspect ratio 4.

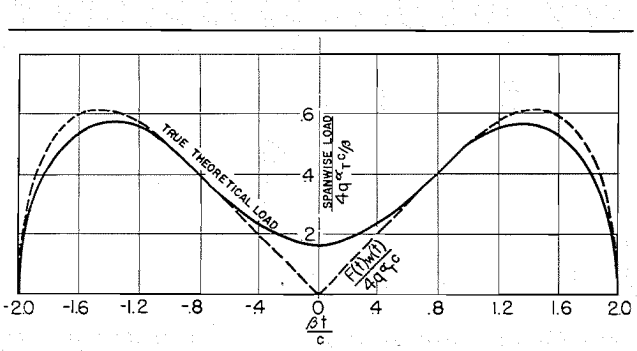

FIG. 8.

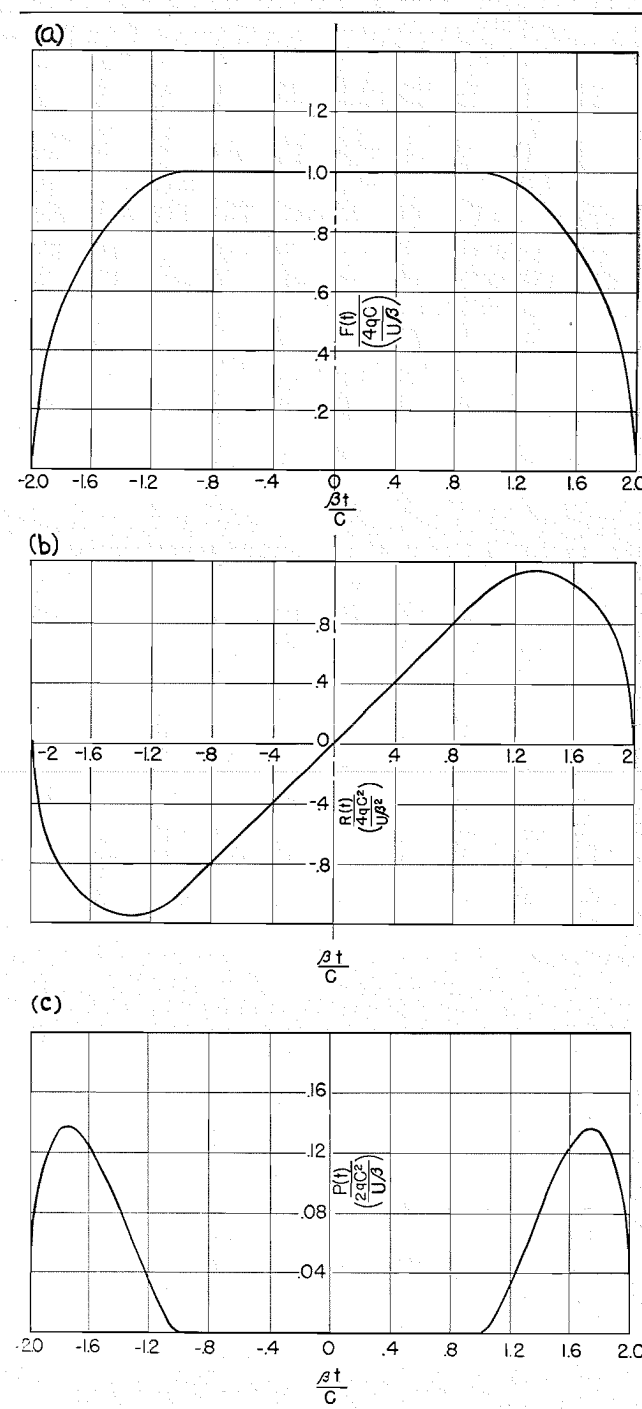

FIG. 9. Influence functions for rectangular wing of effective aspect ratio 4 (β A.R. = 4). (a) $F(t)$ = lift influence function. (b) $R(t)$ = rolling moment influence function (about the wing centerline). (c) $P(t)$ = pitching moment influence function (about the mid-chord).

It is assumed that the upwash can be divided into elements, as indicated in Fig. 3, with the objective of computing the increment of lift from a representative element. The total lift results from the proper addition of increments. Specifically, an upwash element or pulse of unit strength, $w_p\delta\eta = 1$, is placed at spanwise station, $\eta = t$, while everywhere else $w = 0$. The pressure disturbance will spread over the Mach cone from the leading edge and will produce, upon integration, an increment of lift which evidently will be a function of the pulse position t and the geometry of the wing. The methods of solving for the influence of a single pulse are relatively simple and stem from application of the formal solution of Eq. (4) and formulas derivable from it. For given plan forms, the lift due to a unit pulse at t can be expressed as $F(t)$, the integral of pressure over the disturbed region. The total downwash is a continuous distribution of pulses of various strengths $w(t)dt$ at various positions along the span, with the result that, if the lift increment is written

$$dL = [w(t)\ dt]\ F(t)$$

it follows that the total lift is

$$L = \int_{-(b/2)}^{b/2} F(t)w(t)\ dt \tag{5}$$

The function $F(t)$ is the influence function for lift; once it is known for a given plan form, the computation proceeds by determining the area under a single curve, a process similar to approximate strip theories.

Influence Function for Lift

This computation is most easily carried out by use of an expression for pressure coefficient derived from Eq. (4). When the downwash is constant in the chordwise direction, as assumed here, Mirels[5] demonstrates that the difference in pressure coefficients between the top and bottom surfaces at a point (x, y) is given by a single integration

$$\Delta C_p(x, y) = \frac{4}{U\pi}\int_e^f \frac{h(\eta)d\eta}{\sqrt{(x-\xi)^2 - \beta^2(y-\eta)^2}} \tag{6}$$

where $h\ (\eta)$ = upwash velocity = w_p and where the typical paths are along the leading edge between e and f on Fig. 4. The unit pulse, $w_p\delta\eta = 1$, results in zero upwash except for an extremely narrow zone $\delta\eta$ at $\eta = t$; at this point, $\xi = a\eta = at$. The radical is substantially constant over the range of t to $t + \delta\eta$, and therefore Eq. (6) can be evaluated at once as

$$\Delta C_p(x, y) = \frac{4}{U\pi}\left[\frac{1}{\sqrt{(x-at)^2 - \beta^2(y-t)^2}}\right] \tag{7}$$

The regions of influence of the pulse in the central and tip regions are shown in Fig. 5. As a result of the special integration limits in the tip area, there is a section where the pressure cancels and the value of ΔC_p is zero, not that given by Eq. (7). The resultant lift is the influence function and is given by

$$F(t) = q\int\int_B \Delta C_p dxdy = \frac{4q}{U\pi}\int\int_B \frac{dxdy}{\sqrt{(x-at)^2 - \beta^2(y-t)^2}} \tag{8}$$

Fig. 5 shows sample areas of integration. The planform characteristics—chord, span, and leading- and trailing-edge sweep—will define the exact areas B for a given Mach Number and will thus determine the shape of the curve $F(t)$. However, it is significant to note that in any case the areas B are simply Mach cones starting at the leading edge and spreading to the trailing edge; near the tip, the Mach line reflects back from the tip edge. Thus, if the flow were coming from the opposite direction, these areas would represent the fore-cones of points on the downstream edge. This suggests that $F(t)$ is also the solution to a reverse flow.

Let it be assumed that there is a reverse flow over the wing of Fig. 5 at the same Mach Number. Reference to the integral of potential of Eq. (4) and its areas of integration in Fig. 2 shows that the areas B of Fig. 5 are fore-cone areas of integration for calculating a reverse flow potential at the downstream edge. It is convenient to note in this connection that spanwise loading is related to the wing potential at the trailing edge by

$$\frac{dL}{dy} = q\int_{\text{L.E.}}^{\text{T.E.}} \Delta C_p dx = \frac{4q}{U}\int_{\text{L.E.}}^{\text{T.E.}} \frac{\partial\varphi}{\partial x}\,dx = \frac{4q}{U}\,\varphi_{\text{(Trailing Edge)}}$$

A comparison may be made between the influence function, Eq. (8), and the spanwise loading for a uniform reverse flow with unit constant upwash. Using Eq. (4) with $g(\xi, \eta) = 1$ and using the coordinate system of Fig. 5 in which the downstream edge for reverse flow is defined by $x = ay$, the resulting span load is

$$\frac{dL}{dy}(y) = \frac{4q}{U\pi}\int\int_B \frac{d\xi d\eta}{\sqrt{(\xi - ay)^2 - \beta^2(\eta - y)^2}} \tag{9}$$

By comparison, the function $dL/dy(y)$ is identical with $F(t)$. The influence function for lift is, then, the span loading of the reversed wing flying at a constant angle of attack. The span loadings for wings of various plan forms are available,[6] and they can be used directly to obtain the influence function, $F(t)$. For generalized trapezoidal wings it is given below. The wing is split into three spanwise zones, as shown in Fig. 6, having associated with them, respectively, three formulas for the influence function.

For Zone I:

$$F_{\mathrm{I}}(t) = \frac{4q}{U\pi\sqrt{\beta^2 - d^2}}\left\{(c - at - dt)\cos^{-1}\left[\frac{d}{\beta} - \frac{(\beta^2 - d^2)t}{\beta(c - at - dt)}\right] + (c - at + dt)\cos^{-1}\left[\frac{d}{\beta} + \frac{(\beta^2 - d^2)t}{\beta(c - at + dt)}\right]\right\} \quad (10)$$

For Zone II:

$$F_{\mathrm{II}}(t) = \frac{4q}{U\sqrt{\beta^2 - d^2}}(c - at - dt) \quad (11)$$

For Zone III:

$$F_{\mathrm{III}}(t) = \frac{4q}{U\pi}\left\{\frac{c - at - dt}{\sqrt{\beta^2 - d^2}}\cos^{-1}\left[1 - \frac{(\beta + d)(b - 2t)}{c - at - dt}\right] + \sqrt{\frac{2(b - 2t)(c + dt - db - at)}{\beta - d} - (b - 2t)^2}\right\} \quad (12)$$

If the Mach lines from the tip and the root overlap, the influence function in the overlapping region is

$$F(t) = F_{\mathrm{I}}(t) + F_{\mathrm{III}}(t) - F_{\mathrm{II}}(t)$$

Example of Lift Calculation

In general application, the lift is computed from Eq. (5) by multiplying the curve $F(t)$ by $w(t)$ and measuring the included area graphically. However, for illustration, an example is chosen which can also be calculated analytically. Consider a rectangular wing of aspect ratio 2 or greater [for which $F(t)$ is found by letting $a = d = 0$ in Eqs. (10), (11), and (12)] in a field of linear symmetric upwash (Fig. 7). Thus, for the right half-wing,

$$F_{\mathrm{I}}(t) = F_{\mathrm{II}}(t) = 4qc/U\beta$$

$$F_{\mathrm{III}}(t) = \frac{4qc}{U\beta}\left\{\frac{1}{\pi}\cos^{-1}\left[1 - \left(\frac{\beta b}{c} - 2\frac{\beta t}{c}\right)\right] + \frac{1}{\pi}\sqrt{2\left(\beta\frac{b}{c} - 2\beta\frac{t}{c}\right) - \left(\frac{\beta b}{c} - 2\frac{\beta t}{c}\right)^2}\right\}$$

and $w(t) = [U\alpha_T/(b/2)]t$

The product of $F(t)$ and $w(t)$ is shown by the dotted curve in Fig. 8 and encloses an area that can be evaluated analytically to give

$$C_L = \frac{2}{qbc}\int_0^{b/2} F(t)w(t)dt$$

$$= \frac{16\alpha_T}{\beta b^2}\int_0^{(b/2)-(c/\beta)} t\,dt + \frac{16\alpha_T}{\beta b^2}\int_{(b/2)-(c/\beta)}^{b/2}\frac{t}{\pi}\left\{\cos^{-1}\left[1 - \left(\frac{\beta b}{c} - 2\frac{\beta t}{c}\right)\right] + \sqrt{2\left(\frac{\beta b}{c} - 2\frac{\beta t}{c}\right) - \left(\frac{\beta b}{c} - 2\frac{\beta t}{c}\right)^2}\right\}dt$$

$$= (2\alpha_T/\beta)\{1 - (1/\beta\text{A.R.}) + [1/2(\beta\text{A.R.})^2]\}$$

Lagerstrom and Graham[7] treated this case, with the same result, by integrating the pressure coefficients. In addition, the actual span loading that they obtained is plotted in Fig. 8 for comparison with the product $F(t)w(t)$. Although both yield the correct lift coefficient upon integration, only the true loading curve could be used to compute the bending moment about the wing root chord, since an attempt to treat $F(t)w(t)$ as a load distribution curve obviously would produce an erroneous bending moment and is unjustified. Similarly, treating $F(t)w(t)$ as a load distribution curve in general will not correctly give the roll moment on a wing in a nonuniform stream. To compute roll moments in nonuniform fields it is necessary to use a roll moment influence function analogous to the lift function.

Influence Functions for Roll Moments

By similar methods it is possible to derive a rolling moment influence function $R(t)$ such that the total rolling moment around the root chord of a wing is

$$l = \int_{-b/2}^{b/2} w(t)R(t)dt \quad (13)$$

Consider the contribution to rolling moment due to the unit pulse of Fig. 3. The pressure at each point within the disturbed region must be multiplied by its moment arm y and then integrated over the area. The pressures are given by Eq. (7). The contribution of a pulse at station t to the rolling moment is now

$$R(t) = \frac{4q}{U\pi} \int\int_B \frac{y dx dy}{\sqrt{(x - at)^2 - \beta^2(y - t)^2}} \tag{14}$$

The integration areas are again those of Fig. 5. As before, this expression is to be compared with the span loading of a reverse flow. This time the reverse flow contains a linear variation of vertical velocity along the span and is zero at the root with a slope of one—that is, $g(\xi, \eta) = \eta$ in Eq. (4). Again using the coordinate system of Fig. 5, the span loading in reverse flow is

$$\frac{dL}{dy}(y) = \frac{4q}{U\pi} \int\int_B \frac{\eta d\xi d\eta}{\sqrt{(\xi - ay)^2 - \beta^2(\eta - y)^2}} \tag{15}$$

Since the limits of integration are those used previously, Eq. (15) is the same function as Eq. (14). The flow described by Eq. (15), or the roll influence function, is equivalent to the span loading of a reverse uniform flow in which the wing is rolling at 1 rad. per sec. The span loadings on rolling trapezoidal wings have been calculated by Lagerstrom and Graham.[7]

Referring to the zones of Fig. 6 and the work of Lagerstrom and Graham, the influence functions for roll can be obtained.

For Zone I:

$$R_{\mathrm{I}}(t) = \frac{2qbc}{U\pi\beta}\left\{\frac{\left[1 - \frac{t}{c}(a + d)\right]\left[2\frac{\beta t}{c} + \frac{td}{\beta c}(a - d) - \frac{d}{\beta}\right]}{(\beta b/c)[1 - (d^2/\beta^2)]^{3/2}} \cos^{-1}\left[\frac{\frac{d}{\beta} - \frac{\beta t}{c}\left(1 + \frac{ad}{\beta^2}\right)}{1 - (t/c)(a + d)}\right] + \right.$$
$$\left.\frac{\left[1 - \frac{t}{c}(a - d)\right]\left[2\frac{\beta t}{c} - \frac{td}{\beta c}(a + d) + \frac{d}{\beta}\right]}{(\beta b/c)\,[1 - (d^2/\beta^2)]^{3/2}} \cos^{-1}\left[\frac{\frac{d}{\beta} + \frac{\beta t}{c}\left(1 - \frac{ad}{\beta^2}\right)}{1 - (t/c)(a - d)}\right] - \frac{dt}{\beta(b/2)}\frac{\sqrt{1 - \frac{2at}{c} - \frac{t^2}{c^2}(\beta^2 - a^2)}}{1 - (d^2/\beta^2)}\right\} \tag{16}$$

For Zone II:

$$R_{\mathrm{II}}(t) = \frac{2q}{U\beta}\left\{\frac{2t[c - t(a + d)]}{\sqrt{1 - (d^2/\beta^2)}} - \frac{(d/\beta)[c - t(a + d)]^2}{\beta[1 - (d^2/\beta^2)]^{3/2}}\right\} \tag{17}$$

For Zone III:

$$R_{\mathrm{III}}(t) = \frac{2qbc}{U\pi\beta}\left\{\frac{\left[1 - \frac{t}{c}(a + d)\right]\left[2\frac{\beta t}{c} + \frac{td}{\beta c}(a - d) - \frac{d}{\beta}\right]}{(\beta b/c)\,[1 - (d^2/\beta^2)]^{3/2}} \cos^{-1}\left[1 - \frac{\frac{2}{c}\left(\beta + d\right)\left(\frac{b}{2} - t\right)}{1 - (t/c)(a + d)}\right] + \right.$$
$$\sqrt{1 - \frac{t}{b/2}}\sqrt{\frac{\frac{t}{c}(\beta - a) - \frac{b}{2c}(\beta + d) + 1}{(b/2c)(\beta - d)}}\left[\frac{\frac{2t}{c}(\beta + d) - \frac{td}{c\beta}(d + a) + \frac{d}{\beta} - \frac{bd}{\beta c}(\beta + d)}{1 - (d^2/\beta^2)}\right] -$$
$$\left.\frac{2\beta b}{3c}\sqrt{1 - \frac{t}{b/2}}\left[\frac{\frac{t}{c}(\beta - a) - \frac{b}{2c}(\beta + d) + 1}{(b/2c)(\beta - d)}\right]^{3/2}\right\} \tag{18}$$

If the Mach line from the tip and the root overlap, the influence function in the overlapping region is

$$R(t) = R_{\mathrm{I}}(t) + R_{\mathrm{III}}(t) - R_{\mathrm{II}}(t)$$

Influence Functions for Pitching Moments

Proceeding in the same manner, the pitching moment about the η axis of Fig. 5 is expressed in terms of an influence function $P(t)$ by

$$m = \int_{-(b/2)}^{(b/2)} w(t)P(t)dt \tag{19}$$

Computing the pitching moment of a unit pulse gives

$$P(t) = \frac{4q}{U\pi} \int\int_B \frac{x\,dx\,dy}{\sqrt{(x - at)^2 - \beta^2(y - t)^2}} \tag{20}$$

In a uniform reverse flow the function $P(t)$ compares with the span load of wings pitching at 1 rad. per sec. about the downstream η axis. For this case $g(\xi, \eta) = \xi$ in Eq. (4), and

$$\frac{dL}{dy}(y) = \frac{4q}{U\pi} \int\int_B \frac{\xi d\xi d\eta}{\sqrt{(\xi - ay)^2 - \beta^2(\eta - y)^2}} \tag{21}$$

Thus Eqs. (20) and (21) are identified; this relationship is preserved for arbitrary choices of the axis of pitching moment.

The influence function curves for pitching trapezoidal wings are:

For Zone I:

$$P_{\mathrm{I}}(t) = \frac{2qc^2}{U\pi(\beta^2 - d^2)^{3/2}} \left\{ \left[1 - a\frac{t}{c} - d\frac{t}{c}\right]\left[\frac{\beta^2 t}{c}(d - a) + d^2\left(2a\frac{t}{c} - 1\right)\right] \times \right.$$
$$\cos^{-1}\left[\frac{d\left(1 - a\frac{t}{c}\right) - \beta^2\frac{t}{c}}{\beta\left(1 - a\frac{t}{c} - d\frac{t}{c}\right)}\right] + \left[1 - a\frac{t}{c} + d\frac{t}{c}\right]\left[-\beta^2\frac{t}{c}(d + a) + d^2\left(2a\frac{t}{c} - 1\right)\right] \times$$
$$\left. \cos^{-1}\left[\frac{d\left(1 - a\frac{t}{c}\right) + \beta^2\frac{t}{c}}{\beta\left(1 - a\frac{t}{c} + d\frac{t}{c}\right)}\right] + 2d\left(1 - a\frac{t}{c}\right)\sqrt{\beta^2 - d^2}\sqrt{\left(1 - a\frac{t}{c}\right)^2 - \beta^2\frac{t^2}{c^2}} \right\} \tag{22}$$

For Zone II:

$$P_{\mathrm{II}}(t) = \frac{2qc^2}{U\sqrt{\beta^2 - d^2}} \left\{ \left(d\frac{t}{c} - a\frac{t}{c}\right)\left(1 - d\frac{t}{c} - a\frac{t}{c}\right) - \frac{d^2\left(1 - a\frac{t}{c} - d\frac{t}{c}\right)^2}{\beta^2 - d^2} \right\} \tag{23}$$

For Zone III:

$$P_{\mathrm{III}}(t) = \frac{2qc^2}{U\pi(\beta^2 - d^2)^{3/2}} \left\{ \left[1 - a\frac{t}{c} - d\frac{t}{c}\right]\left[(\beta^2 - d^2)\left(d\frac{t}{c} - a\frac{t}{c}\right) - d^2\left(1 - a\frac{t}{c} - d\frac{t}{c}\right)\right] \times \right.$$
$$\cos^{-1}\left[1 - \frac{(\beta + d)\left(\frac{b}{c} - 2\frac{t}{c}\right)}{1 - a\frac{t}{c} - d\frac{t}{c}}\right] + \frac{1}{3}\left(\frac{b}{c} - 2\frac{t}{c}\right)(\beta + d)\left[3\left(1 - 2a\frac{t}{c}\right)(\beta^2 - d^2) - \left(1 - a\frac{t}{c} - d\frac{t}{c}\right) \times \right.$$
$$\left. \left. (\beta^2 + 4d\beta) - \beta(\beta + d)(\beta - 2d)\left(\frac{b}{c} - 2\frac{t}{c}\right)\right] \sqrt{\frac{2}{\left[\frac{(\beta + d)\left(\frac{b}{c} - 2\frac{t}{c}\right)}{1 - 2\frac{t}{c} - d\frac{t}{c}}\right]} - 1} \right\} \tag{24}$$

The influence function in the overlapping region is

$$P(t) = P_{\mathrm{I}}(t) + P_{\mathrm{III}}(t) - P_{\mathrm{II}}(t)$$

The axis of moments for these formulas goes through the middle of the wing root chord.

Discussion

Wing lift, moments of roll, and moments of pitch are readily computed in downwash fields by Eqs. (5), (13), and (19), respectively. For any wing with supersonic leading and trailing edges, the appropriate influence functions have been identified with load distributions in reverse uniform flows. The problem of thickness ratio, not considered in this report, can be treated independently by the linear theory and is the same as in the case of uniform flow; previous results for wave drag due to thickness are valid for nonuniform flows.

The influence functions may be computed by application of Eqs. (8), (14), and (20). They are given here for generalized trapezoidal wings. For rectangular wings, the functions are illustrated in Fig. 9. In general they show, as expected, the effects of three-dimensional flows in the vicinity of roots and wing tips. In comparison with two-dimensional strip theories, the three-dimensional treatment shows marked differences in these root and tip regions, confirming the idea that low aspect ratio wings that consist mostly of root and tip cannot be treated with any success by two-dimensional concepts.

Inspection of influence functions for lift and pitching moment shows that it is possible for different distributions of downwash to produce the same total lift but different moments. Thus, the spanwise distribution of downwash will have an effect on the chordwise center of pressure. From the point of view of tail efficiency, then, the reduction in lift due to downwash might be expressed in terms of one efficiency, while the moment efficiency would have a different value because of the shift in the center of pressure. This fact, which is already known from experiment, is shown by analysis to be an inherent feature of nonuniform downwash distributions flowing over planar tails.

The analysis, however, is restricted by the assumptions of the linearized theory. If, as would be expected, the importance of wing thickness is similar to that in the case of uniform flows, the pitching moment should be modified by a correction such as Busemann's higher order approximation, whereas the lift and rolling moment would be properly predicted for closed profiles by the linear formulas.

The extension of influence functions to include subsonic leading and trailing edges has not been attempted. Such extension would introduce questions concerning the Kutta condition at trailing edges and the proper application of leading-edge suction and would make the problem in general more complicated. The results of an investigation, however, would be of interest to the designers of airfoils having highly swept plan forms.

References

[1] Davis, Theodore, *Experimental Investigation of Downwash and Sidewash Behind a Rectangular Wing at a Mach Number of 1.60*, Meteor Report No. UAC-45, United Aircraft Corporation, January, 1950.

[2] Evvard, John C., *Distribution of Wave Drag and Lift in the Vicinity of Wing Tips at Supersonic Speeds*, N.A.C.A. Report No. TN-1382, July, 1947.

[3] Lagerstrom, P. A., and Van Dyke, M. D., *General Considerations About Planar and Non-Planar Lifting Systems*, Report No. SM-13432, Douglas Aircraft Company, Inc., June, 1949.

[4] Lagerstrom, Paco A., Wall, D., and Graham, Martha E., *Formulas in Three-Dimensional Wing Theory (1) & (2)*, Report No. SM-11901, Douglas Aircraft Company, Inc., July 8, 1946.

[5] Mirels, Harold, *Theoretical Method for Solution of Aerodynamic Forces on Thin Wings in Non-Uniform Supersonic Stream with an Application to Tail Surfaces*, N.A.C.A. Report No. TN-1736, November, 1948.

[6] Harmon, S. M., and Jeffreys, Isabella, *Theoretical Lift and Damping in Roll of Thin Wings with Arbitrary Sweep and Taper at Supersonic Speeds—Supersonic Leading and Trailing Edges*, N.A.C.A. Report No. TN-2114, May, 1950.

[7] Lagerstrom, Paco A., and Graham, Martha E., *Some Aerodynamic Formulas in Linearized Supersonic Theory for Damping in Roll and Effect of Twist for Trapezoidal Wings*, Report No. SM-13200, Douglas Aircraft Company, Inc., March 12, 1948.

Recent Investigation of Temperature Recovery and Heat Transmission on Cones and Cylinders in Axial Flow in the N.O.L. Aeroballistics Wind Tunnel

(*Continued from page 6*)

[12] Fischer, W. W., and Norris, R. H., *Supersonic Convective Heat-Transfer Correlations from Skin-Temperature Measurements on a V-2 Rocket in Flight*, Trans. A.S.M.E., Vol. 71, p. 457, 1949.

[13] Kaye, J., *The Transient Temperature in a Wing Flying at Supersonic Speeds*, Journal of the Aeronautical Sciences, Vol. 17, No. 4, p. 787, 1950.

[14] Lees, L., and Lin, C. C., *Investigation of the Stability of the Laminar Boundary Layer in a Compressible Fluid*, N.A.C.A. T.N. No. 1115, 1946.

[15] Lees, Lester, *The Stability of the Laminar Boundary Layer in a Compressible Fluid*, N.A.C.A. T.N. No. 1360, 1947.

The Interpretation of Failure Loads in the Plastic Theory of Continuous Beams and Frames

P. S. SYMONDS* AND B. G. NEAL†

Brown University and Cambridge University, Respectively

SUMMARY

Plastic failure loads on continuous beams and rigid frames of ductile metal can be simply computed when certain assumptions concerning the moment-curvature relations are made and when it is assumed that individual loads remain in constant ratio to each other during the loading process, so that the load value is defined by a single parameter. The simple theory is mainly concerned with the prediction of the maximum load a structure can carry before "plastic collapse" occurs. However, in some cases it will be desirable to estimate some of the deflections, and a case of a continuous beam is described herein in which the calculation of plastic failure load may be misleading unless accompanied by a deflection analysis. The deflection values that make the plastic analysis meaningful are calculated for this case by a simple approximate method that requires little additional labor after the plastic failure load has been determined. The results are compared with test results previously published by Stüssi and Kollbrunner[11] and by Maier-Leibnitz.[1, 12] The method may be used for general framed structures, and an analysis of a two-story portal frame is given as a further illustration of its use.

(1) INTRODUCTION

THE PLASTIC METHODS OF ANALYSIS and design for beams and frames of ductile metal[1–7] are mainly concerned with the load at which failure by "plastic collapse" would occur. The basic assumption of these methods is that the bending moment at any cross section cannot exceed a value termed "the fully plastic moment." This value corresponds to the spread of plastic zones across the entire cross section, and, as it is approached, large changes in curvature can occur, with negligibly small changes in bending moment. A "plastic hinge" is said to occur at a cross section where the fully plastic moment is developed, since it is assumed that hinge action can then take place at this cross section while the bending moment remains constant.

Under these hypotheses, when the loads on a framed structure are steadily increased in fixed proportion to each other, a critical load is finally reached at which the structure would become a mechanism owing to the formation of plastic hinges at a sufficient number of sections. It has been shown[3–6] how this critical load can be easily calculated as compared with elastic analyses for highly redundant structures.

Received January 19, 1951.

* Associate Professor of Engineering.

† University Demonstrator in Engineering and Fellow of Trinity Hall.

Tests,[1, 3, 8] as well as theoretical considerations, show that in actual structures a certain amount of strain-hardening always takes place at the cross sections where plastic hinges form in the theory, so that the load can be carried slightly above the theoretical collapse value. In practice, complete collapse, with a drop or total loss of load-carrying capacity, occurs only when additional effects arise, such as lateral instability of beams, rupture of welds, additional moments due to large deflections, etc. These effects ordinarily appear only after large plastic deformations have been produced, at loads exceeding the theoretical collapse value. The collapse load of the plastic theory then gives a good estimate, generally conservative, of the observed load at which small load increases produce much larger deflections than at previous load levels.

Although most of the experimental investigations have dealt with mild steel structures, the methods should be useful in cases of structures of other metals of sufficient ductility. The effects of strain-hardening should be qualitatively the same: The actual structure does not collapse at the critical load of the theory but carries loads more or less higher than this, depending on the rate of strain-hardening. Further experimental investigations are needed; questions of failure by rupture or by buckling, among others, must be investigated for the metals that have not yet been studied.

The plastic methods are directly concerned with loads rather than with deflections, although the criterion of failure is the imminence of large plastic deflections. In cases where the precise values of the permissible deflections themselves are the primary quantities that control a design, the plastic theory will probably not be applicable. The exact calculation of deflections in a partially yielded redundant structure is a formidable task, especially if measured stress-strain characteristics are used. Even for simple beams, fairly lengthy calculations are required,[9] while, for redundant structures, trial-and-error procedures must be carried out based on extensive preliminary computations.[10] Except for research purposes, such calculations would never be justified, however. They are necessarily based on assumptions as to constancy of physical properties, such as the yield stress, the strain at which strain-hardening begins, etc., and as to conditions of end-fixing, rigidity of sup-

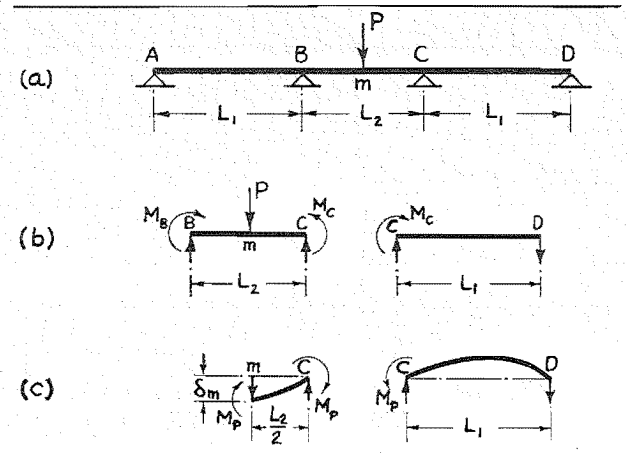

FIG. 1. Type of continuous beam tested by Stüssi and Kollbrunner[11] and Maier-Leibnitz.[12]

ports, absence of residual stresses, and the like. Many tests have shown that in actual structures these conditions may vary by large amounts quite unpredictably. Moreover, if elaborate calculations to determine deflections had to be made, the great advantages of the simplicity and directness of the plastic methods would be lost, and conventional elastic methods would be better employed.

In many cases, however, fairly rough estimates of deflections either at the critical collapse load or at the normal working loads may be desirable, or necessary, and it would be useful to have for these cases a method of estimating important deflections which would require only a small amount of work beyond that needed for the usual plastic analysis. The present paper shows how such deflection estimates can be easily obtained, with some indications as to their probable accuracy.

(2) Continuous Beams

As an example in which deflection estimates are essential in order to make the plastic analysis fully meaningful, consider the continuous beam and loading shown in Fig. 1a. Tests on this type of structure were reported by Stüssi and Kollbrunner,[11] whose main purpose was to investigate the effect of changing the ratio L_1/L_2 on the observed failure load. The concept of failure load used by Stüssi and Kollbrunner was not the plastic collapse load derived from the fully plastic moment values, which is the basis of present-day methods. They were concerned with loads at which complete collapse occurred rather than with the load at which a given load increment first begins to produce much larger plastic deformations than previously.

Let the fully plastic moment of the beam (assumed of uniform section and material) be M_p. Then the load P has reached the plastic collapse value P_c when the bending moments at the midpoint m and at supports B and C have reached the magnitude M_p. To calculate P_c, consider the moment equilibrium equation for the middle span under the given symmetrical loading,

$$(1/4)PL_2 = M_m - (1/2)M_B - (1/2)M_C = M_m - M_C \tag{1}$$

Now, since $M_m \leq M_p$, $M_c \geq -M_p$, it follows that

$$PL_2 \leq 4(M_p + M_p) = 8M_p \tag{2}$$

The critical value P_c is therefore given by

$$P_c = 8(M_p/L_2) \tag{3}$$

This is the highest load that can be applied without violating either the equilibrium conditions or the requirement that the bending moment shall not exceed the fully plastic moment in magnitude at any section.

If the outer spans were removed, leaving the central span simply supported, the collapse load P_c' would be

$$P_c' = 4M_p/L_2 \tag{4}$$

Apparently, therefore, the effect of attaching the outer spans is to double the load at which plastic collapse occurs according to the plastic theory, and this result is true independently of the length L_1. However, if L_1 is made extremely large compared to L_2, the middle span becomes effectively simply supported. There is apparently an inconsistency in the plastic theory, which in the one case predicts a failure load $4M_p/L_2$ and in the other case predicts twice this value for effectively the same simply supported beam. This was pointed out by Stüssi and Kollbrunner, who cited their test results to show that the failure load of the continuous beam with large ratios of L_1/L_2 was less than double the failure load of a beam without outer spans. They concluded, therefore, that the "moment equalization" method, as they called it, was not sound, since it led to an overestimate of the failure load in this case.

There is, in fact, no inconsistency in the plastic theory. According to this, if there are outer spans of any *finite* length, then the rate of increase of deflection with load is finite, since it is limited by the elastic constraint of the outer spans. This is true until the moments at the supports B and C reach the negative fully plastic moment, when theoretically the deflection begins to increase at an infinite rate.

The difficulty in the present example is that if the ratio L_1/L_2 is made extremely large, then a large deflection of the central span will occur before the moments M_B and M_C reach the fully plastic value. Normally, the plastic failure effect is observed as a transition from moderate to much higher rates of deflection with load. In the present case, if L_1/L_2 is made large, this would become increasingly difficult to observe. It is evident that the theoretical collapse load may not, in this case, give a reliable indication of the limiting useful load that the structure can carry; for, if L_1/L_2 is large enough, tolerable deflection values would probably be exceeded before the theoretical failure load is reached. The usual plastic analysis *must* therefore, in this case, be accompanied by an estimate of important deflections.

To estimate the central deflection δ_m in the present case at the instant when the critical load has just been reached, we note that continuity of slope still exists across any section until the full plastic moment is developed there. Therefore, at a load infinitesimally below the critical value there is continuity of slope across the section at C, since it is obvious in this case that the fully plastic moment develops first at the midpoint m and, finally, at C, leading to plastic collapse. Free-body diagrams of the lengths mC and CD are shown in Fig. 1c, with the moments and deflections as they would be just as the failure load is reached.

The following two assumptions will be made:

(1) Each span retains its original flexural rigidity EI except at the cross sections where fully plastic moments are reached.

(2) Rotations occur freely at constant moment values at the cross sections where the fully plastic moments are developed.

The first of these amounts to neglecting the additional flexibility caused by the spread of plastic zones along the length of the members. The second states that the strain-hardening at sections where plastic hinges are formed is to be ignored. The errors caused by these two assumptions tend to cancel each other, so that the calculation of deflections based on them may often be accurate. This calculation can be made directly from the collapse analysis without requiring successive elastic solutions for the beam as various plastic hinges have formed.

The last plastic hinge having formed at C, continuity of slope just as the collapse load is reached requires that

$$\theta_{Cm} = \theta_{CD} \tag{5}$$

these being the clockwise angles of rotation at the ends at C of the spans Cm and CD, respectively. The slope-deflection equations* for these spans are

$$\frac{2EI}{L_2}\theta_{Cm} = \frac{1}{3}M_p - \frac{1}{6}M_p - \frac{4EI\delta_m}{L_2^2} \tag{6}$$

$$(EI/L_1)\theta_{CD} = -(1/3)M_p \tag{7}$$

After equating the expressions for θ_{Cm} and θ_{CD} and solving for δ_m, we obtain

$$\delta_m = (M_p L_2^2/24EI)\,[1 + 4(L_1/L_2)] \tag{8}$$

This result shows at once that the plastic collapse load calculated for the extreme case in which $L_1/L_2 = \infty$ has no practical significance, since the deflection δ_m would also become infinite. This limiting case, however, is of interest mostly as a mathematical curiosity. For spans of reasonable length ratios the failure load and central deflection values of the simple plastic theory have their usual significance of marking the transition from moderate rates of deflection with load to much higher deflection rates, with useful accuracy.

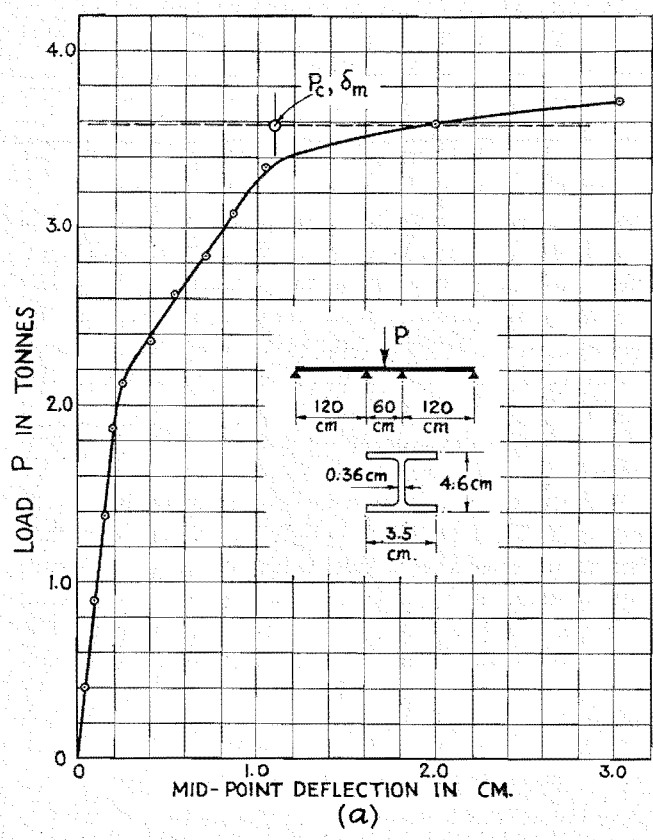

FIG. 2a. Curve shows deflections measured by Stüssi and Kollbrunner[11] on continuous beam of dimensions shown. P_c is collapse load and δ_m is approximate deflection at collapse, determined by simple plastic theory.

Stüssi and Kollbrunner[11] tested steel beams with span ratios L_1/L_2 equal to 3, 2, 1, and $^1/_2$, in addition to a simply supported beam. In all cases L_2 was 60 cm. However, the only curve for load plotted against central deflection reproduced in their paper is that for the case $L_1/L_2 = 2$. The measured points given for this case (beams 532/6 and 534/8) are shown in Fig. 2a, together with the point corresponding to the calculated collapse load and central deflection according to the simple plastic theory. No value of M_p is given in the paper; however, a sufficiently close estimate is obtained by multiplying the yield moment M_y by a shape factor 1.10 appropriate to the rather light I-section used. (The dimensions given are shown in Fig. 2a.)

$$M_p = 1.10M_y = 1.10\sigma_y Z \tag{9}$$

Fig. 2a shows how P_c and δ_m given by the simple theory appear in relation to the curve of load vs. midpoint deflection measured by Stüssi and Kollbrunner. The point with coordinates (P_c, δ_m) does not fall on the measured curve. However, the value P_c gives a fair

* The general form for a span PQ is as follows:

$$(EI/l)(\theta_{PQ} - \theta_{PQ}' - \delta/l) = (1/3)M_{PQ} - (1/6)M_{QP}$$

where EI = flexural rigidity (constant), l = length of span, θ_{PQ} = slope angle of P, θ_{PQ}' = slope angle at P which given span loads would produce if the span were simply supported at P and Q, δ = relative displacement of ends, and M_{PQ}, M_{QP} are end moments at P, Q, respectively. Signs of all slope angles, δ/l, and all end moments are defined by the positive-clockwise convention.

estimate of the plastic failure load, and δ_m indicates roughly the magnitude of the deflection at the load at which large plastic deformations begin to occur. Stüssi and Kollbrunner gave the total failure load for this beam as $P_w = 3.90$ tons, without stating precisely what happened at this load except that "deformation = ∞." Since the usual effect of strain-hardening is to cause the load-deflection curve to rise steadily until an additional effect, such as rupture or buckling, causes a drop in the load-carrying capacity, it is difficult to interpret the meaning of P_w without supposing that one of these effects occurred. The failure load P_c, with which the plastic theory is properly concerned, is conservative, since in almost all cases slightly higher loads can be supported.

Further tests on a beam loaded as shown in Fig. 1a and with $L_1/L_2 = 2$ were made by Maier-Leibnitz.[12] The beam tested was of steel, with area $A = 25.8$ cm.^{2}, section modulus $Z = 90$ cm.^{3}, $I = 453$ cm.^{4}, $L_2 = 60$ cm., $E = 2{,}035$ tons per cm.^{2}, $\sigma_y = 2.455$ tons per cm.^{2}. The latter is the lower yield stress obtained by averaging values from four specimens cut from flanges. The value of M_p calculated from the cross-section dimensions (see Fig. 2b), and the above value of σ_y is 248 ton-cm., corresponding to a "shape factor" of 1.12. With these values the Eqs. (3) and (8) yield the results

$$P_c = 16.5 \text{ tons}, \qquad \delta_m = 1.45 \text{ cm}. \tag{10}$$

This point is plotted in Fig. 2b for comparison with the measured deflection curve. The beam used in these tests was strengthened at the supports and load point, and Fig. 2b shows that this had considerable stiffening effect. If the value for M_p of 262.5 cm. is used, as suggested by Maier-Leibnitz on the basis of tests on a simply supported and centrally loaded beam, the calculated values are $P_c = 17.5$ tons, $\delta_m = 1.54$ cm. This point lies close to the experimental curve. However, it seems advisable to calculate M_p from the measured yield stress and section dimensions in assessing the simple plastic theory. Maier-Leibnitz did not carry the test to complete failure and therefore did not obtain a value of P_w corresponding to that of Stüssi and Kollbrunner.

As a second example of the estimation of deflections at the collapse load of the plastic theory, consider another continuous beam for which Maier-Leibnitz gave test results.[1] In this reference tests are described on the beam shown in Fig. 3a. The supports are at equal heights. For this steel I-section, the author gave the value of M_p as 660 tons per cm., and further data as $L = 80$ cm., $I = 1727$ cm.^{4}, $E = 2100$ tons per cm.^{4}. According to the plastic theory collapse occurs when the magnitudes of the moments at A and I reach the value M_p. The moment equilibrium equations are

$$M_1 = PL + (1/3)M_A \tag{11}$$
$$M_2 = PL + (2/3)M_A \tag{12}$$

From Eq. (11), we obtain

$$PL = M_1 - (1/3)M_A \leq (4/3)M_p \tag{13}$$

Corresponding to the upper limit

$$P_c = (4/3)(M_p/L) \tag{14}$$

the set of bending moments are

M_A	M_1	M_2	M_m
$-M_p$	M_p	$(2/3)M_p$	$(5/6)M_p$

(15)

The theoretical collapse load is, therefore, as given by Eq. (14).

To estimate the deflection at the collapse load under the same simplifying assumptions made previously, the free-body diagrams of Fig. 3b are used. It is assumed that the last plastic hinge to form is at section 1. Continuity of slope across the middle section requires that

$$\theta_{mB} = \theta_{mA} \tag{16}$$

These angles are given by the appropriate slope-deflection equations, in view of the assumed continuity of slope at section 1, as

$$\frac{2}{3}\frac{EI}{L}\theta_{mB} = -\frac{1}{3}\left(\frac{5}{6}M_p\right) - \frac{5}{54}P_cL + \frac{EI}{[(3/2)L]^2}\delta_m \tag{17}$$

$$\frac{2}{3}\frac{EI}{L}\theta_{mA} = \frac{1}{3}\left(\frac{5}{6}M_p\right) + \frac{5}{54}P_cL - \frac{EI}{[(3/2)L]^2}\delta_m \tag{18}$$

The value of δ_m at collapse is found to be

$$\delta_m = (103/144)(M_pL^2/EI) \tag{19}$$

Inserting numerical values, the results are

$$P_c = 11.0 \text{ tons}; \qquad \delta_m = 0.833 \text{ cm}. \tag{20}$$

The point with these coordinates is plotted in Fig. 4 for comparison with the measured load-deflection curve obtained by Maier-Leibnitz. It will be seen that in this case the calculated point locates accurately the load and deflection values when large plastic deflections are imminent.

(3) Rigid Frames

The method of estimating deflections used in the above examples may be applied to portal frames and other types of rigid frames such as that shown in Fig. 5a. It is especially advantageous in these cases because of the high degree of redundancy usually involved.

The method used depended on an assumption as to which plastic hinge of all the plastic hinges that occur in the collapse mode of the structure was the last to form. In the beam examples taken, the choice of the last plastic hinge to form was obvious. However, in more complicated frames, it is rarely obvious which hinge will form last, although usually it is easy to guess where the first few plastic hinges will occur. The procedure is to assume, in turn, that each of the hinges is the last to occur and, by applying the slope-continuity condition to this hinge, to calculate the corresponding value of some particular one of the deflections of the frame. The choice of hinge that yields the largest value of that deflection is the correct one. The reason for this is that imposing a false continuity condition amounts to removing a "kink"—i.e., a discontinuity in slope which was produced at that section in the course of bringing the loads up to the collapse value. However, the only way such a kink can be removed, while maintaining the values of the moments that actually occur at the collapse load, is by a motion of the frame as a mechanism in the *reverse* direction to that which would occur in the actual mode of collapse. Thus, when a condition of slope continuity is assumed across any hinge other than the one actually formed last, the resulting value of the deflection may be considered as the true value diminished by a certain amount due to a backward motion of the frame as a mechanism. No such backward mechanism motion is imposed when the correct choice of hinge is made, and this corresponds, therefore, to the largest value determined by the several choices.

To illustrate by a simple example, consider again the continuous beam of Fig. 1. If the last hinge to form is assumed (erroneously) to be the one at midpoint, then the condition $\theta_{mB} = \theta_{mC}$ is sufficient to determine a value δ_m'. The pertinent slope-deflection equations are

$$\frac{2EI\theta_{mB}}{L_2} = -\frac{1}{6}M_p + \left(\frac{4EI}{L_2^2}\right)\delta_m' \qquad (21)$$

$$\frac{2EI\theta_{mC}}{L_2} = \frac{1}{6}M_p - \left(\frac{4EI}{L_2^2}\right)\delta_m' \qquad (22)$$

Thus, the assumption of continuity of slope at m yields the result

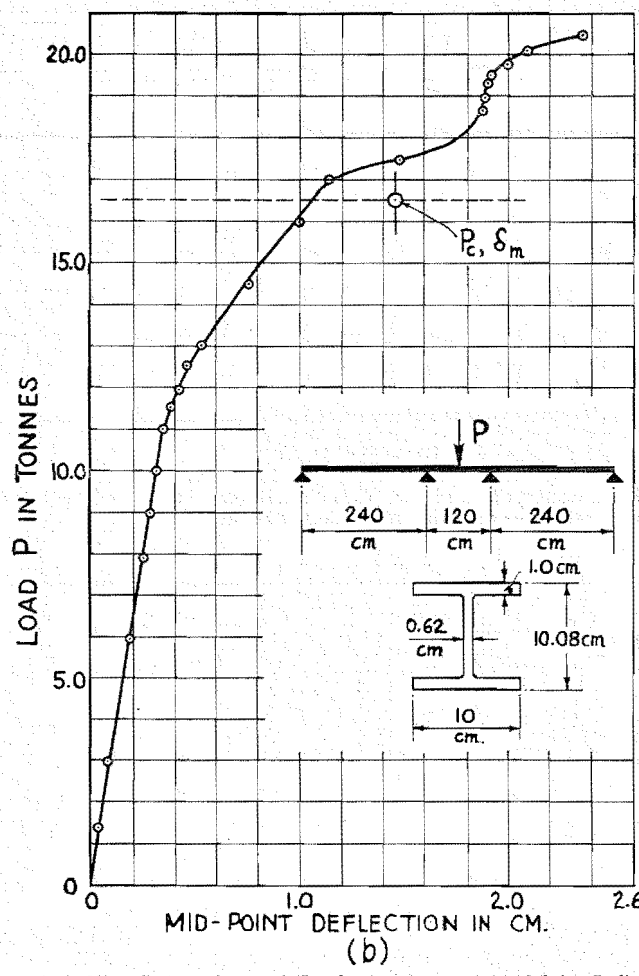

Fig. 2b. Curve shows deflections measured by Maier-Leibnitz on beam of dimensions shown. P_c is collapse load and δ_m is approximate deflection at collapse, from simple plastic theory (ignoring stiffeners actually present at load points).

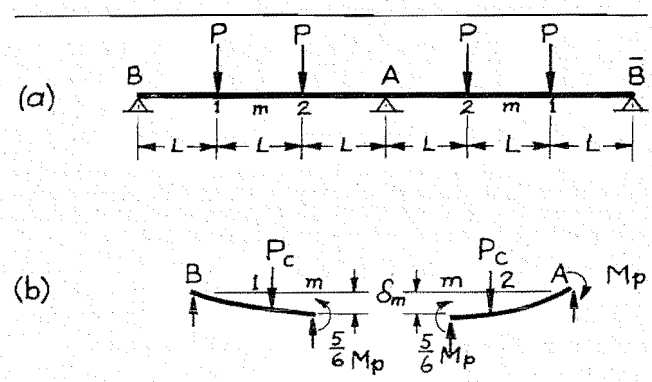

Fig. 3. Type of continuous beam tested by Maier-Leibnitz.[1]

$$\delta_m' = (1/24)(L_2^2 M_p/EI) \qquad (23)$$

Comparing this with the result for δ_m given by Eq. (8), the above value of δ_m' is seen to be smaller than δ_m for any value of L_1 greater than zero. The agreement between the two results for the case $L_1 = 0$ indicates that, when the beam is clamped at B and C, both plastic hinges form simultaneously.

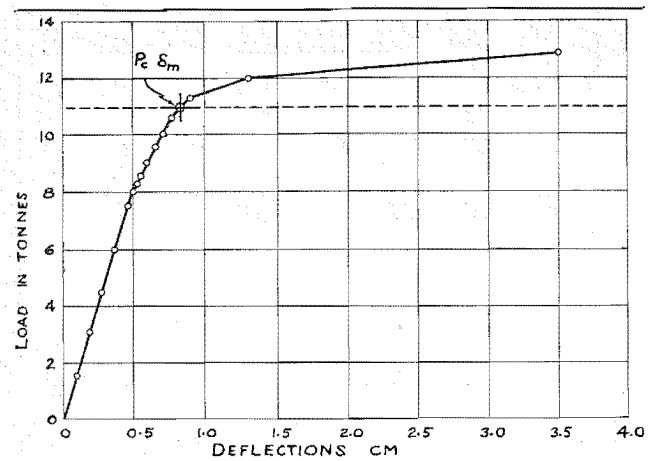

FIG. 4. Comparison of collapse load and deflection at collapse according to simple plastic theory with measured load-deflection curve obtained by Maier-Leibnitz.[1]

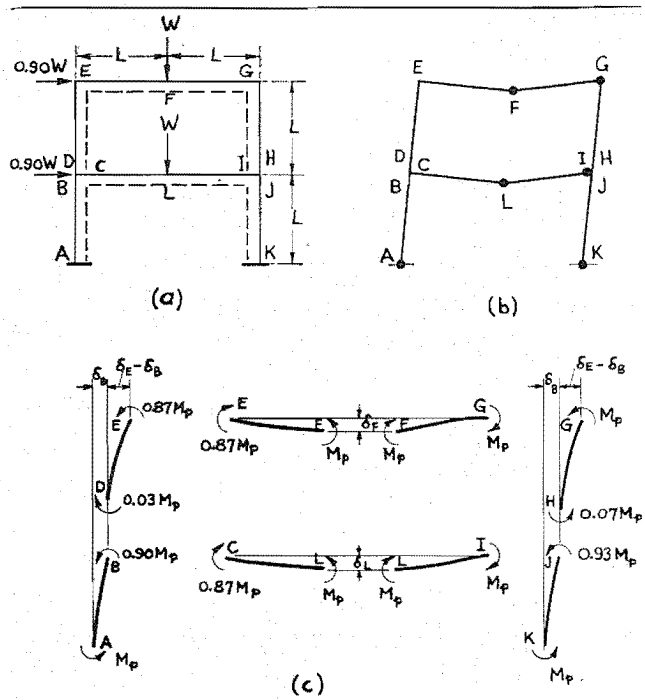

FIG. 5a. Rigid frame and loads used to illustrate deflection calculation. FIG. 5b Mode of collapse; black circles show plastic hinge locations. FIG. 5c Free-body diagrams used in calculation of deflection (shear reactions omitted for simplicity).

If the result Eq. (23) is used to compute the discontinuity in slope across the joint C (or B), we find

$$\theta_{CD} - \theta_{Cm} = -(1/3)/(L_1M_p/EI) \qquad (24)$$

The negative sign indicates slope angle values at section C corresponding to a concave upward shape of the beam. This absurd result is due to having made a false assumption as to continuity of slope at the midpoint. As pointed out above, this false assumption corresponds to removal of a "kink" that actually existed at m by means of a "backward" mechanism motion of the span BmC. This suggests that we can obtain the correct result from Eq. (24) by imposing a "forward" mechanism motion of magnitude just sufficient to cancel the discontinuity given by Eq. (24). In this motion the outer spans are held rigid, all motion occurring at the hinges at B, m, and C. The resulting angle change at C, $-\Delta\theta_{Cm}$, is set equal to $(1/3)(L_1M_p/EI)$. The corresponding increment of deflection $\Delta\delta_m$ is given by

$$\Delta\delta_m = \frac{L_2}{2}(-\Delta\theta_{Cm}) = \frac{1}{6}\frac{L_1L_2M_p}{EI} \qquad (25)$$

The result of adding this to the value of δ_m' given by Eq. (23) is

$$\delta_m' + \Delta\delta_m = \left(\frac{L_2^2}{24} + \frac{L_1L_2}{6}\right)\frac{M_p}{EI} \qquad (26)$$

This is identical with the correct result for δ_m given by Eq. (8). The above process provides a check on the value obtained for δ_m which is useful in more complicated problems.

As an example of deflection calculations for a more complicated frame, the two-story portal frame shown in Fig. 5a will be considered. The vertical loads are taken as W and the horizontal loads as $0.90W$ each. All members are taken to have the same fully plastic moment M_p. The mode of collapse under these circumstances is as indicated by Fig. 5b, the black circles representing plastic hinges. There are six redundant moments in this structure, and the mode of collapse indicated in Fig. 5b has only six plastic hinges. This is a case of incomplete or local collapse,[5, 6] [see Section (5) of this paper] in which the elastic moments are not completely determined by the values of the moments at plastic hinges and conditions of statical equilibrium. However, the elastic moments can readily be calculated, the method of least work being especially convenient for this purpose. It is found that there are four undetermined elastic moments that are related by three equations of equilibrium. The values of these moments can be obtained by minimizing the strain energy of the frame with respect to one of the four moments, taking proper account of the equilibrium equations but regarding the remaining eight moments as constant. The complete set of moments thus obtained is given in Table 1. The moment sign convention used in Table 1 is indicated by the dashed lines in Fig. 5a; positive moments are ones that cause tensile stress in the side of the beam adjacent to this line.

The collapse load W_c is found to be

$$W_c = 2.13(M_p/L) \qquad (27)$$

TABLE 1

Section	A	F	G	I	K	L
Bending Moment / M_p	−1	1	−1	−1	1	1
Section	B	C	D	E	H	J
Bending Moment / M_p	0.90	0.87	0.03	0.87	0.07	−0.93

The details of the analysis to determine the collapse load and the bending moments at collapse need not be given here; references 3–6 may be consulted if necessary.

The first step in the deflection analysis is to draw the free body diagrams of the members of the frame, as shown in Fig. 5c. Using these, one can then calculate any one of the deflections, such as the side-sway δ_B at joint B, from an assumption of slope continuity across any one of the plastic hinges in the collapse mode. Suppose, for example, that the hinge at L is assumed to be the last one to form—i.e., that $\theta_{LC} = \theta_{LI}$. Writing the slope-deflection relations for members CL and LI, we obtain at once

$$-\frac{1}{3}M_p - \frac{0.87}{6}M_p + \Delta_L = \frac{1}{3}M_p - \frac{1}{6}M_p - \Delta_L \tag{28}$$

whence

$$\Delta_L \equiv (EI/L^2)\,\delta_L = 0.323M_p \tag{29}$$

Now, since sections B and C are not plastic hinges, we know also that $\theta_{CL} = \theta_{BA}$ and can write, therefore,

$$\frac{0.87}{3}M_p + \frac{1}{6}M_p + \Delta_L = -\frac{0.90}{3}M_p + \frac{1}{6}M_p + \Delta_B \tag{30}$$

whence

$$\Delta_B \equiv (EI/L^2)\delta_B = 0.913M_p \tag{31}$$

An assumption of slope continuity at each of the other five hinge locations leads, after a similar calculation, to a value of Δ_B [defined as in Eq. (31)]. Some of the calculations are shorter than that just given; others are somewhat longer, but none takes more than a few minutes to work out. It is unnecessary to give the full details. The results are set out in Table 2. The choice of F as the last plastic hinge to form leads to the largest value of δ_B. It is therefore concluded that this is the correct choice and that the value of the side-sway at joint B when the collapse load is just reached is given by

$$\delta_B = 1.363(L^2M_p/EI) \tag{32}$$

As a check, the alternate procedure used in the previous beam example may be applied. The (incorrect) choice of L as the final plastic hinge allows the slope discontinuities to be calculated at all of the hinge locations. For example, the rotation angles at F are found to be given by

$$\theta_{FE} = -0.605(LM_p/EI) \tag{33}$$

$$\theta_{FG} = -0.294(LM_p/EI) \tag{34}$$

TABLE 2

Hinge where slope continuity assumed	F	L	G	I	A	K
Result for $\frac{EI}{L^2M_p}\delta_B$	1.363	0.913	0.908	0.450	0.183	0.178

From these, the slope discontinuity (in the sense indicated in Fig. 5b) is found to be

$$\theta_{FE} - \theta_{FG} = -0.899(LM_p/EI) \tag{35}$$

The negative value of this means, of course, that the choice of L as the location of the last hinge to form is wrong. However, we can now imagine a motion of the frame *as a mechanism* in the actual mode of collapse of just such an amount as to remove this slope discontinuity at F. Let the clockwise rotation of leg AE be ψ; then the relative rotation at F is 2ψ, and this is chosen so that

$$2\psi = 0.899(LM_p/EI) \tag{36}$$

Corresponding to this mechanism motion, there is a side-sway displacement at B equal to

$$\psi L = (0.899/2)(L^2M_p/EI) \tag{37}$$

Adding this to the result for δ_B given by Eq. (31), we obtain

$$\delta_B = \left(0.913 + \frac{0.899}{2}\right)\frac{L^2M_p}{EI} = 1.363\,\frac{L^2M_p}{EI} \tag{38}$$

which agrees with the result obtained previously by assuming the last plastic hinge to be that at F. It may be checked that all of the slope discontinuities are now positive—i.e., in the sense shown in Fig. 5b.

It may be noted that a consideration of deformations in the elastic structure will usually indicate which are the most severely stressed sections. In the present example the joints at A, K, I are obviously highly stressed initially. It would have been a safe guess to assume at the start that none of these is the last plastic hinge to form; this would have eliminated about half of the work involved in the calculation.

(4) Accuracy

As pointed out already the present method of estimating deflections depends on assumptions that amount to neglecting (1) additional flexibility due to spread of plastic zones along the lengths of members and (2) stiffening due to strain-hardening at joints where plastic hinges are assumed to occur.

The accuracy of the method depends on the extent to which these two effects cancel each other. In the cases of continuous beams used as examples in this paper, the bending moments changed in sign at successive joints. This meant that the plastic zones were rather localized, and the additional flexibility due to them was nearly canceled by the stiffening effect of strain-hardening. In other cases some members may be in pure bending, or nearly so, and, if plastic flow occurs in these, the actual deflections may be considerably larger than those predicted by the present method.

The comparisons shown in Figs. 2 and 4 give some indication of the accuracy of the method as applied to

continuous beams. Comparisons between deflections calculated by the simple theory and those observed in tests on small-scale portal frames have been given in another place.[13] The test results were obtained by Baker and Heyman[8] using portal frames of 4-in. span and 2-in. height and loaded by a horizontal load at the beam height and a vertical load at the midpoint of the span. Since the load ratios in these tests were chosen to cause collapse in all the possible modes, they indicate what may be expected for portal frames of rectangular cross section under a wide range of conditions. The comparison between observed deflection curves and calculated points at collapse shows that in many cases the agreement is extremely close. In other cases the calculated deflection is considerably too large and in others too small. However, the agreement in general is good enough so that, in view of its simplicity, the method may be considered a useful means of estimating deflections at the theoretical collapse load of a structure. Such tests as these on model frames must, however, eventually be supplemented by similar tests on full-scale frames made from standard commercial sections using normal fabrication procedures.

(5) Special Cases

Three types of collapse under proportional loading can occur, depending on the structure and the ratios of the loads. Let n be the number of redundant moments in a beam or frame. The type of collapse which most investigators have considered[1–4] is that in which $n + 1$ plastic hinges have formed just as the collapse load is reached; this may be called "complete" collapse. The beams used as examples in this paper failed with complete collapse; in both cases $n = 1$, and there were two hinges at collapse. However, collapse with fewer than $n + 1$ hinges will often occur in practical cases. This has been termed "local" collapse or preferably "incomplete" collapse. For example, the two-story frame of Fig. 5a fails, under the loading shown, with six plastic hinges as in Fig. 5b. In this structure $n = 6$, so this is a case of incomplete collapse (but the term "local" seems inappropriate). Finally, a third type of collapse is possible, although in ordinary structures under normal loadings it is less likely than the other types. This is the type of collapse in which several hinges form simultaneously (in theory) just as the critical failure load is reached, so that in the collapse mode there are more than $n + 1$ plastic hinges. As an example, consider the two-story frame of Fig. 5a, but let the two transverse loads each be W instead of $0.90W$. Then the mode of collapse is actually one with ten plastic hinges, only the moments M_D and M_H being elastic. This sort of failure might be termed "overcomplete" collapse. (Alternatively, the terms "indeterminate," "determinate," and "overdeterminate" might be used to specify the three types of plastic collapse.)

In the rather special cases of overcomplete collapse, the present method for estimating deflections may be difficult to apply, since in order to calculate one of the deflections it will often be necessary to assume slope continuity at a group of hinge locations rather than at merely one. Obviously, there may be many more possible groups than there are plastic hinges. In some cases, however, such as the portal frames whose test results and calculated failure points are discussed in reference 13, the occurrence of more than $n + 1$ hinges does not present any difficulties that cannot be easily resolved by the use of a little judgment concerning the probable behavior of the frame. However, in a more complicated case, such as the two-story frame cited, the situation may be awkward. Probably the simplest expedient is to alter slightly the ratios of the applied loads so that the mode of collapse will be different and of either the complete or incomplete type. In either of these cases there will be no difficulty in making the deflection analysis as described in this paper. The resulting deflection values may either be regarded as sufficiently accurate in themselves or may be taken as a guide in investigating deflections under the original loading.

References

[1] Maier-Leibnitz, H., *Die Bedeutung der Zähigkeit des Stahles für die Berechnung und Bemessung von Stahlhochbauwerken, insbesondere von statisch unbestimmten Konstruktionen: Versuche, Ausdeutung, und Anwendung der Ergebnisse*, Publication of Second Congress of the International Association for Bridge and Structural Engineering, Berlin, p. 103, 1936.

[2] Van den Broek, J. A., *Theory of Limit Design*, John Wiley & Sons, New York, 1948. Also, *Theory of Limit Design*, Trans. A.S.C.E., Vol. 105, p. 638, 1940.

[3] Baker, J. F., *A Review of Recent Investigations into the Behaviour of Steel Frames in the Plastic Range*, J. Instn. Civil Engrs. (London), Vol. 31, p. 188, 1949.

[4] Baker, J. F. *The Design of Steel Frames*, The Structural Engineer (London), Vol. 27, p. 397, 1949.

[5] Neal, B. G., and Symonds, P. S., *The Calculation of Collapse Loads for Frame Structures*, J. Instn. Civil Engrs. (London), Vol. 35, p. 21, 1950–1951.

[6] Symonds, P. S., and Neal, B. G., *Recent Progress in the Plastic Methods of Structural Analysis*, Journal of the Franklin Institute, Vol. 251, Nos. 11, 12, November, December, 1951.

[7] Neal, B. G., *Plastic Collapse and Shakedown Theorems for Structures of Strain-Hardening Material*, Journal of the Aeronautical Sciences, Vol. 17, No. 5, p. 297, May, 1950. See also Symonds, P. S., *The Basic Theorems in the Plastic Theory of Structures*, Readers' Forum, Journal of the Aeronautical Sciences, Vol. 17, No. 10, p. 669, October, 1950.

[8] Baker, J. F., and Heyman, J., *Tests on Miniature Portal Frames*, The Structural Engineer (London), Vol. 28, p. 139, 1950.

[9] Timoshenko, S., *Theory of Elastic Stability*, p. 45; McGraw-Hill Book Company, Inc., New York and London, 1936.

[10] Hrennikoff, A., *Theory of Inelastic Bending with Reference to Limit Design*, Trans. A.S.C.E., Vol. 113, p. 213, 1948.

[11] Stüssi, F., and Kollbrunner, C. F., *Beitrag zum Traglastverfahren*, Bautechnik, Vol. 13, p. 264, 1935.

[12] Maier-Leibnitz, H., *Versuche zur weiteren Klärung der Frage der tatsächlichen Tragfähigkeit durchlaufender Träger aus Baustahl*, der Stahlbau, Vol. 9, p. 153, 1936.

[13] Symonds, P. S., discussion to be published: Yang, C. H., Beedle, L. S., and Johnston, B. G., *Welded Continuous Frames: Plastic Design and the Deformation of Structures*, Welding Journal, Vol. 30, p. 348-s, July, 1951.

Simplified Treatment of the Turbulent Boundary Layer Along a Cylinder in Compressible Flow

HANS U. ECKERT*
Wright Air Development Center

(1) SUMMARY

An attempt is made to determine the effect of lateral surface curvature upon the turbulent boundary layer of a circular cylinder immersed in a compressible fluid with its axis parallel to the direction of flow. The calculation is carried out by means of the momentum theorem with the assumptions that the velocity profile (1/7-power law) and an empirical relation that puts the wall shear stress inversely proportional to the fourth root of the boundary-layer thickness (Blasius Law) are unaffected by the curvature. Further assumptions are constancy of static pressure and total energy. On this basis the following results are obtained: Full thickness and displacement thickness are less than on the flat plate, while momentum thickness and local and mean friction coefficients are higher. For the displacement thickness the deviation from the flat plate value may become appreciable already if the ratio of full boundary-layer thickness to cylinder radius is less than 0.1 and for the full thickness if this ratio is somewhat above 0.1. The friction coefficients on the other side are rather insensitive to curvature and deviate appreciably only if the ratio becomes as large as one. Compressibility in general somewhat increases the effect of curvature except for the displacement thickness where a slight decrease is found. The reliability of the basic assumptions and effects of their variation are discussed.

(2) INTRODUCTION

IN A PRECEDING PAPER,[1] an approximation method has been presented for treatment of the turbulent boundary layer on a flat plate in compressible flow based on von Kármán's momentum theorem and the assumptions of constant static pressure, constant total energy, and a velocity distribution according to the 1/7-power law. A shear stress relation involving the same assumptions has been derived from tests on compressible flow in pipes and applied to the case of the plate in a manner that is consistent with earlier successful procedures in the incompressible régime.

In the same way as it has been shown in that paper already on some parameters for flow in pipes, it can be proved generally for cases of rotational symmetry that, if the velocity profile follows a power law, boundary-layer parameters (as, for instance, mean values for velocity density and temperature or momentum and displacement thickness) can be expressed by corresponding parameters for two-dimensional flow. These consist of the ordinary flat plate term based on the same velocity profile as it occurs on the rotational body and a second term based on a profile with half the exponent of the common profile, which may be called second-order profile. The second term takes account of the lateral surface curvature. It is negative for axial flow inside cylindrical surfaces (concave curvature) and positive for flow outside such surfaces (convex curvature).†

In the present paper the influence of convex surface curvature will be investigated. This case has some practical significance for boundary-layer experiments in wind tunnels where, though ultimately data for two-dimensional flow are desired, cylindrical surfaces are often preferred to flat plates in order to avoid the margin effects. In reverse, the problem emerges if two-dimensional data are to be applied to missiles of large fineness ratio. In cases of model tests with large differences in Reynolds Number an additional scale effect produced by the lateral curvature may have to be taken into consideration. Finally, the problem is of some importance for determination of the base pressure on projectiles since a close relationship between this quantity and the boundary-layer flow has been discovered in recent years.[3, 4]

It can be anticipated that the behavior of the boundary layer along a cylinder will deviate appreciably from that on a flat plate if the boundary-layer thickness becomes comparable in size to the cylinder radius. The question is, however, in which way the boundary layer adapts itself to the changing condition.

Without a detailed knowledge of the mechanism of turbulence one can suppose merely that the following two cases form limits within which the actual behavior may occur. One of these probable limits is that the shear stress at the surface, and thus according to the momentum theorem also the momentum defect of the fluid, remains unaffected by the lateral curvature. For equal momentum thickness it follows, out of the cylinder geometry, that the full thickness of the boundary layer will be smaller on the cylinder than on the plate if the simplifying assumption is made that the velocity distributions within the boundary layer are the same for cylinder and plate. If this limiting

Received April 20, 1951. Revised and received July 30, 1951.
* Research Engineer, Flight Research Laboratory.

† The existence of this relation has been indicated in an earlier paper by Tetervin.[2]

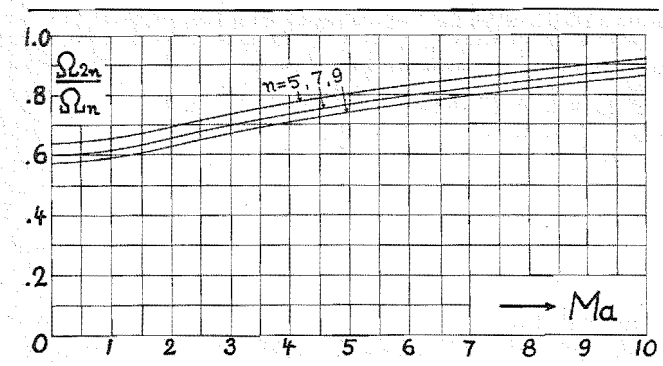

FIG. 1. Nondimensional momentum thickness of second-order velocity profile related to same value of first-order profile vs. free-stream Mach Number for various power law exponents of the first-order profile. Values refer to flat plate flow.

case would be true exact application of friction (and heat transfer) coefficients from flat plates to cylinders and vice versa would be possible.

The other limit may be that the full thickness of the boundary layer remains constant. For same velocity distributions this means higher momentum defect and thus higher shear stress on the cylinder. On this basis Jakob and Dow[5] made an estimation for incompressible laminar and turbulent boundary layers to find out how closely their measurements of heat transfer from cylinders may represent flat plate values. For turbulent boundary layers they assumed a velocity distribution according to the 1/7-power law and obtained for ratios of boundary-layer thickness to cylinder radius between 0.249 and 0.654 ratios of cylinder to plate coefficients between 1.075 and 1.196. The authors find no unequivocal support for the existence of increments of that order by comparing their test results with flat plate values from other experimentators and suggest that in the case of the cylinder the higher "wiping capacity" of the flow will produce a smaller boundary-layer thickness.

The method proposed in the present paper leads to results that are intermediate but closer to the first one of the extreme cases. Instead of keeping the friction coefficient or the boundary-layer thickness constant, it is assumed that the relation between friction coefficient and boundary-layer thickness applied to the flat plate in reference 1 remains applicable to the cylinder. The assumptions regarding velocity profile, static pressure, and total energy are also the same as made for the flat plate in that reference.

(3) THICKNESS OF THE BOUNDARY LAYER ON A CYLINDER

To simplify the calculations it is required that the direction of the free stream just ahead of the cylinder leading edge is parallel to the surface, that the boundary layer is turbulent from the beginning, and that it starts at the leading edge with zero thickness.

Under actual conditions these requirements might be best approximated by equipping the cylinder with a suitably shaped nosepiece and sucking off the boundary layer formed along the nose.

If no pressure gradient has to be taken into account, the momentum theorem reads, for this case,

$$\frac{d}{dx}\int_{y=0}^{y=\delta} \rho u(U-u)2\pi(r+y)\,dy = 2\pi r\tau \qquad (1)$$

where x is the distance from the leading edge along the surface in the flow direction, y is the normal distance from the surface, and δ is the boundary-layer thickness. ρ and u are density and velocity inside, and U is the velocity outside, the boundary layer. r is the cylinder radius, and τ is the shear stress at the surface. All flow characteristics are time-averaged.

The momentum thickness Θ is defined by

$$\Theta \equiv \frac{1}{\rho_U U^2}\int_{y=0}^{y=\delta} \rho u(U-u)\left(1+\frac{y}{r}\right)dy \qquad (2)$$

where ρ_U is the density outside the boundary layer.

Introducing the ratio $\Theta/\delta \equiv \Omega$ and splitting the integral, the following expression is obtained:

$$\Omega \equiv \int_0^1 \frac{\rho u}{\rho_U U}\left(1-\frac{u}{U}\right)d\left(\frac{y}{\delta}\right) + \frac{\delta}{r}\int_0^1 \frac{\rho u}{\rho_U U}\times \left(1-\frac{u}{U}\right)\frac{y}{\delta}\,d\left(\frac{y}{\delta}\right) \qquad (2a)$$

The first integral apparently represents the ratio of the momentum thickness to the full boundary-layer thickness for a flat plate. By applying the same procedure as described in Part (III) of reference 1, it can be shown that the second integral represents half the value of the same ratio for a plate with a velocity profile of half the exponent.

If the profile is denoted as

$$u/U = (y/\delta)^{1/n} \qquad (3)$$

this relation can be indicated by writing Eq. (2a)

$$\Omega_n = \overset{\text{plate}}{\Omega_n} + (\delta/2r)\,\overset{\text{plate}}{\Omega_{2n}} \qquad (4)$$

Numerical values of $\overset{\text{plate}}{\Omega_n}$ as a function of Mach Number up to $Ma = 10$ are given in Fig. 3 of reference 1 with the parameter n varying between 5 and 10. The corresponding values of $\overset{\text{plate}}{\Omega_{2n}}$ can also be determined from the data of Fig. 1 and Eq. (26) of that reference. (NOTE: the term Ω is designated by Θ in reference 1.)

To eliminate the wall shear stress τ from Eq. (1), use is made of Eq. (34) of reference 1, which is the above-mentioned relation derived from pipe-flow experiments. After replacement of the pipe radius $d/2$ by δ, this relation becomes

$$\frac{\tau}{\rho_U U^2} = 0.0233\left(\frac{\mu_U}{U\rho_U\delta}\right)^{1/4}\left(\frac{\bar{T}}{T_U}\right)^{[(\omega+1)/4]-1} \qquad (5)$$

where μ_U is the free stream viscosity, $\bar{T}/T_U$ is the temperature of the mean state across a pipe section related

to temperature at the axis of that section evaluated for 1/7-power law velocity distribution, and ω is the exponent of the viscosity variation power law, in reference 1 taken as 0.8.

Using the identity $\Theta \equiv \Omega\delta$ and Eqs. (2), (4), and (5), we obtain, from Eq. (1),

$$\frac{d}{dx}\left(\delta\Omega_n + \frac{\delta^2}{2r}\Omega_{2n}\right) = 0.0233\left(\frac{\mu_U}{U\rho_U}\right)^{1/4} \times \left(\frac{\bar{T}}{T_U}\right)^{-(3-\omega)/4} \delta^{1/4} \quad (6)$$

The superscript "plate" on Ω has been omitted for simplicity, since only flat plate values of this term appear in the following. Eq. (6) can be readily integrated to give

$$\frac{4}{5}\Omega_n\delta^{5/4} + \frac{4}{9}\Omega_{2n}\frac{\delta^{9/4}}{r} = 0.0233\left(\frac{\mu_U}{U\rho_U}\right)^{1/4}\left(\frac{\bar{T}}{T_U}\right)^{-(3-\omega)/4} x \quad (7)$$

or, if solved for δ/x and with $U\rho_U x/\mu_U \equiv Re$,

$$\frac{\delta}{x} = \frac{0.059\,\Omega_n^{-4/5}\left(\frac{\bar{T}}{T_U}\right)^{-(3-\omega)/5} Re^{-1/5}}{\left(1 + \frac{5}{9}\frac{\Omega_{2n}}{\Omega_n}\frac{\delta}{r}\right)^{4/5}} \quad (7a)$$

For $\delta/r = 0$, Eq. (7a) becomes identical with Eq. (37) of reference 1 for the plate. Dividing Eq. (7a) by the plate equation, the effect of convex lateral wall curvature upon the boundary-layer thickness is obtained.

$$\boxed{\frac{\delta}{\delta_{pl}} = \frac{1}{\left(1 + \frac{5}{9}\frac{\Omega_{2n}}{\Omega_n}\frac{\delta}{r}\right)^{4/5}}} \quad (8)$$

Ω_{2n}/Ω_n has been plotted versus Mach Number in Fig. 1 for $n = 5$, 7, and 9. This ratio increases with Mach Number and decreases with n. Both effects are moderate. For $Ma = 0$, $\Omega_{2n}/\Omega_n = (n+2)/(2n+1)$, which for $n = 7$ yields 0.6. Eq. (8) thus reduces for the incompressible case to

$$\left(\frac{\delta}{\delta_{pl}}\right)_{\text{inc.}} = \frac{1}{[1 + (\delta/3r)]^{4/5}} \quad (8a)$$

The ratio δ/δ_{pl} is plotted vs. δ/r in Fig. 2a with Mach Number as parameter using $n = 7$ which is consistent with the applied shear stress relation. For $Ma = 0$ and $\delta/r = 0.1$ the boundary-layer thickness is about 3 per cent less than on a flat plate under same conditions; for $\delta/r = 1$ the decrement is about 20 per cent. Compressibility slightly increases the effect of curvature.

The fact that Eqs. (8) and (8a) and their graphical representation in Fig. 2a are implicit with respect to δ involves no serious complication for practical purposes. First determine δ_{pl} and use δ_{pl}/r as independent variable to obtain a preliminary value for δ/δ_{pl} from Eq. (8) or Fig. 2a. With this preliminary value, correct that initially used δ_{pl}/r to obtain an improved value for δ/δ_{pl}. If $\delta/r > 0.1$ it may be necessary to repeat the operation.

(4) Friction Coefficients

With δ/r known, the coefficients of local and mean friction can be found in the following way:

The *local* friction coefficient is defined as

$$c_f \equiv 2\tau/\rho_U U^2 \quad (9)$$

With the aid of Eq. (5) and by relating the skin friction value for the cylinder to that for the plate,

$$\frac{c_f}{c_{fpl}} = (\delta_{pl}/\delta)^{1/4} \quad (10)$$

is obtained. Combining Eq. (10) with Eq. (8) yields

$$\boxed{\frac{c_f}{c_{fpl}} = \left(1 + \frac{5}{9}\frac{\Omega_{2n}}{\Omega_n}\frac{\delta}{r}\right)^{1/5}} \quad (11)$$

Numerical values for Eq. (11) are plotted versus δ/r in Fig. 2b for Mach Numbers 0 and 10.

The effect of curvature on c_f is small and becomes appreciable only if δ/r approaches unity.

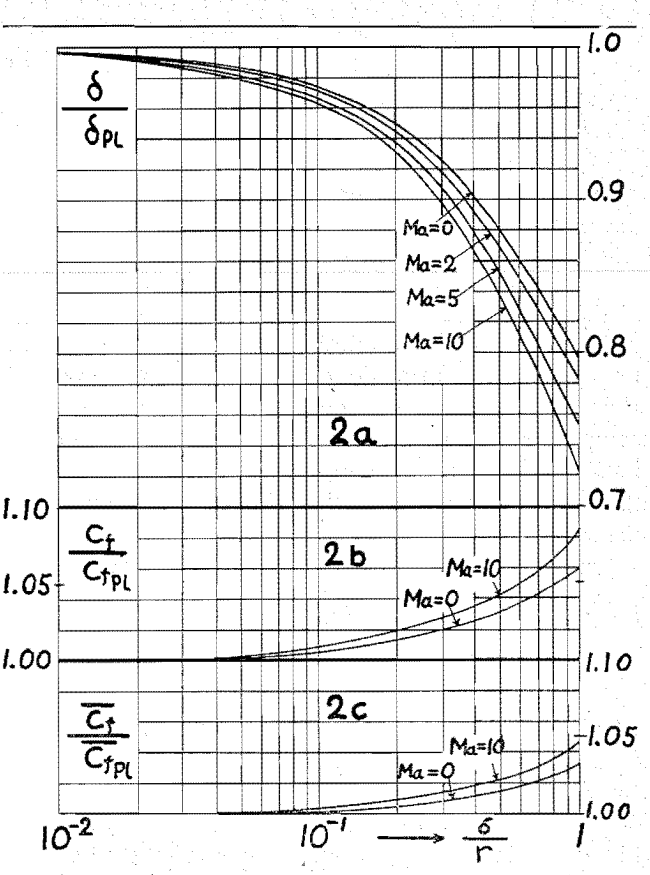

Fig. 2. Characteristics of the turbulent boundary layer along a cylinder in compressible flow related to flat plate values vs. the ratio boundary-layer thickness to radius of the cylinder. 1/7-power law velocity distribution. Parameter: Mach Number. (2a) Full thickness of the boundary layer; (2b) local friction coefficient; (2c) mean friction coefficient.

The *mean* value of the friction coefficient over the distance x is

$$\bar{c}_f \equiv (1/x) \int_0^x c_f \, dx \tag{12}$$

From the integrated momentum Eq. (1) and with the aid of Eqs. (2), (2a), and (4), the ratio of cylinder friction to plate friction is

$$\frac{\bar{c}_f}{\bar{c}_{fpl}} = \frac{\frac{2\delta}{x}\left(\Omega_n + \frac{\delta}{2r}\Omega_{2n}\right)}{(2\delta_{pl}/x)\Omega_n} \tag{13}$$

Using Eq. (8) to eliminate δ/δ_{pl} from Eq. (12) yields

$$\boxed{\frac{\bar{c}_f}{\bar{c}_{fpl}} = \frac{1 + \frac{\delta}{2r}\frac{\Omega_{2n}}{\Omega_n}}{\left(1 + \frac{5}{9}\frac{\delta}{r}\frac{\Omega_{2n}}{\Omega_n}\right)^{4/5}}} \tag{14}$$

The ratio $\bar{c}_f/\bar{c}_{fpl}$ is plotted versus δ/r in Fig. 2c for Mach Numbers 0 and 10. The deviation from the plate value is still smaller than for the local friction coefficient, which is obvious from the fact that the mean friction coefficient includes all values from the leading edge where δ/r, and thus the curvature effect, is smaller than at the downstream end position. Eq. (14) and Fig. 2c also represent the ratio of momentum thickness on the cylinder to that on the flat plate, as is evident from Eqs. (4) and (13).

If in Eq. (13) is set $\delta = \delta_{pl}$ and $\Omega_{14}/\Omega_7 = 0.6$, then

$$\bar{c}_f/\bar{c}_{fpl} = 1 + (3/10)\ (\delta/r) \tag{15}$$

which is the result obtained by Jakob and Dow.[5]

(5) Displacement Thickness

In determining the influence of the cylinder radius upon the displacement thickness it must be remembered that this quantity for higher Mach Numbers becomes comparable to the full thickness of the boundary layer itself, and it is therefore not permissible to disregard the quadratic term as in the case of the momentum thickness.

From the continuity of mass flow, it follows that

$$\rho_U U\pi[(r + \delta - \delta^*)^2 - r^2] = \int_{y=0}^{y=\delta} \rho u 2\pi(r + y)\, dy \tag{16}$$

where δ^* denotes the amount of radial displacement a free-stream line experiences up to its intersection with the "edge" of the boundary layer. This definition differs from that used conventionally for cylindrical surfaces. It is felt, however, to be preferable because it represents the correct influence upon the potential flow.

After rearrangement and division by $2\pi r\delta\rho_U U$, Eq. (16) can be written in nondimensional form

$$\frac{\delta}{2r} + \frac{\delta^{*2}}{2\delta r} - \frac{\delta^*}{\delta} - \frac{\delta^*}{r} + 1 = \int_0^1 \frac{\rho u}{\rho_U U} d\left(\frac{y}{\delta}\right) + \frac{\delta}{r}\int_0^1 \frac{\rho u}{\rho_U U}\frac{y}{\delta} d\left(\frac{y}{\delta}\right) \tag{17}$$

In the same way as for the momentum thickness, it can be shown for the displacement thickness by the procedure in Part (III) of reference 1 that as

$$\int_0^1 \frac{\rho u}{\rho_U U} d\left(\frac{y}{\delta}\right) \equiv 1 - \left(\frac{\delta^*}{\delta}\right)_n^{\text{plate}} \tag{18}$$

there is also

$$\int_0^1 \frac{\rho u}{\rho_U U}\left(\frac{y}{\delta}\right) d\left(\frac{y}{\delta}\right) = \frac{1}{2}\left[1 - \left(\frac{\delta^*}{\delta}\right)_{2n}^{\text{plate}}\right] \tag{19}$$

where again the superscript denotes plate values and the subscript velocity profile parameters as defined by Eq. (3). With Eqs. (18) and (19) and $\Delta \equiv \delta^*/\delta$, Eq. (17) becomes, after rearrangement and canceling out equal terms on both sides,

$$\Delta_n\left(1 + \frac{\delta}{r}\right) - \Delta_n{}^2\frac{\delta}{2r} = \overset{\text{plate}}{\Delta_n} + \frac{\delta}{2r}\overset{\text{plate}}{\Delta_{2n}} \tag{20}$$

or

$$\frac{\Delta_n}{\overset{\text{plate}}{\Delta_n}} = \frac{1 + \frac{\delta}{2r}\left(\frac{\overset{\text{plate}}{\Delta_{2n}}}{\Delta_n}\right)}{1 + \frac{\delta}{r}\left(1 - \frac{\Delta_n}{2}\frac{\Delta_n}{\overset{\text{plate}}{\Delta_n}}\right)} \tag{21}$$

The ratio $(\overset{\text{plate}}{\Delta_{2n}}/\Delta_n)$ which is required for evaluation of Eq. (21) is plotted in Fig. 3 versus Mach Number for $n = 5$, 7, and 9. $\overset{\text{plate}}{\Delta_{2n}}$ has been determined with the aid of Eq. (24) and Fig. 1 of reference 1. The behavior of $(\overset{\text{plate}}{\Delta_{2n}}/\overset{\text{plate}}{\Delta_n})$ is similar to that of $(\overset{\text{plate}}{\Omega_{2n}}/\overset{\text{plate}}{\Omega_n})$. For $Ma = 0$,

$$(\overset{\text{plate}}{\Delta_{2n}}/\overset{\text{plate}}{\Delta_n}) = (n + 1)/(2n + 1)$$

For values of δ/r up to 0.1, the ratio $\overset{\text{plate}}{\Delta_n}/\Delta_n$ can be calculated conveniently and with an error of less than 0.5 per cent in one step from Eq. (21) by setting on the right side $\overset{\text{plate}}{\Delta_n}/\Delta_n = 1$. For larger values of δ/r, one has to use either successive approximation or the solution of the quadratic Eq. (20), which is

$$\Delta_n = \frac{r}{\delta}\left[1 + \frac{\delta}{r} \overset{(+)}{-} \sqrt{1 + \frac{2\delta}{r}(1 - \overset{\text{plate}}{\Delta_n}) + \frac{\delta^2}{r^2}(1 - \overset{\text{plate}}{\Delta_{2n}})}\right] \tag{22}$$

The ratio displacement thickness on the cylinder to displacement thickness on the plate is

$$\delta^*/\delta_{pl}{}^* = (\Delta_n/\overset{\text{plate}}{\Delta_n})\,(\delta/\delta_{pl}) \tag{23}$$

or with Eqs. (8) and (22)

$$\frac{\delta^*}{\delta_{pl}{}^*} = \frac{1 + \frac{\delta}{r} - \sqrt{1 + \frac{2\delta}{r}(1 - \overset{\text{plate}}{\Delta_n}) + \frac{\delta^2}{r^2}(1 - \overset{\text{plate}}{\Delta_{2n}})}}{\frac{\delta}{r}\overset{\text{plate}}{\Delta_n}\left[1 + \frac{5}{9}\frac{\delta}{r}\left(\frac{\Omega_{2n}}{\Omega_n}\right)\right]^{4/5}} \tag{24}$$

$\delta^*/\delta_{pl}{}^*$ is plotted versus δ/r for $n = 7$ and Mach Numbers 0, 2, 5, and 10 in Fig. 4. As can be seen, the influence of lateral curvature on the displacement thickness is larger than on any of the other quantities considered. For incompressible flow, about 90 per cent of the flat plate value are obtained at $\delta/r = 0.1$ and only about 50 per cent at $\delta/r = 1$. It is noteworthy that in this case Mach Number somewhat decreases the effect of curvature.

(6) Supplement

In the absence of experimental data for comparison with the results above, some considerations are required as to the reliability of the basic assumptions and the effects of modifications to which they may be subjected.

Measurements of turbulent boundary layers in compressible flow are at the present time available only for two-dimensional cases. For flat plates the velocity profiles obtained from Pitot tube readings by Wilson, Young, and Thompson[6] at Mach Numbers from 1.6 to 2.2 and Reynolds Numbers from 4×10^6 to 20×10^6 are in good agreement with the 1/7-power law. Except for a region in proximity of the wall, the same can be said about similar tests by Rubesin, Maydew, and Varga[7] at Mach Number 2.5 and Reynolds Numbers varying from 2.7×10^6 to 6.2×10^6. Comparison of the values for δ^*/x and $\overline{c_f}$ derived from these experimental data with the theory of reference 1 indicates their variation with $Re^{-1/5}$, while the Mach Number effect appears to be underestimated by that theory. This does not, however, influence to a great extent the results of the present paper, since its purpose is mainly to show *differences* in the behavior between flow along cylinders and flat plates where only a second-order effect of Mach Number comes into play.

At higher Reynolds Numbers it must be expected that, similarly as for incompressible flow, the 1/7-power law for the velocity profile and the $Re^{-1/5}$ law for the friction coefficient will no longer hold. The velocity profile will probably change to a fuller shape, and the effect of Reynolds Number on skin friction will become weaker. Both effects are interrelated. If $-1/m$ denotes the Reynolds Number exponent, the relation between m and n can be obtained approximately from a dimensional analysis by von Kármán.[12] It reads $m = (n + 3)/2$, which for $n = 9$,† for instance, predicts an effect of Reynolds Number according to $Re^{-1/5}$. Eq. (8), which in the general form reads

$$\frac{\delta}{\delta_{pl}} = \left(1 + \frac{m}{2m - 1}\frac{\Omega_{2n}}{\Omega_n}\frac{\delta}{r}\right)^{-(m-1)/m} \tag{8b}$$

† Wilson[8] obtained from measurements at the wind-tunnel wall for Mach Number 2 a velocity profile close to a power law with $n = 9$. The equivalent flat plate Reynolds Number was determined to 50×10^6.

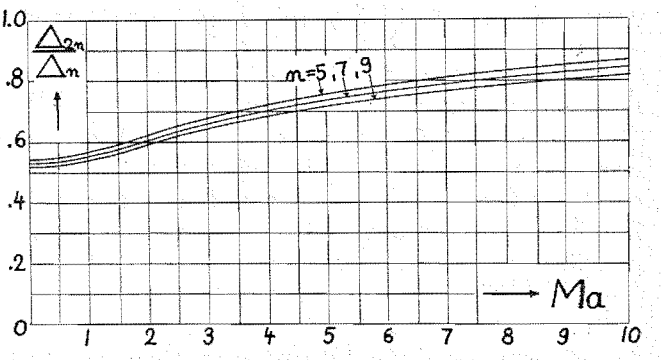

Fig. 3. Nondimensional displacement thickness of second-order velocity profile related to same value of first-order profile vs. free-stream Mach Number for various power law exponents of the first-order profile. Values refer to flat plate flow.

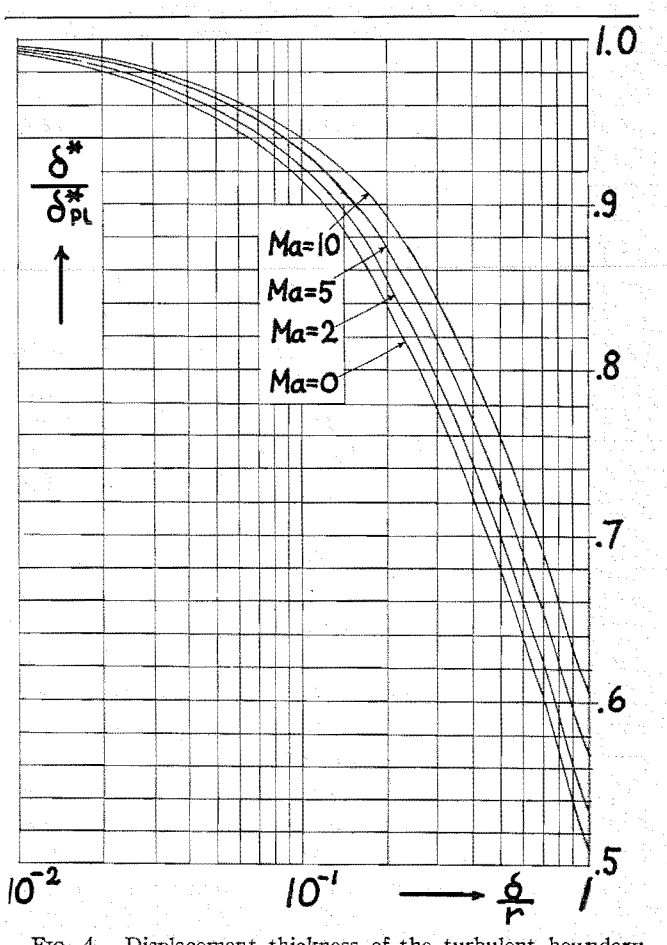

Fig. 4. Displacement thickness of the turbulent boundary layer along a cylinder in compressible flow related to flat plate value vs. the ratio boundary-layer thickness to radius of the cylinder. 1/7-power law velocity distribution. Parameter: Mach Number.

can be written with the relation above

$$\frac{\delta}{\delta_{pl}} = \left(1 + \frac{n+3}{2n+4}\frac{\Omega_{2n}}{\Omega_n}\frac{\delta}{r}\right)^{-(n+1)/(n+3)} \quad (8c)$$

For large values of n, Eq. (8c) converges toward

$$\frac{\delta}{\delta_{pl}} \cong \left(1 + \frac{1}{2}\frac{\Omega_{2n}}{\Omega_n}\frac{\delta}{r}\right)^{-1} \qquad (n \to \infty) \quad (8d)$$

which for the incompressible case reduces to

$$\left(\frac{\delta}{\delta_{pl}}\right)_{\text{inc.}} \cong \left(1 + \frac{\delta}{4r}\right)^{-1} \qquad (n \to \infty) \quad (8e)$$

For $\delta/r = 1$, the value obtained with Eq. (8e) differs by less than 1 per cent from the one obtained with Eq. (8a) where $n = 7$. With respect to the small dependence of the ratio Ω_{2n}/Ω_n upon Mach Number, it can be concluded that Eq. (8d) will give results that are similarly close to the values obtained with Eq. (8) for compressible flow. This means that for $n > 7$ and $\delta/r \leq 1$ the ratio δ/δ_{pl} is practically independent of n.

The ratios of the local and mean friction coefficients decrease in steps of about 0.5 per cent if n is increased in steps of unity between 5 and 9. For $n \to \infty$,

$$c_f/c_{f_{pl}} \to \bar{c}/c_{f_{pl}} \to 1$$

These results are valid for the assumption that the velocity distribution is not influenced by lateral wall curvature. There is reason to expect, however, that the profile will be altered by convex curvature toward larger n—that is, to a fuller shape compared to the flat plate—because the flux of momentum from the free stream toward the wall is concentric. This will lead to higher velocities within the boundary layer and a stronger velocity gradient near the wall.

An effect in this direction has been noticed for incompressible flow by Schultz-Grunow,[9] who found that velocity profiles are fuller on flat plates than in pipes.†

In order to allow an estimation of the effect of different velocity profiles, some calculations have been carried out assuming $n = 9$ and an accordingly altered shear stress relation for the cylinder while retaining $n = 7$ for the plate. For this condition the ratios of cylinder to plate values depend, besides on δ/r, directly on the Reynolds Number, and it is found that for $Re > 10^7$ the friction coefficients may well exceed those on flat plates by 20 per cent. It can be supposed that the effect of curvature on the velocity profile will become significant only if $\delta > r$, but the indication is given that the results of this paper might be low.

The assumptions of constant total energy and constant static pressure have been checked experimentally for two-dimensional flow at Mach Number 2.8 by Spivack.[10] Variations of these quantities with wall distance by about 5 per cent have been noticed. The influence upon integral parameters that enter the present analysis is irrelevant.

It may be added that for a laminar boundary layer and incompressible flow the problem has been treated more fundamentally by starting with the differential form of the boundary-layer equation in a paper by Seban and Bond.[11] Results given for the local friction coefficient are similar to those of the present paper but indicate a stronger effect of lateral curvature. For the behavior of the displacement thickness, no clear result has been obtained because of the limited number of terms retained in the series expansion.

(7) Concluding Remarks

The results obtained by the approximation method above indicate that the growth of the turbulent boundary layer along a cylinder becomes considerably slower compared to the flat plate if the boundary-layer thickness approaches the dimension of the cylinder radius. The effect is still more pronounced on the displacement thickness.

More important for engineering purposes, however, might be that the influence upon the mean friction coefficient comes out to be extremely small and hardly exceeds the uncertainty of present-time experimental determinations even if the boundary-layer thickness equals the cylinder radius. This would substantiate the use of flat plate values for cylinders and vice versa. The reliability of this conclusion depends, of course, upon that of the assumptions involved, mainly the invariance of velocity distribution and shear stress law with curvature radius. It can be expected, however, that the results will, by their presentation as fractions of corresponding plate values, not be sensitive to variation of parameters that simultaneously affect conditions at both cylinder and plate. This is evident from the small influence of Mach Number.

If at higher Mach Numbers or higher Reynolds Numbers the actual behavior of the turbulent boundary layer on the plate does not follow the relations of reference 1, then a similar deviation differing only by higher order effects will also exist for the cylinder and qualitatively useful results can be expected by basing the results of this paper on improved plate values as they may be given, for instance, by the theories developed in references 7 or 8.

Once dependable relations for the case of the flat plate are established, it will be desirable to check also in particular the effect of lateral curvature upon the boundary layer by appropriate experiments.

(8) References

[1] Eckert, H. U., *Characteristics of the Turbulent Boundary Layer on a Flat Plate in Compressible Flow from Measurements of Friction in Pipes*, Journal of the Aeronautical Sciences, Vol. 17, No. 9, pp. 573–584, September, 1950.

(*Continued on page 38*)

† The fact that this difference is rather small in view of the differences in the flow geometry may be due to the pressure drop inherent to subsonic pipe flow which tends to compensate the effect of the concave wall curvature.

On the Flight Dynamics of Slender Special-Purpose Aircraft

R. M. ROSENBERG* AND GEORGE STONER†

Boeing Airplane Company

SUMMARY

In this paper, general equations of motion are derived for slender special-purpose aircraft of nearly circular cross section. It is shown that considerations of steady roll and lack of circular symmetry of cross section lead to Mathieu equations. Aerodynamic force derivatives for flight not near the flutter speed are given which appear to be useful in that their application has resulted in theoretical predictions that agree satisfactorily with flight experience. Finally, some possible instabilities are discussed. The method is illustrated by an example.

INTRODUCTION

FROM THE STANDPOINT of the flight dynamics of modern special-purpose aircraft such as missiles, it is of interest to develop fairly general equations governing the flight of a slender, essentially cylindrical body that is elastic in a sense to be defined later. The solution of these equations leads to the analysis of oscillations that may occur in flight and which may become unstable under certain unfavorable circumstances. The results of the theory presented here have been compared with flight experience, and astonishingly good agreement was achieved.

THE DEGREES OF FREEDOM

The aircraft under consideration is assumed to be slender and to possess geometric, elastic, and inertial characteristics having nearly circular symmetry with respect to all points on a longitudinal axis through the body of the aircraft.

The right-handed orthogonal xyz-system of coordinates is fixed in the craft; it coincides with the principal axes, and the x-axis is positive in a forward direction. Inasmuch as the coordinate system is right-handed, the positive direction of all other quantities relating to the coordinate system are now defined.

The nomenclature and sign convention of the rigid-body degrees of freedom and of certain kinematical and dynamic quantities relating to them are defined in Table 1. All velocities, forces, and moments are positive in the direction of positive displacements.

In addition to the degrees of freedom defined in Table 1, the aircraft is considered to be elastic in the sense that it can execute beam bending vibrations. A vibration in the xy-plane leads to a displacement $\sigma(x, t)$; that in the xz-plane leads to a displacement $\tau(x, t)$. Both vibrations are restricted to occur in the fundamental modes only, and no elastic deformations, except for the two listed, are considered. The nomenclature regarding the kinematical and dynamic quantities referring to the elastic degrees of freedom are listed in Table 2 where $d/dt = D$.

σ is positive in the direction of positive y. τ is positive in the direction of positive z. All other directional quantities in Table 2 are positive when they act in the direction of positive displacements σ and τ.

The aircraft under consideration is assumed to have certain controls having principal actions as listed in Table 3. These are described with reference to an axis system fixed in the aircraft—i.e., they are those seen by an observer on the aircraft. Thus, a side force, for instance, may give rise to a displacement that would appear vertical to an observer on the ground if the application of that force had been precededby a roll displacement of 90°. The symbols in the right-hand column are regarded as indicating the degree of application of the controls leading to the responses indicated in the left-hand column of Table 3. All control actions are positive in that direction in which they give rise to responses in a positive direction.

THE BENDING VIBRATIONS

In an aircraft capable of roll, the inclusion of the vibrational degrees of freedom presents considerable difficulties.

Consider that the aircraft is not rolling and that bending vibrations are set up in the xz-plane, say. If the aircraft is now given a displacement in roll, the plane of the bending vibration does not rotate with the aircraft; it tends to remain fixed in space.[1] Let the plane of bending vibrations be the sx-plane, and, before rolling, the s-axis coincides with the z-axis. When a rolling displacement $\varphi(t)$ takes place, the s-axis remains fixed in space, the z-axis remains fixed in the aircraft, and the angle between the two is $\varphi(t)$. The vibrational displacement τ now has a y-component equal to $\tau(x, t)$ sin $\varphi(t)$ and a z-component equal to $\tau(x, t)$ cos $\varphi(t)$. Obviously, these displacements introduce nonlinearities into the equations of motion which render analytical treatment extremely difficult. If the roll is steady at the angular velocity p_0, the components become $\tau(x, t)$ sin p_0t and $\tau(x, t)$ cos p_0t. In this simpli-

Received March 1, 1951.

* This work was done while Associate Professor of Aeronautical Engineering, University of Washington.

† Assistant Project Engineer.

TABLE 1

Coordinate Axes	Parallel to Coordinate Axes: Velocity	Acceleration	Forces	About Coordinate Axes: Displacement	Velocity	Acceleration	Moment	Inertias
x	u	a_x	X	φ	p	a_φ	L	A
y	v	a_y	Y	θ	q	a_θ	M	B
z	w	a_z	Z	ψ	r	a_ψ	N	C

fied case, the vibrational displacements introduce periodic coefficients into the equations of motion which also make the analysis difficult. Finally, if the aircraft has unequal stiffness in mutually perpendicular directions of beam bending, then the spring restraint becomes, even in steady roll, a periodic function of time. Again, the system of equations will have periodic coefficients leading to Mathieu equations. Because of the difficulties resulting from a consideration of roll, the analysis will be carried out for a nonrolling aircraft, or $\varphi(t) = p(t) \equiv 0$.

When no roll is permitted, the vibrational displacements are

$$\left.\begin{aligned} \sigma(x, t) &= \sigma_0(t)\, f_1(x) \\ \tau(c, t) &= \tau_0(t)\, f_2(x) \end{aligned}\right\} \tag{1}$$

where $f_{1,2}(x)$ are the mode shapes satisfying

$$\int_l f_{1,2}(x)\, dm = 0 \tag{2}$$

where dm is an elemental mass located at x and the symbol $\int_l$ indicates integration along the entire length of the aircraft.

PROCEDURE OF ANALYSIS

The general procedure of analysis will be to write one equation of motion in each degree of freedom. Each equation will be of the form $a = f/m$, where a is an acceleration, linear or angular, f is a force or torque in the direction of the acceleration, and m is a mass or inertia.

Because of the essentially aerodynamic nature of the problem in hand, the natural dependent variables are the velocities rather than the displacements. An exception to this occurs in the vibrational degrees of freedom because vibrational displacements, as well as velocities, produce changes in angle of attack. Thus, as far as the vibrational degrees of freedom are concerned, the displacements will be regarded as the dependent variables.

TABLE 2

Displacement	Velocity	Acceleration	Forces	Natural Frequencies
σ	$\dot\sigma = D\sigma$	$\ddot\sigma = D^2\sigma$	P	ω_1
τ	$\dot\tau = D\tau$	$\ddot\tau = D^2\tau$	Q	ω_2

TABLE 3

Principal Action	Symbol
Thrust	ξ
Side force	η
Vertical force	ζ
Roll torque	ρ
Pitch torque	β
Yaw torque	γ

Inasmuch as the coordinates move in space, the accelerations in the equations of motion are the absolute accelerations of a moving coordinate system. These will, however, differ from the well-known forms of these accelerations in that they contain contributions from the vibrational degrees of freedom. The forces (or torques) in the equations of motion are the summations of all forces that are not inertial in origin. They arise from two sources: One type of force is that arising from the motion of the aircraft. This type of force consists of such quantities as lift, drag, pitching moments, aerodynamic damping, and others, and these will be regarded as response forces; thus, they will appear on the left-hand side of the equations of motion. The second contribution is introduced by activation of the controls. The forces arising from this source will be regarded as exciting forces and will appear on the right-hand side of the equations.

The solutions of the equations of motion give the time histories of the motions; thus, they must clearly depend on the manner of activation of the controls that cause the motion. The equations here derived are completely general in this respect, and the investigator may search for steady-state solutions by introducing periodic control activation, or he may obtain transient solutions to unit-step or arbitrary control activation. The theory here presented was actually applied to transient solutions resulting from unit-step control motion.

THE ACCELERATIONS

Derivation of the linear accelerations presents no great difficulty. They are easily shown to be, respectively (for $p(t) \equiv 0$),

$$\left.\begin{aligned} a_x &= (du/dt) + (w + \dot\tau)q - (v + \dot\sigma)r \\ a_y &= (dv/dt) + (d\dot\sigma/dt) + ur \\ a_z &= (dw/dt) + (d\dot\tau/dt) - uq \end{aligned}\right\} \tag{3}$$

Eqs. (3) are obtainable from purely kinematical considerations.

The angular accelerations must be derived from dynamic relations. They are obtained from Euler's equations of inertia moments of a body rotating about a fixed point coinciding with the center of gravity, and their simple form used here requires that the coordinate axes coincide with the principal axes.

The derivation of the angular acceleration about the x-axis will be shown here. For the other accelerations, only the results are listed.

The angular velocity vector $\bar{\omega}$, whose components are the angular velocities about the xy and z-axes, respectively, is

$$\bar{\omega} = q\bar{j} + r\bar{k}$$

The velocity of a point P located at

$$\bar{r} = x\bar{\imath} + y\bar{j} + z\bar{k}$$

is

$$\bar{v} = \bar{\omega}\bar{r} = v_x\bar{\imath} + v_y\bar{j} + v_z\bar{k}$$

where

$$\begin{aligned} v_x &= (z + \tau)\, q - (y + \sigma)r \\ v_y &= xr \\ v_z &= -xq \end{aligned}$$

Then, the angular momentum of a mass dm located at P is

$$\begin{aligned} \lambda &= \bar{r}\, dm\, \bar{v} \\ &= \lambda_x\bar{\imath} + \lambda_y\bar{j} + \lambda_z\bar{k} \end{aligned}$$

where

$$\begin{aligned} \lambda_x &= dm\, [(y + \sigma)v_z - (z + \tau)v_y] \\ \lambda_y &= dm\, [(z + \tau)v_x - xv_z] \\ \lambda_z &= dm\, [xv_y - (y + \sigma)\, v_x] \end{aligned}$$

The inertia moment due to the mass dm about the x-axis is

$$\begin{aligned} dL &= (d\lambda_x/dt) + q\,\lambda_z - r\lambda_y \\ &= dm\{-x\dot{\sigma}q - x(y + \sigma)\dot{q} - x\dot{\tau}r - x(z + \tau)\dot{r} - \\ &\quad (z + \tau)\,(y + \sigma)q^2 + (z + \tau)\,(y + \sigma)r^2 + \\ &\quad [(y + \sigma)^2 - (z + \tau)^2]qr\} \end{aligned}$$

The total moment is

$$\begin{aligned} L = {} & -\dot{q}\int_l x(y + \sigma)\, dm - \dot{r}\int_l x(z + \tau)\, dm - \\ & q^2\int_l (z + \tau)\,(y + \sigma)\, dm + r^2\int_l (y + \sigma)\,(z + \tau)\, dm + \\ & qr\left[\int_l (y + \sigma)^2\, dm - \int_l (z + \tau)^2\, dm\right] - \\ & q\dot{\sigma}_0\int_l xf_1(x)\,\kappa\, dx - r\dot{\tau}_0\int_l xf_2(x)\,\kappa\, dx \end{aligned}$$

where $\kappa = dm/dx$ is the mass per unit length and use has been made of Eqs. (1). It can be shown that, if the vibrational displacements σ and τ are sufficiently small, the above expression for the moment can be approximated by

$$L = (C - B)qr - q\dot{\sigma}_0\int_l xf_1(x)\kappa\, dx - r\dot{\tau}_0\int_l xf_2(x)\kappa\, dx$$

where higher terms of the small quantities and products of inertia with regard to the vibrations have been neglected. Finally, the acceleration about the x-axis is obtained by dividing the expression for the moment by the moment of inertia of the body about the x-axis, or

$$\begin{aligned} a_\varphi = {} & \frac{C - B}{A}\, qr - \left[\frac{1}{A}\int_l xf_1(x)\kappa\, dx\right]\dot{q}\dot{\sigma}_0 - \\ & \left[\frac{1}{A}\int_l xf_2(x)\kappa\, dx\right] r\dot{\tau}_0 \end{aligned} \tag{4}$$

Because the rolling velocity vanishes identically, particularly simple expressions for the other two angular accelerations are obtained in an exactly analogous manner. They are

$$\left.\begin{aligned} a_\theta &= dq/dt \\ a_\psi &= dr/dt \end{aligned}\right\} \tag{5}$$

The Equations of Motion

Assuming that the force per unit length $\bar{X}$, parallel to the x-axis, is a linear function of all variables and of all controls, the equation of motion of an elemental length of the aircraft (of length dx and mass dm) may be written as

$$\begin{aligned} &(\dot{u} - rv + qw - r\sigma_0 f_1 + q\tau_0 f_2)\, dm = \\ &\qquad \left\{\sum_i \bar{X}_i i + \sum_j \bar{X}_j j + \bar{X}_\sigma\, \sigma_0 f_1 + \bar{X}_{\dot{\sigma}}\dot{\sigma}_0 f_1 + \right. \\ &\qquad \left. \bar{X}_\tau\tau_0 f_2 + \bar{X}_{\dot{\tau}}\dot{\tau}_0 f_2\right\} dx \end{aligned} \tag{6}$$

where i can take on the values u, v, w, q, r; j can take on the values ξ, η, ζ, ρ, β, γ; the subscripts denote partial differentiation; and the bar denotes forces per unit length.

By making use of the following notations

$$\int_l dm = m; \qquad dm = \kappa\, dx; \qquad \bar{X}_i/m = \bar{X}_i$$

$$\int_l \bar{X}_i\, dx = X_i; \qquad d/dt = D$$

and of Eqs. (2), the integral of Eq. (6) over the aircraft length is

$$D(u) - rv + qw - \left\{\sum_i X_i i + \sigma_0 \int_l \tilde{X}_\sigma f_1\,dx + D(\sigma_0)\int_l \tilde{X}_{\dot\sigma} f_1\,dx + \tau_0 \int_l \tilde{X}_\tau f_2\,dx + D(\tau_0)\int_l \tilde{X}_{\dot\tau} f_2\,dx\right\} = \sum_j X_j j \tag{7}$$

Similar equations for the forces parallel to the y- and z-axes are found to be

$$D(v) + ur - \left\{\sum_i Y_i i + \sigma_0 \int_l \tilde{Y}_\sigma f_1\,dx + D(\sigma_0)\int_l \tilde{Y}_{\dot\sigma} f_1\,dx + \tau_0 \int_l \tilde{Y}_\tau f_2\,dx + D(\tau_0)\int_l \tilde{Y}_{\dot\tau} f_2\,dx\right\} = \sum_j Y_j j \tag{8}$$

$$D(w) - uq - \left\{\sum_i Z_i i + \sigma_0 \int_l \tilde{Z}_\sigma f_1\,dx + D(\sigma_0)\int_l \tilde{Z}_{\dot\sigma} f_1\,dx + \tau_0 \int_l \tilde{Z}_\tau f_2\,dx + D(\tau_0)\int_l \tilde{Z}_{\dot\tau} f_2\,dx\right\} = \sum_j Z_j j \tag{9}$$

The equations of torques about the coordinate axes are obtained similarly to Eqs. (7) to (9). Of these, the roll equation does not exist because roll is not an admissible motion.*

With the aid of the following notation:

$$\bar{M}_i/B = \tilde{M}_i, \qquad \int_l \tilde{M}_i\,dx = M_i$$

$$\bar{N}_i/C = \tilde{N}_i, \qquad \int \tilde{N}_i\,dx = N_i$$

the equation of rotation about the y-axis is

$$D(q) - \left\{\sum_i M_i i + \sigma_0 \int_l \tilde{M}_\sigma f_1\,dx + D(\sigma_0)\int_l \tilde{M}_{\dot\sigma} f_1\,dx + \tau_0 \int_l \tilde{M}_\tau f_2\,dx + D(\tau_0)\int_l \tilde{M}_{\dot\tau} f_2\,dx\right\} = \sum M_j j \tag{10}$$

and the equation of rotation about the z-axis is

$$D(r) - \left\{\sum_i N_i i + \sigma_0 \int_l \tilde{N}_\sigma f_1\,dx + D(\sigma_0)\int_l \tilde{N}_{\dot\sigma} f_1\,dx + \tau_0 \int_l \tilde{N}_\tau f_2\,dx + D(\tau_0)\int_l \tilde{N}_{\dot\tau} f_2\,dx\right\} = \sum_j N_j j \tag{11}$$

The remaining equations to be derived are those in the vibrational degrees of freedom. These are most easily obtained by application of Lagrange's equation. That for the σ degree of freedom is

$$D^2(\sigma_0) + \omega_1^2\sigma_0 - \left\{\sum_i i\int_l \tilde{P}_i f_1\,dx + \sigma_0\int_l \tilde{P}_\sigma f_1^2\,dx + D(\sigma_0)\int_l \tilde{P}_{\dot\sigma} f_1^2\,dx + \tau_0\int_l \tilde{P}_\tau f_1 f_2\,dx + D(\tau_0)\times \int_l \tilde{P}_{\dot\tau} f_1 f_2\,dx\right\} = \sum j\int_l \tilde{P}_j f_1\,dx \tag{12}$$

where use has been made of the notation

$$\bar{P}_i/\int_l f_1^2\kappa\,dx = \tilde{P}_i$$

With the notation

$$\bar{Q}_i/\int_l f_2^2\kappa\,dx = \tilde{Q}_i$$

the equation in the τ degree of freedom becomes

$$D^2(\tau_0) + \omega_2^2\tau_0 - \left\{\sum_i i\int_l \tilde{Q}_i f_2\,dx + \sigma_0\int_l \tilde{Q}_\sigma f_1 f_2\,dx + D(\sigma_0)\int_l \tilde{Q}_{\dot\sigma} f_1 f_2\,dx + \tau_0\int_l \tilde{Q}_\tau f_2^2\,dx + D(\tau_0)\times \int_l \tilde{Q}_{\dot\tau} f_2^2\,dx\right\} = \sum_j j\int_l \tilde{Q}_j f_2\,dx \tag{13}$$

* It is not an entirely trivial matter to show the nonexistence of the roll equation because Eq. (4) shows that a roll acceleration does exist even when $p(t) \equiv 0$, and there are undoubtedly nonvanishing forces due to many of the variables that contribute to the roll torque.

The assumption that all forces are linear in their arguments is less satisfactory for the force X than for the others. Therefore, Eq. (7) should be more properly written as

$$D(u) - rv + qw - \left\{\sum_i \int X_i\, di + \int_l \int \tilde{X}_\sigma f_1 d\sigma_0\, dx + \int_l \int \tilde{X}_{\dot{\sigma}} f_1 d\dot{\sigma}_0\, dx + \int_l \int \tilde{X}_\tau f_2 d\tau_0\, dx + \int_l \int \tilde{X}_{\dot{\tau}} f_2 d\dot{\tau}_0\, dx\right\} = \sum_j \int X_j\, dj$$

This equation is seen to introduce nonlinear terms into the system of equations of motion. However, the difficulty is circumvented by the following well-known simplification:

In the conventional analysis of airplane dynamic stability, it is a familiar assumption to consider the variation in forward velocity negligible compared to the mean value of that velocity, or $u = U + u'$, where $u' \ll U$ and U is a constant. In the problem here considered, it is sufficient to regard the maneuvers so small that their effect on the forward velocity need not be considered. For this special case, the first of the equations of motion—i.e., Eq. (7)—must necessarily express the equilibrium between thrust and drag. Thus, Eq. (7) simplifies to

$$X_u U = X_\xi \xi_0 \tag{14}$$

where U is the constant forward velocity and ξ_0 may be regarded as the constant throttle position. Eq. (14) is an equation containing none of the variables under consideration; thus it separates from the system of equations. Those that remain are conveniently written as the matrix equation,

$$[E]\,\{V\} = [C]\,\{\mu\} \tag{15}$$

where

$$[E] = \begin{bmatrix}
(D - Y_v) & (-Y_w) & (-Y_q) & (U - Y_r) & \begin{pmatrix} -\int_l \tilde{Y}_{\dot{\sigma}} f_1\, dx\, D \\ -\int \tilde{Y}_\sigma f_1\, dx \end{pmatrix}\begin{pmatrix} -\int_l \tilde{Y}_{\dot{\tau}} f_2\, dx\, D \\ -\int_l \tilde{Y}_\tau f_2\, dx \end{pmatrix} \\
(-Z_v) & (D - Z_w) & -(U + Z_q) & (-Z_r) & \begin{pmatrix} -\int_l \tilde{Z}_{\dot{\sigma}} f_1\, dx\, D \\ -\int_l \tilde{Z}_\sigma f_1\, dx \end{pmatrix}\begin{pmatrix} -\int_l \tilde{Z}_{\dot{\tau}} f_2\, dx\, D \\ -\int_l \tilde{Z}_\tau f_2\, dx \end{pmatrix} \\
(-M_v) & (-M_w) & (D - M_q) & (-M_r) & \begin{pmatrix} -\int_l \tilde{M}_{\dot{\sigma}} f_1\, dx\, D \\ -\int_l \tilde{M}_\sigma f_1\, dx \end{pmatrix}\begin{pmatrix} -\int_l \tilde{M}_{\dot{\tau}} f_2\, dx\, D \\ -\int_l \tilde{M}_\tau f_2\, dx \end{pmatrix} \\
(-N_v) & (-N_w) & (-N_q) & (D - N_r) & \begin{pmatrix} -\int_l N_{\dot{\sigma}} f_1\, dx\, D \\ -\int_l N_\sigma f_1\, dx \end{pmatrix}\begin{pmatrix} -\int_l \tilde{N}_{\dot{\tau}} f_2\, dx\, D \\ -\int_l \tilde{N}_\tau f_2\, dx \end{pmatrix} \\
\left(-\int_l \tilde{P}_v f_1\, dx\right) & \left(-\int_l \tilde{P}_w f_1\, dx\right) & \left(-\int_l \tilde{P}_q f_1\, dx\right) & \left(-\int_l \tilde{P}_r f_1\, dx\right) & \begin{pmatrix} D^2 - \int_l \tilde{P}_{\dot{\sigma}} f_1^2\, dx\, D \\ -\int_l \tilde{P}_\sigma f_1^2\, dx + \omega_1^2 \end{pmatrix}\begin{pmatrix} -\int_l \tilde{P}_{\dot{\tau}} f_1 f_2\, dx\, D \\ -\int \tilde{P}_\tau f_1 f_2\, dx \end{pmatrix} \\
\left(-\int_l \tilde{Q}_v f_2\, dx\right) & \left(-\int \tilde{Q}_w f_2\, dx\right) & \left(-\int_l \tilde{Q}_q f_2\, dx\right) & \left(-\int \tilde{Q}_r f_2\, dx\right) & \begin{pmatrix} -\int_l \tilde{Q}_{\dot{\sigma}} f_1 f_2\, dx\, D \\ -\int_l \tilde{Q}_\sigma f_1 f_2\, dx \end{pmatrix}\begin{pmatrix} D^2 - \int \tilde{Q}_{\dot{\tau}} f_2^2\, dx\, D \\ -\int_l \tilde{Q}_\tau f_2^2\, dx + \omega_2^2 \end{pmatrix}
\end{bmatrix}$$

$$[C] = \begin{bmatrix}
Y_\xi & Y_\eta & Y_\zeta & Y_\rho & Y_\beta & Y_\gamma \\
Z_\xi & Z_\eta & Z_\zeta & Z_\rho & Z_\beta & Z_\gamma \\
M_\xi & M_\eta & M_\zeta & M_\rho & M_\beta & M_\gamma \\
N_\xi & N_\eta & N_\zeta & N_\rho & N_\beta & N_\gamma \\
\int_l \tilde{P}_\xi f_1\, dx & \int_l \tilde{P}_\eta f_1\, dx & \int_l \tilde{P}_\zeta f_1\, dx & \int_l \tilde{P}_\rho f_1\, dx & \int_l \tilde{P}_\beta f_1\, dx & \int_l \tilde{P}_\gamma f_1\, dx \\
\int_l \tilde{Q}_\xi f_2\, dx & \int_l \tilde{Q}_\eta f_2\, dx & \int_l \tilde{Q}_\zeta f_2\, dx & \int_l \tilde{Q}_\rho f_2\, dx & \int_l \tilde{Q}_\beta f_2\, dx & \int_l \tilde{Q}_\gamma f_2\, dx
\end{bmatrix}$$

$$\{V\} = \begin{bmatrix} v \\ w \\ q \\ r \\ \sigma_0 \\ \tau_0 \end{bmatrix} \qquad \{\mu\} = \begin{bmatrix} 0 \\ \eta \\ \zeta \\ 0 \\ \beta \\ \gamma \end{bmatrix}$$

The Aerodynamic Derivatives

Eq. (15) and the equations defining the matrices of Eq. (15) demonstrate the necessity for determining a large number of aerodynamic derivatives.

It is realized that, in the problem at hand, the aerodynamic forces (whose derivatives with respect to the dependent variables are desired) are those arising from unsteady flow about airfoils. Inasmuch as these forces have been determined for both subsonic incompressible and supersonic flows, their substitution in the equations of motion presents no insurmountable obstacle. However, their use complicates the problem so that a solution without high-speed computing devices seems forbidding.

It is not unrealistic to suppose that the application of the air forces arising from steady flow will predict the dynamic behavior under investigation reasonably well, provided the velocity of translation of the airplane is not near the flutter speed. However, in applying the steady-flow air forces, the investigator deprives himself of the possibility of analyzing flutter.

The analysis here presented was undertaken in an effort to duplicate analytically, in character as well as quantitatively, the appearance of oscillations observed in flight. As a first step, the forces appearing in the equations of motion were considered to be those of steady flow—i.e., the effect of vortices shed into the wake was neglected. The results of this simplified analysis agree well with observation; therefore, it was considered satisfactory to treat the air forces in this simplified manner.

It will be noticed that many aerodynamic derivatives appear simply as partial derivatives of forces with respect to some of the dependent variables, while others are integrals in which the derivatives occur in the integrand. The former are considered here to be quantities known either from theory or from wind-tunnel tests. The latter will be termed integral derivatives for convenience, and it is these that will be considered in this section. Specifically, the integral derivatives will be here computed from the "simple" derivatives.

It is supposed that the simple derivatives (which are known) were obtained by superposition of contributions arising from certain components of the aircraft. Thus, to consider one of these as an example, it is assumed that Y_v was obtained by the operation

$$Y_v = \sum_{n=1}^{k} \frac{\partial \bar{Y}_n}{\partial v} = \sum_{n=1}^{k} \frac{1}{m} \frac{\partial \bar{Y}_n}{\partial v} \qquad (n = 1, 2, \ldots, k) \tag{16}$$

where the k numbers n represent k stations along the x-axis of the aircraft where components (such as airfoils) are located, each giving rise to an aerodynamic contribution to Y_v. If downwash or any other factor should introduce a phase lag between the k components to be added in the manner of Eq. (16), this effect can be taken into consideration by considering some of the $\partial Y_n/\partial v$ as complex quantities. In any case, it is assumed that all components of the simple derivatives and thus their sums are known. It will now be shown how the integral derivatives can be obtained from the "simple" derivatives.

The integral derivatives will be considered in certain groups, the first of these being that in which the differentiation is carried out with respect to a vibrational velocity.

Consider $\bar{P}_{\dot{\sigma}}$ which is the rate of change of the vibrational force per unit length $\bar{P}$ with respect to the vibrational velocity $\dot{\sigma}$. Both the force and the velocity are in the y-direction. Thus, with regard to an element of length of the aircraft, $\bar{P}_{\dot{\sigma}}$ is indistinguishable from $\bar{Y}_v$, or

$$\partial \bar{Y}/\partial v = \partial \bar{P}/\partial \dot{\sigma}$$

But, since

$$\frac{\partial \bar{Y}}{\partial v} = \frac{1}{m} \frac{\partial \bar{Y}}{\partial v}, \quad \frac{\partial \bar{P}}{\partial \dot{\sigma}} = \frac{1}{\int_l f_1^2 \kappa \, dx} \frac{\partial \bar{P}}{\partial \dot{\sigma}}$$

it follows that

$$\partial \bar{P}/\partial \dot{\sigma} = (m/\int_l f_1^2 \kappa \, dx) \; (\partial \bar{Y}/\partial v)$$

In view of Eq. (16), it is clear that

$$\int_l \bar{P}_{\dot{\sigma}} \, f_1^2 \, dx = \frac{m}{\int_l f_1^2 \kappa \, dx} \sum_n \frac{\partial Y_n}{\partial v} \, [f_1(x_n)]^2 \tag{17}$$

where $f_1(x_n)$ is the value of $f_1(x)$ when $x = x_n$—i.e., it is the deflection in the $f_1(x)$-mode at that value of x at which the nth station is located. In a similar manner, all other integral derivatives with respect to linear velocities can be found.

In determining integral derivatives with respect to angular velocities, use is made of the operations

$$\frac{\partial}{\partial r} = \frac{\partial}{\partial v}\frac{\partial v}{\partial r}, \qquad \frac{\partial}{\partial q} = \frac{\partial}{\partial w}\frac{\partial w}{\partial q}$$

However, since the right-handed coordinate system implies $v = rx$ and $w = -qx$, it follows that

$$\partial/\partial r = x(\partial/\partial v)$$

while

$$\partial/\partial q = -x(\partial/\partial w)$$

Thus, for instance,

$$\int_l \bar{P}_r f_1\, dx = \frac{m}{\int_l f_1^2 \kappa\, dx} \sum_n \frac{\partial \bar{Y}_n}{\partial v} x_n f_1(x_n) \qquad (18)$$

But it is found that

$$\int_l \bar{P}_q f_1\, dx = -\frac{m}{\int_l f_1^2 \kappa\, dx} \sum_n \frac{\partial \bar{Y}_n}{\partial w} x_n f_1(x_n) \qquad (19)$$

The next group of integral derivatives to be considered is that of nonvibratory forces with respect to the vibrational velocities.

In view of the fact that, for example,

$$\frac{\partial Y}{\partial v} = \frac{1}{m}\int \frac{\partial \bar{Y}}{\partial v}\, dx = \int \frac{\partial \bar{Y}}{\partial v}\, dx$$

$$\frac{\partial Y}{\partial \dot{\sigma}} = \frac{1}{m}\int_l \frac{\partial \bar{Y}}{\partial \dot{\sigma}}\, dx = \int_l \frac{\partial \bar{Y}}{\partial \dot{\sigma}}\, dx$$

it follows, from reasoning similar to that applied previously, that

$$\int_l \bar{Y}_{\dot{\sigma}} f_1(x)\, dx = \sum_n \frac{\partial \bar{Y}_n}{\partial v} f(x_n) \qquad (20)$$

It remains to evaluate the integral derivatives of forces and moments with respect to the vibrational displacements. The aerodynamic effect of a vibrational displacement on a component of the aircraft is the change in angle of attack which the component experiences.

Consider as an example the quantity $\partial \bar{Y}/\partial \sigma$. This quantity will be first regarded in its relation to the yaw angle ψ. In fact,

$$\partial \bar{Y}/\partial \sigma = (\partial \bar{Y}/\partial \psi)\ (\partial \psi/\partial \sigma)$$

But the yaw angle may be written as

$$\psi = \frac{d\sigma}{dx} = \frac{d}{dx}(\sigma_0 f_1(x)) = \sigma_0 f_1'(x) = \sigma_0 f_1(x)\frac{f_1'(x)}{f_1(x)} = \sigma \frac{f_1'(x)}{f_1(x)}$$

where the prime denotes differentiation with respect to x. Then

$$\partial \bar{Y}/\partial \sigma = (\partial \bar{Y}/\partial \psi)\ [f_1'(x)/f_1(x)]$$

However, ψ is expressible in terms of the sideways velocity v. In fact,

$$\tan \psi = v/U \cong \psi$$

where the approximation was made in view of the small maneuvers considered here. Then,

$$\partial v/\partial \psi = U, \qquad \partial \bar{Y}/\partial \psi = (\partial \bar{Y}/\partial v)\ (\partial v/\partial \psi)$$

or, finally,

$$\partial \bar{Y}/\partial \sigma = (\partial \bar{Y}/\partial v)\ U[f_1'(x)/f_1(x)] \qquad (21)$$

Similar reasoning, together with the fact that $w/U = -\alpha$, leads to

$$\partial \bar{Y}/\partial \tau = -(\partial \bar{Y}/\partial w) U[f_2'(x)/f_2(x)] \qquad (22)$$

From Eqs. (21) and (22), two typical integral derivatives with respect to vibrational displacements are evaluated by methods similar to those employed for Eqs. (17), (18), (19), and (20). They are

$$\int_l \bar{Y}_{\sigma} f_1\, dx = U \sum_n \frac{\partial \bar{Y}_n}{\partial v} f_1'(x_n) \qquad (23)$$

and

$$\int_l \bar{Y}_{\tau} f_2\, dx = -U \sum_n \frac{\partial \bar{Y}_n}{\partial w} f_2'(x_n) \qquad (24)$$

A list of all required integral derivatives is given in Table 4. Their derivation is in all cases analogous to one of those shown in detail in this section.

TABLE 4

DERIVATIVE	EVALUATION	DERIVATIVE	EVALUATION
$\int_l \bar{P}_{\sigma} f_1^2 dx$	$(m/\int_l f_1^2 \kappa dx)\sum_n \frac{\partial \bar{Y}_n}{\partial v} f_1^2(x_n)$	$\int_l \bar{Z}_{\tau} f_2 dx$	$\sum_n \frac{\partial \bar{Z}_n}{\partial w} f_2(x_n)$
$\int_l \bar{P}_{\dot{\sigma}} f_1 f_2 dx$	$(m/\int_l f_1^2 \kappa dx)\sum_n \frac{\partial \bar{Y}_n}{\partial w} f_1(x_n) f_2(x_n)$	$\int_l \bar{M}_{\sigma} f_1 dx$	$\sum_n \frac{\partial \bar{M}_n}{\partial v} f_1(x_n)$
$\int_l \bar{Q}_{\dot{\sigma}} f_1 f_2 dx$	$(m/\int_l f_2^2 \kappa dx)\sum_n \frac{\partial \bar{Z}_n}{\partial w} f_1(x_n) f_2(x_n)$	$\int_l \bar{M}_{\tau} f_2 dx$	$\sum_n \frac{\partial \bar{M}_n}{\partial w} f_2(x_n)$
$\int_l \bar{Q}_{\dot{\tau}} f_2^2 dx$	$(m/\int_l f_2^2 \kappa dx)\sum_n \frac{\partial \bar{Z}_n}{\partial w} f_2^2(x_n)$	$\int_l \bar{N}_{\sigma} f_1 dx$	$\sum_n \frac{\partial \bar{N}_n}{\partial v} f_1(x_n)$
$\int_l \bar{P}_{\dot{\sigma}} f_1 dx$	$(m/\int_l f_1^2 \kappa dx)\sum_n \frac{\partial \bar{Y}_n}{\partial v} f_1(x_n)$	$\int_l \bar{N}_{\tau} f_2 dx$	$\sum_n \frac{\partial \bar{N}_n}{\partial w} f_2(x_n)$
$\int_l \bar{P}_{\dot{\tau}} f_1 dx$	$(m/\int_l f_1^2 \kappa dx)\sum_n \frac{\partial \bar{Y}_n}{\partial w} f_1(x_n)$	$\int_l \bar{Y}_{\sigma} f_1 dx$	$U\sum_n \frac{\partial \bar{Y}_n}{\partial v} f_1'(x_n)$
$\int_l \bar{P}_{\dot{\sigma}} f_1 dx$	$-(m/\int_l f_1^2 \kappa dx)\sum_n \frac{\partial \bar{Y}_n}{\partial w} n f_1(x_n)$	$\int_l \bar{Y}_{\tau} f_2 dx$	$-U\sum_n \frac{\partial \bar{Y}_n}{\partial w} f_2'(x_n)$
$\int_l \bar{P}_{\tau} f_1 dx$	$(m/\int_l f_1^2 \kappa dx)\sum_n \frac{\partial \bar{Z}_n}{\partial w} n f_1(x_n)$	$\int_l \bar{Z}_{\sigma} f_1 dx$	$U\sum_n \frac{\partial \bar{Z}_n}{\partial v} f_1'(x_n)$
$\int_l \bar{P}_{\dot{\tau}} f_1 dx$	$(m/\int_l f_1^2 \kappa dx)\sum_n \frac{\partial \bar{Z}_n}{\partial \dot{\sigma}} f_1(x_n)$	$\int_l \bar{Z}_{\tau} f_2 dx$	$-U\sum_n \frac{\partial \bar{Z}_n}{\partial w} f_2'(x_n)$
$\int_l \bar{Q}_{\sigma} f_2 dx$	$(m/\int_l f_2^2 \kappa dx)\sum_n \frac{\partial \bar{Z}_n}{\partial v} f_2(x_n)$	$\int_l \bar{P}_{\sigma} f^2 dx$	$(mU/\int_l f_1^2 \kappa dx)\sum_n \frac{\partial \bar{Y}_n}{\partial w} f_{(x_n)} f_1'(x_n)$
$\int_l \bar{Q}_{\dot{\sigma}} f_2 dx$	$(m/\int_l f_2^2 \kappa dx)\sum_n \frac{\partial \bar{Z}_n}{\partial w} f_2(x_n)$	$\int_l \bar{P}_{\tau} f_1 f_2 dx$	$-(mU/\int_l f_1^2 \kappa dx)\sum_n \frac{\partial \bar{Y}_n}{\partial w} f_2(x_n) f_1'(x_n)$
$\int_l \bar{Q}_{\dot{\tau}} f_2 dx$	$-(m/\int_l f_2^2 \kappa dx)\sum_n \frac{\partial \bar{Z}_n}{\partial w} n f_2(x_n)$	$\int_l \bar{Q}_{\sigma} f_1 f_2 dx$	$(mU/\int_l f_1^2 \kappa dx)\sum_n \frac{\partial \bar{Z}_n}{\partial w} f_{(x_n)} f_2'(x_n)$
$\int_l \bar{Q}_{\tau} f_2 dx$	$(m/\int_l f_2^2 \kappa dx)\sum_n \frac{\partial \bar{Z}_n}{\partial w} n f_2(x_n)$	$\int_l \bar{Q}_{\tau} f_2^2 dx$	$-(mU/\int_l f_2^2 \kappa dx)\sum_n \frac{\partial \bar{Z}_n}{\partial w} f_2(x_n) f_2'(x_n)$
$\int_l \bar{Q}_{\dot{\sigma}} f_2 dx$	$(m/\int_l f_2^2 \kappa dx)\sum_n \frac{\partial \bar{Z}_n}{\partial \dot{\sigma}} f_2(x_n)$	$\int_l \bar{M}_{\sigma} f_1 dx$	$U\sum_n \frac{\partial \bar{M}_n}{\partial v} f_1'(x_n)$
$\int_l \bar{Y}_{\sigma} f_1 dx$	$\sum_n \frac{\partial \bar{Y}_n}{\partial v} f_1(x_n)$	$\int_l \bar{M}_{\tau} f_2 dx$	$-U\sum_n \frac{\partial \bar{M}_n}{\partial w} f_2'(x_n)$
$\int_l \bar{Y}_{\dot{\tau}} f_2 dx$	$\sum_n \frac{\partial \bar{Y}_n}{\partial w} f_2(x_n)$	$\int_l \bar{N}_{\sigma} f_1 dx$	$U\sum_n \frac{\partial \bar{N}_n}{\partial v} f_1'(x_n)$
$\int_l \bar{Z}_{\sigma} f_1 dx$	$\sum_n \frac{\partial \bar{Z}_n}{\partial v} f_1(x_n)$	$\int_l \bar{N}_{\tau} f_2 dx$	$-U\sum_n \frac{\partial \bar{N}_n}{\partial w} f_2'(x_n)$

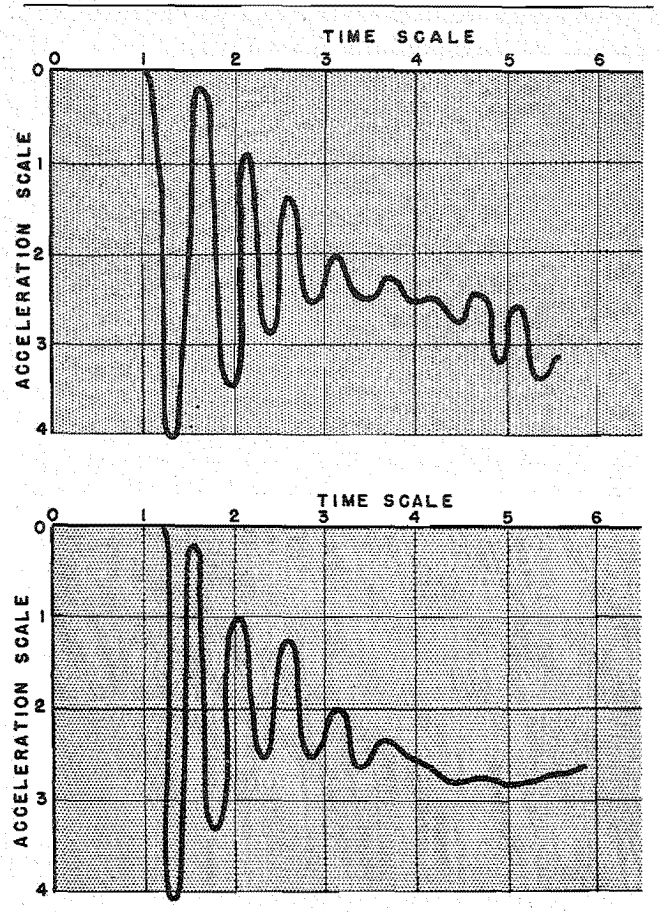

FIG. 1. Upper curve is the result of flight measurements for one flight condition. Lower curve is the result predicted by theory.

A SIMPLE APPLICATION

The foregoing development will be here applied to the following example:

A step-function type of control activation in ζ will be applied at $t = t_0$; all other controls will be left undisturbed. Thus, the controls activity considered will be $\zeta = 1\zeta$, or $1\zeta(t) = 0$ for $t < t_0$ and $1\zeta(t) = 1$ for $t \geqslant t_0$. Furthermore, only "primary" aerodynamic forces will be considered to exist. Thus, the following derivatives vanish—i.e.,

$$Y_w,\ Y_q,\ Y_r,\ \int_l \bar{Y}_\tau f_2\,dx,\ \int_l \bar{Y}_{\dot\tau} f_2\,dx,\ Y_\zeta,\ Z_v,\ Z_q,\ Z_r,$$
$$\int_l \bar{Z}_\sigma f_1\,dx,\ \int_l \bar{Z}_{\dot\sigma} f_1\,dx,\ \int_l \bar{P}_w f_1\,dx,\ \int_l \bar{P}_q f_1\,dx,$$
$$\int_l \bar{P}_\tau f_1 f_2\,dx,\ \int_l \bar{P}_{\dot\tau} f_1 f_2\,dx,\ \int_l \bar{P}_\zeta f_1\,dx,\ \int_l \bar{Q}_v f_2\,dx,$$
$$\int_l \bar{Q}_\tau f_2\,dx,\ \int \bar{Q}_\sigma f_1 f_2\,dx,\ \int_l \bar{Q}_{\dot\sigma} f_1 f_2\,dx,\ \int_l \bar{M}_\sigma f_1\,dx,$$
$$\int_l \bar{M}_{\dot\sigma} f_1\,dx,\ M_v,\ M_r,\ \int_l \bar{N}_\tau f_2\,dx,\ \int_l \bar{N}_{\dot\tau} f_2\,dx,$$
$$N_w,\ N_r,\ N_\zeta$$

are all zero. In an aircraft of conventional design, these derivatives are actually sufficiently small compared to those retained that they may be neglected compared with all others.

For this system, Eq. (15) becomes

$$\begin{bmatrix} (D - Y_v) & \left(-\int_l \bar{Y}_\sigma f_1\,dx\,D\right) & (U) & 0 & 0 \\ \left(-\int_l \bar{P}_v f_1\,dx\right) & \left(D^2 - \int_l \bar{P}_{\dot\sigma} f_1^2\,dx\,D - \int_l \bar{P}_\sigma f_1^2\,dx + \omega_1^2\right) & \left(-\int_l \bar{P}_\tau f_1\,dx\right) & 0 & 0 \\ (-N_v) & \left(-\int_l \bar{N}_{\dot\sigma} f_1\,dx\,D - \int_l \bar{N}_\sigma f_1\,dx\right) & (D - N_r) & 0 & 0 \\ 0 & 0 & 0 & (D - Z_w) & \left(-\int_l \bar{Q}_w f_2\,dx\right) \\ 0 & 0 & 0 & \left(-\int_l Z_{\dot\tau} f_2\,dx\,D - \int \bar{Z}_\tau f_2\,dx\right) & \left(D^2 - \int_l \bar{Q}_{\dot\tau} f_2^2\,dx\,D - \int_l \bar{Q}_\tau f_2^2\,dx + \omega_2^2\right) \\ 0 & 0 & 0 & (-U) & \left(-\int_l \bar{Q}_q f_2\,dx\right) \\ 0 & 0 & 0 & \left(-\int_l \bar{M}_{\dot\tau} f_2\,dx\,D - \int \bar{M}_\tau f_2\,dx\right) & (D - M_q) \end{bmatrix} \begin{bmatrix} v \\ \sigma_0 \\ r \\ w \\ \tau_0 \\ q \end{bmatrix} = 1_\zeta \begin{bmatrix} 0 \\ 0 \\ 0 \\ Z_\zeta \\ \int_l \bar{Q}_\zeta f_2\,dx \\ M_\zeta \end{bmatrix} \quad (25)$$

Clearly, the equations giving rise to the first three rows of Eq. (25) are functions of those variables of which the equations corresponding to the last three are not. This observation is equivalent to noting that in a nonrolling aircraft the longitudinal and lateral motions may be discussed separately.

Inasmuch as the proposed control activity is one giving rise to longitudinal motion, the lateral motion will not be further considered. The longitudinal motion is the solution of the following matrix equation:

$$\begin{bmatrix} (D - Z_w) & \begin{pmatrix} -\int_l \bar{Z}_{\dot\tau} f_2\, dx\, D \\ -\int_l \bar{Z}_\tau f_2\, dx \end{pmatrix} & -U \\ -\int \bar{Q}_w f_2\, dx & \begin{pmatrix} D^2 - \int_l \bar{Q}_{\dot\tau} f_2{}^2\, dx\, D \\ -\int_l \bar{Q}_\tau f_2{}^2\, dx + \omega_2{}^2 \end{pmatrix} & -\int_l \bar{Q}_q f_2\, dx \\ -M_w & \begin{pmatrix} -\int_l \bar{M}_{\dot\tau} f_2\, dx\, D \\ -\int_l \bar{M}_\tau f_2\, dx \end{pmatrix} & (D - M_q) \end{bmatrix} \begin{bmatrix} w \\ \tau_0 \\ q \end{bmatrix} = \begin{bmatrix} Z_\zeta \\ \int_l \bar{Q}_\zeta f_2\, dx \\ M_\zeta \end{bmatrix} 1\zeta \tag{26}$$

If the occurrence of the acceleration $D^2\tau_0$ in the central element of Eq. (26) is considered an inconvenience, it may be eliminated by augmenting the equations of motion by the additional equation $\dot\tau_0 = D\tau_0$. The augmented matrix equation becomes

$$\begin{bmatrix} (D - Z_w) & \begin{pmatrix} -\int_l \bar{Z}_{\dot\tau} f_2\, dx\, D \\ -\int_l \bar{Z}_\tau f_2\, dx \end{pmatrix} & 0 & -U \\ -\int_l \bar{Q}_w f_2\, dx & \begin{pmatrix} -\int_l \bar{Q}_{\dot\tau} f_2{}^2\, dx\, D \\ -\int_l \bar{Q}_\tau f_2{}^2\, dx + \omega_2{}^2 \end{pmatrix} & D & -\int_l \bar{Q}_q f_2\, dx \\ -M_w & \begin{pmatrix} -\int_l \bar{M}_{\dot\tau} f_2\, dx\, D \\ -\int_l \bar{M}_\tau f_2\, dx \end{pmatrix} & 0 & (D - M_q) \\ 0 & -D & 1 & 0 \end{bmatrix} \begin{bmatrix} w \\ \tau_0 \\ \dot\tau_0 \\ q \end{bmatrix} = \begin{bmatrix} Z_\zeta \\ \int_l \bar{Q}_\zeta f_2\, dx \\ M_\zeta \\ 0 \end{bmatrix} 1\zeta \tag{27}$$

Eq. (27) has been applied in a practical case in order to attempt the duplication of observed flight experience. The aerodynamic integral derivatives were computed by the theory presented here. The analytical results showed remarkably good agreement with observed performance. In particular, an oscillation of considerable amplitude was explained qualitatively, as well as quantitatively. The actual task of integrating the equations of motion was entrusted to an electronic analog computer, and the results were obtained as tracings of an oscillograph. These results are shown in Figs. 1 and 2 for two different flight conditions. In both illustrations, the upper curves are the results of flight measurements and the lower are the results of the analysis presented in this paper. The scales are the same in the two illustrations—i.e., the peak acceleration in Fig. 1 is nearly eight times as large as that in Fig. 2. It will be noticed that the agreement between theory and experiment is extremely satisfactory in both cases.

Stability

It appears that the system will be stable if the characteristic equation of the system satisfies the stability criteria of the Routh discriminant. However, for certain types of control motion the system may become unstable even if the Routh discriminant of the left-hand side of Eq. (27) indicates stability. Thus, consider a control activation that is governed by the acceleration as measured somewhere on the aircraft. Then, ζ becomes a function of one or more of the dependent variables. This can either be accomplished by a mass unbalance[2,3] incorporated in the control system or by an accelerometer that governs control action

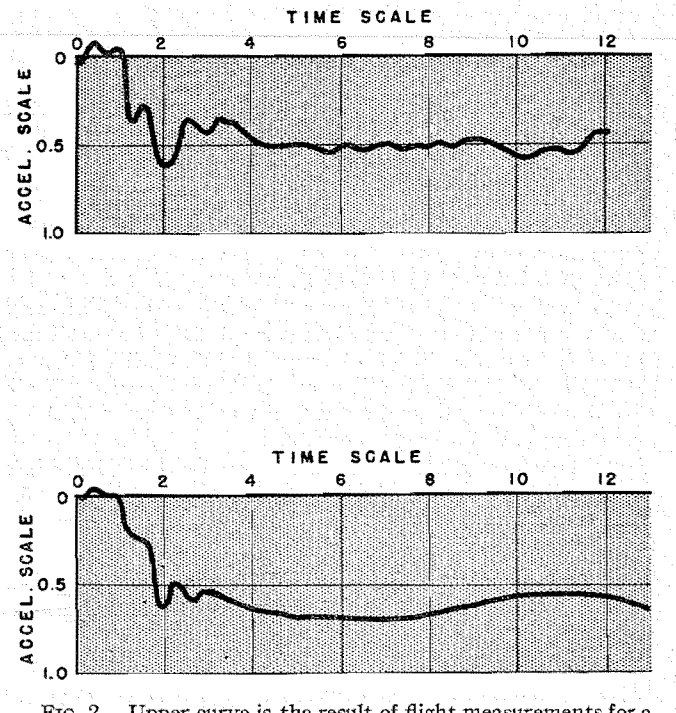

FIG. 2. Upper curve is the result of flight measurements for a flight condition different from that of Fig. 1. Lower curve is the result predicted by theory.

by electric means. If the acceleration-controlled aerodynamic surface is on one side of a node of the vibration mode and the acceleration-sensitive unit is on the other, then the accelerations of these two components will be 180° out of phase with respect to one another. Now assume that the controlling device is adjusted so as to counteract any acceleration experienced by it. This will generally be the case if acceleration control is introduced to produce stability. In that case and for the unfavorable location of the two units in question, the control action now excites the vibration mode at resonance and the system becomes unstable. This same effect can be produced with favorably located components if there is a phase lag equal to an integer multiple of one-half the vibrational frequency between control command and control response. This effect may be analyzed by the equations derived here; it is merely necessary to insert the proper control forces on the right-hand side of the equations of motion.

Concluding Remarks

A theory of the flight dynamics of cylindrical bodies, nearly circular in cross section and elastic in a limited sense, has been presented. A large number of restrictions were introduced in order to render the treatment manageable. These might be grouped into those whose removal would render the treatment more tedious but not theoretically more difficult and into others that make any analytical treatment quite forbidding. Among the restrictions that could be removed without causing undue difficulty are those relating to the elasticity and to the air forces.

The admission of elastic deflections decomposable into $n + 1$ normal modes rather than only one would merely add n equations of motion to the system and n terms to the equations used in this analysis. Thus, the consideration of three normal modes instead of one should certainly be considered feasible.

Consideration of the air forces arising from unsteady flow is possible since these air forces are known. In fact, it appears that even transient solutions could be obtained rather easily if use is made of analog or digital computing machines. However, when nonstationary air forces are introduced, the problem appears to become numerically too complex for solution by means of desk computers.

All restrictions except the two just mentioned were introduced in order to retain differential equations that are linear and have constant coefficients. Theoretical predictions of the flight dynamics of the aircraft under consideration do not appear hopeful if these restrictions are relaxed. However, an analysis in the neighborhood of the problem solved here can be carried out by perturbation methods.

References

[1] Pringle, J. W. S., *The Gyroscopic Mechanism of the Halteres of Dipteria*, Phil. Trans. Roy. Soc. London, 233B, pp. 347–384, 1948.

[2] Phillips, Wm. H., *Effect of Spring and Gravity Moments on the Longitudinal Stability of the Brewster XSBA-1 Airplane*, N.A.C.A. Wartime Report L-263.

[3] Rosenberg, R. M., *Spring and Gravity Moments in the Control System of an Airplane;* presented at the Annual Summer Meeting of the Institute of the Aeronautical Sciences, July, 1944.

Simplified Treatment of the Turbulent Boundary Layer Along a Cylinder in Compressible Flow

(*Continued from page 28*)

[2] Tetervin, N., *Approximate Formulas for the Computation of Turbulent Boundary-Layer Momentum Thicknesses in Compressible Flows*, N.A.C.A. A.C.R. No. L6 A 22, 1946.

[3] Kurzweg, H., *A Few Aspects of Future Supersonic Windtunnel Design and Test Techniques*, Symposium on Experimental Compressible Flow, U.S. N.O.L., White Oak, Md. NOLR 1133, pp. 103–119, 1949. Also, *Interrelationship Between Boundary Layer and Base Pressure*, Journal of the Aeronautical Sciences, Vol. 18, No. 11, pp. 743–748, November, 1951.

[4] Chapman, D. R., *An Analysis of Base Pressure at Supersonic Velocities and Comparison with Experiment*, N.A.C.A. T.N. No. 2137, 1950.

[5] Jakob, M., and Dow, W. N., *Heat Transfer from Cylindrical Surfaces to Air in Parallel Flow with and Without Unheated Starting Section*, Transactions of the A.S.M.E., Vol. 68, No. 2, pp. 123–134, 1946.

[6] Wilson, R. E., Young, E. C., and Thompson, M. J., *2nd Interim Report on Experimental Determination of Turbulent Boundary Layer Characteristics at Supersonic Speeds*, Defense Research Lab., Univ. of Tex. Report CM-501, DRL-196, 1949.

[7] Rubesin, M. W., Maydew, R. C., and Varga, S. A., *An Analytical and Experimental Investigation of the Skin Friction of the Turbulent Boundary Layer on a Flat Plate at Supersonic Speeds*, N.A.C.A. T.N. No. 2305, 1951.

[8] Wilson, R. E., *Turbulent Boundary-Layer Characteristics at Supersonic Speeds—Theory and Experiment*, Journal of the Aeronautical Sciences, Vol. 17, No. 9, pp. 585–594, September, 1950.

[9] Schultz-Grunow, F., *Neues Reibungswiderstandsgesetz fuer glatte Platten*, Luftfahrtforschung, Vol. 17, pp. 239–246, 1940. (Translation, N.A.C.A. T.M. No. 986.)

[10] Spivack, H. M., *Experiments in the Turbulent Boundary Layer of a Supersonic Flow*, North American Aviation Report CM-615, 1950.

[11] Seban, R. A., and Bond, R., *Skin Friction and Heat Transfer Characteristics of a Laminar Boundary Layer on a Cylinder in Axial Flow*, Univ. of Calif. Contract No. W33(038)-ac-15229 with the A.A.F., A.M.C., 1949. Also, Journal of the Aeronautical Sciences, Vol. 18, No 10, pp. 671–675, October, 1951.

[12] von Kármán, Th., *Ueber laminare und turbulente Reibung*, Zeitschrift fuer angewandte Mathematik und Mechanik 1, pp. 233–252, 1921. (Translation, N.A.C.A. T.M. No. 1092.)

Velocity and Temperature Distribution Through the Laminar Boundary Layer in Supersonic Flow*

CARLO FERRARI†

Cornell Aeronautical Laboratory, Inc.

SUMMARY

The laminar boundary layer in a compressible gas is studied in order to obtain the velocity and temperature distributions through the layer in the presence of any pressure distribution whatsoever for the external flow, under the usual assumptions that the pressure is constant through the layer and that the temperature of the constraining surface is constant throughout its extent. The contour of this surface is supposed to be so gently turning that the surface elements may always be considered aligned with the free-stream flow.

The method described is well suited for routine computations. Even though it makes use of successive approximations, only one extensive recomputation is required; after the second approximation is obtained, further approximations, if desired, are carried out by means of short cuts that reduce the labor involved to less than one-tenth of that required in the first recomputation.

A significant effect of scale on the pressure changes in the potential flow exterior to the boundary layer is observed, although the magnitude of the changes in these external pressures is small in the example selected for numerical illustration of the theory. The numerical example shows the progressive change in profile shape up to the point where imminent separation can be expected. Tables and aids to calculation are provided, along with the numerical example.

INTRODUCTION

THIS REPORT DEALS WITH A NEW METHOD for the determination of the velocity and temperature through the laminar boundary layer in supersonic fluid flow. This method is related to one expounded by von Kármán and Tsien[1] and to the ideas suggested by Feinsilber,[2] but the present treatment may be applied to a compressible gas, and it holds for any kind of pressure variation along the boundary in the external stream.

The method discussed here is actually one involving the technique of successive approximations. The degree of approximation associated with the solution desired in this investigation, however, may be considered as more than adequate for practical purposes. The procedure described is, besides, well suited for routine evaluations because of the fact that the numerical values of the functions entering the final formulas have already been tabulated in standard works.

The assumptions upon which this method is based are the same as those that have been employed previously in similar investigations. For instance, it is taken to be permissible to use the "simplified" equations of the boundary layer in order to describe the viscous flow therein, and, hence, it is implied that the static pressure is constant throughout every cross section. The experimental results of Ackeret, Feldmann, and Rott[3] controvert this assumption, of course, more and more as the particular cross section under consideration is selected closer and closer to the one at which the shock wave starts.

Such an assumption of constant pressure, on the other hand, does not preclude the derivation of a formula from which it is possible to deduce how the pressure within the stream external to the boundary layer is modified by the presence of the boundary layer itself.

In a preceding report of this series,[4] it has been shown how, in the case where the Prandtl Number is taken to be unity, the problem can be solved approximately through use of a step-by-step procedure by means of which the pressure variation through the cross section is taken into account at each step of the calculation processes.

Further, it is assumed here, even as was done in the above-mentioned report, that the thermal conductivity of the wetted wall is infinite (so that the temperature of the wall is constant over its whole length), and, in addition, the curvature of the wall is taken to be so small that its surface elements may be considered coincident in direction with the x-axis and the outward normal to be in the direction of the y-axis.

A numerical example is presented to illustrate the application of the suggested method, and the necessary tables employed in the computations are also appended.

PRELIMINARY CONCEPTS

(1) *Symbols*

U = component of the velocity along the x-axis
V = component of the velocity along the y-axis
V_l = limit velocity attained by the free stream when expanded to a vacuum
U_∞ = velocity of the undisturbed stream

Received May 27, 1951. Extended version of manuscript submitted to Cornell Aeronautical Laboratory, Inc., December 20, 1949.

* This research was conducted under Navy BuOrd sponsorship.

† Member of the Cornell Aeronautical Laboratory consulting staff. Professor, Laboratorio di Aeronautica, Politecnico di Torino.

U_e = velocity of the stream on the outer edge of the boundary (for all intents and purposes, this vector is taken to be parallel to the x-axis)
$u = U/V_l$; $v = V/V_l$; $u_e = U_e/V_l$; $u_\infty = U_\infty/V_l$
ρ = density of the fluid; ρ_e = density of the fluid in the external stream; ρ_∞ = density of the fluid in the undisturbed stream; ρ_p = density of the fluid in contact with the wall
p = pressure
T = absolute temperature
μ = viscosity coefficient
ν = kinematic viscosity coefficient

The above symbols with subscripts e, ∞, and p have analogous meanings to those given for ρ.

L = length of the wall; $\xi = x/L$; $\eta = y/L$
R_∞ = Reynolds Number of the asymptotic stream (undisturbed flow at infinity) = $U_\infty L/\nu_\infty$; $\eta^* = \eta\sqrt{R_\infty}$
ψ = stream function (dimensions of a viscosity coefficient)
$\psi_1 = \psi/(\rho_\infty U_\infty L)$; $\psi_1^* = \psi_1\sqrt{R_\infty}$
$z = \mu/\mu_e$; $z_1 = 1 - z$
$Z = (u_e^2/2u_\infty^2) - (u^2/2u_\infty^2)$; $Z_e = u_e^2/2u_\infty^2$; and $\zeta = Z_e - Z = u^2/2u_\infty^2$
c_p = specific heat at constant pressure
γ = adiabatic exponent (= 1.4 for air)
P_r = Prandtl Number (= 0.75 for air)
n = a coefficient defined by $\mu/\mu_e = (T/T_e)^n$ (n = 0.75 for air)

Other symbols are specified in the text.

(2) *General Equations*

On the basis of the fundamental assumption concerning the constancy of the pressure as mentioned in the introduction, the equations defining the flow within the boundary layer are as follows:

Equation of motion:

$$\rho U\frac{\partial U}{\partial x} + \rho V\frac{\partial U}{\partial y} = -\frac{dp}{dx} + \frac{\partial}{\partial y}\left(\mu\frac{\partial U}{\partial y}\right) = \rho_e U_e\frac{dU_e}{dx} + \frac{\partial}{\partial y}\left(\mu\frac{\partial U}{\partial y}\right) \tag{1}$$

Energy equation:

$$c_p\left(\rho U\frac{\partial T}{\partial x} + \rho V\frac{\partial T}{\partial y}\right) = U\frac{dp}{dx} + \frac{c_p}{P_r}\frac{\partial}{\partial y}\left(\mu\frac{\partial T}{\partial y}\right) + \mu\left(\frac{\partial U}{\partial y}\right)^2$$
$$= -UU_e\rho_e\frac{dU_e}{dx} + \frac{c_p}{P_r}\frac{\partial}{\partial y}\left(\mu\frac{\partial T}{\partial y}\right) + \mu\left(\frac{\partial U}{\partial y}\right)^2 \tag{2}$$

The continuity equation is satisfied by writing

$$\left.\begin{aligned}\rho u &= \rho_\infty u_\infty\,(\partial\psi_1/\partial\eta)\\ \rho v &= -\rho_\infty u_\infty\,(\partial\psi_1/\partial\xi)\end{aligned}\right\} \tag{3}$$

Through the use of the transformation previously employed by von Mises,[5] and by letting

$$z = \mu/\mu_e \tag{4}$$

where

$$z = (T/T_e)^n; \qquad \rho/\rho_e = T_e/T = z^{-1/n} \tag{5}$$

and

$$\xi_1 = \int_0^\xi \frac{\mu_e\rho_e}{\mu_\infty\rho_\infty}\,d\xi; \qquad \psi_1^* = \sqrt{R_\infty}\psi_1 \tag{6}$$

while also

$$\left.\begin{aligned}Z &= (u_e^2/2u_\infty^2) - (u^2/2u_\infty^2)\\ Z_e &= u_e^2/2u_\infty^2\end{aligned}\right\} \tag{6'}$$

then from Eq. (1), one obtains

$$\partial Z/\partial\xi_1 = (u/u_\infty)\,(\partial/\partial\psi_1^*)\,[z^{(n-1)/n}(\partial Z/\partial\psi_1^*)] + [(1 - z^{1/n})(dZ_e/d\xi_1)] \tag{7}$$

Applying the von Mises transformation to Eq. (2), one obtains in an analogous manner:

$$\partial z/\partial\xi_1 = (1/P_r)\,(1 - z_1)^{(n-1)/n} \times (\partial/\partial\psi_1^*)[(u/u_\infty)\,(\partial z_1/\partial\psi_1^*)] - z^{(2n-2)/n}(nu_\infty/u) \times [2u_\infty^2/(1 - u_e^2)](\partial Z/\partial\psi_1^*)^2 \tag{8}$$

where $z_1 = 1 - z$. The boundary conditions are:
For Eq. (7):

$$Z = Z_e \text{ for } \psi_1^* = 0; \qquad Z = 0 \text{ for } \psi_1^* = \infty \tag{7'}$$

For Eq. (8):

$$\left.\begin{aligned}z_1 &= 1 - (T_p/T_e)^n \text{ for } \psi_1^* = 0\\ z_1 &= 0 \text{ for } \psi_1^* = \infty\end{aligned}\right\} \tag{8'}$$

wherein T_p, the constant temperature at the wall, is supposed to be known for this phase of the calculations.

Solutions of the Transformed Equations

(3) *External Solution of the Equation Derived from the Equation of Motion Through Use of von Mises Transformation*

Within the boundary-layer region, but near the external stream, it is permissible to write

$$\partial Z/\partial\psi_1^* = z_1 = 0 \qquad \text{and } u/u_\infty = u_e/u_\infty \tag{9}$$

and letting

$$\xi_1^{**} = \frac{1}{P_r}\int_0^{\xi} \frac{u_e}{u_\infty}\, d\xi_1 \tag{10}$$

it follows from Eq. (8) that

$$\partial z_1/\partial\xi_1^{**} = \partial^2 z_1/\partial\psi_1^{*2} \tag{11}$$

which is identical to the equation of heat conduction within a medium having unit diffusivity. Let

$$(z_1)_{\psi_1^*=0} = z_{1,p} = \sum_m A_m \xi_1^{**m} \tag{12}$$

then the integral of Eq. (11) which satisfies condition (8′) is

$$z_1 = \sum_m A_m 2^{2m} m!\, \xi_1^{**m}\, i^{2m} \operatorname{erfc}\left[\psi_1^*/(2\sqrt{\xi_1^{**}})\right] \tag{13}$$

(4) *External Solution of the Equation Derived from the Energy Relation Through Means of the von Mises Transformation*

In order to determine the external solution of Eq. (7), the result just obtained as Eq. (13) will be used directly. Within the region of the boundary layer now under consideration, one may take $z^{(n-1)/n}$ ($= z^{-1/3}$ for air) to be constant, because it varies but slightly within the layer. In fact, there can be no objection to selection of this constant as precisely unity. In addition, letting $u/u_\infty = u_e/u_\infty$, Eq. (7) may be written in the form

$$\partial Z/\partial\xi_1 = (u_e/u_\infty)\,(\partial^2 Z/\partial\psi_1^{*2}) + (1 - z^{1/n})\,(dZ_e/d\xi_1)$$

or also, if we set

$$\xi_1^* = P_r\xi_1^{**} \tag{14}$$

then

$$\partial Z/\partial\xi_1^* = (\partial^2 Z/\partial\psi_1^{*2}) + (1 - z^{1/n})\,(dZ_e/d\xi_1^*)$$

Expanding $1 - z^{1/n}$ in a power series in the neighborhood of $z = 1$ and retaining the first degree term only, one obtains

$$\frac{\partial Z}{\partial\xi_1^*} = \frac{\partial^2 Z}{\partial\psi_1^{*2}} + \frac{1}{n} z_1 \frac{dZ_e}{d\xi_1^*} = \frac{\partial^2 Z}{\partial\psi_1^{*2}} + F \tag{15}$$

Let

$$Z_e = \sum_m B_m \xi_1^{*m} \tag{16}$$

then Eq. (13) yields

$$F = \frac{1}{n}\sum_m A_m 2^{2m} m!\, \xi_1^{**m}\left[i^{2m}\operatorname{erfc}\frac{\psi_1^*}{2\sqrt{\xi_1^{**}}}\right]\sum_s sB_s\xi_1^{*(s-1)} = \sum_m C_m\xi_1^{*m}\left[i^{2m}\operatorname{erfc}\frac{\psi_1^*\sqrt{P_r}}{2\sqrt{\xi_1^*}}\right]\sum_s B_s{}^1\xi_1^{*(s-1)} \tag{17}$$

wherein

$$\left.\begin{aligned} C_m &= (A_m/n)\, 2^{2m} m!\, (1/P_r{}^m) \\ B_s{}^1 &= sB_s \end{aligned}\right\} \tag{18}$$

Thus, it appears feasible to write

$$F = \sum_m \xi_1^{*m}\left[C_0 B^1{}_{m+1} + C_1 B_m{}^1\, i^2 \operatorname{erfc}\frac{\psi_1^*\sqrt{P_r}}{2\sqrt{\xi_1^*}} + C_2 B^1{}_{m-1}\, i^4 \operatorname{erfc}\frac{\psi_1^*\sqrt{P_r}}{2\sqrt{\xi_1^*}} + \ldots + C_m B_1{}^1 i^{2m} \operatorname{erfc}\frac{\psi_1^*\sqrt{P_r}}{2\sqrt{\xi_1^*}}\right] \tag{19}$$

Now return to consideration of Eq. (15). Applying to it the Laplace transform with respect to the variable ξ_1^*, one obtains

$$(d^2\bar{Z}/d\psi_1^{*2}) - p\bar{Z} = -\bar{F} \tag{20}$$

in which

$$\left.\begin{aligned} \bar{Z} &= L(Z) = \int_0^\infty e^{-p\xi_1^*} Z\, d\xi_1^* \\ \bar{F} &= L(F) \end{aligned}\right\}$$

The Laplace transform of such an expression as $\xi_1^{*r} i^{2r} \operatorname{erfc}\left[\psi_1^*\sqrt{P_r}/(2\sqrt{\xi_1^*})\right]$ is discussed in Appendix V of *The Conduction of Heat in Solids* by Carslaw and Jaeger. Using this result, it is noted that

$$L\left\{\xi_1^{*m} i^{2r} \operatorname{erfc}\left[\psi_1^*\sqrt{P_r}/(2\sqrt{\xi_1^*})\right]\right\} = \left[(-1)^{m-r}/4^r\right]\,(d^{m-r}/dp^{m-r})\,(e^{-\psi_1^* q}/p^{1+r}) \tag{21}$$

for $m > r$ and wherein $q = \sqrt{P_r p}$. It follows that $-F$ turns out to be a summation of terms of the type

$$C_{t,g}{}^*\,(e^{-q\psi_1^*}/p^{1+t/2})\psi_1^{*g} \tag{22}$$

where g and t are positive integers. It follows that one may write

$$\bar{Z} = \sum_{t,g} \bar{Z}_{t,g} \tag{23}$$

wherein $\bar{Z}_{t,g}$ is defined by

$$(d^2\bar{Z}_{t,g}/d\psi_1{}^{*2}) - p\bar{Z}_{t,g} = C_{t,g}{}^*\psi_1{}^{*g}\,(e^{-q\psi_1{}^*}/p^{1+t/2}) \quad (24)$$

$$\bar{Z}_{t,g} = 0 \quad (25)$$

where the conditions that for $\psi_1{}^* = 0$, as well as for $\psi_1{}^* = \infty$ must be kept in mind.

One deduces, consequently, that

$$\bar{Z}_{t,g} = \frac{C_{t,g}{}^*}{2p^{(3/2)+(t/2)}}\frac{1}{q[1-(1/\sqrt{P_r})]}\left[e^{-q\psi_1{}^*}\sum_{h=0}^{g} h!\binom{g}{h}\frac{\psi_1{}^{*g-h}}{q^h[1-(1/\sqrt{P_r})]^h} - \frac{e^{-\sqrt{p}\psi_1{}^*}\,g!}{q^g[1-(1/\sqrt{P_r})]^g}\right]$$

$$= \frac{C_{t,g}{}^*}{2(\sqrt{P_r}-1)p^{(2+t/2)}}\left[e^{-q\psi_1{}^*}\sum_{h=0}^{g} h!\binom{g}{h}\frac{\psi_1{}^{*g-h}}{(\sqrt{P_r}-1)^h p^{h/2}} - \frac{e^{-\sqrt{p}\psi_1{}^*}}{p^{g/2}(\sqrt{P_r}-1)^g}\,g!\right] \quad (26)$$

Then noting that

$$L^{-1}\left(\frac{e^{-q\psi_1{}^*}}{p^{1+[(2+t+h)/2]}}\right) = (4\xi_1{}^*)^{(2+t+h)/2}\,i^{2+t+h}\,\mathrm{erfc}\,\frac{\psi_1{}^*\sqrt{P_r}}{2\sqrt{\xi_1{}^*}}$$

and

$$L^{-1}\,(e^{-\sqrt{p}\psi_1{}^*}/p^{1+[(2+t+g)/2]}) = (4\xi_1{}^*)^{(2+t+g)/2}\,i^{2+t+g}\,\mathrm{erfc}\,[\psi_1{}^*/(2\sqrt{\xi_1{}^*})] \quad (27)$$

one obtains

$$Z_{t,g} = \frac{C_{t,g}{}^*}{2(\sqrt{P_r}-1)}\left[\sum_{h=0}^{g}\frac{h!\binom{g}{h}\psi_1{}^{*g-h}}{(\sqrt{P_r}-1)^h}(4\xi_1{}^*)^{(2+t+h)/2}\,i^{(2+t+h)}\mathrm{erfc}\frac{\psi_1{}^*\sqrt{P_r}}{2\sqrt{\xi_1{}^*}} - \frac{g!}{(\sqrt{P_r}-1)^g}(4\xi_1{}^*)^{(2+t+g)/2}\times\right.$$

$$\left. i^{2+t+g}\,\mathrm{erfc}\frac{\psi_1{}^*}{2\sqrt{\xi_1{}^*}}\right] = \frac{C_{t,g}{}^*}{2(\sqrt{P_r}-1)}\left[\sum_{h=0}^{g}\frac{h!\binom{g}{h}\left(\frac{\psi_1{}^*}{2\sqrt{\xi_1{}^*}}\right)^{g-h}}{(\sqrt{P_r}-1)^h}(4\xi_1{}^*)^{(2+t+h)/2}\,i^{(2+t+h)}\,\mathrm{erfc}\,\frac{\psi_1{}^*\sqrt{P_r}}{2\sqrt{\xi_1{}^*}} - \right.$$

$$\left.\frac{g!}{(\sqrt{P_r}-1)^g}(4\xi_1{}^*)^{(2+t+g)/2}\,i^{2+t+g}\,\mathrm{erfc}\,\frac{\psi_1{}^*}{2\sqrt{\xi_1{}^*}}\right] \quad (28)$$

The expression for Z which satisfies Eq. (15), and which, for $\psi_1{}^* = 0$, coincides with the Z_e given by Eq. (16) is therefore

$$Z = \sum_m B_m 2^{2m} m!\,\xi_1{}^{*m} i^{2m}\,\mathrm{erfc}\,\frac{\psi_1{}^*}{2\sqrt{\xi_1{}^*}} + \sum_{t,g} Z_{t,g} \quad (29)$$

Thus, for example, in the most simple case in which

$$Z_e = B_0 + B_1\xi_1{}^* \quad (16')$$

one has

$$Z = B_0\,\mathrm{erfc}\,\frac{\psi_1{}^*}{2\sqrt{\xi_1{}^*}} + B_1 4\xi_1{}^* i^2\,\mathrm{erfc}\,\frac{\psi_1{}^*}{2\sqrt{\xi_1{}^*}} + \sum_{t=0,\,2,\,4,\,\ldots} C_{t,0}{}^*\frac{(4\xi_1{}^*)^{1+t_1}}{2(\sqrt{P_r}-1)}\times$$

$$\left[i^{2(1+t_1)}\mathrm{erfc}\,\frac{\psi_1{}^*\sqrt{P_r}}{2\sqrt{\xi_1{}^*}} - i^{2(1+t_1)}\,\frac{\psi_1{}^*}{2\sqrt{\xi_1{}^*}}\right] \quad (29')$$

wherein $t_1 = t/2$, and

$$C_{t,0}{}^* = 0 \qquad \text{for } t = 1,\,3,\,5,\,\text{etc.}$$
$$C_{t,0}{}^* = -(1/4^{t_1})\,(A_{t_1}/n)\,(2^{2t_1}\,t_1!\,B_1/P_r{}^{t_1}) \qquad \text{for } t = 0,\,2,\,4,\,\text{etc.} \quad (30)$$

(5) *Internal Solution of the Equation Derived from the Energy Relation Through Means of the von Mises Transformation*

In proximity to the solid wall (where $\psi_1{}^* = 0$), Eq. (7) may be written in the form

$$\frac{\partial Z}{\partial\xi_1} = \left\{(u/u_\infty)\,[(n-1)/n]z^{[(n-1)/n]-1}(\partial z/\partial\psi_1{}^*)\right\}_{\psi_1{}^*=0}(\partial Z/\partial\psi_1{}^*) + (u/u_\infty)z_p{}^{(n-1)/n}(\partial^2 Z/\partial\psi_1{}^{*2}) +$$

$$(1 - z_p{}^{1/n})(dZ_e/d\xi_1) \quad (31)$$

But it is true that

$$\left\{(u/u_\infty)\,[(n-1)/n]z^{[(n-1)/n]-1}(\partial z/\partial\psi_1^*)\right\}_{\psi_1^*=0} = [(n-1)/n](\rho_\infty/\rho_e)\,(\partial z/\partial\eta^*)_{\eta^*=0} \tag{32}$$

Now this term vanishes for $n = 1$, whatever the heat exchange ΔQ through the wall happens to be, and it vanishes as well for the case in which $P_r = 1$, regardless of the magnitude of n, if there is no heat exchange ($\Delta Q = 0$). Therefore, it seems allowable, in the case in which $\Delta Q = 0$, for fluids that, like air, have values of n and P_r both close to unity, to disregard the term within brackets. In the general case, we may still consider this term to be so small as to permit, without appreciable error, the substitution of the constant value taken on at the wall by the derivative $\partial Z/\partial\psi_1^*$ for the actually variable value of this quantity. Consequently, one may substitute into Eq. (31) the expression

$$[\,]_{\psi_1^*=0}\frac{\partial Z}{\partial\psi_1^*} \cong \left(\frac{\partial Z}{\partial\psi_1^*}\right)_{\psi_1^*=0}\,[\,]_{\psi_1^*=0} = D_0 Y_0$$

wherein

$$\left.\begin{aligned} D_0 &= [(1-n)/n]\,(\rho_\infty/\rho_e)\,(\partial z/\partial\eta^*)_{\eta^*=0} \\ Y_0 &= -(\partial Z/\partial\psi_1^*)_{\psi_1^*=0} \end{aligned}\right\} \tag{33}$$

In the development given below, the solution of Eq. (31) is obtained by following a procedure analogous to that applied by von Kármán[6] to the study of the same problem in the case of incompressible flow. Let

$$\zeta = Z_e - Z \tag{34}$$

then Eq. (31) yields

$$\partial^2\zeta/\partial\psi_1^{*2} = -(1/\sqrt{2})\,(1/\sqrt{\zeta})\,(z_p^{1/n}/z_p^{(n-1)/n})(dZ_e/d\xi_1^*)\,\sqrt{2}\sqrt{Z_e} + [1/(\sqrt{2}z_p^{(n-1)/n})]\,(1/\sqrt{\zeta})\,[(\partial\zeta/\partial\xi_1^*)\sqrt{2}Z_e + D_0 Y_0] \tag{31'}$$

Analogously to what was done by von Kármán in the above-mentioned report,[6] the latter equation is replaced by

$$\partial^2\zeta/\partial\psi_1^{*2} = (A^*/\sqrt{\zeta})\,[1 - \sqrt{\zeta/\zeta_f}] \tag{31''}$$

wherein

$$A^* = A_0^*(1 + Y_0 A_1^*); \qquad A_0^* = -(Z_e^{1/2}Z_e' z_p^{1/n})/z_p^{(n-1)/n}; \qquad A_1^* = D_0(1/\sqrt{2})\,[1/(z_p^{1/n}Z_e')]; \quad Z_e' = dZ_e/d\xi_1^* \tag{35}$$

while ζ_f denotes the value of ζ which corresponds to the inflection point in the graph of ζ vs. $\psi_1^*/(2\sqrt{\xi_1^*})$ obtained from the internal solution. From Eq. (31''), one deduces that

$$\psi_1^* = (\sqrt{\zeta_f}/A^*)[Y_0 - \sqrt{Y_0^2 + 4A^*\sqrt{\zeta - 2A^*(\zeta/\sqrt{\zeta_f})}}] + (\sqrt[4]{4\zeta_f^3}/\sqrt{A^*}) \times \left\{\arcsin\,(2A^*/\sqrt{4A^{*2} + 2Y_0^2A^*/\sqrt{\zeta_f}}) - \arcsin\,[(2A^* - 2A^*\sqrt{\zeta/\zeta_f})/\sqrt{4A^{*2} + 2Y_0^2A^*/\sqrt{\zeta_f}}]\right\} \tag{36}$$

---

(6) *Join Between the External and Internal Solution of Eq. (7)*

The connection between the solution given by Eq. (36) and the one represented by Eq. (29) is made by following the same procedure as that suggested by von Kármán.[6] From the graph of ζ vs. $\psi_1^*/(2\sqrt{\xi_1^*})$, plotted through means of Eq. (29) for the various parametric values of ξ_1^*, the value of

$$H = -\left\{(\partial Z/\partial[\psi_1^*/(2\sqrt{\xi_1^*})]\right\}[1/(\sqrt{\xi_1^*})]_{\zeta=\zeta_f} \tag{37}$$

is determined.

Hence, by imposing the condition that, for $\zeta = \zeta_f$, the value of $\partial\zeta/\partial\psi_1^*$ given by Eq. (36) must be exactly equal to H, one obtains the condition that

$$H^2 = Y_0^2 + 2A^*\sqrt{\zeta_f} = Y_0^2 + 2\sqrt{\zeta_f}\,A_0^*\,(1 + Y_0 A_1^*) \tag{37'}$$

This relationship permits one to evaluate Y_0. Then, for each ξ_1^*, Eq. (36) gives the value of ψ_1^* in terms of ζ, provided that D_0—that is, $[(\partial z/\partial\eta^*)]_{\eta^*=0}$—is known. The *complete* diagram of ζ in terms of $\psi_1^*/(2\sqrt{\xi_1^*})$, at every given cross section of the boundary, $\xi_1^* = \text{const.}$, is now determined, because for the interval $0 \leq \zeta \leq \zeta_f$, it is given by Eq. (36), and for the interval $\zeta_f \leq \zeta \leq Z_e$, it is defined by Eq. (29).

Detailed Procedures of Solution

(7) *Second Approximation for the Temperature Distribution—i.e., the Law of Variation of the z Values*

In order to determine a second approximation for the distribution of z through the boundary layer, one may proceed as follows. Rewrite Eq. (8) in the form

$$(u/u_\infty)z^{-2(n-1)/n}(\partial z_1/\partial\xi_1) = (1/P_r)\,(u/u_\infty)\,(1 - z_1)^{-(n-1)/n}(\partial/\partial\psi_1^*)\,[(u/u_\infty)\,(\partial z_1/\partial\psi_1^*)] - n[2u_\infty^2/(1 - u_e^2)]\,[\partial Z/\partial\psi_1^*]^2 \quad (8'')$$

Then let

$$F(z) = \int_0^z z^{1/n}dz = \frac{n}{n+1}\,z^{(n+1)/n} \quad (38)$$

and so, Eq. (8″) becomes

$$\partial^2 F/\partial\eta^{*2} = -2nP_r\,[2u_\infty^2/(1 - u_\infty^2)]z\,[(\partial/\partial\eta^*)\sqrt{Z_e - Z}]^2 - P_r(\rho_e/\rho_\infty)^2\,2\sqrt{Z_e}\sqrt{Z_e - Z}\,(1 - z_1)^{-1}\times(\partial z_1/\partial\xi_1^*) = \phi \quad (39)$$

In addition, Eq. (3) may be recast as

$$\eta^* = \int^{\psi_1^*}\frac{\rho_\infty U_\infty}{\rho U}\,d\psi_1^* = \frac{2\sqrt{\xi_1^*}}{\sqrt{2}}\,\frac{\rho_\infty}{\rho_e}\int_0^{\psi_1^*/(2\sqrt{\xi_1^*})}\frac{z^{1/n}}{(Z_e - Z)^{1/2}}\,d\,\frac{\psi_1^*}{2\sqrt{\xi_1^*}} \quad (40)$$

The forms of Eqs. (40) and (39) now suggest a procedure of successive approximations for the determination of the manner in which z varies within the layer. If one introduces into the second member of Eq. (40) the value of z obtained from the external solution, considered as a first approximation, then Eq. (40) permits one to obtain η^* in terms of $\psi_1^*/(2\sqrt{\xi_1^*})$, for each value of ξ_1^*. Now evaluate the quantity

$$\frac{\partial}{\partial\eta^*}\sqrt{Z_e - Z} = -\frac{z^{-1/n}}{\sqrt{2}}\left(\frac{\rho_e}{\rho_\infty}\right)\frac{\partial Z}{\partial[\psi_1^*/(2\sqrt{\xi_1^*})]}\,\frac{1}{2\sqrt{\xi_1^*}}$$

by making use of the values of z given by the external solution. One is then able to evaluate ϕ in terms of η^*, and, hence, obtains

$$F = \int_0^{\eta^*}d\eta^*\int_0^{\eta^*}\phi d\eta^* + \phi_{1,0}\,\eta^* + F_0 \quad (41)$$

wherein

$$\phi_{1,0} = (\partial F/\partial\eta^*)_{\eta^*=0} = z_p^{1/n}(\partial z/\partial\eta^*)_{\eta^*=0}$$

and

$$F_0 = (F)_{\eta^*=0} = [n/(n+1)]z_p^{(n+1)/n}$$

Because Eq. (41) permits the evaluation of F, then one has simply that $z = [(n+1)/n]^{n/(n+1)}F^{n/(n+1)}$ as a second approximation for z. It is easy to see that this procedure may be extended in order to obtain further approximations.

(8) *Practical Method for the Determination of the Motion Within the Layer. Evaluation of the Heat Transmission*

The calculations are generally laborious if the amount of heat ΔQ transferred from the fluid to the wall is taken to be a given quantity; they are simplified if one fixes T_p and consequently evaluates ΔQ. In fact, under these conditions, a first approximation to the distribution of the velocity and temperature is determined within the layer by taking $D_0 = 0$ (this value comes nearer to being the true one as n approaches unity). The procedure just outlined permits one to determine the values of $(\partial z/\partial\eta^*)_{\eta^*=0}$ if the above-mentioned assumptions are employed. Once having obtained this temperature gradient, a second approximation for the values of Z and then of z may be deduced if necessary. It should be noted that the values of D_0 affect the internal solution of Z only. It is not necessary, therefore, to repeat the calculations leading to the external solution of Z, which, in fact, are the only laborious ones, in order to obtain a second approximation for z which will be satisfactory throughout the layer.

One obtains finally that

$$\Delta Q = \int_0^1\lambda_p\left(\frac{\partial T}{\partial\eta}\right)_{\eta=0}d\xi = c_p\mu_p T_p\,\frac{P_r}{n}\sqrt{R_\infty}\int_0^1\frac{1}{z_p}\left(\frac{\partial z}{\partial\eta^*}\right)_{\eta^*=0}d\xi \quad (42)$$

corresponding to the selected value of T_p.

If the system is thermally insulated ($\Delta Q = 0$), a first approximation determination of T_p may be made by taking the value of the latter to be that corresponding to the condition for flow along a flat plate $[(\partial p/\partial\xi) = 0]$. In this case, the following equation, describing the law of variation of the temperature, holds:

$$(T - T_p)/T_p = -(P_r/2)\,U^2/(c_pT_p) - [P_r/(80\gamma^2)]\,(1 - P_r)[U^2/(c_pT_p)](U/U_\infty)^2 + \ldots \quad (43)$$

Therefore, it appears that, in the case now being examined, a parabolic law of variation of T/T_p in terms of $U/\sqrt{c_pT_p}$ is valid throughout almost the whole extent of the layer. If one retains only the term

$$(T - T_p)/T_p = -(P_r/2)\,U^2/(c_pT_p) \quad (43')$$

and imposes the condition that Eq. (43′) should blend, for $U = U_\infty$, into the relationship that holds for the external variation of T, which is, of course, $T_\infty/T_0 = 1 - [U_\infty^2/(2c_pT_0)]$, wherein T_0 is the stagnation tem-

TABLE 1
Complete Velocity Distribution Through Boundary Layer for Three Selected Locations

$\frac{\psi_1^*}{2\sqrt{\xi_1^*}}$	ζ $\xi = 0.1$	$2\sqrt{\zeta}$ $\xi = 0.1$	η^* $\xi = 0.1$	ζ $\xi = 0.3$	$\sqrt{2\zeta}$ $\xi = 0.3$	η^* $\xi = 0.3$	ζ $\xi = 0.5$	$2\sqrt{\zeta}$ $\xi = 0.5$	η^* $\xi = 0.5$
0.00	0.000	0.000	0.000	0.000	0.000	0.000	0.000	0.000	0.000
0.05	0.027	0.230	0.420	0.024	0.211	0.712	0.021	0.190	0.921
0.10	0.053	0.327	0.596	0.048	0.304	1.010	0.042	0.277	1.304
0.15	0.080	0.400	0.726	0.072	0.376	1.227	0.064	0.347	1.580
0.20	0.106	0.461	0.833	0.096	0.439	1.404	0.086	0.405	1.805
0.25	0.132	0.514	0.926	0.120	0.491	1.537	0.108	0.466	1.996
0.30	0.158	0.562	1.008	0.144	0.537	1.693	0.130	0.511	2.163
0.35	0.182	0.604	1.082	0.167	0.579	1.816	0.152	0.552	2.314
0.40	0.206	0.642	1.151	0.190	0.617	1.928	0.173	0.589	2.454
0.45	0.229	0.677	1.214	0.212	0.651	2.032	0.195	0.624	2.583
0.50	0.251	0.709	1.273	0.233	0.683	2.130	0.215	0.655	2.703
0.55	0.272	0.735	1.329	0.253	0.712	2.221	0.234	0.685	2.816
0.60	0.292	0.765	1.381	0.273	0.739	2.308	0.253	0.711	2.923
0.65	0.311	0.789	1.431	0.291	0.763	2.390	0.271	0.736	3.024
0.70	0.329	0.811	1.479	0.308	0.785	2.469	0.287	0.758	3.121
0.75	0.345	0.831	1.525	0.324	0.805	2.545	0.303	0.775	3.195
0.80	0.361	0.849	1.569	0.340	0.824	2.617	0.318	0.797	3.284
0.85	0.375	0.866	1.612	0.353	0.841	2.687	0.332	0.814	3.370
0.90	0.388	0.881	1.653	0.366	0.856	2.755	0.344	0.830	3.453
0.95	0.400	0.894	1.693	0.378	0.869	2.821	0.356	0.844	3.534
1.00	0.411	0.906	1.732	0.389	0.882	2.885	0.367	0.856	3.613
1.10	0.429	0.926	1.807	0.407	0.903	3.009	0.385	0.877	3.765
1.20	0.444	0.943	1.880	0.422	0.919	3.128	0.400	0.894	3.911
1.30	0.456	0.955	1.950	0.434	0.932	3.244	0.412	0.908	4.053
1.40	0.465	0.965	2.019	0.444	0.942	3.356	0.421	0.918	4.191
1.50	0.472	0.972	2.085	0.450	0.949	3.466	0.428	0.925	4.326
1.60	0.477	0.977	2.151	0.456	0.955	3.574	0.434	0.931	4.458
1.70	0.481	0.981	2.216	0.459	0.959	3.681	0.437	0.953	4.589
1.80	0.484	0.984	2.281	0.462	0.961	3.787	0.440	0.938	4.719
1.90	0.486	0.986	2.345	0.464	0.963	3.892	0.442	0.940	4.848
2.00	0.487	0.987	2.408	0.465	0.965	3.996	0.443	0.942	4.976

perature of the potential flow external to the layer, then it is found that

$$T_p/T_0 = 1 - (1 - P_r)\, u_\infty^2 \tag{44}$$

GROSS BOUNDARY-LAYER EFFECTS

(9) *Thickness of the Boundary Layer*

The thickness of the boundary layer may be obtained from Eq. (40) by inserting in it, for each ξ, the value of $\psi_1^*/(2\sqrt{\xi_1^*})$, for which $\zeta^{1/2} = 0.997 Z_e^{1/2}$. This value varies but slightly with ξ, and in the numerical example that follows, it is seen to be close to 2.

Thus, it may be presumed that

$$\delta^* = \sqrt{2\xi_1^*}\,\frac{\rho_\infty}{\rho_e}\int_0^2 \frac{z^{1/n}}{\zeta^{1/2}}\,dx \tag{45}$$

wherein

$$x = \psi_1^*/(2\sqrt{\xi_1^*})$$

(10) *Influence of the Boundary Layer on the External Pressure Distribution*

From the continuity equation, one has

$$(\partial/\partial\xi)\,(\rho u) + [(\partial/\partial\psi_1)\,(\rho v)]\,[\rho u/(\rho_\infty u_\infty)] - [(\partial/\partial\psi_1)\,(\rho u)]\,[\rho v/(\rho_\infty u_\infty)] = 0$$

or

$$(\partial/\partial\xi)\,[(\rho/\rho_\infty)\,(u/u_\infty)] + (\rho^2/\rho_\infty^2)\,(u^2/u_\infty^2)\,(\partial/\partial\psi_1)\,(v/u) = 0$$

whence, it results that, within the layer,

$$\left(\frac{v}{u}\right)_\delta - \left(\frac{v}{u}\right)_0 = -\int_0^{(\psi_1)_\delta} \frac{\rho_\infty^2 u_\infty^2}{\rho^2 u^2}\,\frac{\partial}{\partial\xi}\left(\frac{\rho u}{\rho_\infty u_\infty}\right) d\psi_1 = \int_0^{(\psi_1)_\delta} \frac{\partial}{\partial\xi}\left(\frac{\rho_\infty u_\infty}{\rho u}\right) d\psi_1 \tag{46}$$

If the pressure variation due to the change in direction of the velocity is assumed to be that predicted on the basis of linear theory, $(p - p_\infty)/(\rho_\infty U_\infty^2) = (1/\sqrt{M_\infty^2 - 1})\beta$ and if β denotes the angle between $\vec{U}_e$ and $\vec{U}_\infty$, then the change in pressure is given by

$$\frac{\Delta p_e}{\rho_\infty U_\infty^2} = \frac{1}{\sqrt{M_\infty^2 - 1}}\left[\left(\frac{v}{u}\right)_\delta - \left(\frac{v}{u}\right)_0\right] = \frac{1}{\sqrt{M_\infty^2 - 1}}\int_0^{(\psi_1)_\delta} \frac{\partial}{\partial\xi}\left(\frac{\rho_\infty u_\infty}{\rho u}\right) d\psi_1 \tag{47}$$

wherein $\Delta p_e = \bar{p}_e - p_e$, and $\bar{p}_e$ denotes the pressure on the outer edge of the boundary layer when the presence of the latter is taken into account. But it is true that

$$\int_0^{(\psi_1)_\delta} \frac{\partial}{\partial \xi}\left(\frac{\rho_\infty u_\infty}{\rho u}\right) d\psi_1 = \frac{2\sqrt{\xi_1^*}}{\sqrt{R_\infty}} \frac{\mu_e \rho_e u_e}{\mu_\infty \rho_\infty u_\infty} \int_0^{(x)_{\delta^*}} \frac{\partial}{\partial \xi_1^*}\left(\frac{\rho_\infty u_\infty}{\rho u}\right) dx$$

wherein $(x)_{\delta^*}$ is the value of x that corresponds to $\eta^* = \delta^*$. It follows that

$$\frac{\Delta p_e}{\rho_\infty U_\infty^2} = \frac{1}{\sqrt{M_\infty^2 - 1}} \frac{2\sqrt{\xi_1^*}}{\sqrt{R_\infty}} \frac{\mu_e \rho_e u_e}{\mu_\infty \rho_\infty u_\infty} \int_0^{(x)_{\delta^*}} \frac{\partial}{\partial \xi_1^*}\left(\frac{\rho_\infty u_\infty}{\rho u}\right) dx$$

It appears that the influence of the boundary layer on the pressure distribution in the external stream is dependent upon the Reynolds Number; therefore, while in natural scale the influence may be small, under experimental conditions, which usually correspond to smaller Reynolds Numbers, such influence may be appreciable.

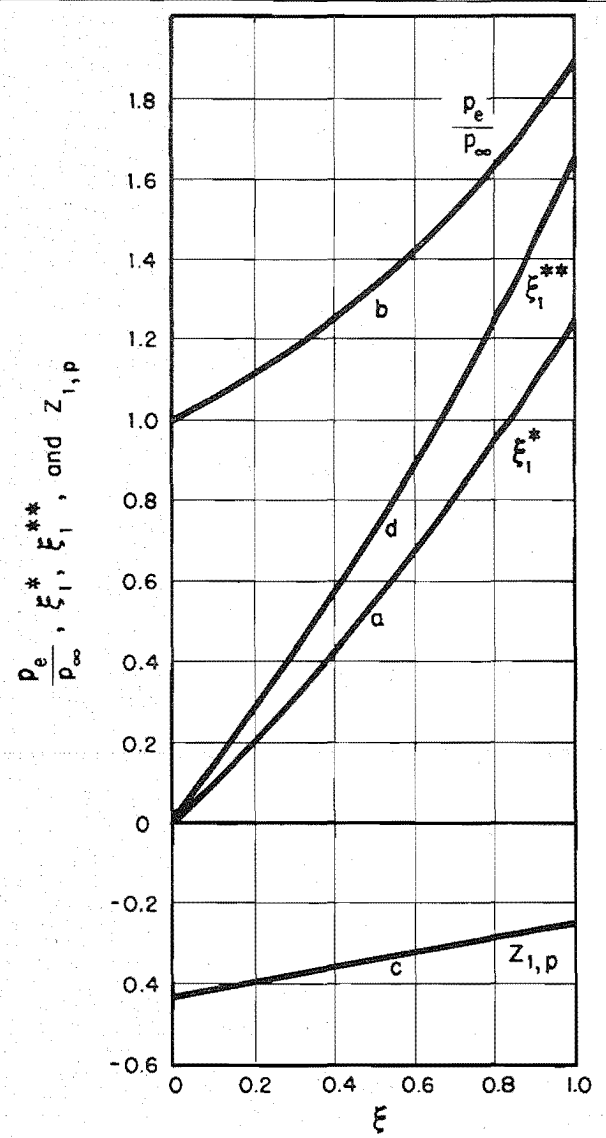

FIG. 1. Successive steps in the numerical procedure of establishing the correspondence between the velocity-related parameter $z_{1,p}$ and the adjusted location along the constraining wall, ξ_1^{**}.

CALCULATED DATA

(11) *Numerical Application*

The procedures described in the preceding paragraphs are now to be applied to the following example.

$$M_\infty = 2$$

whence $u_\infty^2 = 4/9$; $Z_e = 0.5(1 - 0.2\xi_1^*)$; $n = 0.75$; and $P_r = 0.75$.

Only the results of the calculations are presented below. The subsidiary steps are to be found "in extenso" in a Cornell Aeronautical Laboratory report[7] that is available upon request from the Johns Hopkins University, Applied Physics Laboratory.

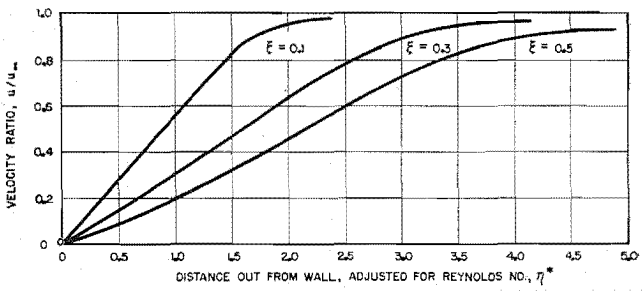

FIG. 2. Complete velocity distribution through the boundary layer at three selected locations.

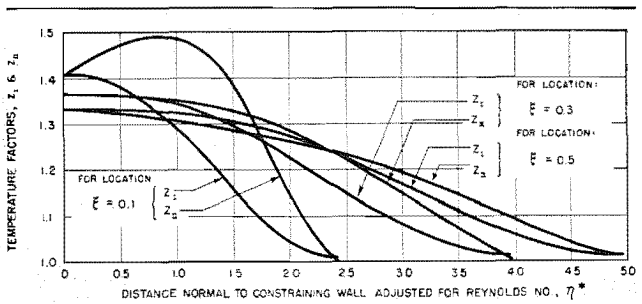

FIG. 3. Comparison of first and second approximations to the temperature profiles encountered at three selected locations spaced along the wetted wall.

TABLE 2
First and Second Approximations to Temperature Factor

$\frac{\psi_1^*}{2\sqrt{\xi_1^*}}$	z_I $\xi = 0.1$	z_{II} $\xi = 0.1$	z_I $\xi = 0.3$	z_{II} $\xi = 0.3$	z_I $\xi = 0.5$	z_{II} $\xi = 0.5$
0.00	1.405	1.405	1.370	1.370	1.337	1.337
0.05	1.386	1.463	1.354	1.353	1.324	1.305
0.10	1.367	1.483	1.338	1.345	1.311	1.291
0.15	1.348	1.493	1.322	1.337	1.297	1.281
0.20	1.329	1.497	1.306	1.330	1.283	1.271
0.25	1.310	1.496	1.289	1.322	1.269	1.262
0.30	1.292	1.492	1.276	1.313	1.255	1.253
0.35	1.274	1.485	1.257	1.304	1.241	1.244
0.40	1.256	1.475	1.241	1.295	1.226	1.235
0.45	1.239	1.464	1.225	1.285	1.212	1.226
0.50	1.222	1.453	1.210	1.275	1.199	1.217
0.55	1.206	1.438	1.196	1.264	1.185	1.208
0.60	1.191	1.422	1.181	1.253	1.172	1.199
0.65	1.176	1.404	1.168	1.242	1.159	1.189
0.70	1.162	1.386	1.154	1.231	1.147	1.180
0.75	1.148	1.368	1.142	1.219	1.135	1.172
0.80	1.135	1.349	1.130	1.208	1.124	1.163
0.85	1.123	1.330	1.118	1.197	1.114	1.154
0.90	1.112	1.310	1.108	1.186	1.104	1.145
0.95	1.101	1.291	1.098	1.174	1.094	1.136
1.00	1.091	1.272	1.088	1.164	1.085	1.127
1.10	1.074	1.235	1.071	1.142	1.069	1.111
1.20	1.059	1.200	1.057	1.123	1.056	1.096
1.30	1.046	1.167	1.045	1.104	1.044	1.081
1.40	1.036	1.137	1.035	1.086	1.034	1.068
1.50	1.027	1.109	1.027	1.070	1.026	1.055
1.60	1.021	1.083	1.020	1.054	1.020	1.042
1.70	1.016	1.060	1.015	1.040	1.015	1.031
1.80	1.011	1.038	1.011	1.026	1.011	1.020
1.90	1.008	1.018	1.008	1.012	1.008	1.010
2.00	1.006	1.000	1.006	1.000	1.006	1.000

Proceeding upon the basis of the above-assumed values, one deduces:

$$T_e/T_\infty = 1.8 - 1.6\,Z_e; \qquad u_\infty/u_e = (1 - 0.2\xi_1^*)^{-1/2}$$

$$\xi = \int_0^{\xi_1^*} (1 + 0.16\xi_1^*)^{-3.25}\,(1 - 0.2\xi_1^*)^{-0.5}\,d\xi_1^*$$

$$p_e/p_\infty = (1.8 - 1.6\,Z_e)^{3.5}$$

Fig. 1 shows the diagrams giving p_e/p_∞, ξ_1^*, ξ_1^{**} in terms of ξ.

From Eq. (44) it follows that $T_p/T_0 = 8/9$, whence

$$T_p/T_e = [1.6/(1.8 - 1.6Z_e)]; \qquad z_{1,\,p} = 1 - [1.6/(1.8 - 1.6Z_e)]^{0.75}$$

From this relationship for $z_{1,\,p}$, one deduces that $z_{1,\,p}$ may be fairly well approximated, in terms of ξ_1^{**}, by the following equation:

$$z_{1,\,p} = \sum_{m=0}^{3} A_m \xi_1^{**m} = -0.4226 + 0.1280\xi_1^{**} - 0.01344\xi_1^{**2} + 0.001479\xi_1^{**3}$$

The complete velocity distribution within the boundary layer, throughout the three cross sections selected as the ones corresponding to locations $\xi = 0.1$, $\xi = 0.3$, and $\xi = 0.5$, is plotted to give the diagrams of Fig. 2, and the values are listed in Table 1.

Fig. 3 and Table 2 give the values of z as a function, respectively, of η^* (distance normal to the constraining wall adjusted for Reynolds Number) and of $\psi_1^*/(2\sqrt{\xi_1^*})$, which is a parameter representing the stream function (nondimensionalized by reference to a viscosity coefficient) that has been "reduced" to account for the value of the local velocity external to the layer. Hence, this curve essentially describes the temperature distribution within the boundary layer as would be calculated as a result of applying the first and then the second approximation procedures to this determination of the temperatures.

It should be remarked that, particularly for cases where $\xi = 0.3$ and $\xi = 0.5$, the values of z obtained as a second approximation are fairly close to those obtained as the first approximation. Consequently, one may safely draw the conclusion that the law of distribution of velocity within the layer as well as the law of variation of the temperature therein, as now obtained in second approximation, is sufficiently accurate. At this point, it should be noted that departure of the true value of z from those assumed as a first approximation has but little influence on the graph of ζ versus $\psi_1^*/(2\sqrt{\xi_1^*})$, so that a continued process of correction would involve solely the redetermination of η^*, which is not a laborious task.

REFERENCES

[1] von Kármán, Th., and Tsien, H. S., *Boundary Layer in Compressible Fluids*, Journal of the Aeronautical Sciences, Vol. 5, No. 6, pp. 227–232, April, 1938.

[2] Feinsilber, A. M., *Reduction of Boundary Layer Equations for Gases to the Type of Thermal Conductivity Equation*, Comptes Rendus (Doklady) de l'Académie des Sciences de l'U.R.S.S., Vol. 51, No. 7, p. 2, 1946.

(*Continued on page 65*)

Computation of the Laminar Boundary Layer with Suction*

FRIEDRICH O. RINGLEB†

Naval Aircraft Factory

SUMMARY

In this paper, the incompressible laminar boundary layer is computed using, as approximate profile for the velocity u tangential to the boundary, an exponential function of a polynomial of the fourth order in y with coefficients that are functions of x. If the velocity outside the boundary layer and the suction (blowing) velocity are given functions of x, the first of those coefficients is determined by an ordinary differential equation of the first order which can be solved by numerical methods in the general case and exactly by simple analytical expressions in many special cases. The other coefficients are determined by elementary functions of the first coefficient and its first derivative. This method, which is convenient and combines high accuracy with uniformity of the procedure, is applied here to the flat plate with and without suction, the stagnation point, the asymptotic suction profile, and some other examples of interest.

NOTATION

x, y	=	coordinates within the boundary layer tangential and normal to the boundary
u, v	=	velocity components in the x- and y-direction within the boundary layer
$p(x)$	=	pressure
$U(x)$	=	velocity outside the boundary layer
$v_0(x)$	=	suction (blowing) velocity
$\tau_0(x)$	=	shear at the boundary
ρ	=	mass density of the fluid
ν	=	kinematic viscosity of the fluid
$a(x)$, $b(x)$, $c(x)$, $d(x)$	=	coefficients of the velocity profile $u = U(1 - e^{ay + by^2 + cy^3 + dy^4})$

INTRODUCTION

THE PRACTICAL VALUE OF boundary-layer suction, especially of continuous (porous) suction in order to diminish the profile drag and to increase the maximum lift, proved by many experiments, led during the last years to a considerable number of investigations about methods for the computation of the laminar boundary layer with and without suction conditions. The literature up to 1938 is discussed in detail in S. Goldstein's *Modern Developments in Fluid Dynamics*, Volume I, Chapter IV. Since that time, a considerable number of papers about the same problem have been published by Schlichting, Falkner, Piercy, Whitehead, Tyler, Thwaites, Trilling, and others.[1–9] Most of these authors are using the momentum equation of the boundary layer. Trilling solved recently the equation in Crocco's form, though in a somewhat complicated manner, by a series of powers of the velocity u with coefficients that are functions of x.

The present paper starts from the boundary-layer equations in the original form (Prandtl) and assumes an approximate profile of the type

$$u = U(1 - e^{a(x)y + b(x)y^2 + c(x)y^3 + d(x)y^4})$$

This choice of the velocity profile is suggested by the following general consideration. It can be assumed that a solution u of the boundary-layer equations can be expanded in the form

$$u = U\left[1 - \exp\left(\sum_{n=1}^{\infty} a_n(x)y^n\right)\right]$$

at least within a neighborhood of $y = 0$ for any x. Replacing now the power series in y by a polynomial in y, satisfying the boundary-layer equations near $y = 0$ as far as possible for the chosen degree of the polynomial, one obtains an approximation near $y = 0$. However, one can expect to obtain in this way, because of the general simplicity of the shape of a velocity profile, even a good approximation for any value $y > 0$ if the coefficient of the highest power in y proves to be negative, because u approaches then the asymptotic value $U(x)$ in an exponential character as it must be expected out of physical reasons and as it is suggested also by the few known correct solutions. Using as degree of the polynomial in y the value 4, one obtains a high accuracy in all well-known examples of the boundary-layer theory not only near $y = 0$ but for every $y > 0$. Another reason for the choice of this velocity profile was the fact that it does not offer particular mathematical difficulties for the computation as normally connected with suction problems especially. Therefore, this method seems to be well suited for theoretical and practical use, combining high accuracy with conceptional simplicity.

(1) DETERMINATION OF THE COEFFICIENTS OF THE ASSUMED VELOCITY PROFILE

The boundary-layer equations in the original form are

Received June 15, 1951.

* Report to the Office of Naval Research, Washington, D.C.

† Research Scientist.

$$\left.\begin{aligned} u\frac{\partial u}{\partial x} + v\frac{\partial u}{\partial y} &= -\frac{p'(x)}{\rho} + \nu\frac{\partial^2 u}{\partial y^2} \\ (\partial u/\partial x) + (\partial v/\partial y) &= 0 \end{aligned}\right\} \tag{1}$$

where u, v are the velocity components of the flow at the point x, y within the boundary layer. $p(x)$ is the given pressure distribution of the flow outside the boundary layer, ρ is the mass density, and ν is the kinematic viscosity of the incompressible fluid. $p'(x)$ means the derivative of $p(x)$ with respect to x.

Outside the boundary layer, Bernoulli's equation

$$UU' + (p'/\rho) = 0 \tag{2}$$

is valid where U is the flow velocity at the border of the boundary layer. If the suction (blowing) velocity along the surface $y = 0$ is denoted by $v_0(x)$, the second of Eqs. (1) yields

$$v = v_0(x) - \int_0^y \frac{\partial u}{\partial x}\,dy$$

and the elimination of p and v from the Eqs. (1) and (2) leads, therefore, to the condition

$$u\frac{\partial u}{\partial x} + \left(v_0(x) - \int^y \frac{\partial u}{\partial x}\,dy\right)\frac{\partial u}{\partial y} - UU' - \nu\frac{\partial^2 u}{\partial y^2} = 0 \tag{3}$$

for u, which may be denoted as the boundary-layer equation.

With $p(x)$ is $U(x)$, a given function. An approximate solution of this equation with the form

$$u = U(1 - e^{ay + by^2 + cy^3 + dy^4}) \tag{4}$$

shall now be determined. Here are $a(x)$, $b(x)$, $c(x)$, $d(x)$ unknown functions of x which are supposed to have continuous derivatives of the first order. It is further supposed that U has a continuous derivative of the second order* and v_0 a continuous derivative of the first order.

The boundary condition $u = 0$ for $y = 0$ is always satisfied by the assumed function [Eq. (4)]. The boundary condition $u = U$ for $y = \infty$ is satisfied if $d < 0$ or, generally, if the coefficient of the lowest power of y which does not vanish is negative. It is then, also, every derivative

$$(\partial^n u/\partial y^n)_{y=\infty} = 0$$

and, further,

$$(\partial u/\partial x)_{y=0} = 0$$

The functions a, b, c, d can be determined by satisfying the boundary-layer equation [Eq. (3)] along $y = 0$ as far as possible. The best way to do this is to differentiate Eq. (3) three times with respect to y. One obtains then, for $y = 0$, inclusive [Eq. (3)], the following four conditions:

$$v_0\frac{\partial u}{\partial y} - UU' - \nu\frac{\partial^2 u}{\partial y^2} = 0$$

$$v_0\frac{\partial^2 u}{\partial y^2} - \nu\frac{\partial^3 u}{\partial y^3} = 0$$

$$\frac{\partial u}{\partial y}\frac{\partial^2 u}{\partial x \partial y} + v_0\frac{\partial^3 u}{\partial y^3} - \nu\frac{\partial^4 u}{\partial y^4} = 0$$

$$2\frac{\partial u}{\partial y}\frac{\partial^3 u}{\partial x \partial y^2} + v_0\frac{\partial^4 u}{\partial y^4} - \nu\frac{\partial^5 u}{\partial y^5} = 0$$

The derivatives that appear in these equations have to be calculated from Eq. (4) for $y = 0$ and substituted here. Thus, the following four conditions for a, b, c, d are obtained:

$$a^2 + 2b = (1/\nu)(av_0 + U')$$

$$a^3 + 6ab + 6c = (v_0/\nu^2)(av_0 + U')$$

$$a^4 + 12a^2b + 12b^2 + 24ac + 24d = -(1/\nu)(U'a^2 + Uaa') + (v_0^2/\nu^3)(av_0 + U')$$

$$2a[U'(a^2 + 2b) + U(2b' + 2aa')] - v_0(a^4 + 12a^2b + 12b^2 + 24ac + 24d) = \nu[a(a^4 + 12a^2b + 12b^2 + 24ac + 24d) + 8b(a^3 + 6ab + 6c) + 36c(a^2 + 2b) + 96ad]$$

The first three of these equations determine the functions b, c, and d as functions of a:

$$\left.\begin{aligned} 2b &= (1/\nu)(av_0 + U') - a^2 \\ 6c &= \left(\frac{v_0}{\nu^2} - \frac{3a}{\nu}\right)(av_0 + U') + 2a^3 \\ 24d &= -\frac{1}{\nu}(U'a^2 + Uaa') - 6a^4 + \\ &\left(\frac{v_0^2}{\nu^3} - 4a\frac{v_0}{\nu^2} + 12\frac{a^2}{\nu}\right)(av_0 + U') - \frac{3}{\nu^2}(av_0 + U')^2 \end{aligned}\right\} \tag{5}$$

If these values for b, c, d are substituted into the fourth equation, the following condition for a is found:

$$\left(\frac{10v_0}{\nu^2} - 28\frac{a}{\nu}\right)(av_0 + U')^2 + \left(55a^3 - 21\frac{a^2v_0}{\nu} + 5\frac{av_0^2}{\nu^2} - \frac{v_0^3}{\nu^3}\right)(av_0 + U') + \frac{2}{\nu}aU\frac{d}{dx}(av_0 + U') + \left(\frac{v_0}{\nu} - 5a\right)Uaa' - 24\nu a^5 + 5a^4v_0 - a^3\frac{v_0^2}{\nu} = 0 \tag{6}$$

Thus we have the results: *The coefficient $a(x)$ is connected with the outside velocity $U(x)$ of the flow and the suction velocity $v_0(x)$ by the relation (6). The coefficients $b(x)$, $c(x)$, and $d(x)$ are functions of $a(x)$, $U(x)$, and $v_0(x$ according to Eq. (5).*

Eq. (6) is an ordinary differential equation of the first order for a if U and v_0 are given functions. It is also an ordinary differential equation of the first order for v_0 if U and a are considered as given functions.

Now the *shear along the boundary $y = 0$ is given by*

$$\tau_0 = \nu\rho(\partial u/\partial y)_{y=0} = -\nu\rho Ua \tag{7}$$

* This supposition is necessary for the theoretical derivation only. The final result will not contain the second derivative.

Thus, if $U(x)$ and the shear $\tau_0(x)$ are given functions, $a(x)$ is determined by Eq. (7) and the ordinary differential equation of first order [Eq. (6)] for v_0 solves approximately the problem of the determination of the suction (or blowing) velocity that is required in order to produce a given shear $\tau_0(x)$.

A *dimensionless form of Eq. (6)* can be obtained replacing the variables x, v_0, U, and a by the dimensionless variables

$$\left.\begin{aligned} \xi &= x/l, & t &= v_0/\nu a \\ \sigma &= U/l\nu a^2 & \zeta &= (1/l\nu a^2)(dU/d\xi) \end{aligned}\right\} \tag{8}$$

where l is any significant length. The differential equation [Eq. (6)] then becomes

$$2\sigma \frac{d}{d\xi}(t+\zeta) = \varphi_0(\zeta) + \varphi_1(\zeta)t + \varphi_2(\zeta)t^2 + \varphi_3(\zeta)t^3 + t^4 + 2\left(\zeta + \frac{5}{4}t - \frac{5}{4}\right)\left(\frac{d\sigma}{d\xi} - \zeta\right) \tag{9}$$

with

$$\left.\begin{aligned} \varphi_0(\zeta) &= 28\zeta^2 - 55\zeta + 24 \\ \varphi_1(\zeta) &= -10\zeta^2 + 77\zeta - 60 \\ \varphi_2(\zeta) &= -25\zeta + 50 \\ \varphi_1(\zeta) &= \zeta - 15 \end{aligned}\right\} \tag{10}$$

However, this general dimensionless representation is not always convenient. Different dimensionless representations will be applied, therefore, in the following from case to case.

(2) The Laminar Boundary Layer Without Suction

Without suction follows from Eq. (6) because of $v_0 = 0$

$$\frac{2}{\nu}UU'' - \frac{28}{\nu}U'^2 + 55U'a^2 - 24\nu a^4 - \frac{5}{2}U\frac{da^2}{dx} = 0 \tag{11}$$

Therefore, *a^2 is a solution of this Riccati's differential equation if there is no suction.* a^2 being determined, the coefficients b, c, d are obtained from

$$\left.\begin{aligned} 2b &= U'/\nu - a^2 \\ 6c &= -3(U'/\nu)a + 2a^3 \\ 24d &= -\frac{2}{5}\frac{UU''}{\nu^2} + \frac{13}{5}\left(\frac{U'}{\nu}\right)^2 - \frac{6}{5}a^4 \end{aligned}\right\} \tag{12}$$

according to Eq. (5).

For the *flat plate without suction* ($U = \text{const.} = U_0$) Eq. (11) reduces to

$$(5/2)U_0(da^2/dx) + 24\nu a^4 = 0$$

which has the general solution

$$1/a^2 = (48/5)(\nu x/U_0) + C$$

where C is a constant of integration. From Eq. (12) there follows

$$b = -a^2/2, \qquad c = a^3/3, \qquad d = -a^4/20$$

The velocity profile [Eq. (4)] of the boundary layer has, therefore, the form

$$u = U_0(1 - e^{ay - (1/2)(ay)^2 + (1/3)(ay)^3 - (1/20)(ay)^4})$$

If now $x = 0$ is the beginning of the flat plate, the initial condition $u \to U_0$ for $x \to 0$ and every $y > 0$ shows that it has to be $C = 0$. Thus,

$$a = -\sqrt{(5/48)(U_0/\nu x)}$$

The shear along the surface of the plate follows from Eq. (7) and has the value

$$\tau_0 = 0.323\rho U_0^2\sqrt{\nu/U_0 x}$$

Blasius' correct solution yields the numerical constant 0.332, the error therefore being 2.7 per cent.

Let us apply Eq. (11) to the boundary layer of the *stagnation point* where

$$U = U_0(x/l)$$

Eq. (11) then gives

$$\frac{da^2}{d\ln x} = -\frac{56}{5}\frac{U_0}{l\nu} + 22a^2 - \frac{48}{5}\frac{a^4}{U_0/l\nu} \tag{13}$$

Approaching the stagnation point with $x \to 0$, a^2 would become infinite if not $da^2/dx \to 0$. From Eqs. (12) and (4), it would follow that $u = 0$ for $x = 0$ and $y > 0$, which would be a contradiction to the velocity distribution of a stagnation point. Only a constant solution a^2 of Eq. (13) therefore comes into question. The two constant solutions of this equation are

$$(l\nu/U_0)a^2 = 1.529, \qquad (l\nu/U_0)a^2 = 0.763$$

Now there has to be, however,

$$24d = \frac{13}{5}\left(\frac{U_0}{l\nu}\right)^2 - \frac{6}{5}a^4 < 0$$

Thus only

$$a = -1.237\sqrt{U_0/l\nu} \tag{14}$$

The shear

$$\tau_0 = 1.237\rho\frac{\nu U_0}{l}\sqrt{\frac{U_0 l}{\nu}}\left(\frac{x}{l}\right)$$

The correct value of the constant calculated by Hiemenz[10] is 1.233, the error of the approximation being 0.32 per cent. With a, the coefficients b, c, d of the velocity profile are also constants. From Eq. (12) it follows, with Eq. (14), that

$$\left.\begin{aligned} b &= -0.264(U_0/l\nu) \\ c &= -0.0115(U_0/l\nu)^{3/2} \\ d &= -0.00855(U_0/l\nu)^2 \end{aligned}\right\} \tag{15}$$

Setting now

$$\eta = y\sqrt{U_0/l\nu}$$

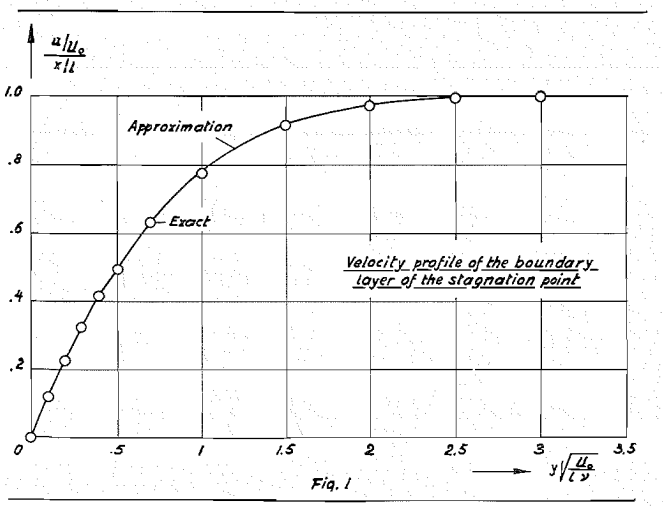

Fig. 1

the velocity profile of the boundary layer becomes

$$u/U_0(x/l) = 1 - e^{-1.237\eta - 0.264\eta^2 - 0.0115\eta^3 - 0.00855\eta^4}$$

This profile is plotted in Fig. 1 as solid curve. Values that Hiemenz obtained by exact computation are indicated by small circles.

The general equation [Eq. (11)] can be simplified considerably. It can be transformed especially into such a type that the second derivative of U disappears, which is convenient for practical applications. This can be done replacing a^2 by the function λ according to

$$a^2 = (\lambda/\nu) + (4/5)(U'/\nu) \tag{16}$$

Eq. (11) then yields, for λ, the condition

$$U\lambda' = 0.256U'^2 + 6.64U'\lambda - 9.6\lambda^2$$

By solving this equation, a^2 and the shear τ_0 [from Eq. (7)] are computable without knowledge of U''. The last coefficient d of the velocity profile, however, requires U'', as follows, from Eq. (12).

This Riccati's equation for λ can be transformed further by the usual substitution

$$\lambda = (U/9.6)(d \ln z/dx) \tag{17}$$

into a linear differential equation of the second order. Replacing the differentiation with respect to x by a differentiation with respect to x/l, and U by U/U_0, this differential equation gets the dimensionless form

$$\frac{d^2z}{d(x/l)^2} - 5.64\frac{d\ln(U/U_0)}{d(x/l)}\frac{dz}{d(x/l)} - 2.4576\left[\frac{d\ln(U/U_0)}{d(x/l)}\right]^2 z = 0 \tag{18}$$

A solution z of this equation yields, because of Eqs. (16) and (17),

$$\frac{lva^2}{U} = \frac{1}{9.6}\frac{d\ln z}{d(x/l)} + \frac{4}{5}\frac{d\ln(U/U_0)}{d(x/l)} \tag{19}$$

If especially

$$U/U_0 = [\alpha + \beta(x/l)]^m$$

(α, β, m are constants), the general solution of Eq. (18) becomes

$$z = K_1\left(\alpha + \beta\frac{x}{l}\right)^{n_1} + K_2\left(\alpha + \beta\frac{x}{l}\right)^{n_2} \tag{20}$$

where

$$n_{1,2} = \frac{Am+1}{2} \pm \sqrt{\left(\frac{Am+1}{2}\right)^2 + Bm^2}$$

and

$$A = 5.64, \qquad B = 2.4576$$

K_1, K_2 are arbitrary constants. For lva^2/U, their ratio only is important and this has to be determined from the initial condition of the particular problem.

In the special case

$$U/U_0 = e^{\alpha + \beta(x/l)}$$

the general solution of Eq. (18) is

$$z = K_1 e^{n_1(x/l)} + K_2 e^{n_2(x/l)} \tag{21}$$

with

$$N_{1,2} = (\beta/2)(A \pm \sqrt{A^2 + 4B})$$

Both cases are convenient for the practical computation of the boundary layer if these two velocity functions are used for a stepwise approximation of any given velocity distribution. Both cases are characterized by the fact that the velocity profiles of boundary layer become similar (Thwaites[9]).

If, finally, x/l in Eq. (18) is replaced by

$$\xi = k_0 + k_1 \int (U/U_0)^{5.64} d(x/l)$$

with two arbitrary constants k_0 and k_1, this equation gets the form

$$\frac{d^2z}{d\xi^2} = 2.4576\left[\frac{d\ln(U/U_0)}{d\xi}\right]^2 z$$

Thus, the investigation of the laminar boundary layer without suction is reduced to a differential equation of the type

$$z'' = f(\xi)z$$

(3) Approximation of the Velocity Profile by a Gauss-curve; Displacement and Momentum Thickness

The main purpose of the following approximation of the velocity profile by a Gauss-curve is to simplify the calculation of the displacement and the momentum thickness of the boundary layer.

If one tries to solve the boundary-layer equations in the same way as before by the simpler expression

$$u = U(1 - e^{ay + \beta y^2}) \tag{22}$$

instead of Eq. (4), the accuracy of the result becomes insufficient. This is not too surprising because the determination of the velocity profile by the given method starts essentially from conditions along $y = 0$ only. An accurate result can be expected, therefore, only if these conditions are sufficiently strong. This was the case with Eq. (4). However, it is possible now to determine a sufficiently accurate Gauss-curve [Eq. (22)] using the results obtained for the exponential solution with four coefficients.

To this purpose, the fourth-order solution [Eq. (4)] shall be replaced by a Gauss-Curve [Eq. (22)] which has the same tangent as Eq. (4) for $y = 0$ and which passes through a certain point of Eq. (4) inside the boundary layer. If

$$E = e^{ay + by^2 + cy^3 + dy^4}$$

it is $(\partial E/\partial y)_{y=0} = a$ and the tangent of this curve $E(y)$ at $y = 0$ passes through the point $y_1 = -1/a$ at the y-axis. The point P_1 of $E(y)$ which belongs to this y_1 has the E-value

$$E_1 = e^{-1 + (b/a^2) - (c/a^3) + (d/a^4)}$$

If this point P_1 of $E(y)$ is chosen as the point through which the curve

$$E = e^{ay + \beta y^2} \tag{23}$$

has to pass, one obtains

$$\beta = b - (c/a) + (d/a^2) \tag{24}$$

The solution (4) with the coefficients a, b, c, d determined by Eqs. (6) and (7) is in this way approximated by the Gauss-curve

$$u = U(1 - e^{ay + \beta y^2})$$

with β given by Eq. (24).

In the case of the stagnation point, because of Eqs. (14) and (15),

$$\beta = -0.2789(U_0/l\nu)$$

If the corresponding Gauss-curve would be plotted in Fig. 1, there would be no perceptible difference with the already plotted curve [Eq. (4)].

Since a, b, c, d have to be found anyway, this simplification to a Gauss-curve as such would not be essential. However, so it is for the determination of the *displacement and the momentum thickness of the boundary layer.*

The displacement thickness $\delta^*(x)$ is defined by

$$\delta^*(x) = \int_0^\infty \left(1 - \frac{u}{U}\right) dy \tag{25}$$

the momentum thickness by

$$\theta^*(x) = \int_0^\infty \left(1 - \frac{u}{U}\right) \frac{u}{U}\, dy \tag{26}$$

With

$$u/U = 1 - e^{ay + by^2 + cy^3 + dy^4} = 1 - E$$

follows, therefore,

$$\delta^*(x) = \int_0^\infty E\, dy \tag{27}$$

$$\theta^*(x) = \delta^*(x) - \int_0^\infty E^2\, dy \tag{28}$$

If E is replaced now by the Gauss-curve [Eq. (23)], the integration can be performed with the aid of Gauss' error integral

$$\phi(x) = \frac{2}{\sqrt{\pi}} \int_0^x e^{-x^2}\, dx \tag{29}$$

and one obtains

$$\delta^*(x) = \frac{\sqrt{\pi}}{2} \frac{e^{-a^2/4\beta}}{\sqrt{-\beta}} \left[1 - \phi\left(-\frac{a}{2\sqrt{-\beta}}\right)\right] \tag{30}$$

The integral $\int_0^\infty E^2\, dy$ in Eq. (28) follows from the same formula with $2a$, $2b$, $2c$, $2d$ instead of a, b, c, d. If we denote, therefore,

$$\bar{\beta} = 2b - (c/a) + (d/2a^2) \tag{31}$$

it is

$$\int_0^\infty E^2\, dy = \frac{\sqrt{\pi}}{2} \frac{e^{-a^2/\bar{\beta}}}{\sqrt{-\bar{\beta}}} \left[1 - \phi\left(-\frac{a}{\sqrt{-\bar{\beta}}}\right)\right] \tag{32}$$

The case of the *flat plate without suction* becomes

$$\beta = -0.883a^2$$

with $a = -0.323\sqrt{U_0/\nu x}$, and, because of Eq. (30), $\delta^* = 1.75\sqrt{\nu x/U_0}$. The correct value of the constant is 1.72. For the same case, $\bar{\beta} = -1.358a^2$ and, because of Eqs. (32) and (28), $\theta^* = 0.641\sqrt{\nu x/U_0}$, the correct value (Blasius) of the constant being 0.664.

(4) The Flat Plate with Constant Suction and the Asymptotic Suction Profile

The flat plate with constant suction was computed by Iglisch[11] in 1944. In order to treat this problem with the present method, the differential equation [Eq. (6)] for a has to be solved under the conditions

$$U = U_0 = \text{const.}, \qquad v_0 = \text{const.} < 0$$

which reduces this equation to

$$U_0\left(3\frac{v_0}{\nu} - 5a\right) a' = 24\nu a^4 - 60v_0 a^3 + 50\frac{v_0^2}{\nu} a^2 - 15\frac{v_0^3}{\nu^2} a + \frac{v_0^4}{\nu^3} \tag{33}$$

It can be solved by direct integration. Introducing the dimensionless variables

$$\xi = (v_0^2/\nu U_0)x, \qquad t = v_0/\nu a \tag{34}$$

one obtains

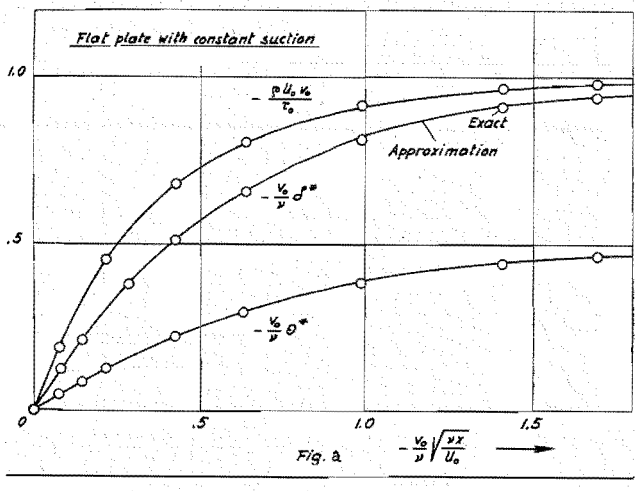

Fig. 2

$$\frac{d\xi}{dt} = \frac{5t - 3t^2}{24 - 60t + 50t^2 - 15t^3 + t^4} \tag{35}$$

Here also, because of Eq. (7),

$$t = -\rho U_0 v_0/\tau_0 \tag{36}$$

If the flat plate extends along the positive x-axis and the fluid flows in the direction of increasing x, the shear τ_0 has to be infinite at $x = 0$, and from Eq. (33) it follows that

$$\xi = \int_t^0 \frac{5t - 3t^2}{24 - 60t + 50t^2 - 15t^3 + t^4}\, dt$$

or

$$\xi = 0.4642 - 2 \ln (1 - t) + 0.25 \ln (2 - t) - 0.351 \ln (10.899 - t) + 2.101 \ln (1.101 - t) \tag{37}$$

The coefficients of the velocity profile of the boundary layer as functions of t are

$$\left.\begin{aligned} a &= (v_0/\nu)/(1/t) \\ b &= \frac{1}{2}\left(\frac{v_0}{\nu}\right)^2\left(\frac{1}{t} - \frac{1}{t^2}\right) \\ c &= \frac{1}{6}\left(\frac{v_0}{\nu}\right)^3\left(\frac{1}{t} - \frac{3}{t^2} + \frac{2}{t^3}\right) \\ d &= \frac{1}{24}\left(\frac{v_0}{\nu}\right)^4 \frac{-2 + \frac{11}{t} - \frac{21}{t^2} + \frac{18}{t^3} - \frac{6}{t^4}}{5 - 3t} \end{aligned}\right\} \tag{38}$$

The results following from these formulas have been plotted in Fig. 2. For various values of $t = -\rho U_0 v_0/\tau_0$, the coordinate $\xi = (v_0^2/\nu U_0)x$ can be calculated directly from Eq. (37). t is plotted versus $\sqrt{\xi}$ in Fig. 3. For the same values of t, the coefficients of the velocity profile follow from Eqs. (38). With a, b, c, d is β known from Eq. (24) and, therefore, also δ^* as function of t and of $\sqrt{\xi}$. With a, b, c, d is also known $\bar{\beta}$ from Eq. (31) and, therefore, θ^* from Eqs. (32) and (28). In Fig. 2 are plotted $-(v_0/\nu)\ \delta^*$ and $-(v_0/\nu)\theta^*$ versus $\sqrt{\xi}$. The small circles in this figure indicate the values calculated by Iglisch. The accordance with the results of the present theory is excellent, and the simplicity of the necessary numerical calculation involved by this method is obvious.

The preceding example includes the asymptotic suction profile. With $\xi \to \infty$ is $t \to 1$, and therefore, because of Eqs. (38),

$$a = v_0/\nu, \qquad b = c = d = 0$$

Thus, indeed,

$$u/U_0 = 1 - e^{(v_0/\nu)y}$$

With $t \to 1$ there follows, in this special case,

$$-\rho U_0 v_0/\tau_0 = 1$$

A *generalization* can be obtained if one asks for the conditions under which, generally,

$$-\rho U v_0/\tau_0 = 1 \tag{39}$$

for variable U and v_0. Because of $\tau_0 = -\nu\rho U a$, the equation has then to be $a = v_0/\nu$. The general differential equation [Eq. (6)] then yields

$$UU'' - 9U'^2 + (v_0^2/\nu)\ U' = 0 \tag{40}$$

and the coefficients of the velocity profile become

$$\left.\begin{aligned} a &= v_0/\nu \\ b &= (1/2)(U'/\nu) \\ c &= -(1/3)(v_0/\nu^2)\, U' \\ d &= \frac{1}{24}\left(-\frac{3}{\nu^2}\, U'^2 + 2\frac{v_0^2}{\nu^3}\, U' - \frac{v_0 v_0'}{\nu^3}\, U\right) \end{aligned}\right\} \tag{41}$$

For any given not constant U exists a suction velocity v_0 determined by Eq. (40), for which Eq. (39) holds under the condition that $d < 0$. If

$$U = U_0 = \text{const.}$$

Eq. (40) is satisfied for every v_0, and from Eq. (41) there follows

$$a = \frac{v_0}{\nu}, \quad b = c = 0, \quad d = -\frac{U_0}{48\nu^3}\frac{dv_0^2}{dx}$$

Thus we obtain

$$u/U_0 = 1 - e^{(v_0/\nu)y - (U_0/48\nu^3)(dv_0^2/dx)y^4} \tag{42}$$

as a suction profile of the flat plate for which $\tau_0 = -\rho U_0 v_0$, under the condition only that

$$dv_0^2/dx > 0$$

This condition includes that the result has a meaning only for an infinite flat plate in both directions with arbitrarily increasing suction velocity in the flow direction. The asymptotic suction profile appears again for $v_0 = \text{const.}$

(5) Exact Solutions of Eq. (9) with Constant Shear

The general equation in the dimensionless form [Eq. (9)] can be integrated exactly if ζ and $d\sigma/d\xi$ are constants. In this case there follows either

$$\left.\begin{aligned} U/U_0 &= (\alpha\xi + \beta)^m \\ \sigma &= \gamma(\alpha\xi + \beta) \end{aligned}\right\} \tag{43}$$

or

$$\left.\begin{aligned} U/U_0 &= e^{\alpha\xi + \beta} \\ \sigma &= \gamma \end{aligned}\right\} \tag{44}$$

where m, α, β, and γ are arbitrary constants. Accordingly,

$$\tau_0 = \rho\sqrt{\nu/l\gamma}(\alpha\xi + \beta)^{(3/2)m - (1/2)} \tag{45}$$

or

$$\tau_0 = \rho\sqrt{\nu/l\gamma}\, e^{(3/2)(\alpha\xi + \beta)} \tag{46}$$

In the special case $m = 1/3$, the first τ_0 is constant. If, moreover,

$$\zeta = m\alpha\gamma = 5/4 \tag{47}$$

and therefore $\alpha\gamma = 15/4$, Eq. (9) has the solution $t = 0$, which means that no suction is necessary. With $\alpha = 1$, $\beta = 0$, it follows *that for the velocity distribution*

$$U/U_0 = \xi^{1/3} \tag{48}$$

outside the boundary layer the shear along the boundary

$$\tau_0 = \frac{2}{\sqrt{15}}\rho\frac{\nu U_0}{l}\sqrt{\frac{U_0 l}{\nu}} \tag{49}$$

is constant without suction. This special case corresponds to the symmetrical flow against a corner with plane surfaces under 90° angle.

The other special value $\alpha = 0$ for which τ_0 is constant leads in both cases to

$$U = U_0 = \text{const.}, \quad \sigma = \sigma_0 = \text{const.}$$

and represents, therefore, *the flat plate in longitudinal flow with constant shear due to suction.* Eq. (9) yields in this case

$$\frac{\xi - \xi_0}{\sigma_0} = 2\int_0^t \frac{dt}{24 - 60t + 50t^2 - 15t^3 + t^4} \tag{50}$$

if suction is applied for $\xi \geq \xi_0$. If τ_{00} is the shear without suction at the point ξ_0 and at the same time the prescribed constant value of the shear for $\xi > \xi_0$, it follows

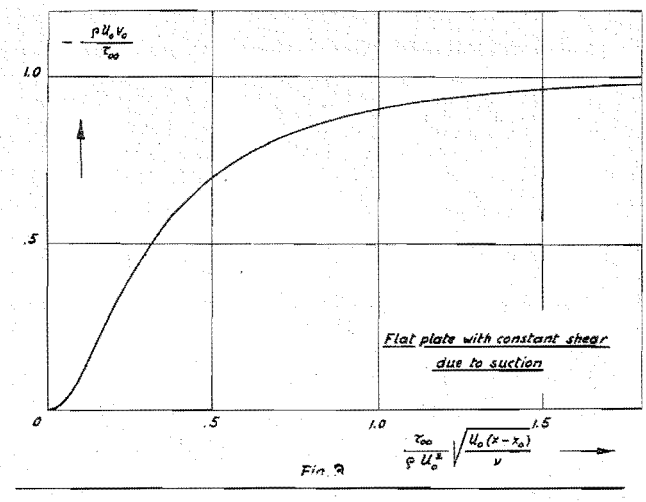

Fig. 3

$$\left.\begin{aligned} t &= -\rho U_0 v_0/\tau_{00} \\ \sqrt{\frac{\xi - \xi_0}{\sigma_0}} &= \frac{\tau_{00}}{\rho U_0^2}\sqrt{\frac{U_0(x - x_0)}{\nu}} \end{aligned}\right\} \tag{51}$$

because of Eq. (8). In Fig. 3, t is plotted versus $\sqrt{(\xi - \xi_0)/\sigma_0}$. This result shows that the suction velocity necessary to keep the shear constant increases rapidly from zero to a constant value corresponding to the asymptotic suction.

References

[1] Goldstein, S., *Modern Developments in Fluid Dynamics*, Chapter IV—The Mathematical Theory of Motion in a Boundary Layer; Oxford, 1938.

[2] Schlichting, H., *Berechnung der laminaren Grenzschicht mit Absaugung*, ZWB, F. B. 1480, 1941.

[3] Schlichting, H., *An Approximate Method for Calculation of the Laminar Boundary Layer with Suction for Bodies of Arbitrary Shape*, Aer. Inst. Braunschweig Ber. No. 43/13, June, 1943. Also, N.A.C.A. T.M. No. 1216, March, 1949; Ing. Archiv 16, 1948.

[4] Falkner, V. M., *Simplified Calculations of the Laminar Boundary Layer*, A.R.C. R.G.M. 1895, 1941.

[5] Piercy, N. A. V., Whitehead, L. G., and Tyler, R. A., *The Laminar Boundary Layer*, Aircraft Engineering, Vol. 20, December, 1948.

[6] Piercy, N. A. V., and Whitehead, L. G., *Boundary Layer Calculations*, Aircraft Engineering, Vol. 21, January, 1949.

[7] Trilling, L., *The Incompressible Boundary Layer wtih Pressure Gradient and Suction*, Journal of the Aeronautical Sciences, Vol. 17, No. 6, pp. 335, June, 1950.

[8] Thwaites, B., *A Theoretical Discussion of High Lift Aerofoils with Leading Edge Porous Suction*, A.R.C. R.G.M. No. 2242, 1946.

[9] Thwaites, B., *On Certain Types of Boundary Layer Flow with Continuous Surface Suction*, A.R.C. R.G.M. 2243, July, 1946.

[10] Hiemenz, K., *Die Grenzschicht an einem in den gleichfoermigen Fluessigkeitsstrom eingetauchten geraden Kreiszylinder* (Diss. Goettingen 1911), Dingl. Polytech. Journal, Vol. 326, 1911.

[11] Iglisch, R., *Exakte Berechnung der laminaren Grenzschicht an der laengs angestroemten ebenen Platte mit homogener Absaugung*, Schriften der Deutschen Akad. der Luftfahrtforschung, Vol. 8B, 1944.

Turbulent Boundary Layer on a Cone in a Supersonic Flow at Zero Angle of Attack

E. R. VAN DRIEST*

North American Aviation, Inc.

ABSTRACT

A simple rule is given for transforming local heat-transfer coefficients from flat plates to cones at zero angle of attack for fully turbulent boundary layers in supersonic flow. The rule is that the cone heat-transfer coefficient is the flat-plate coefficient for one-half the Reynolds Number on the cone, the Mach Number and wall-to-free-stream temperature ratio remaining the same.

INTRODUCTION AND SUMMARY

THE CALCULATION OF THE TEMPERATURE of a cone in supersonic flight requires a knowledge of the heat-transfer coefficient of the boundary layer of the cone. Hantzsche and Wendt[1] solved the problem for laminar boundary layers. They found that the local laminar heat-transfer coefficient on a cone at zero angle of attack can be obtained by merely multiplying by $\sqrt{3}$ the local laminar heat-transfer coefficient on a flat plate. Since heat transfer and skin friction are proportional, this rule applies also to local skin-friction coefficients for cones. Because laminar heat transfer and skin friction vary inversely with the square root of the Reynolds Number, another way of formulating the transformation rule for conical laminar layers is to state that the cone solution is the flat-plate solution for one-third of the Reynolds Number on the cone.

The present report offers a simple transformation rule for fully turbulent boundary layers on cones, similar to that for laminar layers. It is found that, for turbulent boundary layers, the cone solution for local heat transfer is the flat-plate solution for one-half of the Reynolds Number on the cone, the Mach Number and wall-to-free-stream temperature ratio remaining the same. The effect is an increase over the local turbulent heat-transfer or skin-friction coefficient of flat plates of about 10 to 15 per cent. The work is an extension to compressible flow of an analysis by Gazley,[2] who neglected the effect of compressibility and assumed a power law for velocity distribution; his results approach those obtained when the above general rule for turbulent boundary layers is applied to incompressible flow at high Reynolds Numbers.

Received July 26, 1951.

* Aerodynamics Engineer, Aerophysics Laboratory.

MOMENTUM EQUATION FOR THE BOUNDARY LAYER ON A CONE AT ZERO ANGLE OF ATTACK

The von Kármán momentum equation for a boundary layer in steady state on a body of revolution at zero angle of attack is

$$\frac{\partial}{\partial x}\int_0^\delta r\rho u(u_\infty - u)\,dy = -\frac{\partial p}{\partial x}\int_0^\delta r\,dy - r_w\tau_w \qquad (1)$$

In this relation, x is a coordinate distance measured along the body from the forward most point, y is the other coordinate measured from the surface along a normal to the surface, u is the flow velocity relative and parallel to the surface at the point (x, y), ρ is the density of the fluid at (x, y), r is the normal distance from the body axis to (x, y), p is the pressure at (x), τ_w is the shear stress at the surface, and δ is the boundary-layer thickness measured normal to the surface. Subscripts w and ∞ refer to the wall and outer edge of the boundary layer, respectively.

With a cone, when the flow is supersonic and the shock wave is attached, the pressure along the rays is constant for inviscid fluids. Therefore, since the boundary layer is thin ($\delta \ll r$), it is assumed that the pressure is also constant along the boundary layer—i.e., $\partial p/\partial x = 0$. Hence, Eq. (1) for cones reduces to

$$\frac{\partial}{\partial x}\int_0^\delta r\rho u(u_\infty - u)\,dy = -r_w\tau_w \qquad (2)$$

Furthermore, as a consequence of $\delta \ll r$, Eq. (2) becomes

$$\frac{\partial}{\partial x} r_w \int_0^\delta \rho u(u_\infty - u)\,dy = -r_w\tau_w \qquad (3)$$

or

$$\frac{\partial}{\partial x}\int_0^\delta \rho u(u_\infty - u)\,dy + \frac{1}{r_w}\frac{\partial r_w}{\partial x}\int_0^\delta \rho u(u_\infty - u)\,dy = -\tau_w \qquad (4)$$

But for the cone

$$(1/r_w)(\partial r_w/\partial x) = 1/x \qquad (5)$$

so that, finally, from Eq. (4), the momentum equation for thin boundary layers on a cone in supersonic flight at zero angle of attack is

$$\tau_w = \frac{\partial}{\partial x}\int_0^\delta \rho u(u_\infty - u)\,dy + \frac{1}{x}\int_0^\delta \rho u(u_\infty - u)\,dy \quad (6)$$

For turbulent flow, the fluid properties, ρ and u, in this equation take on mean values.

Turbulent Skin Friction and Heat Transfer on a Cone

It is assumed that the same flow mechanism holds locally on a cone as on a flat plate. Hence, the same procedure is followed for skin friction on cones as was used in the writer's previous report[3] on turbulent boundary layers on flat plates. According to that procedure, it was at first shown that the apparent shear stress was given by

$$\tau = -\overline{(\rho v)'u'} \quad (7)$$

whence, when $\bar{v} \approx 0$ for thin boundary layers and the triple correlation $\overline{\rho' u' v'}$ is neglected,

$$\tau = -\bar{\rho}\,\overline{u'v'} \quad (8)$$

where ρ is the fluid density and u and v are the velocity components parallel to the free stream and normal to the plate, respectively. The primes indicate fluctuation from the mean. Introduction of the Prandtl mixing length l then gave

$$\tau = \bar{\rho} l^2 (d\bar{u}/dy)^2 \quad (9)$$

The shear was next assumed constant and equal to the wall value, and l was taken as Ky. The mean local density was related to the mean local velocity by using

$$\frac{\bar{T}}{T_w} = \frac{T_w}{T_\infty} - \left(\frac{T_w}{T_\infty} - 1\right)\frac{\bar{u}}{u_\infty} + \frac{\gamma - 1}{2} M_\infty^2 \frac{\bar{u}}{u_\infty}\left(1 - \frac{\bar{u}}{u_\infty}\right) \quad (10)$$

in

$$\bar{\rho}/\rho_w = T_w/\bar{T} \quad (11)$$

to obtain

$$\frac{\bar{\rho}}{\rho_w} = 1\Big/\left[1 + B\frac{\bar{u}}{u_\infty} - A^2\left(\frac{\bar{u}}{u_\infty}\right)^2\right] \quad (12)$$

where

$$A^2 = [(\gamma - 1)/2]M_\infty^2/(T_w/T_\infty)$$

and

$$B = (\{1 + [(\gamma - 1)/2]M_\infty^2\}/(T_w/T_\infty)) - 1$$

and where T is temperature, γ is the ratio of the specific heats, M is the Mach Number, and w and ∞ refer to wall- and free-stream conditions, respectively. Integration of Eq. (9) then yielded

$$\frac{1}{A}\sin^{-1}\frac{2A^2(\bar{u}/u_\infty) - B}{(B^2 + 4A^2)^{1/2}} + \frac{1}{A}\sin^{-1}\frac{B}{(B^2 + 4A^2)^{1/2}} = \frac{1}{u_\infty}\sqrt{\frac{\tau_w}{\rho_w}}\left(F + \frac{1}{K}\ln\sqrt{\frac{\tau_w}{\rho_w}}\cdot\frac{y}{\nu_w}\right) \quad (13)$$

where F is a constant and ν is the fluid kinematic viscosity.

With flat plates, the von Kármán momentum relation constitutes only the first term on the right-hand side of Eq. (6). Substitution of Eqs. (12) and (13) in that term then gave

$$\tau_w = \frac{D\mu_w u_\infty}{K}\cdot\frac{d}{dx}\left\{Ja^2\exp\left[\frac{a}{A}\sin^{-1}\frac{B}{(B^2 + 4A^2)^{1/2}}\right]\right\} \quad (14)$$

where

$$D = e^{-FK}$$

$$a = Ku_\infty/\sqrt{\tau_w/\rho_w}$$

$$J = \int_0^1 \frac{z(1 - z)}{(1 + Bz - A^2Y^2)^{3/2}}\cdot \exp\left[\frac{a}{A}\sin^{-1}\frac{2A^2z - B}{(B^2 + 4A^2)^{1/2}}\right]dz$$

$$z = \bar{u}/u_\infty$$

In these equations, coordinate x is the distance measured from the leading edge of the plate in the free-stream direction. The integral J was expanded in a series and terms of higher order than $1/a^2$ were neglected, since a was large, resulting in

$$J = \frac{1}{a^2(1 + B - A^2)^{1/2}}\cdot\exp\left[\frac{a}{A}\sin^{-1}\frac{2A^2 - B}{a^2(B^2 + 4A^2)^{1/2}}\right] \quad (15)$$

After rearrangement, Eq. (14) became

$$\frac{\rho_w u_\infty}{\mu_w} = \frac{D}{K^3}\cdot\frac{1}{(1 + B - A^2)^{1/2}}\cdot a^2\cdot\frac{d}{dx}\left\{\exp\left[\frac{a}{A}(\sin^{-1}\alpha + \sin^{-1}\beta)\right]\right\} \quad (16)$$

where

$$\alpha = (2A^2 - B)/(B^2 + 4A^2)^{1/2}$$

and

$$\beta = B/(B^2 + 4A^2)^{1/2}$$

The lower limit on a for $x = 0$ was taken as zero, since the shear at the leading edge of the plate was assumed to be infinite. Integration of Eq. (16) then yielded, for large values of a and negligible variation of wall temperature with x,

$$\frac{\rho_w u_\infty x}{\mu_w} = \frac{D}{K^3}\cdot\frac{1}{(1 + B - A^2)^{1/2}}\cdot a^2\cdot\exp\left[\frac{a}{A}(\sin^{-1}\alpha + \sin^{-1}\beta)\right] \quad (17)$$

from which came the form of the local skin-friction (heat-transfer) formula

$$\frac{2^{1/2}}{Ac_{f\infty}{}^{1/2}(T_w/T_\infty)^{1/2}}(\sin^{-1}\alpha + \sin^{-1}\beta) = \text{const.} + \frac{1}{K}\left[\ln R_\infty c_{f\infty} - \left(\frac{1}{2}+\omega\right)\ln\frac{T_w}{T_\infty}\right] \quad (18)$$

since

$$\begin{aligned}
\rho_w &= \rho_\infty(T_w/T_\infty)^{-1}\\
\mu_w &= \mu_\infty(T_w/T_\infty)^{\omega}\\
c_{f\infty} &= 2\tau_w/\rho_\infty u_\infty{}^2\\
c_{fw} &= c_{f\infty}(T_w/T_\infty)\\
R_w &= R_\infty(T_w/T_\infty)^{-(1+\omega)}\\
R_\infty &= \rho_\infty u_\infty x/\mu_\infty
\end{aligned}$$

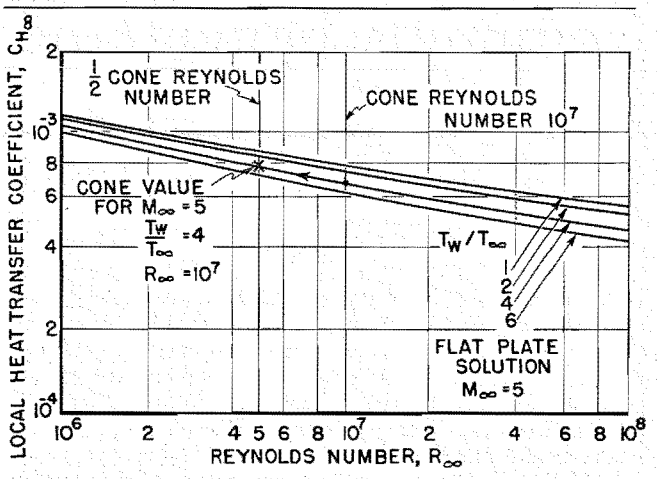

FIG. 1. Method of obtaining the local cone heat-transfer coefficient from the flat-plate solution.

A similar development can be traced for the cone in supersonic flow with attached shock wave. Instead of Eq. (16), one obtains, starting with Eq. (6),

$$\frac{\rho_w u_\infty}{\mu_w} = \frac{D}{K^3}\cdot\frac{1}{(1+B-A^2)^{1/2}}\cdot a^2\left[\frac{d}{dx}\left\{\exp\left[\frac{a}{A}(\sin^{-1}\alpha+\sin^{-1}\beta\right]\right\}+\frac{1}{x}\left\{\exp\left[\frac{a}{A}(\sin^{-1}\alpha+\sin^{-1}\beta)\right]\right\}\right] \quad (19)$$

Now, with the assumption that a is large, Eq. (19) can be written as

$$\frac{\rho_w u_\infty}{\mu_w} = \frac{D}{K^3}\cdot\frac{1}{(1+B-A^2)^{1/2}}\cdot\left[\frac{d}{dx}\left\{a^2\exp\left[\frac{a}{A}(\sin^{-1}\alpha+\sin^{-1}\beta)\right]\right\}+\frac{a^2}{x}\left\{\exp\left[\frac{a}{A}(\sin^{-1}\alpha+\sin^{-1}\beta)\right]\right\}\right] \quad (20)$$

Rearrangement gives

$$\frac{\rho_w u_\infty}{\mu_w}\cdot x\,dx = \frac{D}{K^3}\cdot\frac{1}{(1+B-A^2)^{1/2}}\cdot d\left\{xa^2\exp\left[\frac{a}{A}(\sin^{-1}\alpha+\sin^{-1}\beta)\right]\right\} \quad (21)$$

which integrates to

$$\frac{1}{2}\cdot\frac{\rho_w u_\infty x}{\mu_w}\cdot x = \frac{D}{K^3}\cdot\frac{1}{(1+B-A^2)^{1/2}}\cdot x\cdot a^2\exp\left[\frac{a}{A}(\sin^{-1}\alpha+\sin^{-1}\beta)\right] \quad (22)$$

or

$$\frac{1}{2}\cdot\frac{\rho_w u_\infty x}{\mu_w} = \frac{D}{K^3}\cdot\frac{1}{(1+B-A^2)^{1/2}}\cdot a^2\exp\left[\frac{a}{A}(\sin^{-1}\alpha+\sin^{-1}\beta)\right] \quad (23)$$

Comparison of Eqs. (23) and (17) shows that, for the same cone Mach Number and wall-to-free-stream temperature ratio, the cone solution for local skin friction (and therefore heat-transfer coefficient, since they are proportional) is the same as the flat-plate solution when the cone Reynolds Number is divided by 2. The use of this rule is shown in Fig. 1 in which the local heat-transfer coefficient is plotted as a function of Reynolds Number and temperature ratio at a Mach Number of 5 for flat plates. For example, if the cone free-stream Mach Number is 5, the wall-to-free-stream temperature ratio 4, and the cone Reynolds Number 10^7, then the cone local heat-transfer coefficient is found in Fig. 1 on the temperature ratio 4 curve at Reynolds Number 5×10^6. Thus, in this particular case, it is found that the heat-transfer coefficient for the cone is 1.140 times that of a flat plate under the same conditions. This ratio will vary with all of the above flow parameters.

(*Continued on page 72*)

Column Behavior Under Conditions of Impact

GEORGE GERARD* AND HERBERT BECKER†

New York University and Combustion Engineering-Superheater, Inc., Respectively

SUMMARY

The magnitude of the stress introduced into a long slender bar by velocity impact depends only upon the conditions of impact. Thus, buckling of this bar under impact loading can only take place after the compressive stress wave has propagated over a "critical" length of the bar. Column behavior under impact is studied theoretically and by a novel experimental technique, and it is concluded that a column can momentarily support a dynamic compressive stress of any magnitude which may be introduced by impact.

INTRODUCTION

THE INVESTIGATION OF COLUMN BEHAVIOR under conditions of dynamic loading has been studied by several investigators. Meier[1] has studied the behavior of columns containing initial imperfections by investigating the motion of the center of the column for loads below the Euler load and above. Although Meier speculates that the column can carry loads in excess of the Euler load, a study of his analytical results fails to bear out this conclusion.

Hoff[2] has studied a similar problem but has specified the displacement at the end of the column rather than the load. His investigation is concerned with an initially imperfect column in which one end of the column has been displaced at a constant velocity. Under such conditions it has been shown analytically that the column can carry loads in excess of the Euler load because of the lateral inertia of the imperfect column.

In both the above investigations, it has been assumed that the period of the lateral motion of the column is small relative to the time required for a stress wave to propagate from one end of the bar to the other. Thus, it has been assumed that the stress is constant throughout the entire length of the column. In contrast, the investigation contained herein is concerned with the propagation of an elastic stress discontinuity in the column and accounts for the fact that the stress is instantaneously not constant over the entire length of the column. Under conditions of compressive stress wave propagation, it has been found useful to adopt the point of view of determining the critical length of a column subject to a given stress rather than finding the critical stress of a column of given length.

It is the objective of this investigation to show that under certain conditions of impact loading, the compressive stress momentarily supported by a perfect column at buckling may be of *any magnitude* in excess of its static Euler load. Under sufficiently high velocities of impact, the critical length of the column is determined by the magnitude of the stress being propagated, which is contrary to the usual situation of static buckling in which the critical stress is determined by the effective length of the column. This phenomenon is due to the fact that the magnitude of the stress at the end of the bar which is introduced by velocity impact depends only upon the velocity of impact and the modulus and density of the material. Initially, the stress is only at the struck end. Since there is no stress in the remainder of the bar, it is only after the stress has been transmitted over a critical length of the bar that buckling can possibly occur.

SYMBOLS

A = area
c = velocity of propagation
E = elastic modulus
I = moment of inertia
L = length
L_e = length traversed by stress wave in time t, $L_e = ct$
$L_{cr.}$ = critical length in which buckling occurs
m = mass
t = time
U = elastic strain energy
v = velocity
V = volume, $V = LA$
w = lateral displacement
x = coordinate along length
σ = stress
σ_u = ultimate tensile strength
ϵ = strain
ρ = radius of gyration
φ = density

TEST TECHNIQUE

Fig. 1 is a photograph of a long thin column in which buckling was caused by the propagation of a compressive stress wave. The impact loading was achieved experimentally in a simple manner. The specimen was

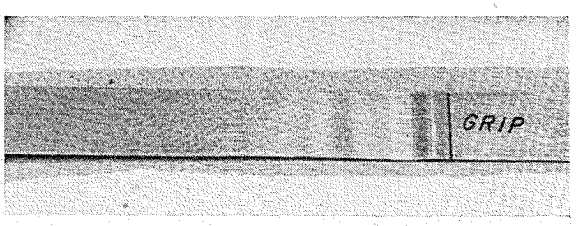

FIG. 1

Received August 1, 1951.

* Assistant Professor of Aeronautical Engineering, College of Engineering.

† Structures Engineer.

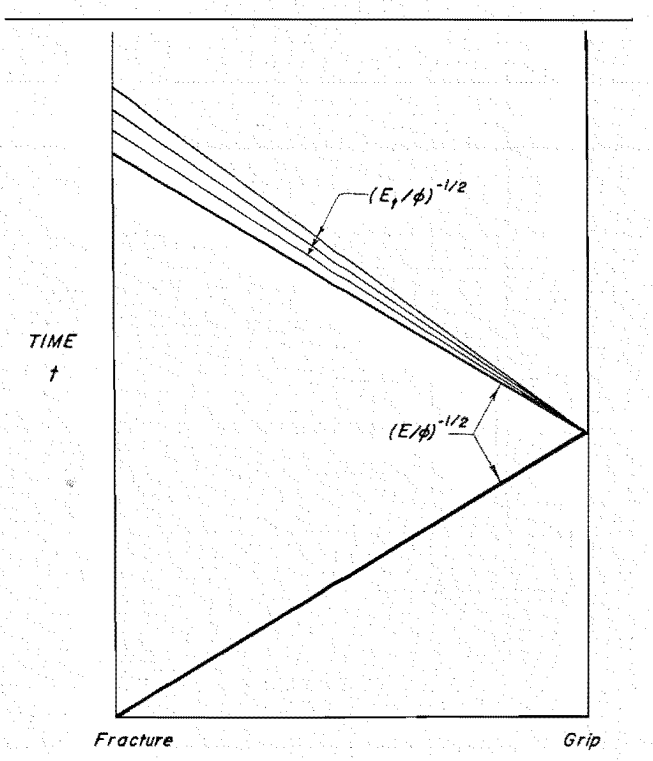

FIG. 2.

loaded in tension until fracture occurred. At fracture, the elastic strain energy stored in the specimen was

$$U = (\sigma_u^2/2E)V \tag{1}$$

This energy is available as impact energy. Thus,

$$mv^2/2 = \sigma_u^2 m/2E\varphi \tag{2}$$

Noting that $c = (E/\varphi)^{1/2}$ for longitudinal wave propagation, the effective impact velocity obtained is given by*

$$v = (c/E)\sigma_u \tag{3}$$

Since for a given material the effective impact velocity is a linear function of the stress in the bar, a simple technique for obtaining various impact velocities is suggested. By using different size notches at some point in the bar, the stress in the unnotched portion of the bar can be varied as desired. While the average fracture stress at the notch would be σ_u, the stress in the unnotched portion would be lower. According to Eq. (3), this would result in a lower effective impact velocity.

The compressive stress wave that buckled the column shown in Fig. 1 was a reflection of the unloading wave (negative tension) which followed fracture at the relatively massive grips that held the specimen. The wave propagation following fracture is depicted in Fig. 2. The velocity of the unloading wave is that associated with the elastic modulus of the material, since the unloading path is elastic. Upon reflection, however, the stress may reach the plastic portion of the dynamic stress-strain curve, and therefore the plastic stresses will propagate at lower velocities than the elastic stresses. With this technique of compressive impact loading, the effective origin of the dynamic stress-strain curve is essentially shifted to the fracture point of the static tension stress-strain curve.

* For a rigorous development of Eq. (3), see Timoshenko, S., *Theory of Elasticity*, 1st Ed., pp. 381–384, McGraw-Hill Book Company, Inc., New York.

COLUMN BEHAVIOR

In its gross features, column behavior under compressive stress wave propagation can be represented by the model shown in Fig. 3. To the long slender bar fixed at the lower end, a given weight is assumed attached at successively increasing distances from the lower end. When the weight has moved a sufficient distance from the fixed end, buckling of the bar will occur in the length between the lower end and the weight. Under the corresponding conditions of compressive stress wave propagation, the magnitude of the stress wave is fixed by impact conditions. As the wave front moves away from the fixed end, buckling will occur when the "critical" length corresponding to this stress magnitude has been traversed.

In the following analysis, it is assumed that the stresses are elastic, and therefore the stress wave is propagated as a single discontinuity and is constant over the length traversed by the wave. The equilibrium differential equation for the column is

$$EI\partial^4 w/\partial x^4 + \sigma A\partial^2 w/\partial x^2 = 0 \tag{4}$$

This equation can be rewritten in the following form:

$$\rho^2\partial^4 w/\partial x^4 + \epsilon\partial^2 w/\partial x^2 = 0 \tag{5}$$

The assumed boundary conditions are clamping at the fixed end of the bar ($x = 0$) from which point the compressive stress wave originates. The additional boundary conditions must be prescribed not at the other end of the bar but at the stress wave front where the first influence of the disturbance is felt. Since there can be no lateral deflection in front of the stress wave, continuity conditions prescribed the boundary conditions at the wave front. Thus,

$$\left.\begin{aligned} w(0) &= \partial w/\partial x(0) = 0 \\ w(L_e) &= \partial w/\partial x(L_e) = 0 \end{aligned}\right\} \tag{6}$$

where $L_e = ct$ and is the distance the stress wave has traveled along the bar. A solution that satisfies Eq. (5), as well as the boundary conditions of Eqs. (6), is given by

$$w = a[1 - (\cos 2\pi x/L_e)] \quad \text{for } 0 \leq x \leq L_e \tag{7}$$

By substituting the appropriate derivatives of Eq. (7) into Eq. (5),

$$[16\rho^2(\pi/L_e)^4 - 4\epsilon(\pi/L_e)^2]a[1 - (\cos 2\pi x/L_e)] = 0 \tag{8}$$

For a nontrivial solution, the first bracketed term must vanish. Consequently,

$$L_{cr.} = 2\pi\rho\epsilon^{-1/2} \tag{9}$$

and the critical length of the bar in which buckling occurs depends upon the magnitude of the stress wave. If use is made of Eq. (3), then Eq. (9) becomes

$$L_{cr.}/\rho = 2\pi(c/v)^{1/2} \tag{10}$$

The dependence of the critical slenderness ratio upon the impact velocity given by Eq. (10) is shown in Fig. 4. In cases where $v > c$, the compressive stress wave would still be propagated at a velocity equal to c. Therefore, for $L_{cr.}/\rho \leq 2\pi$, buckling can never occur.

It is interesting to note that, if the usual method of running static column tests (in which a column of fixed slenderness ratio is subject to increasing stress until buckling occurs) is used for dynamic loading, then buckling always occurs over the entire length of the column. This is due to the fact that the impact velocities would be increased only until the proper stress magnitude for buckling in the entire length is reached and then not continued. If the buckling tests are run according to the model shown in Fig. 3, then buckling will take place in a critical length less than the actual length of the bar.

The solution for the critical length given by Eq. (9) is based on the assumption that the stress wave is elastic. If the stress is of such a magnitude so as to be in the plastic region, then the plastic portions of the stress are propagated at lower velocities than the elastic portion as shown in Fig. 2. In this case, the elastic portion of the stress wave traverses the critical length of the bar first. Therefore, to a first approximation, it appears that the value of the critical length may be closely associated with the proportional limit stress, which in itself may be high because of the large strain rates associated with the impact velocities under consideration. The behavior of the column under conditions of plastic stress wave propagation requires detailed investigation, however, and therefore the above remark is merely an intuitive suggestion.

Experimental Data

Several column tests were run using the experimental technique outlined previously for obtaining compressive impact loadings of high velocity. A $^1/_2$-in. strip of 0.010-in. 24S-T3 aluminum alloy of 10-in. length was held in a testing machine by Templin grips. The specimens were loaded to failure in tension, and it was observed (as shown in Fig. 1) that a series of short wavelength buckles formed immediately above the grip after reflection of the unloading wave. The wave length of the buckles of four similar specimens was approximately $^1/_4$ in. The ultimate tensile strength of the specimens averaged 64,000 lbs. per sq.in. It is to be noted that, in

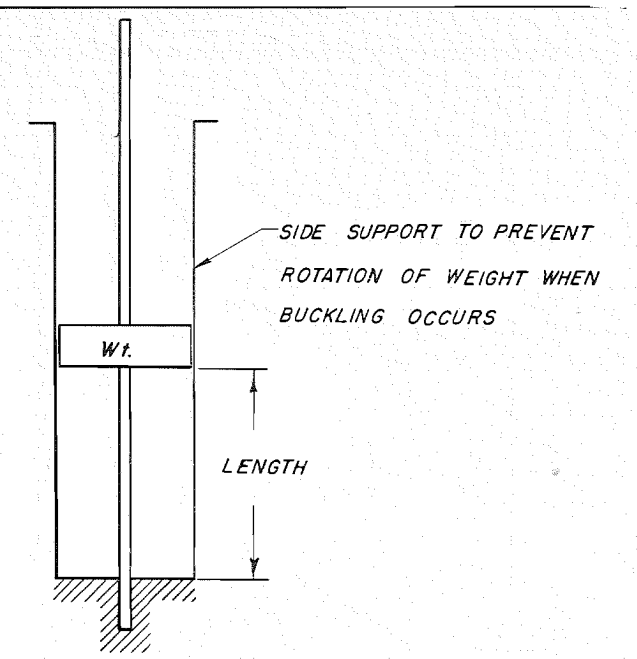

Fig. 3.

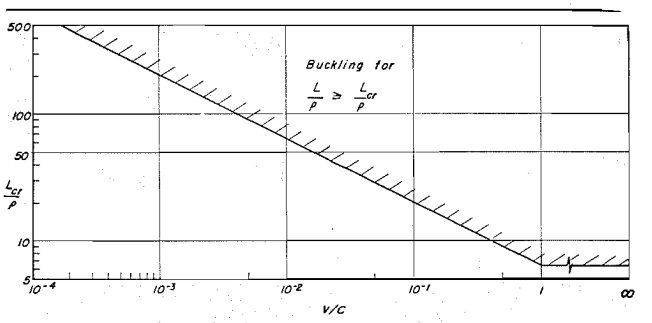

Fig. 4.

stretching the bar to fracture, any initial imperfections in the column are effectively removed and the column as tested is essentially perfect.

From Eq. (9), the estimated critical length based on the assumption of elastic buckling was 0.23 in., which certainly is of the order of magnitude of the wave lengths observed.

Conclusions

Both experiment and theory indicate that, under conditions of velocity impact in which the magnitude of the compressive stress wave may be far in excess of the load required to cause buckling of the column under static conditions, buckling may be confined to a length less than the actual length of the column. This phenomenon indicates that a column can momentarily support a dynamic compressive stress of any magnitude that may be introduced by impact. Therefore, dynamic buckling does not place an upper limit to the compressive stress that can be carried by a slender bar in the sense of static buckling.

(*Continued on page 65*)

On Supersonic Flow of a Two-Dimensional Jet in Uniform Stream*

S. I. PAI†
University of Maryland

SUMMARY

It is well known that a supersonic gas jet issuing from a reservoir into a medium at rest has a periodic structure if the difference of pressure of the jet from the medium is not large. This paper investigates a similar situation when a supersonic gas jet is issuing into a uniform stream. It is found that if the uniform stream is subsonic, the supersonic jet has *almost* periodic structure, and the approximate wave length increases with the Mach Number of the surrounding stream for a given Mach Number of the jet. If the uniform stream is supersonic, the supersonic jet does not have periodic structure. The transmission and the reflection of small disturbance at the boundary of the jet—i.e., a vortex sheet—are investigated. Factors of transmission and reflection of disturbances on the vortex sheet are found. They are functions of the Mach Numbers of the jet and that of uniform stream. The reflection wave may be of the same sign or of opposite sign of the incident wave or zero according to the Mach Numbers of the two streams.

LIST OF SYMBOLS

A	=	constant
B	=	constant
$f(z)$	=	function of z
$F(z)$	=	function of z
$g(z)$	=	function of z
M	=	Mach Number of basic flow
R	=	reflection factor defined by Eq. (24)
T	=	transmission factor defined by Eq. (23)
u	=	x-wise velocity of component of the resultant flow
U	=	velocity of the basic flow
v	=	y-wise velocity component of the resultant flow
x	=	distance along the axis of the jet
y	=	distance perpendicular to the axis of the jet
β_i	=	$\sqrt{\lvert M_i^2 - 1 \rvert}$ $(i = 1 \text{ or } 2)$
θ	=	wave-length factor defined by Eq. (10)
λ	=	frequency or eigenvalue
ϕ	=	velocity potential of disturbance
subscript 1	=	values for quantity in the jet
subscript 2	=	values for quantity in the surrounding stream

(I) INTRODUCTION

IN HIS EXPERIMENTAL INVESTIGATIONS of a jet of gas issuing from an orifice into the medium at rest, Emden[1] found that, if the velocity of the jet is supersonic and the excess pressure of the jet over the surrounding medium is not large, the jet has periodic structure. It was Prandtl[2] who first attempted to explain this phenomenon from a theoretical point of view by the method of small perturbation and reasonable good agreement of the theory with experimental results was found. Several other authors had discussed this problem from a theoretical point of view.[3–5] However, the behavior of the supersonic gas jet in a uniform stream has not yet been studied. This paper is to study the case of a supersonic gas jet in a uniform stream when the pressure of the jet differs slightly from that of surrounding stream. Because the behaviors of the subsonic and the supersonic uniform stream are entirely different, we have to treat these two cases separately.

Since the pressure difference between the jet and the uniform stream is not large, we may assume that the gas velocity normal to the jet axis is small—in other words, that the jet expands very little—hence, the method of small perturbation may be used in this problem. We also assume that there exist velocity potentials inside the jet, as well as in the uniform stream—i.e., even if shock wave may happen in the jet, the strength of the shock is assumed to be small. Thus, the vorticity introduced is still negligible. Both viscosity and heat conduction are neglected.

In this paper we shall consider only the two-dimensional flow. Here, besides the discussion of periodicity of the supersonic jet, some interesting phenomena of a small disturbance reflected from, and transmitted through, a surface of discontinuity have been obtained.

The author also found that, as far as periodicity is concerned, the two-dimensional and the axially symmetrical jets behave similarly. However, in case of reflection and transmission of disturbance on a surface of discontinuity, the axially symmetrical case is much more complicated. Hence, the results of the axially symmetrical supersonic jet in uniform stream will be reported in another paper elsewhere.

(II) FORMULATION OF THE PROBLEM

The schematic diagram of the problem is shown in Fig. 1. At the exit of the nozzle $x = 0$, the jet has the following characteristics:

$$\left.\begin{aligned} u &= U_1 + u_0(y); \quad v = v_0(y) \\ M &= M_1 + M_0(y) \end{aligned}\right\} \tag{1}$$

where $u_0 \ll U_1$, $u_0 \sim v_0$; $M_0 \ll M_1$, where M_1 is the Mach Number corresponding to U_1, and U_1 is certain mean

Received July 23, 1951.

* This work was carried out under Contract AF 33(038)-10481 sponsored by the Office of Air Research.

† Research Associate, Institute for Fluid Dynamics and Applied Mathematics.

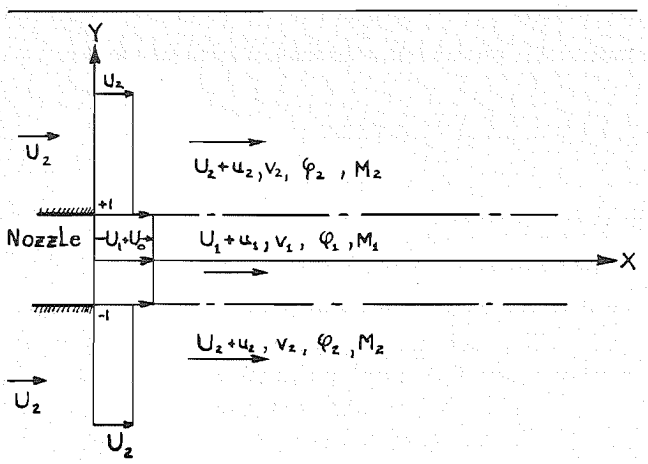

FIG. 1. Supersonic jet in uniform stream.

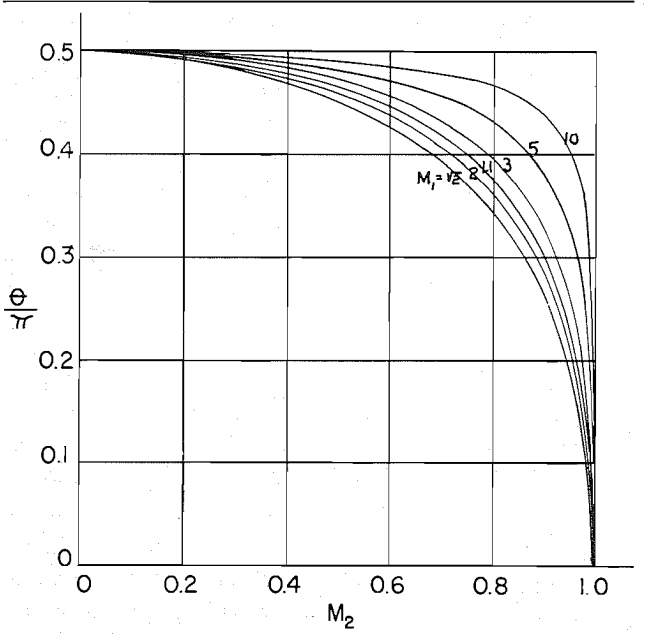

FIG. 2. Function θ against M_2.

velocity in the jet where the pressure in the jet is equal to the pressure of the undisturbed uniform stream.

Inside the jet we have

$$u = U_1\left(1 + \frac{\partial\phi_1}{\partial x}\right), \quad v = U_1\frac{\partial\phi_1}{\partial y} \tag{2}$$

where $U_1\phi_1$ is the velocity potential of the disturbance in the jet.

The uniform stream is of a velocity U_2 and Mach Number M_2 when it is not disturbed. The velocity components in the surrounding stream after it meets the jet will be

$$u = U_2\left(1 + \frac{\partial\phi_2}{\partial x}\right), \quad v = U_2\frac{\partial\phi_2}{\partial y} \tag{3}$$

where $U_2\phi_2$ is the velocity potential of the disturbance in the surrounding stream.

We also have

$$1 \gg \partial\phi_i/\partial x,\ \partial\phi_i/\partial y$$

where $i = 1$ or 2.

The differential equation that governs ϕ_i is

$$(1 - M_i^2)\frac{\partial^2\phi_i}{\partial x^2} + \frac{\partial^2\phi_i}{\partial y^2} = 0 \tag{4}$$

The boundary conditions of the problem are as follows:

(1) By symmetry, at the axis of the jet, the y-wise velocity component is always zero—i.e.,

$$\partial\phi_1/\partial y = 0 \tag{5}$$

at $y = 0$ for all x.

(2) On the surface of the jet $y = \pm 1$, we have two boundary conditions:

(a) The pressures are the same on both sides of the interface—i.e.,

$$\partial\phi_1/\partial x = (M_2^2/M_1^2)\,(\partial\phi_2/\partial x) \tag{6}$$

at $y = \pm 1$.

(b) The inclinations of the flow are the same on both sides of the interface—i.e.,

$$\partial\phi_1/\partial y = \partial\phi_2/\partial y \tag{7}$$

at $y = \pm 1$.

(3) The boundary conditions at infinity depend on whether the uniform stream is supersonic or subsonic.

(a) If the uniform stream is subsonic—i.e., $M_2 < 1$—we have that the disturbance will die out at infinity—i.e.,

$$\partial\phi_2/\partial x = \partial\phi_2/\partial y = 0 \tag{8a}$$

at $y = \pm\infty$.

(b) If the uniform stream is supersonic—i.e., $M_2 > 1$—we assume that no disturbances come from infinity and that all disturbances are generated from the interface—i.e.,

$$\varphi_2 = F(x - \beta_2|y|) \tag{8b}$$

where F is an arbitrary function that is going to be determined and where $\beta_2^2 = M_2^2 - 1$.

Since the nature of the subsonic and of the supersonic flow of the surrounding stream differ entirely from each other, we have to treat the problem separately for these two cases.

(III) Supersonic Jet in Subsonic Uniform Stream

Since the differential Eq. (4) is linear, the method of superposition is applicable. It is then sufficient for us to consider one typical fundamental solution only in the analysis. In order to satisfy the boundary conditions [Eqs. (5) and (8)], we have the fundamental solution of ϕ_i as follows:

$$\left.\begin{aligned}\phi_1 &= \cos \lambda\beta_1 y\ (A_1 \sin \lambda x + B_1 \cos \lambda x)\\ \phi_2 &= e^{-\lambda\beta_2|y|}\ (A_2 \sin \lambda x + B_2 \cos \lambda x)\end{aligned}\right\} \quad (9)$$

where A_i and B_i are arbitrary constants, λ is the eigenvalue of the problem, and $\beta_1^2 = M_1^2 - 1$ and $\beta_2^2 = 1 - M_2^2$.

In order to satisfy the boundary conditions, Eqs. (6) and (7), we obtain the eigenvalue equation as follows:

$$\tan \lambda\beta_1 = \frac{M_1^2}{M_2^2}\sqrt{\frac{1 - M_2^2}{M_1^2 - 1}} = \tan \theta \quad \text{(say)} \quad (10)$$

where $0 \leq \theta \leq \pi/2$.

The eigenvalue λ is then

$$\lambda = (\theta + n\pi)/\beta_1 \quad (11)$$

where $n = 0, 1, 2, 3, \ldots$.

The complete solution of the problem is

$$\phi_1 = \sum_{n=0}^{\infty} \cos (\theta + n\pi) y \left[A_{1n} \sin \frac{\theta + n\pi}{\beta_1} x + B_{1n} \cos \frac{\theta + n\pi}{\beta_1} x\right] \quad (12)$$

$$\phi_2 = \sum_{n=0}^{\infty} e^{-(\beta_2/\beta_1)(\theta + n\pi)|y|} \left[A_{2n} \sin \frac{\theta + n\pi}{\beta_1} x + B_{2n} \cos \frac{\theta + n\pi}{\beta_1} x\right] \quad (13)$$

The coefficients A_{1n} and B_{1n} can be determined from the initial conditions Eq. (1). After A_{1n} and B_{1n} are known, A_{2n} and B_{2n} can be determined by either Eq. (6) or (8).

It is interesting to know that ϕ_1 and ϕ_2 of Eqs. (12) and (13), respectively, are, in general, not periodic functions but that they are *almost periodic functions* which were first introduced by Bohr.[6] Hence, the flow pattern in the supersonic jet in uniform subsonic stream is only almost periodic. As a first approximation, the wave length of this almost periodic structure is

$$L = (2\pi/\theta)\ \beta_1 \quad (14)$$

The variations of θ with M_1 and M_2 are shown in Figs. 2 and 3. It is seen that this wave length increases as M_2 increases for a given M_1. As $M_2 = 0$, $L = 4\beta_1$, which is the Prandtl's formula for two-dimensional supersonic jet.

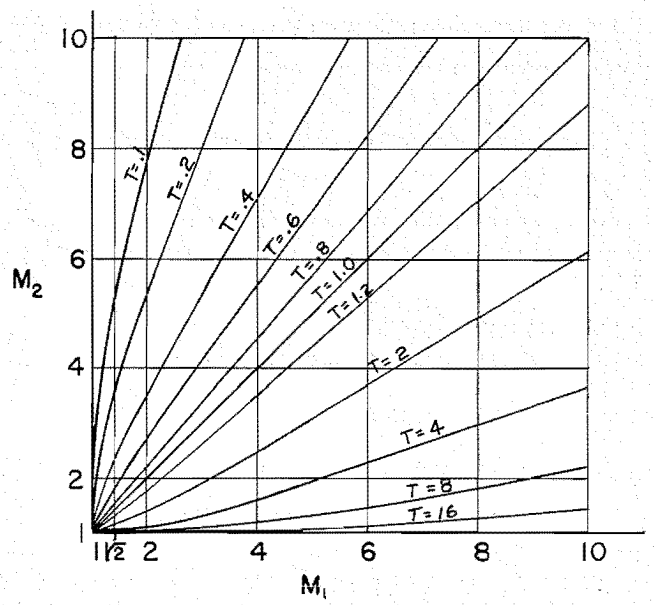

FIG. 4. Transmission factors.

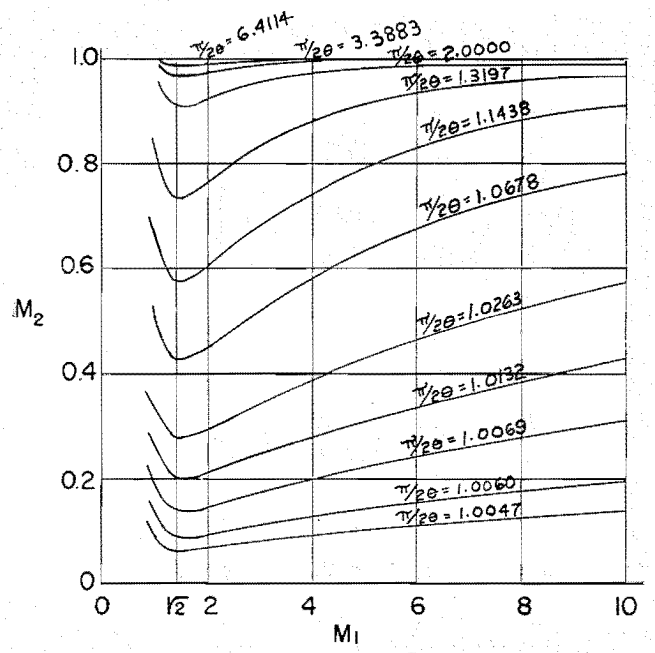

FIG. 3. Variation of wave length with M_1 and M_2.

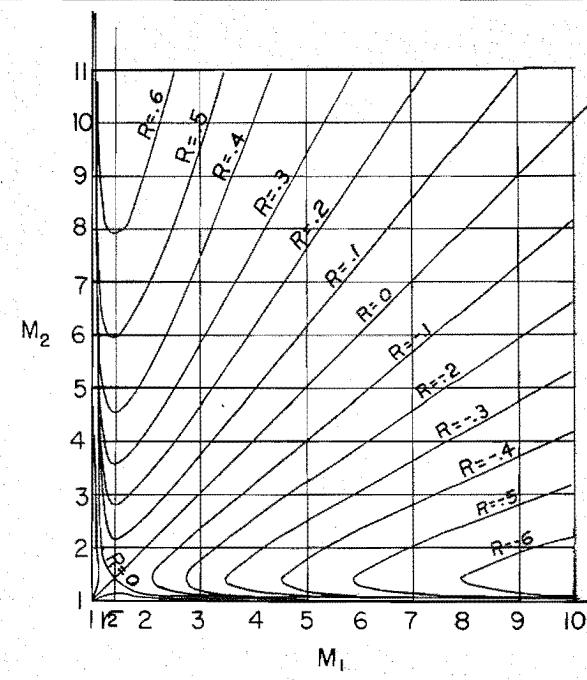

FIG. 5. Reflection factor.

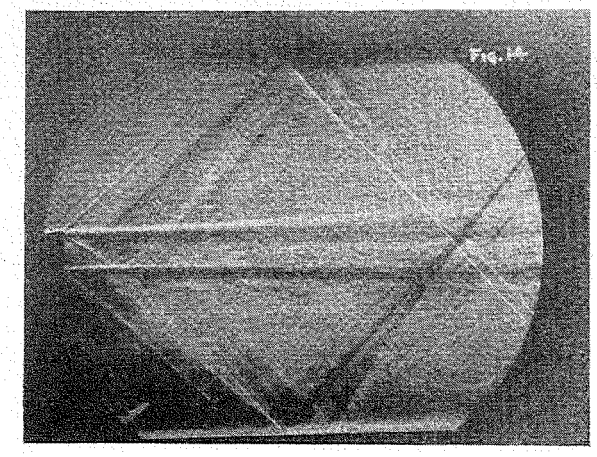

FIG. 6. Supersonic jet in uniform stream ($M_1 = 1.98$; $M_2 = 1.40$). (Fig. 14 of reference 7; courtesy of J. G. Wilder, Jr., Cornell Aeronautical Laboratory, Inc.)

(IV) Supersonic Jet in Supersonic Uniform Stream

First, we would like to know whether or not the supersonic jet still has periodic or almost periodic structure. We put

$$\left.\begin{aligned}\phi_1 &= \cos\lambda\beta_1 y\,[A_1 \sin\lambda x + B_1 \cos\lambda x] \\ \phi_2 &= A_2 \sin\lambda(x - \beta_2|y|) + B_2 \cos\lambda(x - \beta_2|y|)\end{aligned}\right\} \quad (15)$$

so that the boundary conditions [Eqs. (5) and (8)] are satisfied. In order to satisfy the boundary conditions [Eqs. (6) and (7)], we have the eigenvalue equation as follows:

$$\left[\frac{M_1^4}{M_2^4}\frac{\beta_2^2}{\beta_1^2} + \tan^2\lambda\beta_1\right][1 + \cot^2\lambda\beta_2] = 0 \quad (16)$$

It is evident that there is no real eigenvalue λ that satisfies Eq. (16). Hence, the supersonic jet will not have periodic or almost periodic structure.

The solution of this case may be obtained by method of characteristics. It is also possible to find some analytic solution for simple cases, as follows:

The most general solution of this case is

$$\left.\begin{aligned}\phi_1 &= f(x - \beta_1 y) + g(x + \beta_1 y) \\ \phi_2 &= F(x - \beta_2|y|)\end{aligned}\right\} \quad (17)$$

where f, g, and F are arbitrary functions to be determined from the initial conditions. In order to bring out the essential feature of the flow pattern, we consider the simple case that, at $x = 0$,

$$u_0(y) = AU_1, \quad v_0(y) = 0 \quad (18)$$

for $-1 \leq y \leq 1$, where A is a small constant.

In order to satisfy the boundary conditions on the interface $y = \pm 1$, we have

$$\phi_1 = f_0(x - \beta_1 y) + f_1(x - \beta_1 y) + \ldots + f_n(x - \beta_1 y) + \ldots + g_0(x + \beta_1 y) + g_1(x + \beta_1 y) + \ldots + g_n(x + \beta_1 y) + \ldots \quad (19)$$

where

$$\left.\begin{aligned} f_n(x - \beta_1 y) &= R^n \cdot \frac{A}{2}(x - \beta_1 y) && \text{for } (2n-1)\beta_1 < x - \beta_1 y < (2n+1)\beta_1 \\ &= 0 && \text{for } x - \beta_1 y \begin{matrix} > (2n+1)\beta_1 \\ < (2n-1)\beta_1 \end{matrix} \\ g_n(x + \beta_1 y) &= R^n \cdot \frac{A}{2}(x + \beta_1 y) && \text{for } (2n-1)\beta_1 < x + \beta_1 y < (2n+1)\beta_1 \\ &= 0 && \text{for } x + \beta_1 y \begin{matrix} > (2n+1)\beta_1 \\ < (2n-1)\beta_1 \end{matrix} \end{aligned}\right\} \quad (20)$$

and

$$\phi_2 = F_1(x - \beta_2|y|) + F_2(x - \beta_2|y|) + \ldots + F_n(x - \beta_2|y|) + \ldots \quad (21)$$

where

$$\left.\begin{aligned} F_n(x - \beta_2|y|) &= TR^{n-1} \cdot \frac{A}{2}(x - \beta_2|y|) && \text{for } 2n\beta_1 - \beta_2 < x - \beta_2|y| < 2(n+1)\beta_1 - \beta_2 \\ &= 0 && \text{for } x - \beta_2|y| \begin{matrix} > 2(n+1)\beta_1 - \beta_2 \\ < 2n\beta_1 - \beta_2 \end{matrix} \end{aligned}\right\} \quad (22)$$

T is the transmission factor that is the ratio of the nondimensional magnitude of disturbance in the uniform stream to that in the jet and which is given by the following formula:

$$T = 2/\left(\frac{M_2^2}{M_1^2} + \sqrt{\frac{M_2^2 - 1}{M_1^2 - 1}}\right) \tag{23}$$

The values of T for various M_1 and M_2 are shown in Fig. 4.

R is the reflection factor that is the ratio of the magnitude of the reflected disturbance from the surface of discontinuity to the magnitude of the incident disturbance and which is given by the following formula:

$$R = \left(\frac{M_2^2}{M_1^2} - \sqrt{\frac{M_2^2 - 1}{M_1^2 - 1}}\right)\Big/\left(\frac{M_2^2}{M_1^2} + \sqrt{\frac{M_2^2 - 1}{M_1^2 - 1}}\right) \tag{24}$$

Its value lies between -1 to $+1$. The values of R for various M_1 and M_2 are shown in Fig. 5. It is seen that the reflected disturbance may be of the same sign, or of opposite sign of the incident disturbance, or zero according to the values of M_1 and M_2.

There are few experimental data to check the present theory. However, the schlieren pictures (Fig. 6) taken by Wilder[7] indicate that there is no periodic structure in the supersonic jet in uniform supersonic stream. Since the difference between M_1 and M_2 is small in Wilder's pictures, R is extremely small; as a result, in most of his pictures, only the first transmitted disturbance $F_1(x - \beta_2 |y|)$ is seen without reflection. In only a few cases, the first reflected disturbances $f_1(x - \beta_1 y)$ and $g_1(x + \beta_1 y)$ are seen.

REFERENCES

[1] Emden, R., *Über die Ausströmungserscheinungen permanenter Gase*, Annalen der Physik und Chemie (G. Wiedermann) 69; Leipzig, 1899.

[2] Prandtl, L., *Über die stationären Wellen in einem Gasstrahle*, Phys. Zeit., Vol. 5, p. 599, 1904.

[3] von Kármán, Th.: *Über stationären Wellen in Gasstrahlen*, Phys. Zeit., Vol. 8, p. 207, 1907.

[4] Lord Rayleigh, *On the Discharge of Gases under High Pressures*, Phil. Mag., Vol. 32, 1916.

[5] Pack, D. C., *A Note on Prandtl's Formula for the Wavelength of a Supersonic Gas Jet*, Quart. Jour. Mech. Appl. Math., Vol. III, Part 2, 1950.

[6] Bohr, H., *Almost Periodic Functions;* Chelsea Publishing Company, New York, 1947; Julius Springer, Berlin, 1933.

[7] Wilder, J. G., Jr., *Part I of Final Report of Phase I of The Study of Air Exchange Problems in Supersonic Tunnels*, Cornell Aeronautical Laboratory Report AD-570-A5, 1949.

Velocity and Temperature Distribution Through the Laminar Boundary Layer in Supersonic Flow

(*Continued from page 47*)

[3] Ackeret, J., Feldmann, F., and Rott, N., *Untersuchungen an Verdichtungsstoessen und Grenzschichten in schnell bewegten Gasen*, Mitteilung aus dem Inst. für Aerodynamik, No. 10, Zurich. Also translated as N.A.C.A. T.M. No. 1113, *Tests on Compression Shocks and Boundary Layers in Fast-Moving Gases*, January, 1947.

[4] Ferrari, C., *Study of the Laminar Boundary Layer at Supersonic Speeds*, Cornell Aeronautical Laboratory Report CAL/CF-1007 (Available from Johns Hopkins University, Applied Physics Laboratory, Silver Spring, Md.), June 15, 1948.

[5] von Mises, R., *Bemerkungen zur Hydrodynamik*, Zeit. für angewandte Mathematik und Mechanik, Vol. 7, No. 6, 1927.

[6] von Kármán, Th., and Millikan, C. B., *On the Theory of Laminar Boundary Layers Involving Separation*, N.A.C.A. T.R. No. 504, Washington, 1934.

[7] Ferrari, C., *Velocity and Temperature Distribution Through the Laminar Boundary Layer in Supersonic Flow*, Cornell Aeronautical Laboratory Report CAL/CM-585 (Available from Johns Hopkins University, Applied Physics Laboratory, Silver Spring, Md.), May, 1950.

Column Behavior Under Conditions of Impact

(*Continued from page 60*)

REFERENCES

[1] Meier, J. H., *On the Dynamics of Elastic Buckling*, Journal of the Aeronautical Sciences, Vol. 12, No. 4, pp. 433–440, October, 1945.

[2] Hoff, N. J., *The Dynamics of the Buckling of Elastic Columns*, Journal of Applied Mechanics, Vol. 18, No. 1, pp. 68–74, March, 1951.

Readers' Forum

BRIEF REPORTS of investigations in the aeronautical sciences and discussions of papers published in the JOURNAL are presented in this special department. Publication will be completed approximately 8 to 10 weeks after receipt of the material. The Editorial Committee does not hold itself responsible for the opinions expressed by the correspondents. Contributions should not exceed 800 words in length.

Buckling of an N-Section Column

G. Sri Ram and G. V. R. Rao
Research Student and Assistant Professor, Respectively, Indian Institute of Science, Bangalore, India
September 22, 1951

CONSIDER A COLUMN BUILT IN at one end and free at the other, subject to an axial load P. The failure of the column is assumed to take place due to lateral instability rather than by direct compression. When the column is made of n-sections along its length, an analytical solution for the critical load P_{cr}. can be obtained as shown in Fig. 1.

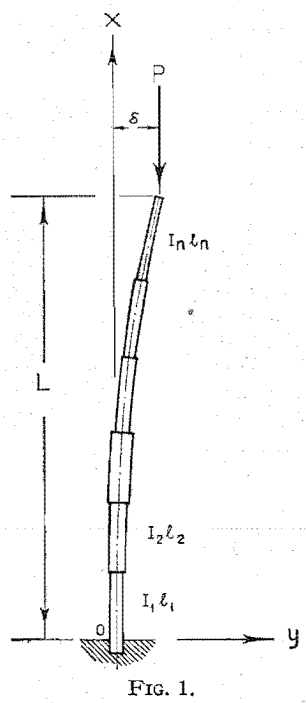

FIG. 1.

Let the i-th section of the column have a length $l_i = L_i - L_{i-1}$ and moment of inertia I_i. This section can be characterized by $k_i l_i$, where $k_i^2 = P/EI_i$. The governing differential equation for the deflection of the column in

$$L_{i-1} < x < L_i$$

is

$$EI_i(d^2y_i/dx^2) = P(\delta - y_i) \qquad (1)$$

Thus for the n-sections along the length we have n such differential equations. One can assume

$$y_i = \delta + A_i \cos k_i x + B_i \sin k_i x \qquad (2)$$

as a solution of Eq. (1). From the continuity of the deflection curve of the column we can equate the deflection and the slope of the column at the i-th joint obtained from the $i - 1$ section and i-th section. These together with the conditions at the ends of the column give equations to determine the constant coefficients, A_i and B_i. If these coefficients should have nonzero solutions, one must satisfy a determinantal equation. The expansion of the determinant leads to a transcendental equation, the solution of which gives the critical load of the column.

For example, in the case of a column built up in two sections the equation

$$0 = 1 - (K_1/K_2) \tan k_1 l_1 \tan k_2 l_2$$

gives the buckling load of the column. This condition is the same as that given in references 1 and 2, whereas, for $n = 3$, there seems to be an error in reference 2. For $n = 3$, we must satisfy

$$0 = 1 - (K_1/K_2) \tan k_1 l_1 \tan k_2 l_2 - (K_1/K_3) \tan k_1 l_1 \tan k_3 l_3 - (K_2/K_3) \tan k_2 l_2 \tan k_3 l_3$$

For $n = 4$, we must satisfy

$$0 = 1 - \Sigma(K_q/K_r) \tan k_q l_q \tan k_r l_r + (K_1/K_2)(K_3/K_4) \tan k_1 l_1 \tan k_2 l_2 \tan k_3 l_3 \tan k_4 l_4$$

where, in the summation, $r = 1, 2, 3, 4$ and $q < r$.

In general, for n-sections we obtain an equation of the form

$$0 = 1 - \Sigma(f_i/K_i) \tan k_i l_i \qquad (i = 2, 3, \ldots, n) \qquad (3)$$

Each f_i in the above equation depends upon the functions $f_2, f_3, \ldots, f_{i-1}$,

$$f_i = f_{i-1} + k_{i-1} \tan k_{i-1} l_{i-1} \quad [1 - \Sigma(f_r/k_r) \tan k_r l_r] \qquad (4)$$

summed for $r = 2, 3, \ldots, i - 2$, and $f_2 = K_i \tan k_i l_i$.

With the above formula one can write the characteristic equation for any number of sections in the length of the column. The equation that gives the critical load can only be solved by trial and error. As n increases, the work becomes laborious. In practice, one can see that $\tan k_i l_i$ is small and that products of $\tan k_i l_i$ four times or more can be neglected. Eq. (3) will then reduce to

$$0 = 1 - \Sigma(K_q/K_r) \tan k_q l_q \tan k_r l_r \qquad (5)$$

where $r = 1, 2, \ldots$ and $q < r$.

One can easily show that the f_i in Eq. (3) are all positive. Further, Eq. (4) shows that the approximation made by neglecting higher powers of products of $\tan k_i l_i$ gives a higher value for f_i. Considering the plot of the right-hand sides of Eqs. (3) and (5) against P, one can easily prove that the solution of the approximate Eq. (5) is always lower than the solution of the complete Eq. (3).

From the application of the energy method, one obtains an approximate buckling load, always higher than the true buckling load. Therefore, the method outlined above helps to obtain bounds on the buckling load of a column.

A symmetrical column with both ends pinned can be reduced to the case treated above by considering only half the length of the column. For an unsymmetrical column pinned at both ends, similar formulas can easily be obtained. A numerical example is carried out applying this method for a column built up in four sections. The following data are taken for the example:

I_1 is the section of the column at the built-in end and

$$\frac{I_2}{I_1} = 0.81, \quad \frac{I_3}{I_1} = 0.64, \quad \frac{I_4}{I_1} = 0.36$$

$$l_1 = l_2 = l_3 = l_4 = L/4$$

L = length of the column. The approximate solution obtained from Eq. (5) gives a critical load of $P_{cr.} = 1.979\ (EI_1/L^2)$. From the strain energy method, by assuming a deflection curve $y = \delta[1 - \cos(\pi x/2L)]$, one obtains a critical load of $P_{cr.} =$

2.034 (EI_1/L^2). The analytical solution as given from Eq. (3) yields $P_{cr.} = 2.019(EI_1/L^2)$.

REFERENCES

[1] Timoshenko, S., *Theory of Elastic Stability*, pp. 129–130; McGraw-Hill Book Company, Inc., New York, 1936.

[2] Thomson, W. T., *Matrix Solution of the n-Section Column*, Journal of the Aeronautical Sciences, Vol. 16, No. 10, pp. 623–624, October, 1949.

A Solution of the Surging Problem in Axial-Flow Compressors

John Mitchell Stephenson*
Farnborough, England

August 21, 1951

SUMMARY

If an axial-flow compressor has many stages on a single rotor shaft, and adiabatic flow, there is only one combination of pressure ratio and mass flow for which the efficiency of compression is a maximum. This is called the "design point" on the performance graph and usually corresponds to full load or thereabouts. At any other point the efficiency is reduced, and surging may occur with catastrophic results. This effect places an upper limit of about six on the design pressure ratio of such a compressor.

The reason for this limitation is analyzed, and the known ways of avoiding it are enumerated. A further solution is then described, which depends on extraction of heat from the gas during compression. It is shown that high pressure ratios can be achieved with good efficiency and stability and without mechanical complications.

(1) INTRODUCTION

THE FLOW THROUGHOUT AN AXIAL-FLOW COMPRESSOR can most conveniently be deduced in terms of the performance of each stage, by which is meant each pair of annular blade rows. To compress efficiently, none of the blades of the compressor must be stalled. But the chief limit to the operation of axial compressor is surging, which occurs when most of the stages are stalled. The mechanism of surging is not fully understood, but the effect of violent fluctuations of pressure is well known. Surging must always be prevented, and the most important characteristics of a compressor is the surge line, which describes the maximum steady pressure ratio attainable with a given mass flow.

We shall show that the line of most efficient running of a single shaft adiabatic compressor is close to the surge line. This fact limits the design pressure ratio of such a compressor to about six. Above this it is not usually possible to avoid surging at part loads.

(2) THE EFFICIENCY OF AN ELEMENTARY COMPRESSION

Consider a gas flowing steadily along a uniform tube, such that at one section there is an infinitesimal pressure rise dp. If the work put into the gas to effect this compression is dW per unit mass flow, we may define the efficiency η of the process as the ratio of pressure energy produced to the work applied. That is,

$$\eta = dp/\rho\, dW$$

where ρ is the density of the gas.

If the compression is adiabatic dW is equal to the change of enthalpy, $Cp\, dT$. But if an amount of heat dQ per unit mass flow is extracted from the gas during the compression, we have

$$dW = Cp\, dT + dQ$$

We now define a cooling factor ζ as the ratio of heat extracted to the work done, or

$$\zeta = dQ/dW$$

Combining these equations we have

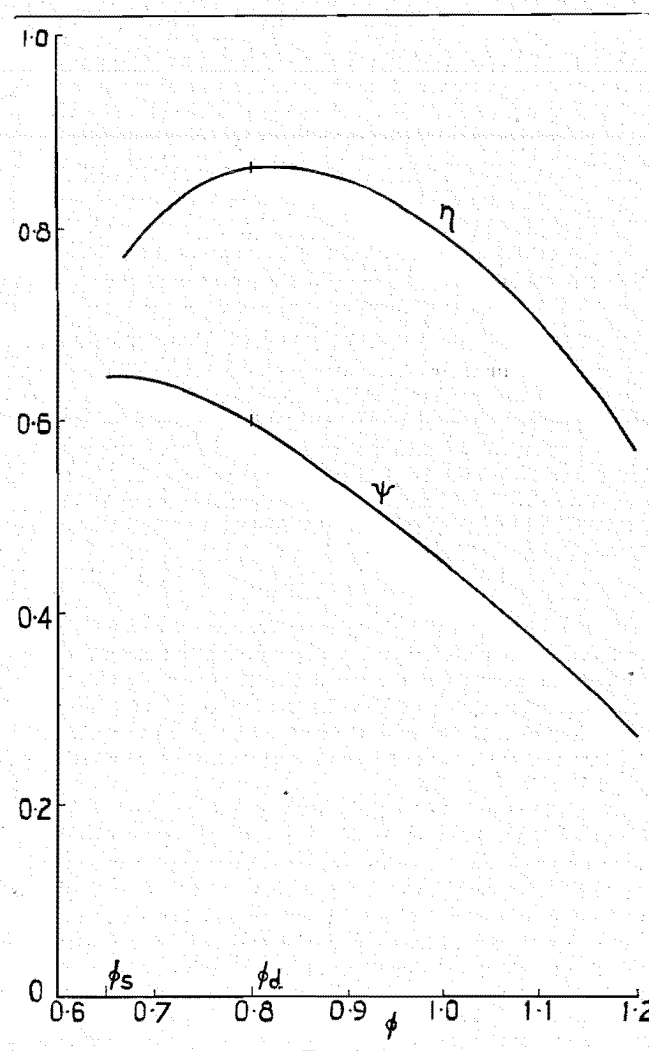

FIG. 1.

$$\eta/(1 - \zeta) = (dp/\rho)/(Cp\, dT)$$

The differential law relating pressure and temperature is approximately

$$dp/p = [n/(n - 1)](dT/T)$$

where $n = \gamma$ for an isentropic compression (i.e., $\eta = 1 = \zeta$). Hence, using the perfect gas equation of state,

$$p = \rho RT = \left(\frac{\gamma - 1}{\gamma}\right)\rho CpT$$

we have

$$\frac{\eta}{1 - \zeta} = \left(\frac{\gamma - 1}{\gamma}\right)\left(\frac{n}{n - 1}\right) \qquad (1)$$

In the particular numerical case that we shall consider later, $\gamma = 7/5$ and $\eta = 6/7$, so that

$$n = 3/(2 + \zeta) \qquad (1a)$$

Note that, if $\zeta = 0$, the compression is adiabatic; while if $\zeta = 1$, we have $n = 1$ and the compression is isothermal. We shall assume here that ζ always lies between these limits so that no heating or refrigeration is applied. Clearly, for a given value of the efficiency (which is independent of the cooling), we can reduce n from the adiabatic value to any other value greater than one simply by cooling the gas.

* Now at Bristol Aeroplane Company, England.

(3) The Flow Range of a Single Compressor Stage

The dimensional analysis of a compressor stage shows that there are a small number of coefficients in terms of which the performance can be described. For a stage of given geometrical design the only quantities that may be varied independently are

- va = the mean velocity of the gas in the axial direction
- u = the tangential velocity of the rotor blades at a reference radius
- l = a length giving the geometrical scale of the stage
- ν = the kinematic viscosity of the gas at same point
- a = the velocity of sound in the gas at inlet

The variables can be combined to form three dimensionless ratios, each a measure of one aspect of the physical behavior of the gas. These are the Reynolds Number, $Re = val/\nu$; the Mach Number, $M = va/a$; and the flow coefficient $\phi = va/u$.

The dependent quantities of interest are the pressure rise per unit mass, $\Delta p/\rho$, and the efficiency. The pressure rise of a single stage is as a rule sufficiently small to use the elementary efficiency η as defined in Section (2). The pressure rise can be expressed in the dimensionless form

$$\psi = \Delta p/(1/2)\rho u^2$$

We may say, therefore, that the performance of a stage is given by ψ and η, which are unique but as yet unknown functions of the independent parameters ϕ, Re, and M. The effect of the last two is known to be small, provided that $Re > 3 \times 10^5$ and $M < 0.5$, approximately. Thus the performance can be expressed simply in terms of ϕ, which determines the angle of attack of the gas on the blades.

We shall not now derive ψ and η analytically in terms of ϕ and the blade shape but shall simply show the characteristics of a typical stage in Fig. 1. This stage is designed to operate at the point of best efficiency, where $\phi = \phi_d$. We see that there is only a small range of ϕ over which the stage works efficiently. And at values less than ϕ_s, ψ has a negative slope, and the blades are stalled. If the stage is running alone, the flow surges at these points. However, when several stages are combined in series, surging does not occur until most of the stages are stalled.

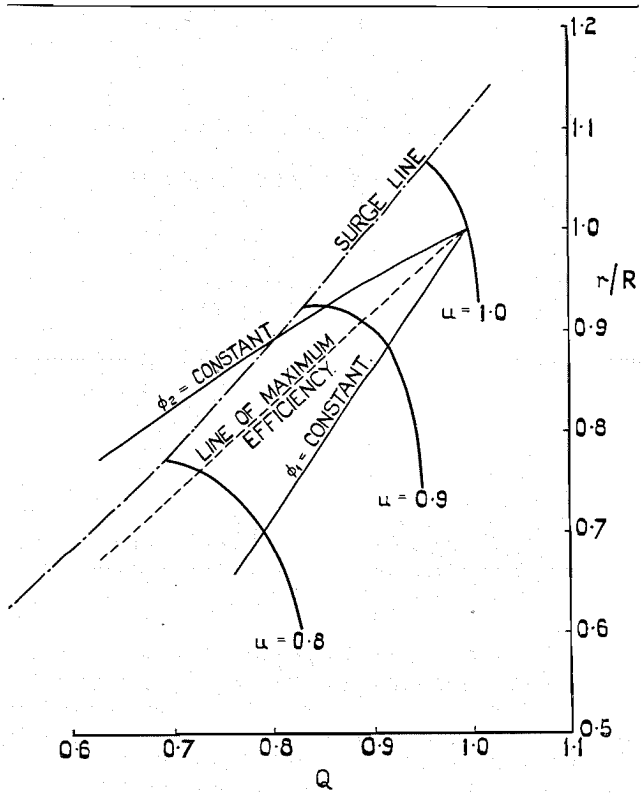

FIG. 2.

(4) The Combination of Several Stages in Series

The problem of combining stages so as to produce a high pressure ratio is to ensure that all the stages operate at or near the design value of ϕ under all likely conditions of operation.

Consider a compressor with many stages, each having the performance shown in Fig. 1. We take any two separated stages in this compressor and refer to them with suffixes 1 and 2. The mass flow Q is given for any section of area A by

$$Q = \rho A\, Va$$

The law of compression is

$$\rho_2/\rho_1 = (p_2/p_1)^{1/n} = r^{1/n}$$

Hence,

$$\frac{\phi_2}{\phi_1} = \left(\frac{Q_2 A_1 u_1}{Q_1 A_2 u_2}\right)\left(\frac{1}{r^{1/n}}\right) \tag{2}$$

Now the area ratio A_1/A_2 is determined for a particular density ratio and is fixed thereafter. Let us suppose that this corresponds to a design pressure ratio R, when there is no cooling ($\zeta = 0$) and the efficiency is $\eta = 6/7$. Then, from Eq. (1a), we have $n = 3/2$.

If also at the design point $u_1 = u_2/k$ where k is a constant and $Q_1 = Q_2$, then

$$A_1/A_2 = kR^{2/3}$$

and Eq. (2) becomes

$$\phi_2/\phi_1 = (Q_2 u_1/Q_1 u_2)(kR^{2/3}/r^{1/n}) \tag{3}$$

A typical simple compressor has continuous adiabatic flow and a single shaft. Thus $u_1 = u_2/k$, $Q_1 = Q_2$, and n = constant (approximately) for all r. It is clear from Eq. (3) that in this case

$$\phi_2 > \phi_1 \text{ for all } r < R$$

Thus, the stages are never all working at maximum efficiency, except at the design pressure ratio and mass flow. The (r, Q, u) diagram of such a compressor is shown in Fig. 2 with the surge line.

Now $\phi_1 = Q_1/\rho_1 A_1 u_1$, and therefore the condition that ϕ_1 is constant implies that Q_1/u_1 is constant. Similarly, ϕ_2 is constant implies that $Q_1/u_1 r^{1/n}$ is constant. The lines of constant ϕ are shown in Fig. 2 for the case where section 1 is at inlet and section 2 at outlet. Since as we have seen, $\phi_2 > \phi_1$, neither of these lines corresponds to efficient compression, and in the second case the compressor surges when $r < 0.9$. The line of best efficiency actually lies somewhere between these two and corresponds to constant ϕ for a stage midway between inlet and outlet. It is parallel to the surge line, which approximately corresponds to stalling of the midway stage.

To ensure stable running, especially when R is large, it is therefore necessary to design every stage, and in particular the first few, to have a large flow range. We shall not consider this subject here, but there are more general solutions of this problem, some of which are well known.

(5) Solutions

(a) The most simple and specialized solution is to keep the pressure ratio always at the design value R. When a compressor forms part of a closed system with a continuously circulating gas, it is sometimes possible to alter the inlet density level at will. In this way the mass flow and power may be altered over the whole range, while the rotational frequency remains constant. Thus the efficiency is always a maximum. This solution is most suitable in connection with constant speed electrical apparatus.

(b) A device that has long been used on airplane propellers is to rotate the blades about a radial axis. In this way the flow co-

TABLE 1

R	3	4	5	6	7	8	9	10	11	12	13	14	15
r_0	2.06	2.50	2.92	3.30	3.67	4.02	4.35	4.66	4.96	5.24	5.53	5.79	6.09

efficient ϕ_d corresponding to maximum efficiency can be varied over a large range. Of course the twist of the blades cannot be altered, so that the efficiency falls off slightly when they are rotated. It is difficult to adjust the rotor blades, but, if only the stators are rotated, the efficiency can be improved and surging avoided. For example, when $r < R$, the entry stator blades and the stators of the first few stages should be rotated to a high stagger (fine pitch), while the stators of the last few stages are moved to low stagger (coarse pitch).

From Eq. (3) however, we see that $\phi_1 = \phi_2$ can be maintained for all pressure ratios less than R by reducing either (c) Q_2/Q_1, (d) u_1/u_2, (e) n. We discuss these in turn.

(c) In a compressor with inlet at atmospheric pressure it is easy to reduce Q_2/Q_1 below the usual value of one by blowing off gas between the stages. However, a great deal of power is lost in doing this, so that the efficiency of any plant incorporating such a device is low. Blowoff is only defensible therefore for transient conditions in starting or decelerating compressors.

(d) u_1/u_2 can be appropriately reduced below the design value k if all the rotors are able to turn independently. This arrangement was suggested by Dr. A. A. Griffith in 1929. It is complicated but is frequently approached by dividing the stages into two groups on separate shafts.

(e) The solution put forward here and which is in theory most promising for many applications is to reduce the exponent n by cooling the gas during the compression, such that n is given by Eq. (1). A device to effect this was patented by the author and Power Jets Ltd. in July, 1948.

(6) Cooled Compression

We consider a single shaft compressor without blowoff, so that Eq. (3) becomes

$$\phi_2/\phi_1 = R^{2/3}/r^{1/n}$$

and we wish to adjust n so that $\phi_2 = \phi_1$ for all r. Hence, we require

$$\log r/\log R = 2n/3$$

Using Eq. (1a) we have

$$\log r/\log R = 2/(2 + \zeta)$$

If ζ is varied according to this formula, all the stages work at their design efficiency. But since we have assumed that $\zeta < 1$, there is a value r_0 below which it is not possible to reduce n when $n = 1$ and the flow is isothermal. Then

$$\log r_0/\log R = 2/3$$

Values of r_0 and R are compared in Table 1. We see that, if a single-shaft isothermal (or adiabatic) compressor will run stably up to a design pressure ratio of five, then a cooled compressor having the cooling shut off at full load can be designed for a pressure ratio of eleven, *with the same stability*.

In practice it may not be desirable to vary ζ and n continuously. If, for example, full cooling is applied up to one-half the required pressure ratio and switched off completely above that the compressor may be sufficiently stable.

Suppose the cooling is achieved by spraying liquid into the stream, so that the liquid is at the temperature of the stream and does not evaporate. Then, if the specific heat of the liquid is C and the liquid-gas ratio m by weight, we have

$$dQ = mC\,dT$$

Hence

$$\zeta = mC/(Cp + mC)$$

Note that, for isothermal compression, $m \to \infty$. For air and water, $Cp = 0.24C$ and

$$\zeta = m/(0.24 + m)$$

An approach to the solution given here is made by varying the thermal ratio of an intercooler placed between two multistage compressors that operate in series. This is an easy way to achieve freedom from surging troubles on an intercooled gas-turbine engine.

Plastic Buckling of a Simply Supported Plate in Compression

Richard A. Pride
Aeronautical Research Scientist, Langley Aeronautical Laboratory, Langley Air Force Base, Va.
September 25, 1951

THE APPLICATION OF THEORIES OF PLASTICITY to plate buckling problems has resulted in widespread controversy in recent years. In the case of long simply supported flanges, a large discrepancy exists between the predictions of buckling theories based on deformation or finite theories of plasticity[1, 2] and those based on flow or incremental theories of plasticity.[3] The experimental data are in excellent agreement with deformation-type buckling theories and appear to contradict altogether the flow type of buckling theory. It has been both suggested[4] and denied[5] that the discrepancy between the experimental results and the predictions of flow-type buckling theories can be ascribed to the effects of the initial imperfections. A crucial question in such a debate is how large the initial imperfections actually were.

In the case of simply supported plates the discrepancy between the two types of theory is generally much less pronounced. Here also experimental results[6] are in much better agreement with deformation than flow-type buckling theories. Several investigators have questioned the validity of this comparison, however, because two of the deformation type of buckling theories used in the comparison were based on the Shanley principle of buckling with increase in load, whereas the flow type of buckling theory was based on the assumption of constant loading during buckling. Pearson[7] has recalculated the buckling load predicted by flow-type theories for simply supported plates taking the Shanley principle into account and found that this modification substantially improved the agreement with experiment in the lower stress range. Although Bijlaard[8] has pointed out that a large part of the improvement is due to the use of the simplifying assumption that Poisson's ratio is one-half in the elastic, as well as the plastic, range, it seemed desirable to provide an experimental check in a region in which the discrepancy between the two types of theories is much more pronounced.

The discrepancy between the theories becomes greater at high buckling stresses—that is, for plates having large thickness-width ratios. However, it would not be satisfactory to go far in this direction because the thin plate equations on which all of the plastic buckling theories have been based would cease to be applicable. A better way to provide the desired check is to use

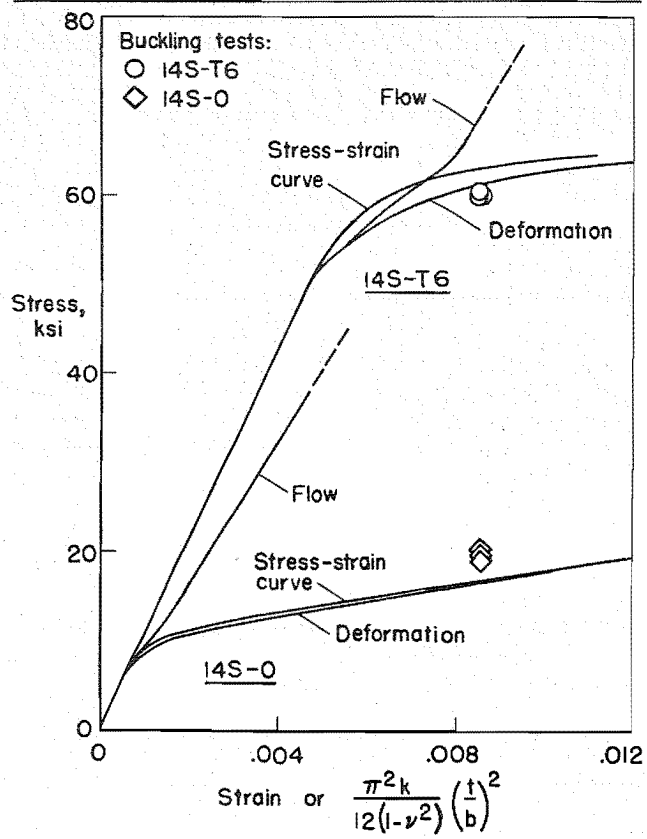

FIG. 1. Plastic buckling theories compared with tests.

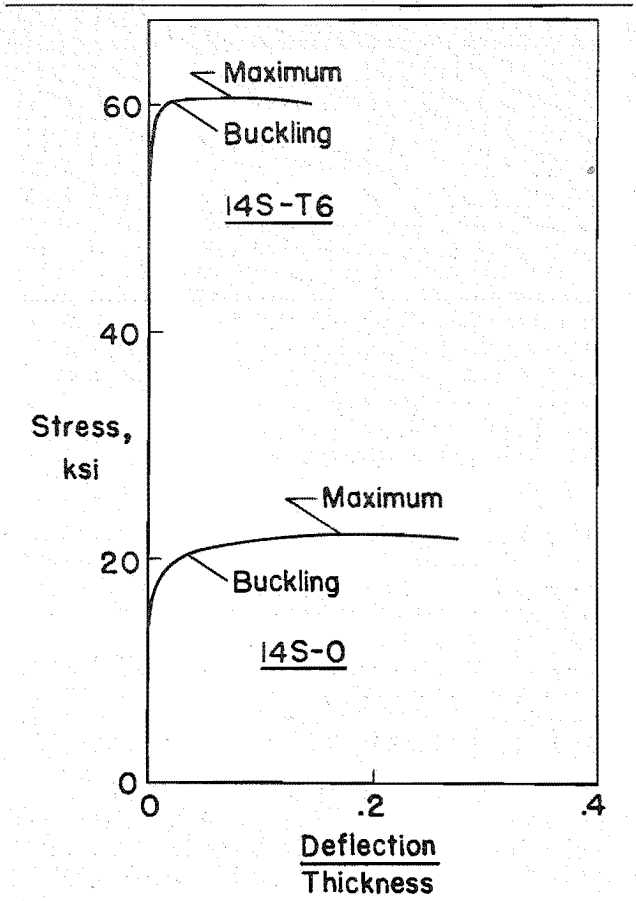

FIG. 2. Stress-deflection diagrams from buckling tests. (Plate thickness, $t = 0.154$ in.)

a material with a low yield stress. With this purpose in mind, square tubes of 14S-T6 aluminum alloy similar to those with the highest buckling stress in a previous experimental program[6] were annealed before being buckled, producing the results shown in Fig. 1. The yield stress was reduced from 62,400 to 12,300 lbs. per sq.in., and the buckling stress was reduced from an average (three tests each) of 60,400 to 19,700 lbs. per sq.in. as a result of annealing the material.

Deformation-type plastic buckling theories continue to be in good agreement with these tests. Flow-type theories, however, are completely inadequate even with Pearson's modification. The dashed portions of the flow theory curves in Fig. 1 indicate the trend of the theory if the stress-strain curve is assumed to rise to a correspondingly high stress. On this basis Pearson's analysis gives the same buckling stress for the low-strength annealed material as for the high-strength material. Since for reasonable strains the stress-strain curve of the material does not rise indefinitely, the flow theory curves probably should be cut off in the vicinity of the ends of the solid lines, Fig. 1. This would seem to imply that buckling could not occur at all for the annealed tubes tested.

The small scatter of the test results makes it seem doubtful that the large discrepancy between these results and the predictions of flow-type buckling theories can be ascribed to the effects of initial imperfections. However, this evidence alone cannot be considered conclusive. Additional data bearing on this possible explanation are provided by the representative stress-deflection curves shown in Fig. 2, from which the order of magnitude of the initial imperfections can be inferred.

The results just discussed taken in conjunction with the previously established results for buckling of long simply supported flanges confirm the view that for practical purposes the buckling stresses of well-made plates are in good agreement with the predictions of buckling theories based on deformation theories of plasticity without modification for effects of initial eccentricity.

REFERENCES

[1] Bijlaard, P. P., *A Theory of Plastic Stability and Its Application to Thin Plates of Structural Steel*, Koninklijke Nederlandsche Akad v. Wetenschappen, Proc., Vol. XLI, No. 7, pp. 731–743, 1938.

[2] Stowell, E. Z., *A Unified Theory of Plastic Buckling of Columns and Plates*, N.A.C.A. Report No. 898, 1948 (formerly N.A.C.A. T.N. No. 1556, 1948).

[3] Handelman, G. H., and Prager, W., *Plastic Buckling of a Rectangular Plate Under Edge Thrusts*, N.A.C.A. Report No. 946, 1949 (formerly N.A.C.A. T.N. No. 1530, 1948).

[4] Cicala, P., *On Plastic Buckling of a Compressed Strip*, Readers' Forum, Journal of the Aeronautical Sciences, Vol. 17, No. 6, pp. 378–379, June, 1950.

[5] Bijlaard, P. P., *On the Plastic Buckling of Plates*, Readers' Forum, Journal of the Aeronautical Sciences, Vol. 17, No. 11, pp. 742–743, November, 1950.

[6] Pride, R. A., and Heimerl, G. J., *Plastic Buckling of Simply Supported Compressed Plates*, N.A.C.A. T.N. No. 1817, 1949.

[7] Pearson, C. E., *Bifurcation Criterion and Plastic Buckling of Plates and Columns*, Journal of the Aeronautical Sciences, Vol. 17, No. 7, pp. 417–424, 455, July, 1950.

[8] Bijlaard, P. P., *On the Plastic Buckling of Plates According to the Flow Theory*, Readers' Forum, Journal of the Aeronautical Sciences, Vol. 17, No. 12, pp. 810–811, December, 1950.

A Method for Calculating Airfoils with Prescribed Pressure Distribution

Dr.-Ing. N. Scholz

Institute of Fluid Mechanics, Technical University of Braunschweig, Germany

September 28, 1951

THE PROBLEM OF CALCULATING AIRFOILS with prescribed pressure distribution is important for laminar airfoils and suction

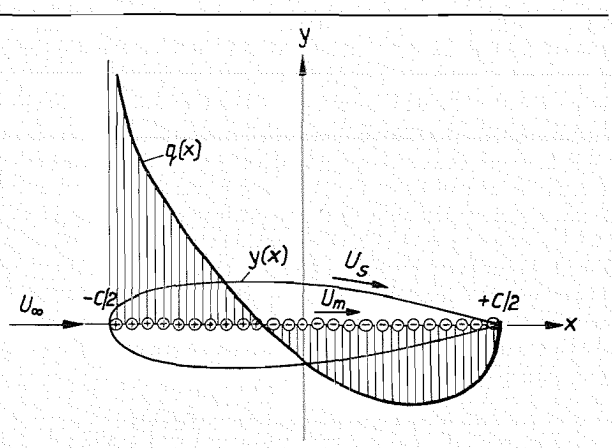

FIG. 1. Source distribution and airfoil shape in the x, y-plane.

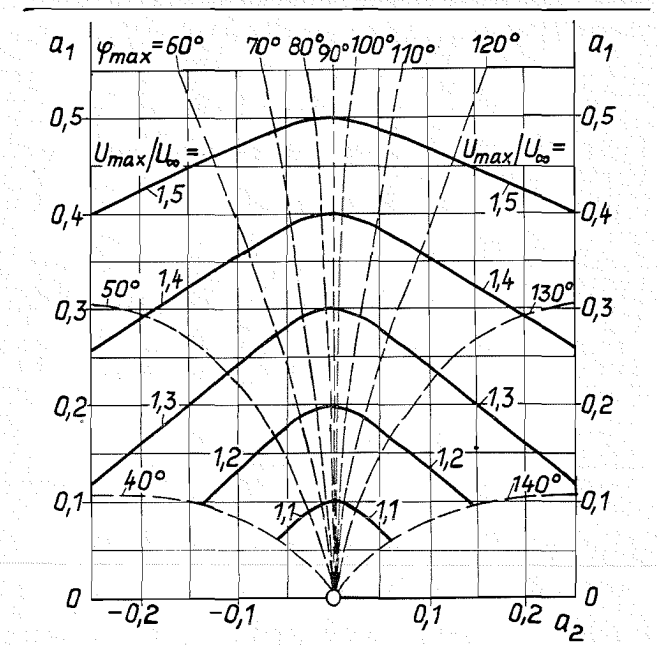

FIG. 2. Diagram for evaluating the coefficients a_1 and a_2.

airfoils. Furthermore, the problem of cavitation in fluid flow and the problem of critical Mach Number at subsonic flow are related herewith. A solution by means of the method of singularities has been given by Riegels[1] and Allen.[2] In this note we give an extension of the method by Riegels suited for practical application.

The starting point of our calculations is the relation given by Riegels[3] between the velocity of the potential flow on the surface of the airfoil, U_s, and on its mean line, U_m, see Fig. 1,

$$U_s(x) = U_m(x)/\sqrt{1 + (dy/dx)^2} \tag{1}$$

$y(x)$ being the shape of the profile. Between the source distribution $q(x)$, which induces velocities on the mean line, and the airfoil shape the following relation holds:

$$dy/dx = (1/2)\,[q(x)/U_\infty] \tag{2}$$

Therefore one gets from Eq. (1) for the velocity at the surface of the airfoil

$$U_s(x) = U_\infty \left\{ \frac{1 + \frac{1}{\pi}\int_{x'=-c/2}^{+c/2} \frac{dy}{dx'}\frac{dx'}{x - x'}}{\sqrt{1 + (dy/dx)^2}} \right\} \tag{3}$$

For the airfoil shape $y(x)$, at first supposed to be symmetrical, we give an expression, which fulfills identically the condition of a closed contour ($y = 0$ for $x = \pm c/2$), φ being the well-known trigonometric variable,

$$\left.\begin{aligned} x/(c/2) &= -\cos\varphi \\ y/(c/2) &= \sum_{n=1}^{\infty} a_n \sin(n\varphi) \\ \frac{dy}{dx} &= \sum_{n=1}^{\infty} n a_n \frac{\cos(n\varphi)}{\sin\varphi} \end{aligned}\right\} \tag{4}$$

with $0 \le \varphi \le \pi$ for $-c/2 \le x \le +c/2$. The integral in Eq. (3) then becomes (compare also reference 2),

$$\frac{1}{\pi}\int_{x'=-c/2}^{+c/2} \frac{dy}{dx'}\frac{dx'}{x - x'} = \frac{1}{\pi}\int_{\varphi'=0}^{\pi} \times \left(\sum_{n=1}^{\infty} n(a_n)\frac{\cos(n\varphi')}{\sin\varphi'}\right)\frac{\sin\varphi'}{\cos\varphi' - \cos\varphi}\,d\varphi' = \sum_{n=1}^{\infty} n(a_n)\frac{\sin(n\varphi)}{\sin\varphi} \tag{5}$$

Herewith one obtains finally from Eq. (3) after some simple calculation

$$\sum_{n=1}^{\infty} n(a_n)\sin(n\varphi) = \sin\varphi \times \left\{\frac{U_s(\varphi)}{U_\infty}\sqrt{1 + \left(\sum_{n=1}^{\infty} n(a_n)\frac{\cos(n\varphi)}{\sin\varphi}\right)^2} - 1\right\} \equiv f(\varphi) \tag{6}$$

For slender airfoils the square root at the right-hand side of this equation is only a little different from 1 for nearly the whole range of values of φ. Therefore, it can be taken as a correction term that can be approximated in a simple way as given below. With $U_s(\varphi)$ given, the right-hand side of Eq. (6) can be regarded as a known function $f(\varphi)$, from which the coefficients a_n can be calculated by Fourier analysis

$$a_n = \frac{2}{\pi(n)}\int_{\varphi=0}^{\pi} f(\varphi)\sin(n\varphi)\,d\varphi \tag{7}$$

Then the shape of the airfoil is obtained from Eq. (4). By the aid of the Prandtl-Glauert rule, the effect of compressibility can simply be introduced by putting

$$f(\varphi)_{\text{incompr.}} = \sqrt{1 - M_\infty^2}\, f(\varphi)_{\text{compr.}} \tag{8}$$

M_∞ being the free-stream Mach Number.

For the first approximation of $f(\varphi)$, only the coefficients a_1 and a_2 are taken into account. These can simply be obtained from Fig. 2 dependent on the following two parameters of the prescribed velocity distribution:

(1) Maximum velocity of the potential flow, $U_{max.}/U_\infty$.

(2) Position of maximum velocity, $[x/(c/2)]_{U_{max.}}$ corresponding to $\varphi_{max.}$

This diagram has been obtained from the "generalized" Joukowsky airfoils (with rounded trailing edge), which are obtained from Eq. (4), if all coefficients are zero, except for a_1 and a_2. (The case $a_2 = a_1/2$ gives the "special" Joukowsky airfoils with sharp trailing edge.) The first approximation for $f(\varphi)$ obtained in this way yields the coefficients a_n according to Eq. (7) and herewith a good approximation for the shape of the airfoil. From these coefficients, a_n, a second approximation for $f(\varphi)$ can be obtained, which in most cases then yields the shape of the airfoil with fully sufficient accuracy. It is sufficient to calculate in the first approximation the coefficients until $n = 4$, and in the second approximation until $n = 8$. For the evaluation of the coefficients a_n and the coordinates of the airfoil, a simple general scheme has been set up which reduces the whole numerical work to forming simple products and their sums. Fig. 3 gives the

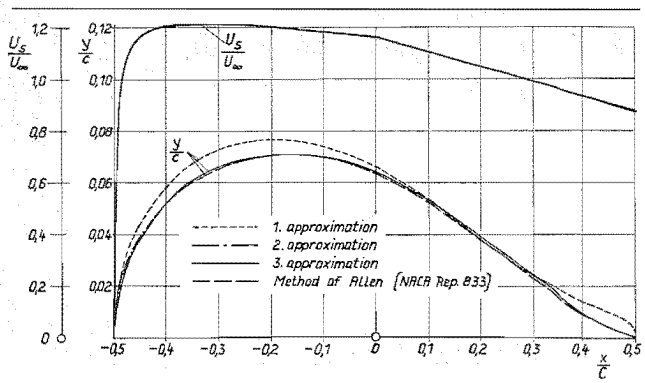

FIG. 3. Prescribed velocity distribution and calculated airfoil shapes. (Airfoil thickness is enlarged to five times the actual thickness.)

results of the first, second, and third approximation of our calculation compared with the result of Allen[2] for one of his examples (base airfoil velocity for "semi-low-drag-airfoil"). Up to now, only symmetrical airfoils with the same velocity distribution on both sides of the airfoil were dealt with. But it can easily be shown that the same procedure can be applied if the prescribed velocity distribution is different on the lower and upper surface of the airfoil. The procedure then has to be applied separately for the lower and the upper surface and yields the airfoil coordinates for both sides.

A pure source distribution $q(x)$ yields the velocity distribution $(U_{up} + U_{low})/2$, a pure vorticity distribution $\gamma(x)$ yields the velocity distribution $(U_{up} - U_{low})$. Both together above the chord yield a velocity normal to the chord

$$v_{up} = \frac{q}{2} + \frac{1}{2\pi}\int_{x'=-c/2}^{+c/2} \frac{\gamma(x')}{x - x'}\, dx' \qquad (9)$$

which might also be obtained from a pure source distribution of the strength $q_{up} = 2v_{up}$. Then Eq. (2) holds for the slope of the upper surface with the required source distribution q_{up}, and in the same way for the lower surface. Therefore, all relations given here hold also for asymmetrical airfoils.

If, however, the airfoil has an angle of attack of some magnitude, Eq. (4) is inconvenient for the shape of the airfoil, because the Fourier series with only sine terms is incomplete, as it gives always $y = 0$ at $x = -c/2$. For small angles of incidence, as they mostly occur in practice, this failure is of minor importance. For larger angles of incidence, it can be overcome by splitting off that part of the induced velocity which gives the angle of incidence. From Glauert's theory of thin airfoils and with regard to Eq. (1), one obtains for the angle of incidence,

$$\alpha_g = \frac{1}{4}\int_{\varphi=0}^{\pi} \left\{ \frac{U_{up} - U_{low}}{U_\infty} \sqrt{1 + \left(\frac{dy}{dx}\right)^2} \right\} \sin\frac{\varphi}{2}\, d\varphi \qquad (10)$$

where the braces mean the distribution of vorticity γ of the airfoil. The reduced velocity distribution having no angle of incidence is, then,

$$U_{\substack{up \\ low}}{}^{*} = U_{\substack{up \\ low}} \mp \frac{\alpha_g \operatorname{ctg}(\varphi/2)}{\sqrt{1 + (dy/dx)^2}} \qquad (11)$$

In Eqs. (10) and (11) the slope dy/dx has to be taken from the symmetrical basic airfoil.

REFERENCES

[1] Riegels, F., *Aerodynamische Berechnung von Tragflügelprofilen*, 4, Bericht, ZWB, UM-Bericht 3019, 1943.

[2] Allen, H. J., *General Theory of Airfoil Sections*, N.A.C.A. Report No. 833, 1945.

[3] Riegels, F., *Das Umströmungsproblem bei inkompressiblen Potentialströmungen*, I. und II. Mitteilung., Ing.-Archiv, Vol. 16, p. 373, 1948, and Vol. 17, p. 94, 1949.

Turbulent Boundary Layer on a Cone in a Supersonic Flow at Zero Angle of Attack

(*Continued from page 57*)

REFERENCES

[1] Hantzsche, W., and Wendt, H., *The Laminar Boundary Layer on a Cone in a Supersonic Air Stream at Zero Angle of Attack*, Jahrbuch 1941 der Deutschen Luftfahrtforschung. Also available as Translation No. RAT-6, Project RAND, November, 1947.

[2] Gazley, C., Jr., *Theoretical Evaluation of the Turbulent Skin Friction and Heat Transfer on a Cone in Supersonic Flight*, General Electric Company, Project HERMES, Number R49A0524, November, 1949.

[3] Van Driest, E. R., *Turbulent Boundary Layer in Compressible Fluids*, Journal of the Aeronautical Sciences, Vol. 18, No. 3, pp. 145–160, March, 1951.

SUGGESTIONS *for* CONTRIBUTORS
to the Publications of the
INSTITUTE *of the* AERONAUTICAL SCIENCES

The Institute of the Aeronautical Sciences invites both members and nonmembers from any country to submit papers for publication in the JOURNAL OF THE AERONAUTICAL SCIENCES and the AERONAUTICAL ENGINEERING REVIEW. The Institute, following the practice of other societies, does not pay for contributions.

The following directions for the preparation of papers, if followed by authors, will save correspondence, avoid the return of papers for changes, minimize the work of preparation for the printer, and save the expense due to the charges made for "author's corrections."

MANUSCRIPTS: The original typewritten copy of the paper desired, double or triple spaced on one side of white paper sheets, consecutively numbered. There should be wide margins to allow for the marking of directions to the printer. Correcting, changing, or adding to papers after they are in type is costly. It is, therefore, imperative that papers submitted be in final form. Typographical errors may be corrected on proofs, but if authors wish to add material, they may do so at their own expense. In mailing, drawings may be rolled but manuscripts should be sent flat. Send by first-class mail (register if you wish, for your own protection) to the Editorial Office, Institute of the Aeronautical Sciences, 2 East 64th Street, New York 21, N.Y. All manuscripts will be examined by the Editorial Committee and by the Editor. Authors will be advised as promptly as possible whether the paper is acceptable for publication.

TITLES: The title of the paper should be brief. The name and initials of the author should be written as he prefers. The use of the full name of an author is advocated because of the frequent duplication of initials and surnames which sometimes makes it difficult to establish the identity of the author. This is particularly important for large annual indexing and abstracting services. All titles and degrees or honors are omitted. The name of the organization with which the author is associated should be placed after his name on a separate line. The date on which the paper is received will be inserted by the Editor. The author's title should be indicated in a footnote.

SUMMARIES OR ABSTRACTS: An abstract to be printed at the beginning should accompany each article. It should be adequate as an *index* and as a *summary*. It should contain a statement of major conclusions reached, since summaries in many cases constitute the only source of information used in compiling scientific reference indexes. Abstracts printed in other journals, especially foreign, in most cases, consist of summaries from printed papers. The summary should explain as adequately as possible the major conclusions to a nonspecialist in the subject and should contain from 100 to 300 words, depending on the length of the paper.

SUBHEADINGS: Subheadings should be inserted by the author at frequent intervals. The work of editorial preparation will be simplified by the author providing many subheadings.

MATTER USUALLY DELETED: Photographs or illustrations of little technical interest and not showing advances in general practice. Too detailed tabular matter (general results of such tables may be included in the text). Lengthy descriptions of materials or processes or of preliminary experiments or theories that preceded final results; salient features only are of interest.

REFERENCES AND FOOTNOTES: References should appear as footnotes only, numbered consecutively, grouped together at the end of the manuscript. The arrangement should be as follows: (For books)—[1] Durand, W. F., *Aerodynamic Theory*, 1st Ed., Vol. 1, p. 23; Julius Springer, Berlin, 1934. (For Magazines)—[1] Englund, C. R., Crawford, A. B., and Mumford, W. W., *Some Results of a Study of Ultra-Short-Wave Transmission Phenomenon*, Proc. I. R. E., Vol. 20, No. 12, pp. 481–482, March, 1933. Please give author, title, edition, volume, page, publisher, and date of publication as indicated. Omission of one required fact causes much extra editorial work and possible inaccuracies.

ILLUSTRATIONS: Illustrations should accompany manuscripts, and each should always be referred to in the text, by number. Drawings or graphs should not be larger than 12 × 16 inches, and must be made with jet black India ink on white paper or tracing cloth, the latter being preferred. *Do not use typewriter for lettering.* The smallest lettering on 8- × 10-inch figures should be no less than 1/4 inch high. Cross-section paper (white with black lines) may be used but should not have more than 4 lines per inch. If finer ruled paper is used, the major division lines should be drawn in with black ink, omitting the finer divisions. In the case of finely ruled paper, only blue-lined paper can be accepted. *Tracing paper and blueprints* are not acceptable. Lettering and all markings must be large enough to be readable after reduction. Mail rolled or flat, never fold. Drawings that cannot be reproduced (including pencil drawings) will be returned to the author for redrawing, thus delaying publication of the paper. Photographs should be distinct and show clear black and white contrasts. They must be on glossy white paper. Avoid round and oval photographs.

CAPTIONS AND LEGENDS: Legends or captions must accompany each drawing or photograph submitted. If written on the drawing or photograph, they should be placed below and well outside the part to be reproduced. Each table should have a caption such as Table 1, Table 2, Table 3, etc. Captions should be complete in themselves so as to make the data intelligible to the reader without reference to the text. A duplicate list of captions for figures should be included as the last page of the manuscript. Use "Fig. 1" (not Figure 1), Figs. 3 and 4, etc., in both the text and the numbering of illustrations. In the text, "Eq. (1)," or "Eqs. (1) and (2)" are used, not "Equation (1)." In captions and legends, except for "Fig." and "Eq." and in table headings, write all words in full; do not abbreviate.

MATHEMATICAL WORK: Only the simplest formulas should be typewritten; all others should be carefully written in pen and ink, the writing to be large enough so that ample room is provided to mark mathematical matter for the printer. A considerable spacing for marking should be allowed above and below all equations. All complicated equations should be repeated on separate sheets with plenty of space left for marking. The solidus should be used for simple fractions appearing within the text. Make all expressions clear to the typesetter. Greek letters used in formulas should be clearly designated by name on the margin of the manuscript. All symbols should be clearly written and carefully checked. The difference between capital and lower-case letters should be clearly distinguished and care taken to avoid confusion between zero (0) and the letter (o), between the numeral (one) and the letter (ell) and the prime (′), between alpha and a, kappa and k, u and mu, v and nu, n and eta. All subscripts and exponents should be clearly marked, and dots and bars over letters or mathematical expressions should be avoided. Avoid complicated exponents and subscripts. When it is necessary to repeat a complicated expression, it should be represented by some convenient symbol.

NOMENCLATURE AND ABBREVIATIONS: Standard abbreviations should be used, and it should be noted that most abbreviations are lower case such as m.p.h., b.m.e.p., i.hp., b.hp., hp., ... etc.

CORPORATE MEMBERS
OF THE
INSTITUTE OF THE AERONAUTICAL SCIENCES

ACADEMY OF AERONAUTICS, INC.
ADAMS RITE MANUFACTURING COMPANY
AEROJET ENGINEERING CORPORATION
AEROLAB DEVELOPMENT COMPANY
AEROPRODUCTS DIVISION, GENERAL MOTORS CORPORATION
AEROQUIP CORPORATION
AGAWAM AIRCRAFT PRODUCTS, INC.
AIRBORNE ACCESSORIES CORPORATION
AIRBORNE INSTRUMENTS LABORATORY, INC.
AIRCRAFT RADIO CORPORATION
AIRESEARCH MANUFACTURING COMPANY, DIVISION OF THE GARRETT CORPORATION
ALLIS-CHALMERS MANUFACTURING COMPANY
ALLISON DIVISION, GENERAL MOTORS CORPORATION
ALUMINUM COMPANY OF AMERICA
AMERICAN AIRLINES SYSTEM
AMERICAN BOSCH CORPORATION
AMERICAN HELICOPTER COMPANY, INC.
AMERICAN PHENOLIC CORPORATION
AMERICAN STEEL & WIRE COMPANY
ASSOCIATED AVIATION UNDERWRITERS
ATLAS SUPPLY COMPANY
BAKER STEEL & TUBE COMPANY
BEECH AIRCRAFT CORPORATION
BELL AIRCRAFT CORPORATION
BENDIX AVIATION CORPORATION
- BENDIX INTERNATIONAL DIVISION
- BENDIX PRODUCTS DIVISION
- BENDIX RADIO DIVISION
- ECLIPSE-PIONEER DIVISION
- FRIEZ INSTRUMENT DIVISION
- SCINTILLA MAGNETO COMPANY

THE BG CORPORATION
BOEING AIRPLANE COMPANY
- SEATTLE DIVISION
- WICHITA DIVISION

BREEZE CORPORATIONS, INC.
- ALDRICH COMPANY
- FEDERAL LABORATORIES, INC.

BROOKS AND PERKINS, INC.
CAL-AERO TECHNICAL INSTITUTE, A DIVISION OF GRAND CENTRAL AIRCRAFT COMPANY
CALIFORNIA PANEL & VENEER COMPANY
CANADAIR, LTD.
CESSNA AIRCRAFT COMPANY
CHASE AIRCRAFT COMPANY, INC.
CHASE NATIONAL BANK OF THE CITY OF NEW YORK
THE CLEVELAND PNEUMATIC TOOL COMPANY
CLIFFORD MANUFACTURING COMPANY, DIVISION OF STANDARD-THOMSON CORPORATION
CONSOLIDATED VULTEE AIRCRAFT CORPORATION
- FORT WORTH DIVISION

CONTINENTAL MOTORS CORPORATION
CORNELL AERONAUTICAL LABORATORY, INC.
CORNELL UNIVERSITY
CURTISS-WRIGHT CORPORATION
- ELECTRONICS DIVISION
- PROPELLER DIVISION
- WRIGHT AERONAUTICAL DIVISION

DOELCAM CORPORATION
DOUGLAS AIRCRAFT COMPANY, INC.
- EL SEGUNDO PLANT
- LONG BEACH PLANT
- SANTA MONICA PLANT
- TULSA DIVISION

THE DOW CHEMICAL COMPANY
DZUS FASTENER COMPANY, INC.
EASTERN AIR LINES, INC.
EATON MANUFACTURING COMPANY
EDO CORPORATION
ELASTIC STOP NUT CORPORATION OF AMERICA
ELECTROL INCORPORATED
ESSO STANDARD OIL COMPANY
ETHYL CORPORATION
FAIRCHILD CAMERA & INSTRUMENT CORPORATION
- FAIRCHILD AERIAL SURVEYS, INC.

FAIRCHILD ENGINE AND AIRPLANE CORPORATION
- AL FIN DIVISION
- FAIRCHILD AIRCRAFT DIVISION
- FAIRCHILD ENGINE DIVISION
- FAIRCHILD GUIDED MISSILES DIVISION
- STRATOS DIVISION

FEDERAL TELEPHONE AND RADIO CORPORATION
- RADIO AND TELEPHONE DIVISION

THE FIRESTONE TIRE & RUBBER COMPANY OF CALIFORNIA
FLETCHER AVIATION CORPORATION
FLIGHT REFUELING, INC.
FLIGHT REFUELLING (CANADA) LTD.
FLIGHT SAFETY FOUNDATION
GENERAL ELECTRIC COMPANY
- AIRCRAFT GAS TURBINE DEPARTMENT
- AVIATION DEPARTMENT

GLOBE CORPORATION, AIRCRAFT DIVISION
THE B. F. GOODRICH COMPANY
THE GOODYEAR TIRE & RUBBER COMPANY
GRUMMAN AIRCRAFT ENGINEERING CORPORATION
W. & L. E. GURLEY
HARVEY MACHINE COMPANY, INC.
INDUSTRIAL SOUND CONTROL
INSURANCE COMPANY OF NORTH AMERICA COMPANIES
THE INTERNATIONAL NICKEL COMPANY, INC.
IRVING AIR CHUTE COMPANY, INC.
JACK & HEINTZ, INC
JOHNS-MANVILLE SALES CORPORATION
EARL M. JORGENSEN COMPANY
THE M. W. KELLOGG COMPANY
WALTER KIDDE & COMPANY, INC.
KOLLSMAN INSTRUMENT CORPORATION
LAVELLE AIRCRAFT CORPORATION
LEAR, INCORPORATED
THE LIQUIDOMETER CORPORATION
LOCKHEED AIRCRAFT CORPORATION
- GEORGIA DIVISION

LONGINES-WITTNAUER WATCH COMPANY, INC.
MARMAN PRODUCTS COMPANY, INC.
MARQUARDT AIRCRAFT COMPANY
THE GLENN L. MARTIN COMPANY
McDONNELL AIRCRAFT CORPORATION
MELETRON CORPORATION
MINNEAPOLIS-HONEYWELL REGULATOR COMPANY
NATIONAL CREDIT OFFICE, INC.
NORTH AMERICAN AVIATION, INC.
- COLUMBUS DIVISION
- ELECTRO-MECHANICAL DIVISION

NORTHROP AIRCRAFT, INC.
PAN AMERICAN WORLD AIRWAYS, INC.
THE PARKER APPLIANCE COMPANY
PESCO PRODUCTS DIVISION, BORG-WARNER CORPORATION
PHILLIPS PETROLEUM COMPANY
PIASECKI HELICOPTER CORPORATION
THE PURE OIL COMPANY
RADIOPLANE COMPANY
REPUBLIC AVIATION CORPORATION
E. V. ROBERTS AND ASSOCIATES
A. V. ROE CANADA LIMITED
JOHN A. ROEBLING'S SONS COMPANY
ROHR AIRCRAFT CORPORATION
SCHRILLO AERO TOOL ENGINEERING COMPANY
SEABOARD & WESTERN AIRLINES, INC.
SERVOMECHANISMS, INC.
SHELL OIL COMPANY, INC.
SIMMONDS AEROCESSORIES, INC.
SOCONY-VACUUM OIL COMPANY, INC.
SOLAR AIRCRAFT COMPANY
SPERRY GYROSCOPE COMPANY, DIVISION OF THE SPERRY CORPORATION
STANDARD OIL COMPANY OF CALIFORNIA
STANDARD OIL COMPANY (INDIANA)
THE STEEL PRODUCTS ENGINEERING COMPANY
STURGESS, INC.
SUMMERS GYROSCOPE COMPANY
TELECOMPUTING CORPORATION
THE H. I. THOMPSON COMPANY
THOMPSON PRODUCTS, INC.
TINNERMAN PRODUCTS, INC.
TOOLKO ENGINEERING COMPANY
TRANS WORLD AIRLINES INC.
TURBO PRODUCTS INC.
UNION CARBIDE AND CARBON CORPORATION
- BAKELITE CORPORATION
- ELECTRO METALLURGICAL COMPANY
- HAYNES STELLITE COMPANY
- LINDE AIR PRODUCTS COMPANY
- NATIONAL CARBON DIVISION

UNITED AIR LINES, INC.
UNITED AIRCRAFT CORPORATION
- CHANCE VOUGHT AIRCRAFT DIVISION
- HAMILTON STANDARD DIVISION
- PRATT & WHITNEY AIRCRAFT DIVISION
- SIKORSKY AIRCRAFT DIVISION
- UNITED AIRCRAFT EXPORT CORPORATION
- UNITED AIRCRAFT SERVICE CORPORATION

UNITED STATES AVIATION UNDERWRITERS, INC.
VARD, INC.
VICKERS, INC.
WESTERN GEAR WORKS
WESTINGHOUSE ELECTRIC CORPORATION
- AVIATION GAS TURBINE DIVISION

WESTON ELECTRICAL INSTRUMENT CORPORATION
WYMAN-GORDON COMPANY
YOUNG RADIATOR COMPANY

Jim Launder

JOURNAL OF FLUID MECHANICS

SPALDING & CHI

Turbulent

C_f etc.

VOLUME 18
1964

CAMBRIDGE
AT THE UNIVERSITY PRESS
1964

The drag of a compressible turbulent boundary layer on a smooth flat plate with and without heat transfer

By D. B. SPALDING AND S. W. CHI

Mechanical Engineering Department,
Imperial College of Science and Technology, London, S.W. 7

(Received 10 May 1963)

The theoretical treatments given by earlier authors are classified, reviewed and where necessary extended; then the predictions of twenty of these theories are evaluated and compared with all available experimental data, the root-mean-square error being computed for each theory. The theory of van Driest–II gives the lowest root-mean-square error (11·0 %).

A new calculation procedure is developed from the postulate that a unique relation exists between $c_f F_c$ and RF_R where c_f is the drag coefficient, R is the Reynolds number, and F_c and F_R are functions of Mach number and temperature ratio alone. The experimental data are found to be too scanty for both F_c and F_R to be deduced empirically, so F_c is calculated by means of mixing-length theory and F_R is found semi-empirically. Tables and charts of values of F_c and F_R are presented for a wide range of M_G and T_S/T_G. When compared with all experimental data, the predictions of the new procedure give a root-mean-square error of 9·9 %.

1. Introduction

In many circumstances of interest to aeronautical engineers, it is necessary to predict the frictional drag at a surface along which a gas is flowing at high speed and through which heat is being transferred. This is not only important in the prediction of the frictional drag itself but also in the prediction of the heat transfer, for example by means of a 'modified Reynolds analogy'. This knowledge is required in connexion with many processes, for example, in the cooling of combustion-chamber walls, gas-turbine blades, hypersonic ram-jet intakes, rocket-motor nozzles and high-speed aircraft skins.

Often the velocity of the mainstream fluid is not uniform. In a rocket-nozzle it increases with distance downstream, whilst in a ram-jet intake it decreases; the main-stream pressure is accordingly non-uniform. Despite these facts, it is necessary to restrict attention in the present paper mainly to the case in which the pressure gradient is zero; that is, to that of the boundary layer on a flat plate. The reason is that this is the simplest case, which must be understood first.

There have been numerous investigations of the problem, both theoretical and experimental; these will be described in some detail in the following §§2, 3. Nevertheless, as will appear below, present knowledge of the subject is defective in two respects. First, there is considerable uncertainty as to which of various theories gives the best prediction; for each theory contains fairly drastic simplifi-

cations, and has usually been compared with only a small selection of the available experimental data. Secondly, some of the methods of prediction (including unfortunately those which give the most accurate predictions) are difficult to use; the prospective user of the method has to carry out extensive numerical work, because the necessary auxiliary functions have not been computed and tabulated once for all.

It is intended below to pay particular attention to remedying the above defects. As far as possible, uncertainty will be eliminated by comparing the existing theories with all published experimental data and by developing a new calculation procedure based upon accumulated theoretical and experimental knowledge of the compressible turbulent boundary layer; and graphs and tables will be presented which permit friction to be calculated for a wide range of conditions as a result of merely a few minutes' work.

The tables cover Mach numbers (M_G) between 0 and 15, and ratios of wall temperature to main-stream temperature (T_S/T_G) between 0·05 and 30.

Sections 2 and 3 below are mainly devoted to a review of earlier work. These lead to a development of the present method which is presented in §4. Readers solely concerned with the use of the method should turn to §4.6 which contains a summary of the prediction procedures which are recommended for use.

Notation

a, b	see equations (13) and (14)
c_f	local frictional drag coefficients based upon main-stream fluid properties, equation (17)
$\bar{c}_f$	overall frictional drag coefficient based upon main-stream fluid properties, equation (26)
E	a constant, equation (2)
F_c	function multiplying c_f in universal drag law, equations (11) and (19)
$F_{\bar{c}}$	function multiplying $\bar{c}_f$ in universal drag law, equation (11)
$F_{R\delta}$	function multiplying R_δ in universal drag law, equations (12) and (20)
F_{Rx}	function multiplying R_x in universal drag law, equations (12) and (25)
h	specific enthalpy, equation (32), (B.Th.U./lb.)
h^0	stagnation enthalpy, equation (32), (B.Th.U./lb.)
K	a constant ($\approx 0{\cdot}4$), equation (2)
M_G	Mach number of main stream, equation (13)
n, p, q	exponents, equations (44) and (51)
P	Prandtl number, equation (36)
r	recovery factor, equation (35)
R_δ	Reynolds number based upon momentum thickness and main-stream fluid properties, equation (3)
R_x	Reynolds number based upon x and main-stream fluid properties, equation (21)
T	temperature, equation (13), (°R)
u	velocity in x-direction, equation (1), (ft./h)
x	distance measured along main-stream direction from effective start of turbulent boundary layer, implied in the definition of R_x, (ft.)

u^+ non-dimensional value of u, equation (2)
y distance from wall, equation (1), (ft.)
y^+ non-dimensional value of y, equation (2)
z a different non-dimensional value of u, equation (2)
δ_2 momentum thickness, equation (3), (ft.)
γ specific heat ratio, equation (13)
ϕ function appearing in equations (2), (5), etc.
ψ_δ, ψ_x, Ψ functions appearing in the generalized drag laws, equations (18), (24) and (27)
ρ density, equation (1), (lb./ft.^{3})
μ viscosity, equation (3), (lb./ft.h)
τ shear stress in boundary layer, equation (1), (lb./ft. h^2)

Subscripts

av average conditions in laminar sublayer
G main-stream fluid state, equation (2)
i uniform property flow, equation (43)
N state near the wall, equation (43)
S state at the wall, equation (2)
1 outer edge of laminar sublayer, table 1

2. Survey of previous theoretical work

2.1. *General characteristics of analyses*

There are a number of theories for the prediction of the frictional-drag coefficient in the compressible turbulent boundary layer on a smooth flat plate (see the references marked with an asterisk in the list at the end of the paper). According to the nature of the principal assumptions used by various authors, the theories can be grouped into five types, namely, (i) theories based upon the Prandtl differential equation, (ii) theories based upon the von Kármán differential equation, (iii) theories based upon other differential equations, (iv) theories based upon a fixed velocity profile, and (v) theories based upon the incompressible formulae with fluid properties inserted at a 'reference' state. The main features of the analyses for each of those groups will be summarized in the following five sections (§§2.2–2.6), and the characteristics of individual theories belonging to these groups will be indicated in tables 1–5. Table 6 includes miscellaneous analyses which do not belong to any of the five groups mentioned above.

2.2. *Theories based upon the Prandtl differential equation*

By 'the Prandtl differential equation' we mean that postulated by Prandtl (see Schlichting 1960, p. 477) relating the shear stress in the turbulent part of the boundary layer to the velocity gradient and other properties, namely

$$\tau = \rho K y^2 \left(\frac{du}{dy}\right). \tag{1}$$

Author and year	Hypothesis for E	Nature of ϕ	Method of evaluating R_δ integral
Smith & Harrop (1946)	$E = 11{\cdot}24$	$\phi = (\rho/\rho_S)^{\frac{1}{2}} = (1+bz-a^2z^2)^{-\frac{1}{2}}$	Approximate analytical (A)*
van Driest–I (1951)	$E = 13{\cdot}1$ (for ψ_x)†		Approximate analytical (B)*
Kalikman (1956)	$2y_1 u_{av}\rho_{av}/\mu_{av} = (11{\cdot}5)^2$ $y_1^+ = u_G^+(z_1 + \frac{1}{2}bPz_1^2 + \frac{1}{3}bPz_1^3)$		Exact numerical
Dorrance (1960)	$E = 13{\cdot}1$ (for ψ_x)		Exact numerical (approximate integration used later to yield $c_f(R_x)$)
Kutateladze & Leont'ev (1961)	$y_1^+ = 11{\cdot}6(T_G/T_S)^{\omega+\frac{1}{2}}$ $z_1 = 11{\cdot}6 \times$ ($\frac{1}{2}$ drag coefficient in uniform-property flow at same R_δ)$^{\frac{1}{2}}$	$\phi = (\rho/\rho_S)^{\frac{1}{2}} = [1+(b-0{\cdot}1a^2)z - 0{\cdot}0a^2z^2]^{-\frac{1}{2}}$	Approximate analytical (B)

* These methods of evaluating R_δ integral are summarized in the Appendix.
† 'For ψ_x' means that the value of E specified here is for the c_f *vs.* R_x expression.

TABLE 1. Theories based upon Prandtl differential equation

Author and year	Hypothesis for E	Nature of ϕ	Method of evaluating R_δ integral
Frankl & Voishel (1937)	$u_1^+ = 11{\cdot}5$ $(du^+/dy^+)_1 = 0{\cdot}289$	$\phi = (\rho/\rho_S)^{\frac{1}{2}}$ $= (1+bz-a^2z^2)^{-\frac{1}{2}}$	Approximate analytical—by expanding integrand in series of b and a^2, and neglecting higher terms
Wilson (1950)	$u_1^+ = 11{\cdot}6$ $(du^+/dy^+)_1 = 0{\cdot}218$	$\phi = (\rho/\rho_S)^{\frac{1}{2}}$ $= (1-a^2z^2)^{-\frac{1}{2}}$ (adiabatic only)	Approximate analytical (B)
Rubesin, Maydew & Varga (1951)	$u_1^+ = 11{\cdot}5$ $(du^+/dy^+)_1 = 0{\cdot}218$	$\phi = (\rho/\rho_S)^{\frac{1}{2}}$ $= (1+bz-a^2z^2)^{-\frac{1}{2}}$	Exact numerical
van Driest–II (1955)	$E = 13{\cdot}1$ (for ψ_x)		Approximate analytical (B)
Deissler & Loeffler (1959)	$y_1^+ = 26$ For $y^+ \leqslant 26$, $\tau_S = (\mu + 0{\cdot}01188\rho uy)\dfrac{du}{dy}$ $q_S = (k + 0{\cdot}01188\rho uy)\dfrac{dT}{dy}$	$\phi = (\rho/\rho_S)^{\frac{1}{2}}$ $= \left[\dfrac{T_1}{T_S} - \dfrac{q_S}{c_p T_S\sqrt{(\rho_S\tau_S)}}(u^+ - u_1^+) - \dfrac{\tau_S}{2c_p T_S\rho_S}(u^{+2} - u_1^{+2})\right]^{-1}$	Exact numerical

Author and year	*Nature of differential equation*	*Method of evaluating R_3 integral*
Clemmow–I (1950)	$\tau_S = \rho K^2 y^2 \left(\frac{du}{dy}\right)^2 + uK^2 y^2 \frac{du}{dy}$	Approximate analytical (B)
Clemmow–II (1950)	$\tau_S = K^2 \frac{(du/dy)^3}{(d^2u/dy^2)^2}\left(\rho \frac{du}{dy} + u \frac{d\rho}{dy}\right)$	
Ferrari (1950)	$\sqrt{\frac{\tau_S}{\rho_S}} = \frac{\rho K y (du/dy)}{\rho_S\left\{1 + \text{const.} \times z\left[1 + \frac{2}{(\gamma-1)\,M_G^2}\right]^{-\frac{1}{2}}\right\}}$ The value of constant is unknown	Approximate numerical
Li & Nagamatsu (1951)	$\tau_S = \rho K^2 y^2 (du/dy)^2 + f(M_G)\, uK^2 y^2 \frac{d\rho}{dy}\frac{du}{dy}$ The function of M_G, $f(M_G)$ is unknown	Approximate analytical (B)
Kosterin & Koshmarov (1960)	$\tau_S = \rho K^2 y^2 (du/dy)^2 + \int K^2 y u \frac{d\rho}{dy}\frac{du}{dy}\,dy$	Exact numerical

TABLE 3. Theories based upon other differential equations

Author and year	Assumed velocity profile	Expression of ρ/ρ_S	Method of evaluating R_3 integral
Cope–I (1943)	$u^+ = 8{\cdot}7y^{+\frac{1}{7}}$	$\rho/\rho_S = (1 - a^2z^2)^{-1}$ (adiabatic only)	Exact numerical
Cope–II (1943)	$y^+ = E^{-1}\exp(Ku^+)$		Approximate analytical (B)
Monaghan (1950)	$y^+ = E^{-1}\exp(Ku^+)$	$\rho/\rho_S = (1 + bz - a^2z^2)^{-1}$	Approximate analytical (B)

TABLE 4. Theories based upon fixed velocity profile

Author and year	Expression of T_R/T_G
von Kármán (1935)	$T_R/T_G = 1 + \frac{1}{2}(\gamma-1)\,M_G^2$ (adiabatic only)
Tucker (1951)	$T_R/T_G = 1 + \frac{1}{4}(\gamma-1)\,M_G^2$ (adiabatic only)
Young & Janssen (1952)	For $M_G \leqslant 5{\cdot}6$: $T_R/T_G = 0{\cdot}42 + 0{\cdot}58(T_S/T_G) + 0{\cdot}035\,M_G^2$ For $M_G > 5{\cdot}6$: $T_R/T_G = 0{\cdot}42 + 0{\cdot}58(T_S/T_G) + 0{\cdot}023\,M_G^2$
Sommer & Short (1955)	$T_R/T_G = 0{\cdot}55 + 0{\cdot}45(T_S/T_G) + 0{\cdot}035M_G^2$
Eckert (1955)	$T_R/T_G = 0{\cdot}5 + 0{\cdot}5(T_S/T_G) + 0{\cdot}11P^{\frac{1}{3}}(\gamma-1)\,M_G^2$ or $h_R/h_G = 0{\cdot}28 + 0{\cdot}5(h_S/h_G) + 0{\cdot}22(h_{ad,\,S}/h_G)$

TABLE 5. Theories based upon incompressible formulae (ψ_w) with reference properties

With the assumption $\tau = \tau_S$, the velocity distribution in the turbulent boundary layer is derived,

$$y^+ = E^{-1} \exp\left(K u_G^+ \int_0^z \phi \, dz\right), \tag{2}$$

where $y^+ \equiv y(\tau_S \rho_S)^{\frac{1}{2}}/\mu_S$, $u^+ \equiv u/(\tau_S/\rho_S)^{\frac{1}{2}}$, $z \equiv u/u_G$, $\phi \equiv (\rho/\rho_S)^{\frac{1}{2}}$, K = a mixing length constant, E = an integrating constant, and subscript G refers to the main stream, i.e. the outer 'edge' of the boundary layer, subscript S refers to the fluid conditions immediately adjacent to the wall, i.e. to the inner 'edge' of the boundary layer.*

Equation (2) leads to the integral for R_δ:

$$R_\delta = \frac{\mu_S}{\mu_G} \frac{K}{E} (u_G^+)^2 \int_0^1 \phi^3 z(1-z) \exp\left(K u_G^+ \int_0^z \phi \, dz\right) dz, \tag{3}$$

where $$R_\delta \equiv \frac{\rho_G u_G \delta_2}{\mu_G}, \quad \delta_2 \equiv \int_0^{y_G} \frac{\rho}{\rho_G} \frac{u}{u_G} \left(1 - \frac{u}{u_G}\right) dy.$$

The above features are common to all analyses of this group. The differences between them are in either: (i) an hypothesis for E (or other method of determining the integration constant), (ii) the nature of the ϕ function, or (iii) the method of evaluating the R_δ integral. Accordingly, the individual members of the group are distinguished by the nature of these three items in table 1.

2.3. *Theories based upon the von Kármán differential equation*

The differential equation postulated by von Kármán (see Schlichting 1960, p. 485) as the connexion between τ, du/dy and other quantities is

$$\tau = \rho K^2 (du/dy)^4/(d^2u/dy^2)^2. \tag{4}$$

The assumption $\tau = \tau_S$ leads to the velocity distribution

$$y^+ = (K/E) \int_0^{u^+} \exp\left(K u_G^+ \int_0^z \phi \, dz\right) du^+. \tag{5}$$

This leads further to the R_δ integral

$$R_\delta = \frac{\mu_S}{\mu_G} \frac{K}{E} u_G^{+2} \int_0^1 \phi^2 z(1-z) \exp\left(K u_G^+ \int_0^z \phi \, dz\right) dz. \tag{6}$$

Equations (4)–(6) are common to all the methods of this group; individual methods are classified in table 2 by reference to either (i) their hypotheses for E, (ii) the nature of the ϕ function, or (iii) the method of evaluating the R_δ integral.

2.4. *Theories based upon other differential equations*

Analyses of this group start from various differential equations but the assumption of $\tau = \tau_S$ is also made as in the above two groups (§§2.2, 2.3). Generally speaking, all proposed differential equations lead to equations for the velocity distribution which are identical in form with (2) or (5). However, the nature of ϕ in this expression differs from that in §§ 2.2 and 2.3, that is, ϕ here is no longer

* A mnemonic: $G \equiv$ gas stream; $S \equiv$ surface.

equal to $(\rho/\rho_S)^{\frac{1}{2}}$. The Reynolds-number integral for the analyses of the group is either

$$R_\delta = \frac{\mu_S}{\mu_G}\frac{K}{E}u_G^{+2}\int_0^1 \phi\frac{\rho}{\rho_S}z(1-z)\exp\left(Ku_G^+\int_0^z \phi\,dz\right)dz, \tag{7}$$

or

$$R_\delta = \frac{\mu_S}{\mu_G}\frac{K}{E}u_G^{+2}\int_0^1 \frac{\rho}{\rho_S}z(1-z)\exp\left(Ku_G^+\int_0^z \phi\,dz\right)dz, \tag{8}$$

depending on whether the velocity distribution of (2) or that of (5) is appropriate. Methods of this group are distinguished in table 3 by reference to either (i) the nature of the differential equation, or (ii) the method of evaluating the R_δ integral.

2.5. *Theories based upon a fixed velocity profile*

In this group, it is assumed that the velocity profile is independent of compressibility, for example,

$$y^+ = E^{-1}\exp(Ku^+), \tag{9}$$

for which the R_δ integral becomes

$$R_\delta = \frac{\mu_S}{\mu_G}\frac{K}{E}u_G^{+2}\int_0^1 \frac{\rho}{\rho_S}z(1-z)\exp(Ku_G^+)dz. \tag{10}$$

Methods of this group are distinguished in table 4 by reference to (i) the assumed fixed velocity profile, (ii) the expression for ρ/ρ_S, and (iii) the method of evaluating the R_δ integral.

2.6. *Theories based upon incompressible formulae with reference properties*

Methods of this group imply the existence of a universal relationship between frictional-drag coefficient and Reynolds number, if properties are evaluated at a reference temperature (or reference enthalpy). They are distinguished in table 5 by reference to (i) the method by which the reference temperature was determined, and (ii) the expression for T_R/T_G or (h_R/h_G).

2.7. *Miscellaneous other methods*

Methods which do not belong to those groups discussed in §§ 2.2–2.6 include the use of various transformations and the direct use of empirical data. We have placed in this category the theories of Lin & Shen (1951), Shen (1951), Donaldson (1952), Spence (1959), Winkler (1961), Burgraff (1962) and Coles (1962).

The validity of the assumptions and simplifications involved in various theories can only be verified by comparison with experiment. This will be done systematically in the next section.

3. Comparison between the theoretically and experimentally obtained data

3.1. *Purpose of comparison*

As pointed out above, all theoretical treatments discussed in § 2 have been based upon assumptions and simplifications. Further, their predictions differ significantly, as has been shown, for example, by Chapman & Kester (1953) for the adiabatic-wall case. It is therefore necessary to establish the relative validity of all theories by comparing them with experimental data. Other authors, for

example, Rubesin, Maydew & Varga (1951), Sommer & Short (1955), Monaghan (1950), Matting, Chapman, Nyholm & Thomas (1961), Winkler (1961) and Peterson (1963) have compared some theories with experiments; but they either used relatively few sets of experimental data or used a qualitative method of comparison in the form of numerous figures, so their conclusions are still rather indecisive. We shall compare the various theories with all published experimental data of c_f and $\bar{c}_f$ versus R_δ and R_x at various M_G and T_S/T_G, and shall evaluate for each theory a quantitative measure of its agreement with experiment. After that, we shall be able to see which of the available theories is best, and so learn which assumptions for the compressible turbulent boundary layer are most plausible. This examination forms the starting point for the development of an improved calculation procedure, which is also presented below.

3.2. *Experimental data*

If experimental data were accurate, a few sets of data at desired conditions (Mach number and heat-transfer rates) would suffice to test the validity of the various theories. Such data are, however, not available. For this reason, the greatest possible number of experimental data have been collected (see references marked with a double dagger) and tabulated.* They include measurements on a flat plate and on a cylinder with axis parallel to the stream direction and radius large in comparison with the boundary-layer thickness. Figures 1–3 show the collected data in the form of c_f *vs* R_δ, c_f *vs* R_x and $\bar{c}_f$ *vs* R_x, and figure 4 shows the conditions (i.e. values of M_G and T_S/T_G) which have been explored experimentally. Although it must be expected that the data are not all equally reliable, we have made no attempt to estimate their accuracy or to introduce any corresponding weighting factors.

3.3. *Theoretical data*

Theoretical friction-coefficient data corresponding to the experimental Reynolds number (R_δ or R_x), Mach number (M_G) and temperature ratio (T_S/T_G) have been obtained by the various methods discussed in § 2; however, some authors have not worked out all the relations which are required if their theories are to be compared with all the collected experimental data. Extensions can, however, be made to those theories without conflicting with the authors' original argument. The methods used by us in making the extensions are summarized below.

Conversion of R_x to R_δ and vice versa. The results of some analyses, viz. Clemmow (1950), Cope (1943), Monaghan (1950), Smith & Harrop (1946), Van Driest (1950, 1955), Wilson (1950) and the theories of table 5, imply that a unique relation exists between $c_f F_c$ and RF_R where F_c and F_R are functions of Mach number and temperature ratio alone. As will be shown in § 4, the relations between F_c, $F_{\bar{c}}$, $F_{R\delta}$ and F_{Rx} are such that

$$F_c = F_{\bar{c}}, \tag{11}$$

$$F_{Rx} = F_{R\delta}/F_c, \tag{12}$$

where F_c and $F_{\bar{c}}$ are the functions of M_G and T_S/T_G multiplying c_f and $\bar{c}_f$ respectively, and $F_{R\delta}$ and F_{Rx} are the functions of M_G and T_S/T_G multiplying R_δ and R_x.

* The table is not printed here. Copies may be obtained by interested readers on application to the authors.

respectively. Hence equations (11) and (12) enable the determination of the c_f *vs* R_x relation of one of these theories from the corresponding $\bar{c}_f$ *vs* R_x or c_f *vs* R_δ relations, and vice versa.

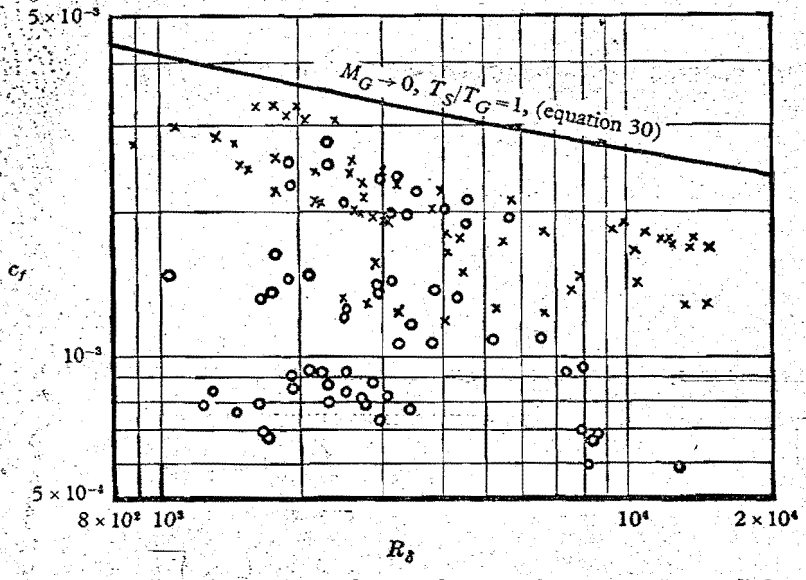

FIGURE 1. Collected experimental data of c_f *vs* R_δ in compressible turbulent boundary layer. ×, adiabatic; ○, with heat transfer.

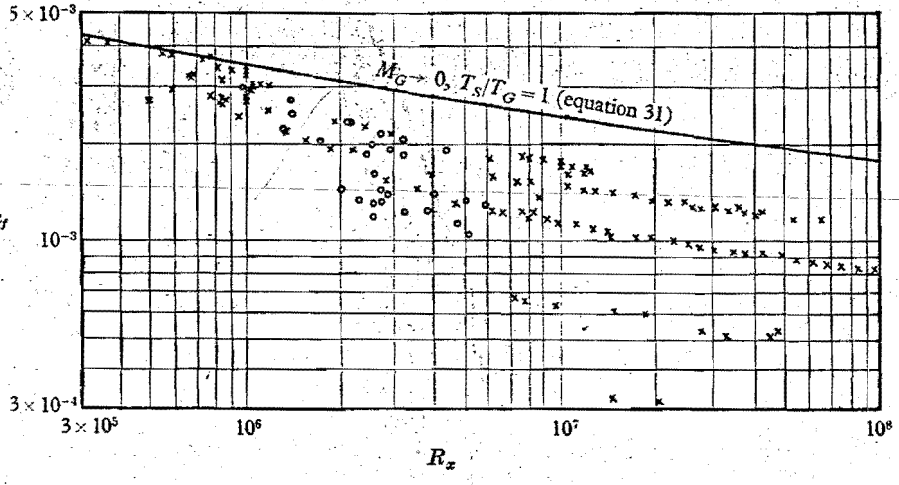

FIGURE 2. Collected experimental data of c_f *vs* R_x in compressible turbulent boundary layer. ×, adiabatic; ○, with heat transfer.

Extension of theories derived for the adiabatic wall to the case of heat transfer. When only the adiabatic-wall case is considered and the Reynolds analogy between momentum and energy transfer is assumed, as in the theories of Cope (1943), Donaldson (1952), Wilson (1950), etc., the temperature-distribution equation is

$$T/T_S = 1 - a^2 z^2, \tag{13}$$

where

$$a^2 \equiv [\tfrac{1}{2}(\gamma-1)M_G^2]/(1+\tfrac{1}{2}(\gamma-1)M_G^2),$$

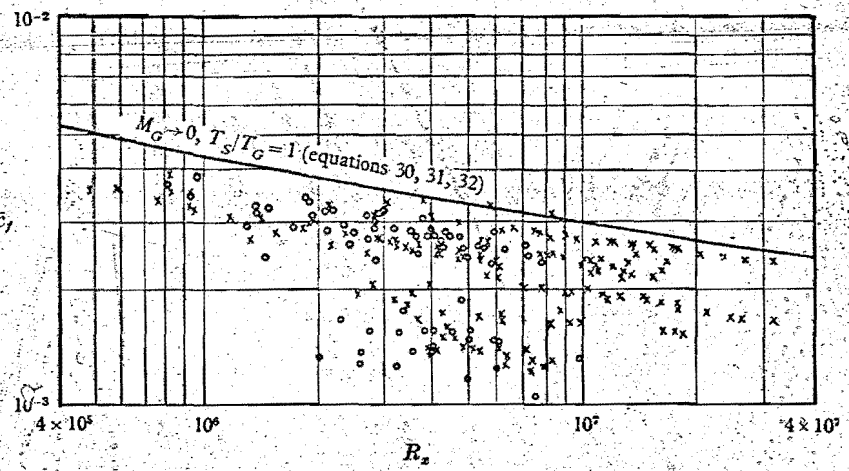

FIGURE 3. Collected experimental data of $\bar{c}_f$ *vs* R_x in compressible turbulent boundary layer. ×, adiabatic; ○, with heat transfer.

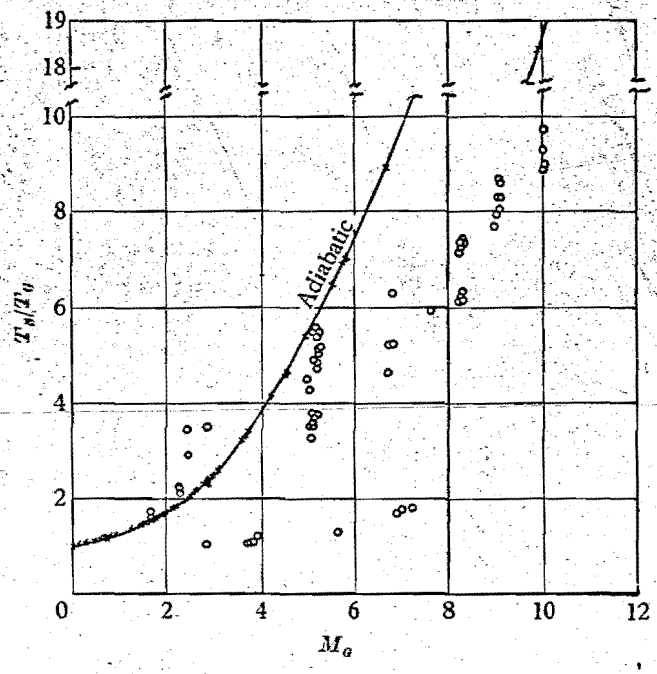

FIGURE 4. Area of conditions explored experimentally.

$z \equiv u/u_G$, $T \equiv$ absolute temperature (°R), and suffixes G and S refer to free stream and surface, respectively.

We have extended equation (13) to include the effect of heat transfer as follows:

$$T/T_S = 1 + bz - a^2 z^2, \tag{14}$$

where $$b \equiv [\{1 + \tfrac{1}{2}(\gamma - 1) M_G^2\}/(T_S/T_G)] - 1$$

and $$a^2 \equiv \{\tfrac{1}{2}(\gamma - 1) M_G^2\}/(T_S/T_G).$$

Viscosity law. The viscosity law recommended by the original authors has been used in most cases for applying their theory to experimental conditions. When this is not possible, or no law is recommended, the following power law has been used

$$\mu \propto T^{0.76}. \tag{15}$$

Although Sutherland's viscosity law, given by

$$\frac{\mu}{\mu_G} = \frac{T}{T_G}\,\frac{T_G + 198\,^\circ\mathrm{R}}{T + 198\,^\circ\mathrm{R}} \tag{16}$$

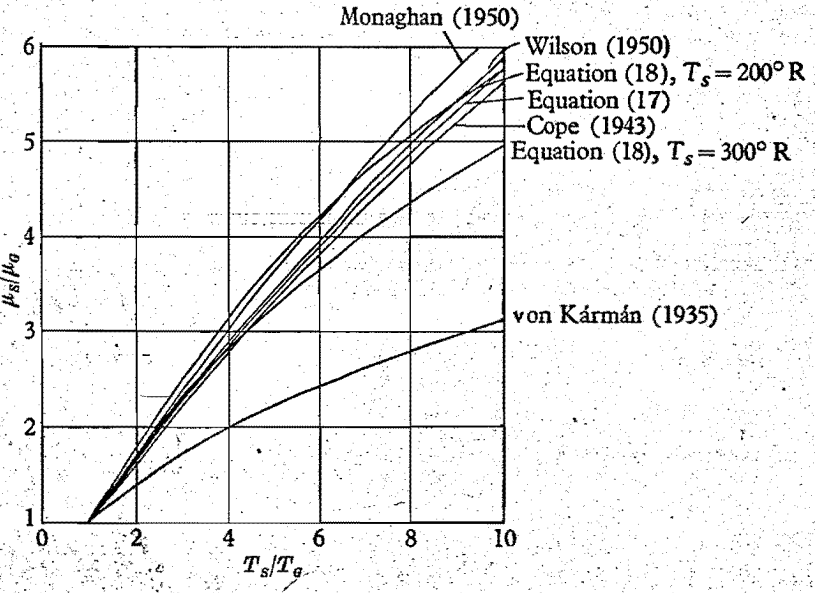

FIGURE 5. Comparison of various viscosity-temperature laws.

is more accurate than the power law, the absolute value of T_G was not reported by most experimenters. Figure 5 shows the viscosity-temperature relations used in the various theories. Since μ has only a weak influence on c_f, it is unlikely that the use of different viscosity laws for different theories has any appreciable effect on our final conclusions.

Drag laws for incompressible flow. Each of the authors whose works we have studied incorporates in his theory, implicitly or explicitly, a relationship between drag coefficient and Reynolds number (either R_δ or R_x) valid for incompressible flow. We have in each case used the relationship recommended by the author in question, without attempting to calculate separately its effect on the accuracy of the theory. However, in the Reynolds-number range of the experiments, the drag coefficients calculated from the various formulae differ only by 1 or 2 %, so there is no reason to expect that the use of a single relationship would have appreciably modified our final conclusion.

3.4. *Comparison between theories and experiments*

Twenty out of twenty-nine collected theories (see references marked with an asterisk) are compared in this report; they are believed to include all the essential assumptions used by various authors. Nine theories (theories which have been

Principal assumptions	Authors and years	R.M.S. error for adiabatic wall (%)	R.M.S. error for heat transfer (%)	Total R.M.S. error (%)
Prandtl differential equation	Smith & Harrop (1946)	20·3	37·9	32·3
	van Driest–I (1951)	13·3	17·3	14·7
	Kutateladze & Leont'ev (1961)	9·5	16·2	12·0
von Kármán differential equation	Frankl & Voishel (1937)	20·3	41·7	28·7
	Wilson (1950)	10·4	13·6	11·5
	van Driest–II (1955)	9·7	13·6	11·0
Other differential equations	Clemmow–I (1950)	11·5	21·5	15·2
	Clemmow–II (1950)	20·7	31·7	24·7
Fixed velocity profile	Cope–I (1943)	16·7	24·7	19·1
	Cope–II (1943)	12·6	25·0	17·4
	Monaghan (1950)	13·5	25·3	18·0
Reference temperature	von Kármán (1935)	25·0	38·7	29·9
	Tucker (1951)	9·6	22·5	14·9
	Young & Janssen (1952)	12·7	22·8	16·5
	Sommer & Short (1955)	12·0	17·1	13·8
	Eckert (1955)	12·2	20·2	15·1
Miscellaneous other assumptions	Donaldson (1952)	12·4	20·6	15·4
	Spence (1959)	12·2	18·2	14·3
	Winkler (1961)	14·0	23·7	17·6
	Burgraff (1962)	16·1	26·1	19·8
	Present procedure	8·6	12·5	9·9

TABLE 6. Comparison of theories with experimental data of the references marked with a cross

compared are listed in table 6) are not included, either because they still have indeterminate constants or because they involve lengthy time-consuming numerical work which is believed not to be profitable at the present state of knowledge of turbulence.

The criterion used for comparison is the root-mean-square of

$$(c_{f,\exp} - c_{f,\mathrm{th}})/c_{f,\mathrm{th}},$$

where $c_{f,\exp}$ is the experimental local or overall friction coefficient and $c_{f,\mathrm{th}}$ is the theoretical local or overall friction coefficient*, the corresponding experimental Reynolds number (R_δ or R_x), Mach number (M_G) and temperature ratio (T_S/T_G). In evaluating the above root-mean-square value for each of 20 theories, all the experimental data of Appendix A (plotted in figures 1–3) have been used.

The evaluation of the root-mean-square values of $(c_{f,\exp} - c_{f,\mathrm{th}})/c_{f,\mathrm{th}}$ was carried out by the Mercury digital computer of London University. A computer program was written for each of the twenty theories. Then each theory was applied to each of the 491 experimental conditions for which $c_{f,\exp}$ data were available, yielding appropriate values of $c_{f,\mathrm{th}}$. The root-mean-square value of $(c_{f,\exp} - c_{f,\mathrm{th}})/c_{f,\mathrm{th}}$ was then computed for each theory in an obvious manner.

The results of the comparison are shown in table 6. They give a quantitative indication of the accuracy of the various theories when compared with present empirical knowledge of the compressible turbulent boundary layer.

It is seen from table 6 that the three best theories are those of van Driest–II (1955), Wilson (1950) extended by us, and Kutateladze & Leont'ev (1961). They are all based upon the mixing-length theory used in the method of §§ 2.2 or 2.3, that is, tables 1 or 2. Table 6 also reveals that all theories exhibit a greater error when compared with the data for finite heat-transfer rates than when compared with data obtained under adiabatic conditions.

4. Development of an improved calculation procedure

4.1. *Fundamental functions*

We first seek a relation between c_f and R_δ. For the constant-pressure boundary layer, we may expect that

$$c_f = c_f(R_\delta, M_G, T_S/T_G). \tag{17}$$

The nature of the function can be determined either theoretically (§ 2) or experimentally.

Now many of the theoretical expressions, viz. theories of Clemmow–I & II (1950), Cope–II (1943), Monaghan (1950), Smith & Harrop (1946), van Driest–I & II (1951, 1955), Spence (1959), Wilson (1950), Winkler (1961) and table 5 can be written in the form

$$\tfrac{1}{2}c_f F_c = \psi_\delta(R_\delta F_{R\delta}), \tag{18}$$

where the function ψ_δ is independent of Mach number and temperature ratio, the

* For the sake of simplicity, here and on some other occasions, c_f stands for both c_f and $\bar{c}_f$, as is clear in the text.

effects of which are wholly accounted for by the functions F_c and $F_{R\delta}$. The latter functions are such that

$$F_c = F_c(M_G, T_S/T_G),$$
$$= 1, \quad \text{for} \quad M_G = 0, \quad T_S/T_G = 1; \tag{19}$$
$$F_{R\delta} = F_{R\delta}(M_G, T_S/T_G),$$
$$= 1, \quad \text{for} \quad M_G = 0, \quad T_S/T_G = 1. \tag{20}$$

Some of the other theoretical expressions, for example, those of Kutateladze & Leont'ev (1961), and Burgraff (1962), if expressed in the form of equation (18), would imply that $F_{R\delta}$ exhibits a weak dependence on c_f; however, this is by no means certain, as is shown by our comparison between theories and experiments (table 6) and we shall ignore this dependence.

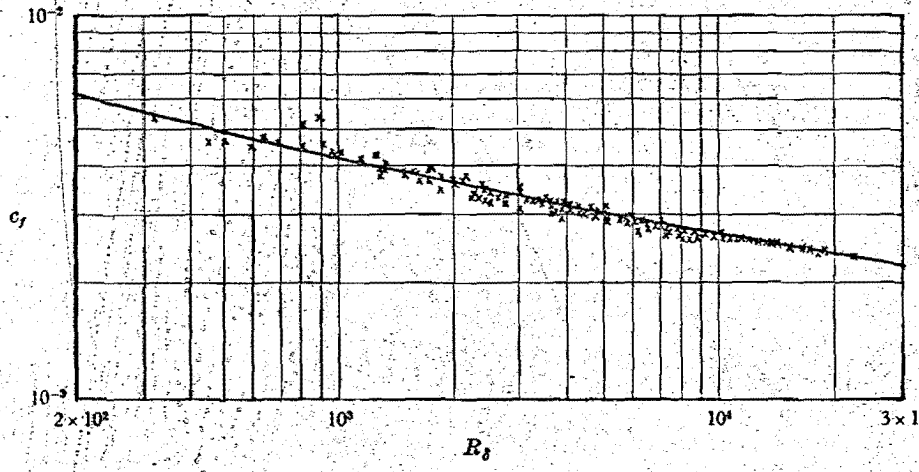

FIGURE 6. Comparison of equation (28) with uniform-property data, c_f *vs* R_δ.

Secondly, we will consider the relation between c_f and R_x. The integral momentum equation for the boundary layer on a flat plate (see Schlichting 1960, p. 536) leads to

$$\tfrac{1}{2}c_f = dR_\delta/dR_x. \tag{21}$$

Rewriting equation (21) in integral form, we obtain

$$R_x = \int_0^{R_\delta} (2/c_f)\, dR_\delta. \tag{22}$$

By multiplication of equation (22) by $F_{R\delta}/F_c$, there is obtained

$$\frac{F_{R\delta}}{F_c} R_x = \int_0^{F_{R\delta}R_\delta} \frac{2}{c_f F_c}\, d(F_{R\delta} R_\delta). \tag{23}$$

We have already postulated the existence of a unique relation between $c_f F_c$ and $R_\delta F_{R\delta}$ in equation (18), which is independent of Mach number and temperature ratio. With this, equation (23) yields

$$\tfrac{1}{2}c_f F_c = \psi_x(R_x F_{Rx}), \tag{24}$$

where the function ψ_x is independent of Mach number and temperature ratio, F_c and $F_{R\delta}$ are the same functions as those of equations (19) and (20), and F_{Rx} is related to $F_{R\delta}$ and F_c by

$$F_{Rx} = F_{R\delta}/F_c = 1, \quad \text{for} \quad M_G = 0, \quad T_S/T_G = 1. \tag{25}$$

Finally, consider $\bar{c}_f$ as a function of R_x. From the definition of $\bar{c}_f$,

$$\tfrac{1}{2}\bar{c}_f \equiv (R_x)^{-1}\int_0^{R_x} (c_f/2)\,dR_x, \tag{26}$$

it can be shown by the method of the preceding paragraph that

$$\tfrac{1}{2}\bar{c}_f F_c = \overline{\psi}(R_x F_{Rx}), \tag{27}$$

where the function $\overline{\psi}$ is again independent of Mach number and temperature ratio, and F_c and F_{Rx} are defined by equations (19) and (25).

To summarize, it has been shown that, if $F_{R\delta}$ is independent of $\frac{1}{2}c_f$, the following functions exist,

$$\tfrac{1}{2}c_f F_c = \psi_\delta(F_{R\delta} R_\delta), \tag{18}$$

$$\tfrac{1}{2}c_f F_c = \psi_x(F_{Rx} R_x), \tag{24}$$

$$\tfrac{1}{2}\bar{c}_f F_c = \overline{\psi}(F_{Rx} R_x), \tag{27}$$

where ψ_δ, ψ_x and $\overline{\psi}$ are independent of Mach number and temperature ratio. Now analytic functions exist which adequately represent the relations between $\frac{1}{2}c_f$ and R_δ, $\frac{1}{2}c_f$ and R_x, and $\frac{1}{2}\bar{c}_f$ and R_x, in uniform-density flow (Spalding 1962*a*), namely*

$$R_\delta = \tfrac{1}{6}(u_G^+)^2 + (KE)^{-1}[\{1-(2/Ku_G^+)\}\exp(Ku_G^+) + (2/Ku_G^+) + 1 - \tfrac{1}{6}(Ku_G^+)^2 - \tfrac{1}{12}(Ku_G^+)^3 - \tfrac{1}{40}(Ku_G^+)^4 - \tfrac{1}{180}(Ku_G^+)^5], \tag{28}$$

$$R_x = \tfrac{1}{12}(u_G^+)^2 + (K^3E)^{-1}[\{6 - Ku_G^+ + (Ku_G^+)^2\}\exp(Ku_G^+) - 6 - 2Ku_G^+ - \tfrac{1}{12}(Ku_G^+)^4 - \tfrac{1}{20}(Ku_G^+)^5 - \tfrac{1}{60}(Ku_G^+)^6 - \tfrac{1}{252}(Ku_G^+)^7], \tag{29}$$

$$\tfrac{1}{2}\bar{c}_f = R_\delta/R_x, \tag{30}$$

where $u_G^+ = (2/c_f)^{\frac{1}{2}}$, $K = 0{\cdot}4$ and $E = 12$.

Figures 6, 7 and 8 show the comparison between the above three functions, equations (28), (29) and (30), and the incompressible turbulent boundary-layer experimental data from those references marked with a dagger. The agreement is good throughout the whole range of Reynolds number; indeed the values of E and K have been chosen so as to give a minimum value of root-mean-square error in a manner similar to that described above, Chi (1962).† Now, our problem reduces to the determination of F_c and $F_{R\delta}$ as functions of Mach number and temperature ratio.

4.2. *Determination of the F_c-function*

Since the functions ψ_δ, ψ_x, and $\overline{\psi}$ are known [equations (28), (29) and (30)], and since numerous data for compressible turbulent boundary layers [references marked with a double dagger] have been collected, it might seem to be possible

* These are of course not the only equations which may be used; and they are certainly not the simplest. They are used because they are consistent with a formula for the universal velocity profile which is both simple and in good agreement with experimental data.

† On a c_f basis, the root-mean-square error would be about 2 %.

to deduce the F_c and F_{Rs} functions solely from experiment. An attempt to do this, however, soon showed that the data were too scanty and inaccurate to allow success. Some theoretical guidance is therefore sought for the determination of one of the functions. F_c is the obvious choice.

In § 3, it was shown that theories based upon the mixing-length hypothesis of tables 1 and 2 gave the best prediction of all the previous theories; it was also discovered that the corresponding methods lead to the following expression for F_c

$$F_c = \left[\int_0^1 (\rho/\rho_G)^{\frac{1}{2}} dz\right]^{-2}. \quad \checkmark \tag{31}$$

The expression for F_{Rs}, by contrast, varies considerably from one theory to the next. Equation (31) has been adopted for the F_c function in the present theory.

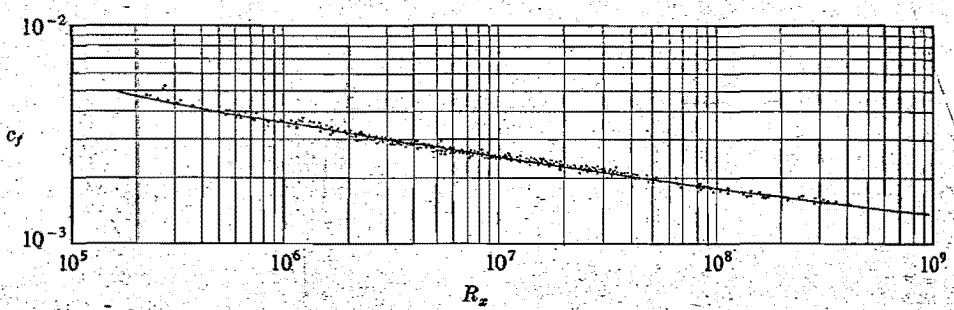

FIGURE 7. Comparison of equation (29) with uniform-property data, c_f *vs* R_x.

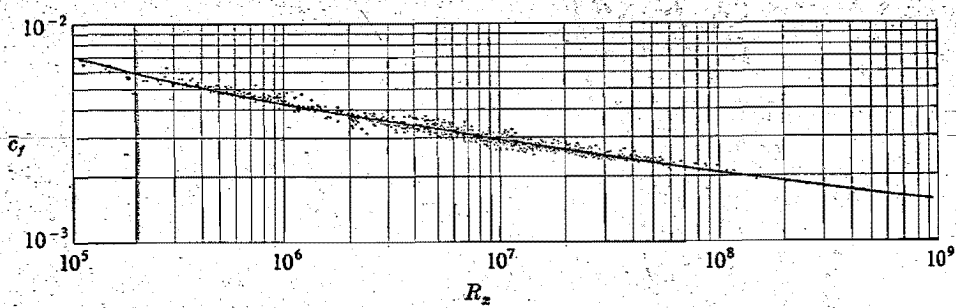

FIGURE 8. Comparison of equation (30) with uniform-property data, $\bar{c}_f$ *vs* R_x.

Evaluation of F_c from equation (31) requires the density to be expressed as a function of z, where z is defined as u/u_G. This relationship may be derived from the Reynolds analogy between energy and momentum transfer, modified for non-unity Prandtl number in the following manner.

From the Reynolds analogy, we have

$$\frac{h^0 - h_S^0}{h_G^0 - h_S^0} = \frac{u - u_S}{u_G - u_S}, \tag{32}$$

where h^0 is the stagnation enthalpy, u is the velocity in the x-direction, subscripts G and S refer to the main stream and the fluid adjacent to the wall, respectively.

Now $u_S = 0$, $h^0 = c(T + \frac{1}{2}(\gamma-1)M_G^2 T_G z^2)$ for a perfect gas, $h_S^0 = h_S = cT_S$, where c is the specific heat at constant pressure, and T is the temperature in degrees absolute. Equation (32) can then be written as

$$T/T_G = (T_S/T_G) + \{1 + \tfrac{1}{2}(\gamma-1)M_G^2 - (T_S/T_G)\}z - \tfrac{1}{2}(\gamma-1)M_G^2 z^2. \quad (33)$$

For the adiabatic-wall case, the coefficient of z of equation (33) is zero, and T_S is equal to the adiabatic-wall temperature, $T_{ad,S}$. Hence

$$T_{ad,S}/T_G = 1 + \tfrac{1}{2}(\gamma-1)M_G^2. \quad (34)$$

This holds for a Prandtl number of unity. For non-unity Prandtl number,

$$T_{ad,S}/T_G = 1 + \tfrac{1}{2}r(\gamma-1)M_G^2, \quad (35)$$

where r is the recovery factor. For gases of $P \approx 0{\cdot}7$, measurements of recovery factor by various investigators, Brevoort & Arabian (1958), Brinich (1961), Kaye (1954), Hilton (1951), Slack (1952) and Stalder, Rubesin & Tendeland (1950), showed that the value of recovery factor lies between 0·88 and 0·9; 0·89 is a fair mean of all measurements. Now equation (33) can be modified to satisfy the boundary condition at the wall for the adiabatic-wall case, by writing

$$T/T_G = (T_S/T_G) + \{1 + \tfrac{1}{2}r(\gamma-1)M_G^2 - (T_S/T_G)\}z - \tfrac{1}{2}r(\gamma-1)M_G^2 z^2, \quad (36)$$

where $r = 0{\cdot}89$ for $P \approx 0{\cdot}7$. For an ideal gas at constant pressure,

$$\rho/\rho_G = (T/T_G)^{-1}. \quad (37)$$

On substitution of equation (36) into equation (37), there is obtained

$$\rho/\rho_G = [(T_S/T_G) + \{1 + \tfrac{1}{2}r(\gamma-1)M_G^2 - (T_S/T_G)\}z - \tfrac{1}{2}r(\gamma-1)M_G^2 z^2]^{-1}. \quad (38)$$

Hence from equations (31) and (38), we have

$$F_c = \left\{\int_0^1 \frac{dz}{[(T_S/T_G) + \{1 + \tfrac{1}{2}r(\gamma-1)M_G^2 - (T_S/T_G)\}z - \tfrac{1}{2}r(\gamma-1)M_G^2 z^2]^{\frac{1}{2}}}\right\}^{-2}, \quad (39)$$

where $r = 0{\cdot}89$. Equation (39) is the F_c function which we have used.

4.3. *Determination of the $F_{R\delta}$ function*

Though the theoretically derived expressions for $F_{R\delta}$ are rather uncertain, they can generally be written as

$$F_{R\delta} = (\mu_G/\mu_S)(\rho_S/\rho_G)^{\beta}(E/E_i), \quad (40)$$

where E_i is the value of E for uniform-property flow and is a constant. For example,

(*a*) In the van Driest–I method, $\beta = \frac{1}{2}$, $E = E_i$, hence

$$F_{R\delta} = (\mu_G/\mu_S)(\rho_S/\rho_G)^{\frac{1}{2}} = (T_G/T_S)^{1{\cdot}26} \quad \text{for} \quad \mu_G/\mu_S = (T_G/T_S)^{0{\cdot}76}. \quad (41)$$

(*b*) In the van Driest–II method, $\beta = 0$, $E = E_i$, hence

$$F_{R\delta} = (\mu_G/\mu_S) = (T_G/T_S)^{0{\cdot}76} \quad \text{for} \quad \mu_G/\mu_S = (T_G/T_S)^{0{\cdot}76}. \quad (42)$$

(c) In other methods, e.g. those of Kalikman (1956), Kutateladze & Leont'ev (1961)

$$E/E_i = f(T_N/T_S), \tag{43}$$

where T_N is the value of the temperature at some point near the wall.

Hence such theories commonly lead to an expression for $F_{R\delta}$ of the form

$$F_{R\delta} = (T_S/T_G)^p\,(T_N/T_S)^n, \tag{44}$$

where p and n are two constants which are still indeterminate and are to be determined from experiments as in the following paragraphs.

For the adiabatic-wall case, the temperature gradient at the wall is zero, and so the temperature near the wall is approximately equal to T_S. Hence equation (44) reduces to

$$F_{R\delta} = (T_S/T_G)^p. \tag{45}$$

Using the functions ψ_δ, ψ_x, $\overline{\psi}$ and F_c of equations (28), (29), (30) and (39), respectively, and all the collected experimental data for the adiabatic-wall case (summarized in Appendix A and figures 1–3), we have determined the value of p which gives the smallest root-mean-square value of $(c_{f,\exp} - c_{f,\mathrm{th}})/c_{f,\mathrm{th}}$. This value of p is $-0{\cdot}702$. Thus, for the adiabatic-wall case,

$$F_{R\delta} = (T_S/T_G)^{-0{\cdot}702}, \tag{46}$$

where T_S is of course the adiabatic-wall temperature which is obtained by equation (35).

The index q can be found from the drag coefficient in the presence of heat transfer. When there is heat transfer at the wall, the temperature gradient at the wall has a finite value and it is plausible that the ratio of the temperature in the vicinity of the wall to the wall temperature, T_N/T_S, is

$$T_N/T_S = 1 + z_N[d(T/T_S)/dz]_S, \tag{47}$$

where $z_N = u_N^+/u_G^+$, u_N^+ is the value of u^+ at the relevant distance from the wall. It is probable that u_N^+ is small so that u_G^+ is usually much larger than u_N^+; hence equation (47) can be written equally well as

$$T_N/T_S = \{1 + [d(T/T_S)/dz]_S\}^{z_N}. \tag{48}$$

Now, by differentiation of equation (36), we obtain

$$\left(\frac{d(T/T_S)}{dz}\right)_S = \left(1 + \tfrac{1}{2}r(\gamma-1)M_G^2 - \frac{T_S}{T_G}\right)\frac{T_G}{T_S}, \tag{49}$$

then

$$T_N/T_S \approx \left\{1 + \left[\frac{1 + \tfrac{1}{2}r(\gamma-1)M_G^2}{T_S/T_G} - 1\right]\right\}^{z_N}$$

$$= (T_{ad,S}/T_S)^{z_N}. \tag{50}$$

Substituting equation (50) into equation (44), we have

$$F_{R\delta} = (T_S/T_G)^p\,(T_{ad,S}/T_S)^q, \tag{51}$$

where $p = -0{\cdot}702$ obtained above and $q\,(= nz_N)$ is a constant to be determined empirically with the use of frictional-drag coefficient data in the presence of heat transfer. A computer program was written which varied q and minimized the

root-mean-square value of $(c_{f,\exp}-c_{f,\mathrm{th}})/c_{f,\mathrm{th}}$ for all the available heat-transfer experiments, p being given the value $-0{\cdot}702$ as derived earlier. The minimum root-mean-square error was found when q was 0·772. The recommended $F_{R\delta}$ is accordingly

$$F_{R\delta} = (T_S/T_G)^{-0{\cdot}702}\,(T_{ad,S}/T_S)^{0{\cdot}772}, \qquad (52)$$

which reduces to equation (46) for the adiabatic wall.

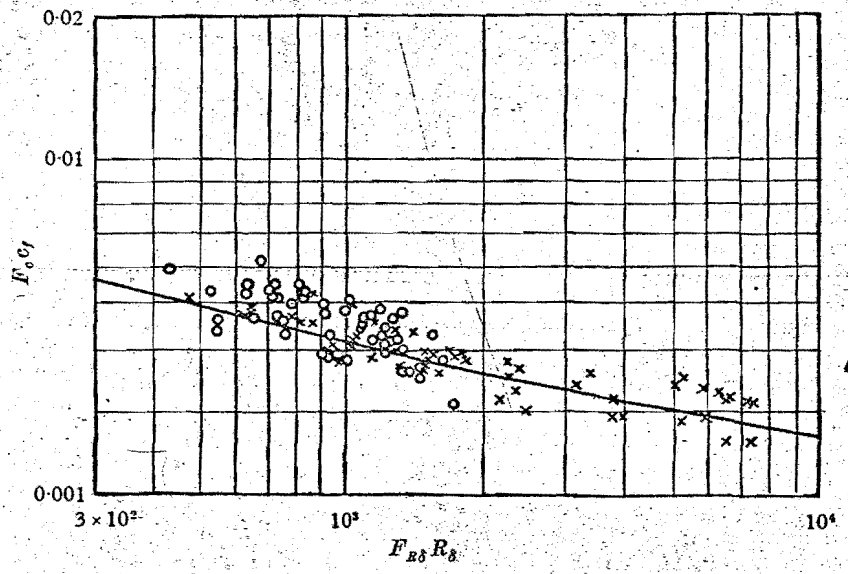

FIGURE 9. Comparison between theoretical and experimental $F_c c_f$ *vs* $F_{R\delta}R_\delta$. ×, experiments, adiabatic; ○, experiments with heat transfer; —, theory equation (28).

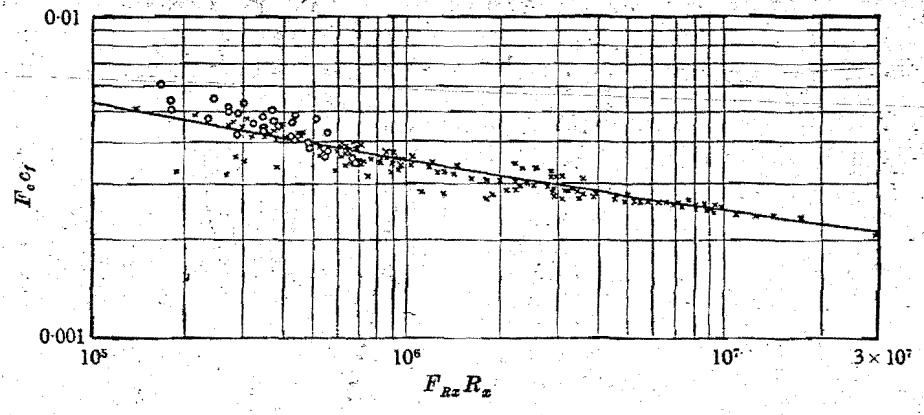

FIGURE 10. Comparison between theoretical and experimental $F_c c_f$ *vs* $F_{Rx}R_x$. ×, experiments, adiabatic; ○, experiments with heat transfer; —, theory equation (29).

4.4. *Comparison of the present method with other theories and experiments*

The root-mean-square value of $(c_{f,\exp}-c_{f,\mathrm{th}})\,c_{f,\mathrm{th}}$ for the present theory has been calculated and inserted in table 6 in order to compare it with the other theories. The present theory gives the lowest root-mean-square value, namely 9·9 %. This is to be expected because we have derived $F_{R\delta}$ directly from the experi-

mental data. In figures 9–11, the experimental and theoretical $F_c c_f$ *vs* $F_{R\delta}R_\delta$, $F_c c_f$ *vs* $F_{Rx}R_x$ and $F_c \bar{c}_f$ *vs* $F_{Rx}R_x$ are plotted. The agreement between theory and experiments is again satisfactory.

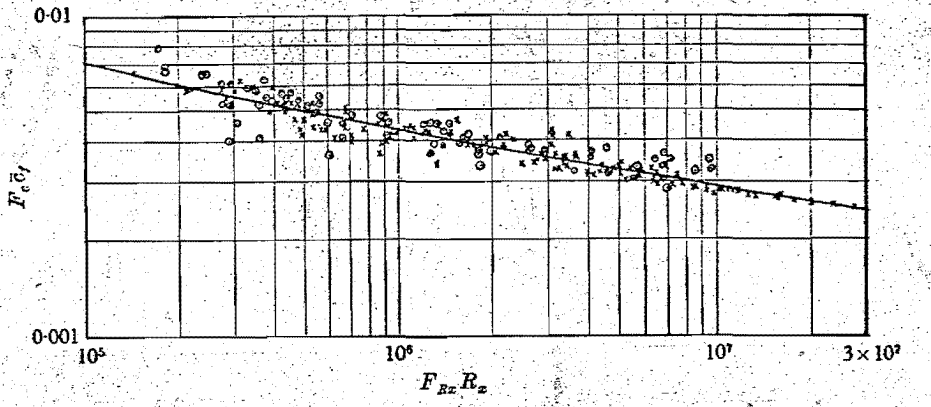

FIGURE 11. Comparison between theoretical and experimental $F_c \bar{c}_f$ *vs* $F_{Rx}R_x$. ×, experiments, adiabatic; ○, experiments with heat transfer; —, theory equation (30).

$F_c c_f$	$F_c \bar{c}_f$	$F_{R\delta}R_\delta$	$F_{Rx}R_x$	$F_c c_f$	$F_c \bar{c}_f$	$F_{R\delta}R_\delta$	$F_{Rx}R_x$
0·0010	0·001117	$2{\cdot}878\times10^7$	$5{\cdot}758\times10^{10}$	0·0060	0·008205	233·0	$5{\cdot}679\times10^4$
0·0015	0·001716	$3{\cdot}955\times10^5$	$4{\cdot}610\times10^8$	0·0065	0·009105	177·6	$3{\cdot}901\times10^4$
0·0020	0·002333	$5{\cdot}425\times10^4$	$4{\cdot}651\times10^7$	0·0070	0·010042	140·4	$2{\cdot}796\times10^4$
0·0025	0·002967	$1{\cdot}386\times10^4$	$9{\cdot}340\times10^6$	0·0075	0·011014	114·4	$2{\cdot}078\times10^4$
0·0030	0·003621	5030	$2{\cdot}778\times10^6$	0·0080	0·012016	95·62	$1{\cdot}592\times10^4$
0·0035	0·004299	2283	$1{\cdot}062\times10^6$	0·0085	0·01304	92·49	$1{\cdot}251\times10^4$
0·0040	0·005006	1208	$4{\cdot}828\times10^5$	0·0090	0·01409	70·91	$1{\cdot}006\times10^4$
0·0045	0·005747	716·0	$2{\cdot}492\times10^5$	0·0095	0·01516	62·55	$8{\cdot}253\times10^3$
0·0050	0·006526	462·3	$1{\cdot}417\times10^5$	0·0100	0·01624	55·87	$6{\cdot}883\times10^3$
0·0055	0·007345	319·4	$8{\cdot}697\times10^4$	0·0105	0·01732	50·46	$5{\cdot}826\times10^3$

TABLE 7. Values of $F_c c_f$, $F_c \bar{c}_f$, $F_{R\delta}R_\delta$ and $F_{Rx}R_x$

4.5. *Summary of results*

To facilitate calculation, the main results derived earlier in this section are presented in the form of tables and figures. Table 7 gives the corresponding values of $F_c c_f$ and $F_c \bar{c}_f$ *vs* $F_{R\delta}R_\delta$ and $F_{Rx}R_x$, table 8 gives the values of F_c at various M_G and T_S/T_G, and table 9 gives the values of $F_{R\delta}$ at various M_G and T_S/T_G. Values from tables 8 and 9 are plotted in figure 12 for convenience of use.

4.6. *Recommended method of calculation*

In the most common cases, the problem is to find the drag coefficient when the Reynolds number, Mach number and temperature ratio are known. The procedure for solving this problem by use of the present method is as follows. First, the value of F_c is determined from table 8 or figure 12. Then the value of $F_{R\delta}$ is

T_S/T_G \ M_G	0	1	2	3	4	5	6	7
0·05	0·3743	0·4036	0·4884	0·6222	0·7999	1·0184	1·2759	1·5713
0·1	0·4331	0·4625	0·5477	0·6829	0·8628	1·0842	1·3451	1·6444
0·2	0·5236	0·5530	0·6388	0·7756	0·9584	1·1836	1·4491	1·7534
0·3	0·5989	0·6283	0·7145	0·8523	1·0370	1·2649	1·5337	1·8418
0·4	0·6662	0·6957	0·7821	0·9208	1·1069	1·3370	1·6083	1·9194
0·5	0·7286	0·7580	0·8446	0·9839	1·1713	1·4031	1·6767	1·9903
0·6	0·7873	0·8168	0·9036	1·0434	1·2318	1·4651	1·7405	2·0564
0·8	0·8972	0·9267	1·0137	1·1544	1·3445	1·5802	1·8589	2·1785
1	1·0000	1·0295	1·1167	1·2581	1·4494	1·6871	1·9684	2·2913
2	1·4571	1·4867	1·5744	1·7176	1·9130	2·1572	2·4472	2·7809
3	1·8660	1·8956	1·9836	2·1278	2·3254	2·5733	2·8687	3·2092
4	2·2500	2·2796	2·3678	2·5126	2·7117	2·9621	3·2611	3·6066
5	2·6180	2·6477	2·7359	2·8812	3·0813	3·3336	3·6355	3·9847
6	2·9747	3·0044	3·0927	3·2384	3·4393	3·6930	3·9971	4·3493
8	3·6642	3·6938	3·7823	3·9284	4·1305	4·3863	4·6937	5·0505
10	4·3311	4·3608	4·4493	4·5958	4·7986	5·0559	5·3657	5·7259
12	4·9821	5·0117	5·1003	5·2470	5·4504	5·7088	6·0204	6·3832
14	5·6208	5·6505	5·7391	5·8860	6·0898	6·3491	6·6621	7·0271
16	6·2500	6·2797	6·3683	6·5153	6·7196	6·9795	7·2937	7·6603
18	6·8713	6·9010	6·9897	7·1368	7·3413	7·6019	7·9170	8·2851
20	7·4861	7·5157	7·6045	7·7517	7·9564	8·2175	8·5334	8·9027
25	9·0000	9·0297	9·1184	9·2658	9·4711	9·7330	10·0505	10·4222
30	10·4886	10·5183	10·6071	10·7546	10·9602	11·2228	11·5415	11·9149

T_S/T_G \ M_G	8	9	10	11	12	13	14	15
0·05	1·9041	2·3738	2·6803	3·1233	3·6027	4·1186	4·6707	5·2591
0·1	1·9812	2·3552	2·7660	3·2134	3·6976	4·2180	4·7748	5·3680
0·2	2·0958	2·4756	2·8925	3·3462	3·8366	4·3636	4·9269	5·5267
0·3	2·1882	2·5723	2·9937	3·4522	3·9974	4·4792	5·0475	5·6523
0·4	2·2692	2·6569	3·0820	3·5443	4·0435	4·5794	5·1518	5·7608
0·5	2·3429	2·7336	3·1620	3·6276	4·1303	4·6697	5·2458	5·8584
0·6	2·4115	2·8049	3·2362	3·7048	4·2105	4·7531	5·3324	5·9483
0·8	2·5379	2·9360	3·3721	3·8459	4·3570	4·9051	5·4901	6·1117
1	2·6542	3·0562	3·4966	3·9748	4·4905	5·0434	5·6333	6·2599
2	3·1564	3·5725	4·0282	4·5228	5·0556	5·6263	6·2345	6·8801
3	3·5929	4·0184	4·4846	4·9904	5·5353	6·1187	6·7401	7·3993
4	3·9964	4·4290	4·9030	5·4176	5·9719	6·5653	7·1972	7·8673
5	4·3792	4·8174	5·2979	5·8196	6·3817	6·9833	7·6240	8·3033
6	4·7477	5·1905	5·6764	6·2041	6·7727	7·3814	8·0297	8·7169
8	5·4549	5·9050	6·3994	6·9368	7·5161	8·1365	8·7972	9·4977
10	6·1347	6·5904	7·0913	7·6363	8·2241	8·8539	9·5247	10·2359
12	6·7955	7·2556	7·7618	8·3129	8·9077	9·5452	10·2245	10·9449
14	7·4422	7·9058	8·4164	8·9727	9·5734	10·2174	10·9040	11·6321
16	8·0778	8·5444	9·0587	9·6194	10·2251	10·6748	11·5676	12·3026
18	8·7045	9·1737	9·6912	10·2556	10·8657	11·5204	12·2187	12·9598
20	9·3238	9·7952	10·3154	10·8832	11·4971	12·1562	12·8595	13·6059
25	10·8467	11·3225	11·8482	12·4227	13·0446	13·7128	14·4263	15·1841
30	12·3418	12·8209	13·3509	13·9305	14·5586	15·2339	15·9556	16·7225

TABLE 8. Values of F_c at various M_G and T_S/T_G

T_S/T_G \ M_G	0	1	2	3	4	5	6	7
0·05	82·7405	93·8950	125·3092	173·1153	234·1638	306·3489	388·2642	478·9229
0·1	29·7852	33·8006	45·1092	62·3185	84·2949	110·2803	139·7684	172·4040
0·2	10·7221	12·1676	16·2385	22·4336	30·3447	39·6990	50·3142	62·0625
0·3	5·8983	6·6934	8·9328	12·3407	16·6926	21·8384	27·6779	34·1406
0·4	3·8598	4·3801	5·8456	8·0757	10·9236	14·2910	18·1123	22·3414
0·5	2·7779	3·1524	4·2071	5·8121	7·8618	10·2853	13·0355	16·0792
0·6	2·1233	2·4095	3·2157	4·4424	6·0091	7·8615	9·9636	12·2900
0·8	1·3895	1·5768	2·1043	2·9071	3·9323	5·1445	6·5201	8·0425
1	1·0000	1·1348	1·5145	2·0923	2·8301	3·7025	4·6926	5·7883
2	0·3600	0·4085	0·5452	0·7532	1·0188	1·3328	1·6892	2·0837
3	0·1980	0·2247	0·2999	0·4143	0·5604	0·7332	0·9292	1·1462
4	0·1296	0·1471	0·1963	0·2711	0·3667	0·4798	0·6081	0·7501
5	0·0933	0·1058	0·1412	0·1951	0·2639	0·3453	0·4377	0·5398
6	0·0713	0·0809	0·1080	0·1491	0·2017	0·2639	0·3345	0·4126
8	0·0466	0·0529	0·0706	0·0976	0·1320	0·1727	0·2189	0·2700
10	0·0336	0·0381	0·0508	0·0702	0·0950	0·1243	0·1575	0·1943
12	0·0257	0·0291	0·0389	0·0537	0·0726	0·0950	0·1204	0·1485
14	0·0204	0·0232	0·0310	0·0428	0·0579	0·0757	0·0959	0·1183
16	0·0168	0·0191	0·0254	0·0351	0·0475	0·0622	0·0788	0·0972
18	0·0141	0·0160	0·0214	0·0295	0·0400	0·0523	0·0662	0·0817
20	0·0121	0·0137	0·0183	0·0253	0·0342	0·0447	0·0567	0·0700
25	0·0087	0·0099	0·0132	0·0182	0·0246	0·0322	0·0408	0·0503
30	0·0066	0·0075	0·0101	0·0139	0·0188	0·0246	0·0312	0·0385

T_S/T_G \ M_G	8	9	10	11	12	13	14	15
0·05	577·5949	683·7162	796·8344	916·5768	1042·629	1174·722	1312·620	1456·116
0·1	207·9243	246·1261	286·8467	329·9519	375·3286	422·8798	472·5207	524·1767
0·2	74·8492	88·6012	103·2599	118·7770	135·1119	152·2295	170·0993	188·6946
0·3	41·1745	48·7395	56·8032	65·3392	74·3250	83·7414	93·5716	103·8009
0·4	26·9444	31·8949	37·1718	42·7577	48·6380	54·8000	61·2328	67·9268
0·5	19·3920	22·9549	26·7527	30·7729	35·0050	39·4398	44·0696	48·8873
0·6	14·8221	17·5454	20·4482	23·5210	26·7557	30·1455	33·6842	37·3665
0·8	9·6995	11·4816	13·3812	15·3920	17·5088	19·7271	22·0428	24·4525
1	6·9808	8·2634	9·6305	11·0777	12·6012	14·1977	15·8643	17·5986
2	2·5130	2·9747	3·4668	3·9878	4·5362	5·1109	5·7109	6·3352
3	1·3824	1·6364	1·9071	2·1937	2·4954	2·8115	3·1416	3·4850
4	0·9046	1·0708	1·2480	1·4355	1·6330	1·8398	2·0558	2·2806
5	0·6511	0·7707	0·8982	1·0332	1·1752	1·3241	1·4796	1·6413
6	0·4976	0·5891	0·6862	0·7897	0·8983	1·0121	1·1309	1·2545
8	0·3256	0·3855	0·4493	0·5168	0·5878	0·6623	0·7401	0·8210
10	0·2344	0·2774	0·3233	0·3719	0·4231	0·4767	0·5326	0·5909
12	0·1791	0·2121	0·2471	0·2843	0·3234	0·3643	0·4071	0·4516
14	0·1427	0·1690	0·1969	0·2265	0·2576	0·2903	0·3244	0·3598
16	0·1172	0·1388	0·1617	0·1860	0·2116	0·2384	0·2664	0·2955
18	0·0985	0·1167	0·1359	0·1564	0·1779	0·2004	0·2239	0·2484
20	0·0844	0·0999	0·1164	0·1339	0·1523	0·1716	0·1917	0·2127
25	0·0607	0·0719	0·0838	0·0964	0·1096	0·1235	0·1380	0·1531
30	0·0464	0·0549	0·0640	0·0737	0·0838	0·0944	0·1055	0·1170

TABLE 9. Values of F_{Rs} at various M_G and T_S/T_G

determined from equation (52), table 9 or figure 12, and where necessary the value of F_{Rx} is obtained from the equation

$$F_{Rx} = F_{R\delta}/F_c. \tag{25}$$

Finally, by using the input value of R_δ (or R_x) and the values of $F_{R\delta}$ (or F_{Rx}) and F_c above, c_f or $\bar{c}_f$ can be obtained from table 7 or figures 9–11.

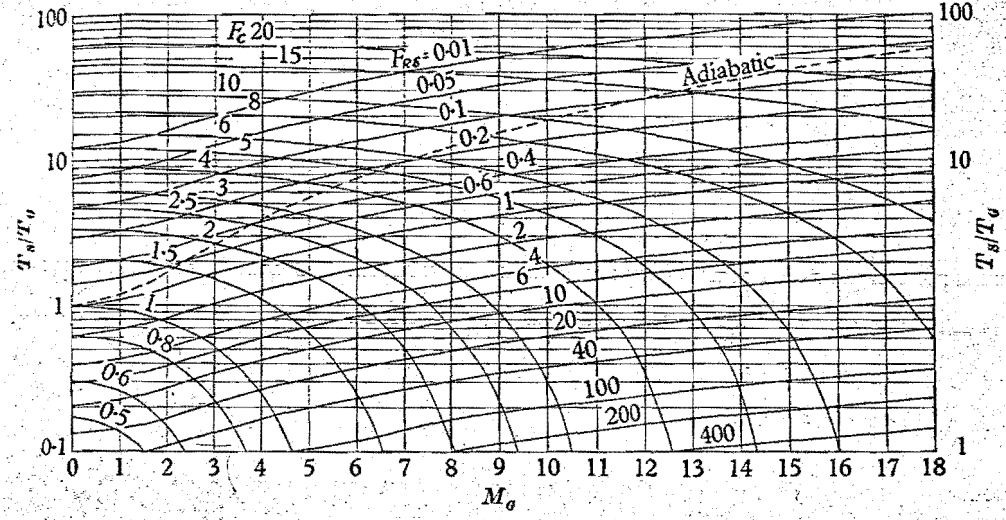

FIGURE 12. Chart of constant F_c and $F_{R\delta}$ lines in T_S/T_G and M_G co-ordinates.

The above calculation can be performed in a few minutes with an accuracy of 1%. The latter is of course well within the limit of experimental accuracy at present.

5. Conclusions

In conclusion, the results of this work can be summarized as follows.

A procedure has been developed semi-empirically for predicting the drag coefficient on a smooth surface of zero stream-wise pressure gradient at various Reynolds numbers, Mach numbers and ratios of surface temperature to stream temperature.

The extent to which the procedure correlates the existing experimental data can be judged by inspection of figures 9–11, whereby it must be remembered that the experiments have been carried out in several entirely different pieces of apparatus and are not of high or uniform accuracy. The correlation is better than that given by any of the other existing theories as can be seen from table 6. The value of the present procedure is that it does not make use of the more arbitrary assumptions of earlier theories; it lets the data speak for themselves.

The procedure is simple and quick to use in engineering calculations and its accuracy is only limited (at the present time) by the accuracy of experimental data from which it is in part derived.

The necessary auxiliary functions have been tabulated (tables 7–9) and plotted in figures 9–12 for ready reference. However, it must be remembered

that experiments have not yet been carried out over the whole range of conditions covered by the tables and figures. Figure 4 shows how remarkably restricted has been the range of experimental conditions so far.

The procedure is capable of greater refinement when more accurate experimental data are available, say by modification of the $F_{R\delta}$ function. It can also be extended to include mass transfer (Spalding 1962*b*).

Finally, it should be noted that the calculation procedure which has been recommended is based on no new physical hypothesis. The expression recommended for F_c implies the assumption of one or other variety of the mixing-length theory; but the expression for $F_{R\delta}$ is entirely empirical. It may indeed be rather hard to find a physical hypothesis to fit the empirically derived $F_{R\delta}$ function; for, whereas the exponent of (T_S/T_G) in equation (52) has a sign and magnitude which allows us to ascribe its effects to the role of the viscosity near the wall, the sign of the exponent of $(T_{ad,S}/T_S)$ is quite unexpected. This point certainly deserves explanation. However, we have thought it better at the present stage to provide quantitative results against which old and new hypotheses can be tested than to advance such hypotheses ourselves.

REFERENCES

†Abbot, I. H. 1953 *AGARD* Memo. AG/8M4.

Brevoort, M. J. & Arabian, B. D. 1958 *Nat. Adv. Comm. Aero., Wash., Tech. Note*, no. 4248.

Brinich, P. F. 1961 *Nat. Aero. Space Admin., Tech. Note*, no. D-1047.

†Brinich, P. F. & Diaconis, N. S. 1952 *Nat. Adv. Comm. Aero., Wash., Tech. Note*, no. 2742.

*Burgraff, O. R. 1962 *J. Aero. Sci.* **29**, 434.

Chapman, D. R. & Kester, R. H. 1953 *J. Aero. Sci.* **20**, 441.

†Chapman, D. R. & Kester, R. M. 1954 *Nat. Adv. Comm. Aero., Wash., Tech. Note*, no. 3097.

Chi, S. W. 1962 Unpublished work at Imperial College.

*Clemmow, D. M. 1950 *Aero. Res. Counc., London*, no. 14051, F.M. 1568, DGWRD Rep. 50/6.

†Coles, D. 1954 *J. Aero. Sci.* **21**, 433.

*Coles, D. E. 1962 *Rand Corporation*, Rep. no. R-403-PR.

*Cope, W. F. 1943 *Aero. Res. Counc., London, Rep. & Mem.*, no. 2840.

†Cope, W. F. 1952 *Proc. Roy. Soc.* A, **215**, 84.

††Dahwan, S. 1952 *Nat. Adv. Comm. Aero., Wash., Tech. Note*, no. 2567.

*Deissler, R. G. & Loeffler, A. L. 1959 *Nat. Aero. Space Admin., Tech. Rep.*, no. R-17.

*Donaldson, C. dup 1952 *Nat. Adv. Comm. Aero., Wash., Tech. Note*, no. 2962.

*Dorrance, W. H. 1960 *Convair Sci. Res. Lab. Res. Rep.* no. 6.

‡Dutton, R. A. 1957 *Aero. Res. Counc., London, Rep. & Mem.*, no. 3058.

*Eckert, E. R. G. 1955 *J. Aero. Sci.* **22**, 585.

‡Falkner, V. M. 1943 *Aircraft Engng*, **15**, 65.

*Ferrari, C. 1950 *Quart. Appl. Math.* **18**, 33.

*Frankl, F. & Voishel, V. 1937 Translation *Nat. Adv. Comm. Aero., Wash., Tech. Note*, no. 1052 (1943).

†Goddard, F. E. 1959 *J. Aero./Sp. Sci.* **26**, 1.

†Hakkinen, R. J. 1955 *Nat. Adv. Comm. Aero., Wash., Tech. Note*, no. 3486.

‡Hama, F. R. 1947 *Rep. Inst. Sci. and Tech., Tokyo, Japan*, **1**, 13 and 19.

†Hill, F. K. 1956 *J. Aero. Sci.* **23**, 35.

†Hill, F. K. 1959 *Phys. Fluids*, **2**, 668.

Hilton, W. F. 1951 *J. Aero. Sci.* **18**, 97.

‡Hughes, G. 1952 *Trans. Inst. Nav. Arch.* **94**, 287.

*Kalikman, L. E. 1959 *Dokl. Akad. Nauk, SSSR*, **106**, 123.

Kaye, J. 1954 *J. Aero. Sci.* **21**, 117.

‡Kempf, G. 1929 *Werft, Reed., Hafen.* **11**, 234.

‡Klebanoff, P. S. & Diehl, Z. W. 1951 *Nat. Adv. Comm. Aero., Wash., Tech. Note*, no. 2475.

†Korkegi, R. H. 1956 *J. Aero. Sci.* **23**, 97.

*Kosterin, S. I. & Koshmarov, Y. A. 1960 *Soviet Phys.* **4**, 819.

*Kutateladze, S. S. & Leont'ev, A. I. 1961 *Discussion of Heat and Mass Transfer, Akad. Nauk BSSR, Minsk*, 1, Translation TIL T5258.

‡Landweber, L. & Siao, T. T. 1958 *J. Ship Res.* **1**, 21.

*Li, T. Y. & Nagamatsu, H. T. 1951 *J. Aero. Sci.* **18**, 696.

*Lin, C. C. & Shen, S. F. 1951 *Nat. Adv. Comm. Aero., Wash., Tech. Note*, no. 2542.

‡Ludwig, H. & Tillmann, W. 1949 Translation *Nat. Adv. Comm. Aero., Wash., Tech. Mem.*, no. 1285.

†‡Matting, F. M., Chapman, D. R., Nyholm, J. R. & Thomas, A. G. 1951 *Nat. Aero. Space Admin., Tech. Rep.*, no. R-82.

‡Mickley, H. S. & Davis, R. S. 1957 *Nat. Adv. Comm. Aero., Wash., Tech. Note*, no. 4017.

*Monaghan, R. J. 1950 *Aero. Res. Counc., London*, no. CP 45.

†Monaghan, R. J. & Cooke, J. R. 1953*a* *Aero. Res. Counc., London*, no. CP 139.

†Monaghan, R. J. & Cooke, J. R. 1953*b* *Aero. Res. Counc., London*, no. CP 140.

†Monaghan, R. J. & Johnson, J. E. 1952 *Aero. Res. Counc., London*, no. CP 64.

†O'Donell, R. M. 1954 *Nat. Adv. Comm. Aero., Wash., Tech. Note*, no. 3122.

†Pappas, C. C. 1954 *Nat. Adv. Comm. Aero., Wash., Tech. Note*, no. 3222.

Peterson, J. B. 1963 *Nat. Aero. Space Admin., Tech. Note*, no. D-1795.

*†Rubesin, M. W., Maydew, R. C. & Varga, S. A. 1951 *Nat. Adv. Comm. Aero., Wash., Tech. Note*, no. 2305.

Schlichting, H. 1960 *Boundary Layer Theory*, 2nd ed. Translated by J. Kestin. London: McGraw-Hill.

‡Schoenherr, K. E. 1932 *Trans. Soc. Nav. Arch. Mar. Engrs*, **40**, 279.

‡Schultz-Grunow, F. 1940 Translation *Nat. Adv. Comm. Aero., Wash., Tech. Note*, no. 986.

*Shen, S. F. 1951 *Nat. Adv. Comm. Aero., Wash., Tech. Note*, no. 2543.

Slack, E. G. 1952 *Nat. Adv. Comm. Aero., Wash., Tech. Note*, no. 2686.

‡Smith, D. W. & Walker, J. H. 1958 *Nat. Adv. Comm. Aero., Wash., Tech. Note*, no. 423.

*Smith, F. & Harrop, R. 1946 *Roy. Aircraft Estmt, Tech. Note*, Aero. 1759.

*†Sommer, S. C. & Short, B. J. 1955 *Nat. Adv. Comm. Aero., Wash., Tech. Note*, no. 3391.

Spalding, D. B. 1962*a* *Int. J. Heat Mass Transfer*, 5, 1133.

Spalding, D. B. 1962*b* *Northern Research and Engineering Corporation, Camb., Mass. Rep.* no. 1058-1.

*Spence, D. A. 1959 *Roy. Aircraft Estmt, Rep.* Aero. 2631.

†Spivak, H. M. 1950 *Aero. Phys. Lab., Nor. Am. Aviation, Inc., Rep.* no. CM-615, CAL-1052.

Stalder, J. R., Rubesin, M. W. & Tendeland, T. 1950 *Nat. Adv. Comm. Aero., Wash., Tech. Note*, no. 2077.

*Tucker, M. 1951 *Nat. Adv. Comm. Aero., Wash., Tech. Note*, no. 2337.

*van Driest, E. R. 1951 *J. Aero. Sci.* 18, 145.
*van Driest, E. R. 1955 *50 Years of Boundary Layer Theory* (Ed. H. Görtler and W. Tollmien), p. 257. Braunschweig: F. Vieweg u. Sohn.
*von Kármán, Th. 1935 *Proc. 5th Volta Congress, Rome*, p. 255.
‡Wieghart, K. 1944 Translation *Nat. Adv. Comm. Aero., Wash., Tech. Mem.*, no. 1314 (1951).
*†Wilson, R. E. 1950 *J. Aero. Sci.* 17, 585.
*†Winkler, E. M. 1961 *J. Appl. Mech., Trans A.S.M.E.* 28, Ser. E, 323.
*Young, C. B. M. & Janssen, E. 1952 *J. Aero. Sci.* 19, 229.

Appendix

Summary of the methods of evaluating R_δ integral, approximations A and B, appearing in tables 1–4

Approximate analytical (*A*)

Taking equation (3) of § 2.2, for example, we have

$$R_\delta = \frac{\mu_S K u_G^{+2}}{\mu_G E}\int_0^1 \phi^3 z(1-z)\exp\left\{Ku_G^+\int_0^z \phi\,dz\right\}dz. \tag{3}$$

As the magnitude of the integrand is small at small z,

$$\int_0^z \phi\,dz$$

is replaced by Nz, where

$$N = \frac{1}{0{\cdot}9}\int_0^{0{\cdot}9}\phi\,dz;$$

the equation (3) now becomes

$$R_\delta = \frac{\mu_S K u_G^{+2}}{\mu_G E}\int_0^1 \phi^3 z(1-z)\exp\left(KNu_G^+ z\right)dz. \tag{A 1}$$

On integrating equation (A 1) by parts twice, there is obtained

$$\begin{aligned} R_\delta &= \frac{\mu_S u_G^+}{\mu_G EN}\left[\phi^3 z(1-z)\exp\left(KNu_G^+ z\right)\right. \\ &\qquad \left. -\int_0^1 [\phi^3(1-2z)+z(1-z)\,(d\phi^3/dz)]\exp\left(KNu_G^+ z\right)dz\right]_0^1 \\ &= \frac{\mu_S}{\mu_G KN^2 E}\left[\phi^3\exp\left(KNu_G^+ z\right)\right]_0^1 + \text{smaller terms} \\ &\approx \frac{\mu_S \phi_G^3}{\mu_G KEN^2}\exp\left(KNu_G^+ z\right). \end{aligned} \tag{A 2}$$

Hence

$$R_\delta = \frac{\mu_S \phi_G^3}{\mu_G N^2 KE}\exp\left\{KN\left(\frac{2T_G}{c_f T_S}\right)^{\frac{1}{2}}\right\}. \tag{A 3}$$

Approximate analytical (*B*)

Taking equation (3) of § 2.2, for example, we have

$$R_\delta = \frac{\mu_S K u_G^{+2}}{\mu_G E}\int_0^1 \phi^3 z(1-z)\exp\left\{Ku_G^+\int_0^z \phi\,dz\right\}dz. \tag{3}$$

Equation (3) is re-written as

$$R_\delta = \frac{\mu_S K u_G^{+2}}{\mu_G E} \exp\left(K u_G^+ \int_0^1 \phi\, dz\right) \int_0^1 \phi^3 z(1-z) \exp\left(K u_G^+ \int_1^z \phi\, dz\right) dz. \quad \text{(B 1)}$$

Replace $$\exp\left(K u_G^+ \int_1^z \phi\, dz\right) \text{ by } z^n,$$

where n is so chosen that the gradient is the same, then, on differentiation, we have $K u_G^+ \phi = n$. Now equation (B 1) can be re-written as

$$\begin{aligned} R_\delta &\approx \frac{\mu_S K u_G^{+2}}{\mu_G E} \exp\left(K u_G^+ \int_0^1 \phi\, dz\right) \int_0^1 \phi^3 z(1-z) z^n\, dz \\ &\approx \frac{\mu_S \phi_G^3 K u_G^{+2}}{\mu_G E} \exp\left(K u_G^+ \int_0^1 \phi\, dz\right) \int_0^1 (z^{n+1} - z^{n+2})\, dz \\ &= \frac{\mu_S \phi_G^3 K u_G^+ \exp\left(K u_G^+ \int_0^1 \phi\, dz\right)}{\mu_G [E(K\phi_G u_G^+ + 2)(K\phi u_G^+ + 3)]}. \end{aligned} \quad \text{(B 2)}$$

As $K u_G^+ \phi \gg 3$ in general, equation (B 2) can be approximately written as

$$R_\delta = \frac{\mu_S \phi_G}{\mu_G K E} \exp\left(K u_G^+ \int_0^1 \phi\, dz\right). \quad \text{(B 3)}$$

Hence

$$R_\delta = \frac{\mu_S \phi_G}{\mu_G K E} \exp\left\{K \left(\int_0^1 \phi\, dz\right) \left(\frac{2T_G}{c_f T_S}\right)^{\frac{1}{2}}\right\}. \quad \text{(B 4)}$$

Jim a. Penland

The origin and some of the consequences of aerodynamic heating are discussed, with emphasis on calculation of the rate of transfer of heat from the air into the surface of a high-speed vehicle and on boundary-layer control by surface cooling.

The Problem of Aerodynamic Heating

E. R. van Driest*
North American Aviation, Inc.

Symbols

Variables and Parameters

- x, y = geometrical coordinates parallel and normal to a body surface with origin at leading edge or stagnation point
- u = velocity in x-direction
- c_f = local skin-friction coefficient
- C_f = mean skin-friction coefficient
- h = heat-transfer coefficient, $q_w/(T_r - T_w)$
- ρ = fluid density
- μ = coefficient of fluid viscosity
- k = coefficient of thermal conductivity, height of wire trip
- c_p = specific heat at constant pressure
- γ = ratio of specific heats at constant pressure and constant volume
- T = absolute temperature
- q_w = heat transfer at the wall
- M = Mach Number
- r = recovery factor
- s = Reynolds analogy factor
- $c_{H\delta}$ = Stanton Number, $h/\rho_\delta u_\delta c_p$
- $c_{H\infty}$ = Stanton Number, $h/\rho_\infty u_\infty c_p$
- $Re_{x\delta}$ = Reynolds Number, $\rho_\delta u_\delta x/\mu_\delta$
- $Re_{D\infty}$ = Reynolds Number, $\rho_\infty u_\infty D/\mu_\infty$
- Pr = Prandtl Number, $c_p\mu/k$
- l = mixing length
- n = power in viscosity-temperature power law
- β = constant in $u_\delta = \beta x$
- D = diameter
- ϵ = height of roughness
- δ = thickness of boundary layer
- δ_k^* = displacement thickness of boundary layer at position of wire trip
- u' = root-mean-square of turbulence fluctuations
- $Re_{\delta T}$ = transition Reynolds Number, $\rho_\delta u_\delta x_T/\mu_\delta$
- Re_{δ_0} = transition Reynolds Number on a smooth body

Subscripts

- δ = condition at outer edge of boundary layer
- w = condition at wall
- ∞ = conditions in undisturbed flow
- r = recovery
- T = transition
- 0 = condition for smooth body or in tunnel supply chamber
- $*$ = ratio to free-stream conditions
- ins = insulated plate

Presented at the Aerodynamic Heating: Aerodynamic Aspects Session, National Summer Meeting, IAS, Los Angeles, June 18-21, 1956.

* Chief Scientist, Missile Development Division.

Introduction

Aerodynamic heating is the heating of an object as a result of the flow of air at high speed about that object. Friction between the fluid filaments while they stream along the body and compression at and near the stagnation regions of forward surfaces convert the kinetic energy of motion into heat within a thin layer of air which blankets the body. Such a region is shown in Fig. 1. The temperature of this layer increases with the square of the speed so that, already at a Mach Number of 3, the boundary-layer temperature attains a value of about 600°F. Since this temperature is concentrated in the air at the surface of the aircraft, heat will flow readily from the boundary layer to the aircraft, the ease with which it flows increasing also with speed. Because of the increase of heat transfer with speed, it appears that a "thermal barrier" exists much as it appeared in the past that a "sonic barrier" existed. However, like the sonic (drag) barrier, which was eventually hurdled by informed design practices, it is believed that the thermal barrier can also be overcome by realistic and proper engineering design. The problems differ somewhat in that the drag barrier existed over a narrow band of Mach Number, whereas the thermal barrier does not occur over a limited range of Mach Number but rather tends to increase in severity as Mach Number is increased. In attempting to solve the thermal problem, the first question that arises is: What is the rate at which heat enters the surface of a high-speed vehicle? Subsequent questions are: Where does the heat go? What happens when the heat gets there? How can the designer live with it?

The first question, which must be answered by the aerothermodynamicist, will be generally dealt with in this paper. The subsequent questions must be engaged by a host of engineers from the structures man through the detail designer.

Status of Calculation Procedure for Aerodynamic Heating

The rate of heat transfer from a hot boundary layer to a cooler wall follows the modified Newtonian law

$$q_w = h(T_r - T_w) \qquad (1)$$

where T_r is the recovery boundary-layer temperature, T_w the wall temperature, and h the heat-transfer coefficient. The boundary-layer temperature T_r is usually written in terms of a recovery factor r defined by

$$T_r = T_\delta\{1 + r\cdot[(\gamma - 1)/2]M_\delta^2\} \qquad (2)$$

where T_δ and M_δ are the local stream temperature and Mach Number, respectively, at the outer edge of the boundary layer, and γ the ratio of the specific heat at constant pressure c_p to the specific heat at constant volume c_v. Furthermore, the heat-transfer coefficient h can be expressed in dimensionless form by

$$c_{H\delta} = h/\rho_\delta u_\delta c_p \qquad (3)$$

which is called the Stanton Number. The Stanton Number is proportional to the local skin-friction coefficient $c_{f\delta}$ in a modified Reynolds analogy form

$$c_{H\delta} = (1/s)\cdot(c_{f_\delta}/2) \qquad (4)$$

In Eq. (3), the symbols ρ_δ and u_δ are the density and velocity, respectively, just outside the boundary layer, and, in Eq. (4), the term s is called the Reynolds analogy factor. Eq. (1) may now be written as

$$q_w = c_{H\delta}\rho_\delta u_\delta c_p\left[T_\delta\left(1 + r\cdot\frac{\gamma - 1}{2}M_\delta^2\right) - T_w\right] \qquad (5)$$

Thus, according to Eq. (5), it is necessary to know the Stanton Number $c_{H\delta}$ and the recovery factor r in order to compute the rate of heat transfer. Now r will vary from about 0.85 for laminar flow to about 0.88 for turbulent flow, so that the exact value will not make or break a design. The coefficient $c_{H\delta}$, on the other hand, varies considerably from laminar to turbulent flow and furthermore, for turbulent flow, is a strong function of Mach Number. Also, the point of transition from laminar to turbulent flow is not yet predictable. Therefore, so long as $c_{H\delta}$ is indefinite, it appears that the state of the art of heat-transfer calculation is rather shaky. Nevertheless, with certain assumptions, calculations can be made. Calculation of heat transfer with laminar flow is felt to be quite reliable, since the fundamental equations are amenable to mathematical solution. Calculation of heat transfer involving entirely turbulent flow is less reliable, because the physical

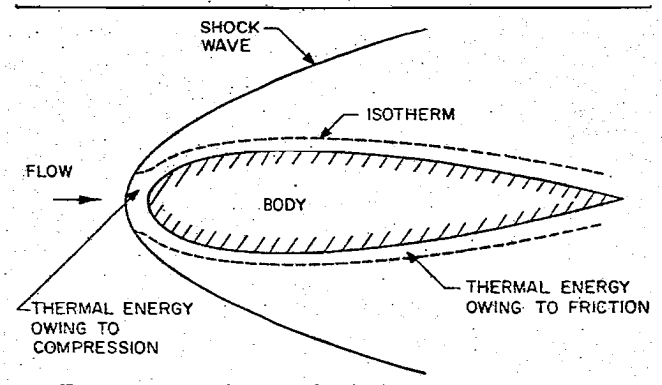

FIG. 1. Hot region covering body at supersonic speed.

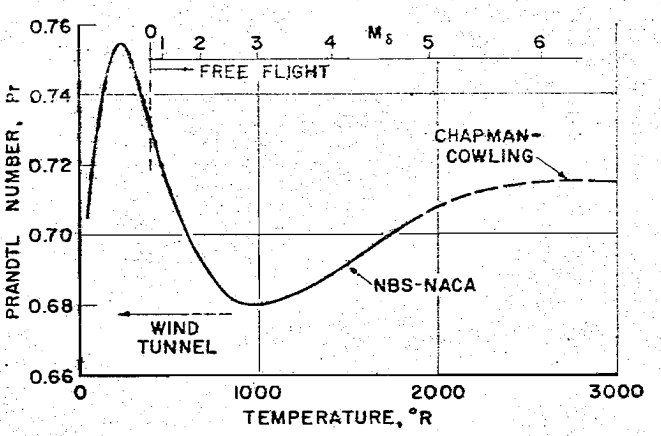

FIG. 2. Prandtl Number of dry air.

phenomenon is not well understood. Least reliable of all is the calculation of heat transfer in the transition range, since little is known about the location of the transition point. The state of knowledge in each of the above areas will now be discussed.

FLAT PLATES

Although pressure and temperature gradients along the surface of a body affect heat transfer appreciably, the primary constant-free-stream-velocity boundary layer with constant wall temperature will be discussed first. Later the heat transfer to blunt bodies will be described.

The heat-transfer coefficient depends also upon whether the boundary layer is laminar, turbulent, or transitional. Since laminar-flow heating rates are significantly lower than turbulent rates, it is important to study the laminar results, owing to the possibility of maintaining laminar flow by suitable control.

Laminar Flow

As mentioned above, the two necessary items to be known for heat-transfer calculation are the recovery factor and the Stanton Number.

Recovery Factor—In order to compute the recovery factor, it is necessary to solve the momentum and energy equations for the boundary layer simultaneously. This has been done carefully for completely variable properties, such as density, viscosity, Prandtl Number, and specific heat.[1] Since the Prandtl Number $(c_p\mu/k)$ is the most important parameter influencing the recovery factor and since it varies strongly with temperature, it is indicated in Fig. 2 (cf. reference 1). Fig. 3 shows the theoretical results for recovery factor for a plate in free flight at zero angle of attack with $T_\delta = 400°R$. In the Figure the Prandtl Number $Pr_\delta = (c_p\mu/k)_\delta$, where k is the coefficient of thermal conductivity. Subscript *ins* denotes insulated-plate condition. It is first noted from the Figure that the recovery factor is not constant but rather a function of both Mach Number and heat transfer. This variation is due largely, although not entirely, to Prandtl Number variation within the boundary layer. Second, it is seen that the numerical spread of r is only from about 0.82 to about 0.85. And

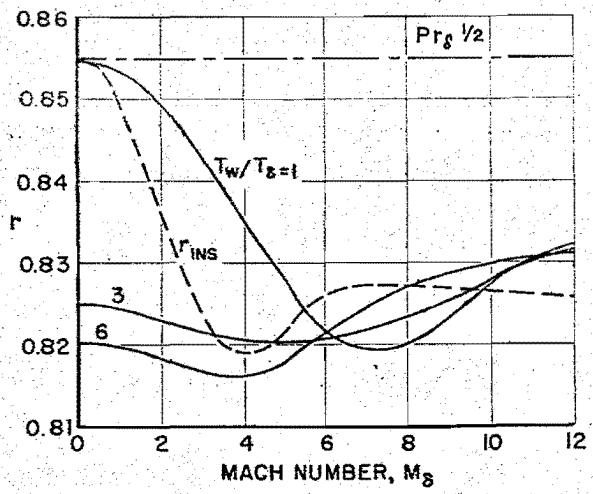

FIG. 3. Recovery factor for a laminar boundary layer on a flat plate in free flight.

third, one notes that the quantity of $Pr_\delta^{1/2}$ represents that range within engineering accuracy and can be used for most engineering calculations. It is interesting to note that $Pr_\delta^{1/2}$ is very closely equal to r only at $M_\delta = 0$ and $T_w/T_\delta = 1$.

When experimental work is conducted in a wind tunnel, the free-stream condition becomes cold, unless the air is heated. At any rate, during such experimentation, one is usually operating at the lower temperature end of the scale for the various property variations. For a wind tunnel with various degrees of heating, the exact recovery-factor calculations are plotted in Fig. 4, a numerical value of 0.85 again roughly representing the results. These calculations have been substantiated by experimental measurements at the Naval Ordnance Laboratory[2] and the Massachusetts Institute of Technology,[3] as shown in Fig. 5. Apparently the recovery factor for laminar flow is well accounted for.

Stanton Number—As with the recovery factor, the Stanton Number can be computed exactly for laminar flow, including variable properties. The results for flat plates in free flight and in heated wind tunnels are given in Figs. 6 and 7, respectively. The curves of Fig. 7 represent only the insulated plate case. Comparison of the figures for the insulated plate case show that the effect of Mach Number is much smaller in the wind tunnel that in free flight, certainly at the lower tunnel supply temperatures. Thus, at supply temperatures around 100°F., one could hardly expect to see any effect of Mach Number on wind-tunnel heat-transfer data. This conclusion, as well as fair substantiation of the theory, is indicated in Fig. 8 in which are plotted NOL heat-transfer data[2] corresponding to some of the recovery-factor data in Fig. 5.

As far as laminar flow is concerned, it appears that, for moderate supersonic speeds, the theory can be depended upon to yield accurate heat-transfer coefficients, in spite of the scatter of experimental data owing to the difficulty of measuring the generally low laminar-flow heat-transfer rates on flat plates. This conclusion follows because the analysis is exact and the fluid properties are well known at moderate temperatures.

Application to Cones—The above results for flat plates can be applied to cones in axial flow by merely multiplying the flat-plate heat-transfer coefficient at the same local Mach Number, local Reynolds Number, and wall-to-local-free-stream temperature ratio by $\sqrt{3}$.

Turbulent Flow

Until the day comes when the boundary layer can be controlled and held laminar, it will be necessary to live with a certain amount of turbulent flow. Indeed, for insurance, the designer should assume fully turbulent flow. The bitter consequences of such an assumption will be seen later in Fig. 22 where it is seen that, for a Reynolds Number of 10^7 and moderate supersonic Mach Numbers, the turbulent heat-transfer coefficient is about 10 times the laminar value.

Recovery Factor—With turbulent flow, the energy equation (in terms of mean quantities) can still be integrated, and a general expression for recovery factor in terms of shear stress (to be obtained from the momentum equation) derived.[1, 4] However, with turbulent flow, the momentum equation cannot be integrated for lack of complete knowledge of the turbulent mechanism, and therefore simplifying assumptions concerning shear and velocity distribution must be made. Assuming a linear shear distribution with distance from the wall and dividing the viscous subregion into the laminar and transitional layers as von Kármán had done,[5] one arrives at the following formula for recovery factor:[1, 4]

$$r = Pr_T\left[1 + \frac{2}{K}\sqrt{\frac{c_f}{2}}(1 - Pr_T)\left[\frac{\pi^2}{6} + \frac{3}{2}(1 - Pr_T)\right] + 25 \cdot \frac{c_f}{2}\left\{\left(\frac{Pr_L}{Pr_T} - 1\right) + 2\ln\left[1 + \frac{5}{6}\left(\frac{Pr_L}{Pr_T} - 1\right)\right] + \ln 6 \cdot \ln\left[1 + \frac{7}{8}\left(\frac{Pr_L}{Pr_T} - 1\right)\right] - \ln 6 \cdot \ln\left[1 + \frac{1}{4}\left(\frac{Pr_L}{Pr_T} - 1\right)\right]\right\}\right] \quad (6)$$

for $0.7 \leqq Pr_T \leqq 1$. In this expression, Pr_L and Pr_T represent the laminar and turbulent Prandtl Numbers, respectively, and K is the mixing length proportionality

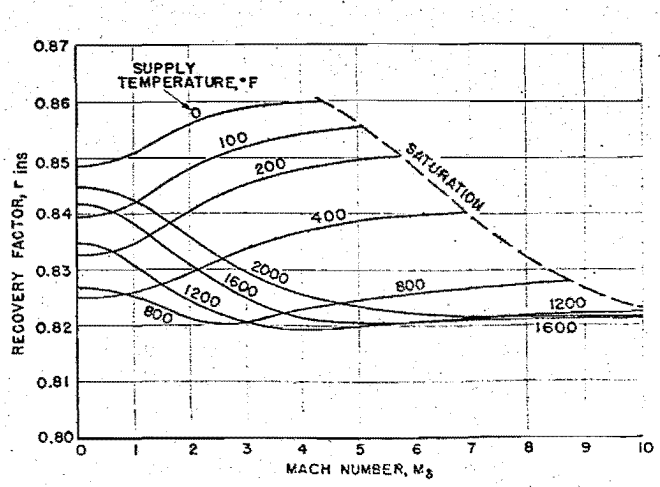

FIG. 4. Recovery factor for a laminar boundary layer on an insulated flat plate in a wind tunnel for air.

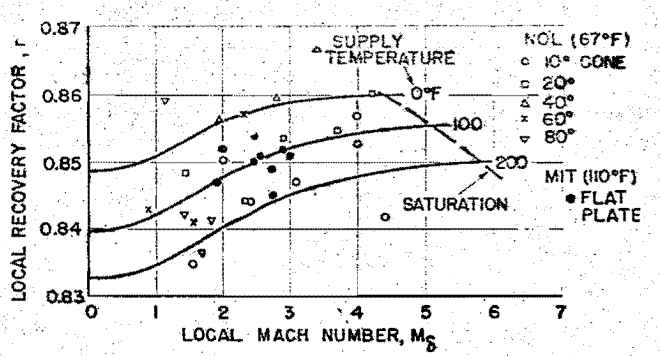

FIG. 5. Comparison of theory and experiment on recovery factor for laminar boundary layers on flat plates and cones in a wind tunnel.

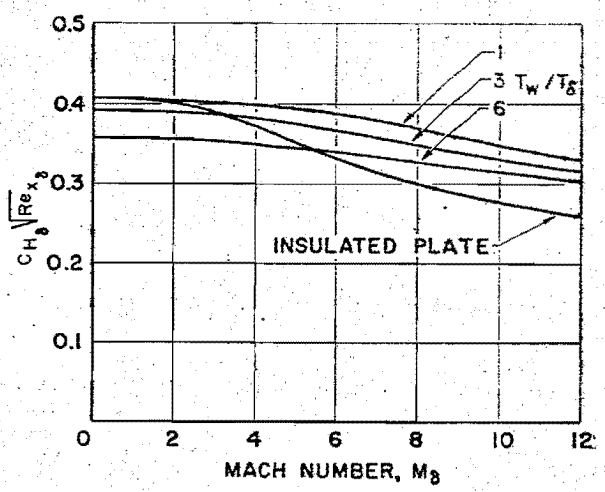

FIG. 6. Local heat-transfer coefficient for a laminar boundary layer on a flat plate in free flight.

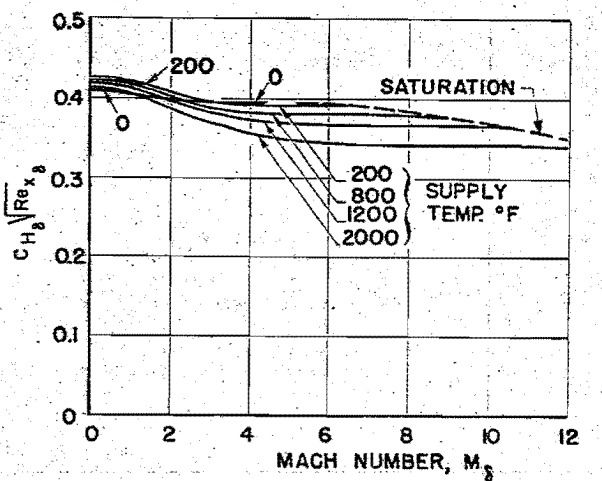

FIG. 7. Local heat-transfer coefficients for a laminar boundary layer on an insulated flat plate in a wind tunnel.

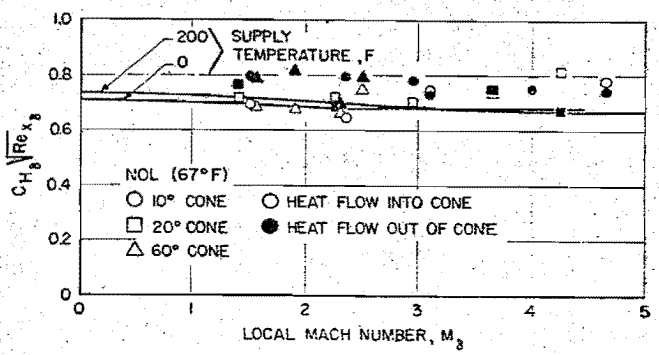

FIG. 8. Comparison of theory and experiment on local heat-transfer coefficient for laminar boundary layers on cones in a wind tunnel.

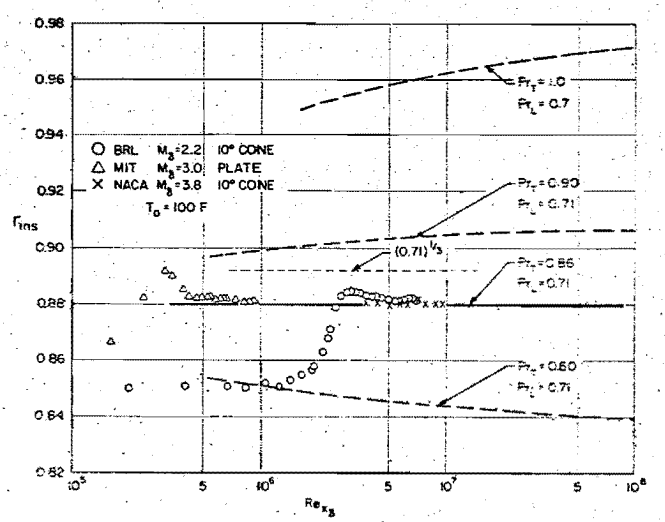

FIG. 9. Recovery factor for a turbulent boundary on a flat plate as a function of Reynolds Number for air ($M_\delta = 0$).

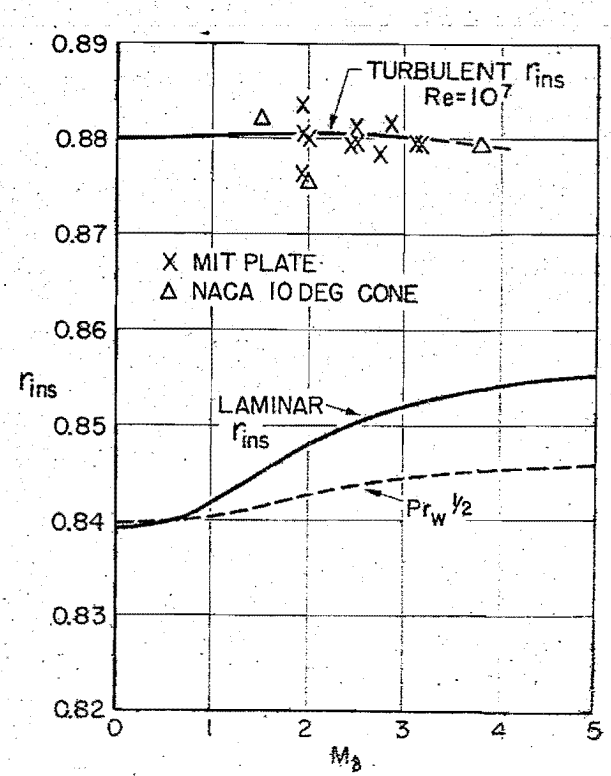

FIG. 10. Recovery factor for a turbulent boundary layer on a flat plate in air in a wind tunnel.

factor usually taken at 0.4. Although the expression was derived for incompressible flow, it can yield approximate trends for compressible flow. With laminar flow, the recovery factor was independent of Reynolds Number. When the recovery factor as well as the turbulent Prandtl Number are assumed independent of Reynolds Number in turbulent flow, it will be uniquely necessary that $r = 0.88$ and $Pr_T = 0.86$. Hence, out of these assumptions comes also a numerical value for the turbulent Prandtl Number.

Fig. 9 shows Eq. (6) for various values of Pr_T, but with $Pr_L = 0.71$. Also plotted in Fig. 9 are some experimental data from the Ballistics Research Laboratory,[6] M.I.T.,[3] and NACA.[7] The independence of the recovery-factor data with Reynolds Number appears to be a good assumption, and the data fall close to the theoretical value of $r = 0.88$ corresponding to $Pr_T = 0.86$. It is seen that Squire's $Pr_L^{1/3} = (0.71)^{1/3} = 0.892$ is a good approximation to Eq. (6) for $Pr_T = 0.86$.

Eq. (6) for recovery factor can be extended to compressible flow, approximately, when wall conditions are introduced in the friction coefficient. Thus the factor

$$\left(1 + r \cdot \frac{\gamma - 1}{2} M_\delta^2\right)$$

should be multiplied into c_f wherever c_f appears in Eq. (6), and then the compressible flow values of c_f are used (see Fig. 13). It will then be found that the recovery factor is essentially independent

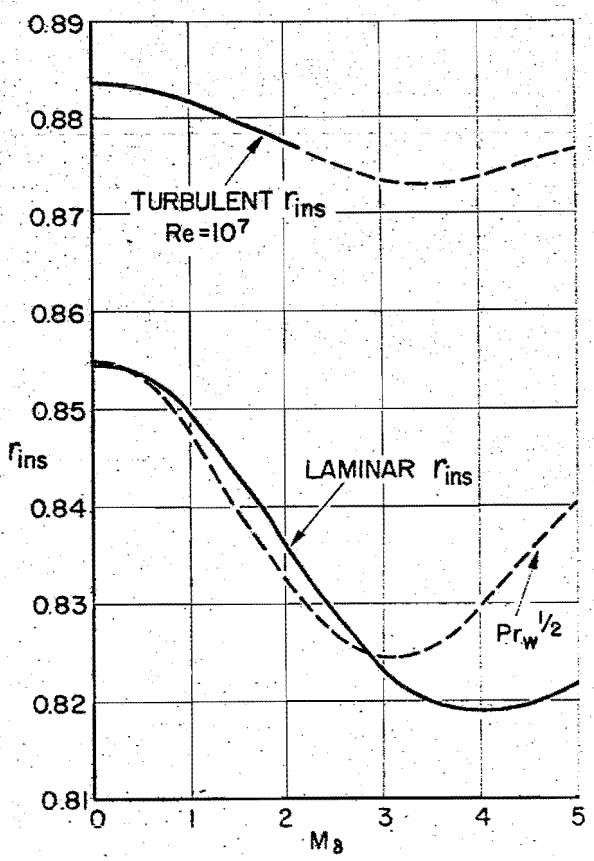

FIG. 11. Recovery factor for a turbulent boundary layer on a flat plate in free flight in air.

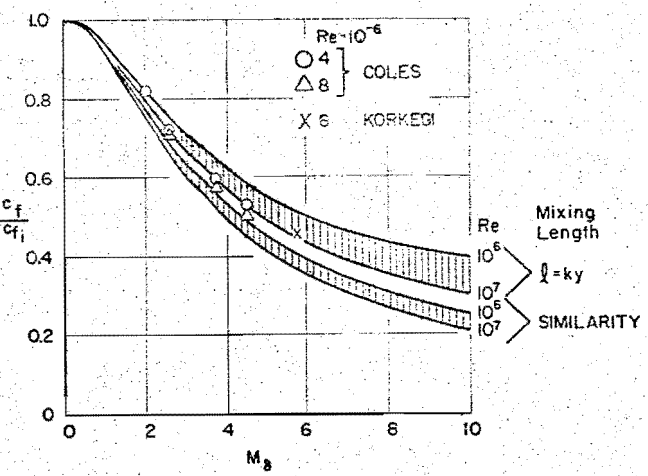

FIG. 12. Comparison of theory and experiment on local skin-friction coefficient for turbulent boundary layers on insulated flat plates.

of Mach Number at least for moderate supersonic speeds, therefore justifying the use of the data in Fig. 9 when the theory was plotted for $M_\delta = 0$. This independence is indicated in Fig. 10 where Eq. (6) (with $Pr_T = 0.86$) is plotted vs. Mach Number for a flat plate in a wind tunnel at a Reynolds Number of 10^7. Fig. 11 shows the variation of recovery factor for a flat plate in free flight in the atmosphere. The stronger variation with Mach Number is due essentially to the stronger variation in laminar Prandtl Number in free flight than in the unheated wind tunnel. The laminar-flow recovery factors are shown in Figs. 10 and 11 for comparison purposes.

In conclusion, it appears that a recovery factor of 0.90 is accurate enough for most engineering calculations assuming a turbulent boundary layer.

Stanton Number—As mentioned above, it is not possible to integrate the momentum equation for turbulent motion, and therefore other means must be utilized in order to include the role of the momentum law in the calculation of heat transfer. What is wanted from the momentum equation is the momentum defect, or, rather, the friction coefficient, for use in Eq. (4). Also, as seen from Eq. (4), it is necessary to compute the Reynolds analogy factor s, which, like the recovery factor, will depend upon the friction.

(*a*) *Friction coefficient:* A semianalytical method of obtaining the local friction coefficient for high-speed turbulent flow is through an extension of von Kármán's mixing-length incompressible-flow theory to take into account density and viscosity variation with temperature. The result is[1, 4]

$$\frac{0.242}{c_{f_\delta}^{1/2}\left(\frac{\gamma - 1}{2} M_\delta^2\right)^{1/2}} (\sin^{-1}\alpha + \sin^{-1}\beta) = 0.41 + \log_{10}(Re_{x_\delta} \cdot c_{f_\delta}) - f(n)\log_{10}(T_w/T_\delta) \quad (7)$$

where

$$\alpha = (2A^2 - B)/(B^2 + 4A^2)^{1/2}$$
$$\beta = B/(B^2 + 4A^2)^{1/2}$$

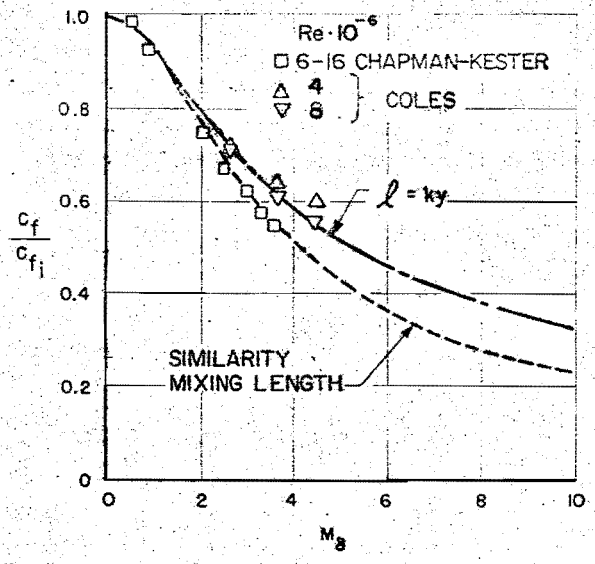

FIG. 13. Effect of Mach Number on mean skin-friction coefficient for insulated surfaces in wind tunnels at Reynolds Numbers of approximately 10^7.

$$A^2 = \left(\frac{\gamma - 1}{2} M_\delta^2\right) \Big/ (T_w/T_\delta)$$

$$B = \left[\left(1 + \frac{\gamma - 1}{2} M_\delta^2\right) \Big/ (T_w/T_\delta)\right] - 1$$

and in which $f(n)$ is a function of the exponent n in the power viscosity law $\mu = \text{const.} \cdot T^n$. It will be found that $f(n)$ depends upon the law assumed for mixing length l. Thus, when the Prandtl mixing length $l = Ky$ is assumed, where y is the distance from the wall normal to the flow, then $f(n) = (1/2) + n$; and when the von Kármán mixing length $l = K(du/dy)/(d^2u/dy^2)$ is assumed, then $f(n) = n$.

There seems to be no really valid theoretical reason for favoring either assumption for mixing length. For $T_w/T_\delta = 1$, both assumptions lead to the same result. However, for $T_w/T_\delta \neq 1$, the above difference in $f(n)$ appears. Therefore, it seems that the choice of mixing-length law must be left to experiment.

Fig. 12 shows a plot of the theory for local skin friction on an insulated plate using the two choices of mixing-length law. The ordinate is the ratio of compressible to incompressible friction. Also plotted are floating-element data of Coles[8] and Korkegi.[9] The data seem to fall between the two mixing-length choices. (Of course, it must be considered that probably too much is being expected of the mixing-length theory itself.)

Another test of the theory can be made using average skin-friction data. The equation for the average friction coefficient defined by

$$C_{f_\delta} = \frac{1}{x} \int_0^x c_{f_\delta}\, dx$$

is

$$\frac{0.242}{C_{f_\delta}^{1/2} \left(\frac{\gamma - 1}{2} \cdot M_\delta^2\right)^{1/2}} (\sin^{-1} \alpha + \sin^{-1} \beta) =$$

$$\log_{10}(Re_{x_\delta} \cdot C_{f_\delta}) - f(n) \log_{10}(T_w/T_\delta) \quad (8)$$

For insulated plates, the ratio of compressible to incompressible average friction is shown in Fig. 13. The directly measured mean data of Chapman and Kester[10] and the integrated local data of Coles[8] are also plotted in the Figure. It appears that these sets of data are not sufficiently consistent to allow a decision on the mixing-length law if the mixing-length theory is to be adhered to. More experiments are required, particularly at hypersonic Mach Numbers where the effects are greatest.

A further check on the theory can be obtained from free-flight data. Under transient conditions of free flight, the wall-to-free-stream temperature ratio T_w/T_δ is close to unity, whereupon the last term in Eq. (8) and the effect of $f(n)$ disappears. For $T_w/T_\delta = 1$, the effect of $f(n)$ would also disappear from Eq. (7). In Fig. 14 is plotted the mean-friction theory of Eq. (8), assuming the similarity law for mixing length—i.e., $f(n) = n$, where n is taken as 0.76. Also plotted in the Figure are free-flight total-friction-drag data of Sommer and Short.[11] The theory and data appear to agree well for $T_w/T_\delta = 1$.

(*b*) *Reynolds analogy factor:* Fundamentally, the key to the rate of heat transfer within a substance is in the availability of energy to be transported and in the ability of the substance to transport that energy. This is expressed by the Prandtl Number, which is a dimensionless grouping of the specific heat thermal conductivity, and by viscosity—i.e., $Pr = c_p\mu/k$. Thus the Prandtl Number should strongly influence the convective heat-transfer processes. Indeed, the Prandtl Number is embodied mainly in the Reynolds analogy factor s of Eq. (4), with the Prandtl Number having a small effect in turn upon the friction coefficient c_f.

As with the recovery factor, integration of the energy equation also yields a general expression for the Reynolds analogy factor.[1, 4] And then, again, when a linear shear distribution with distance from the wall is assumed and the boundary layer is divided into a laminar sublayer, a transitional layer, and a wholly

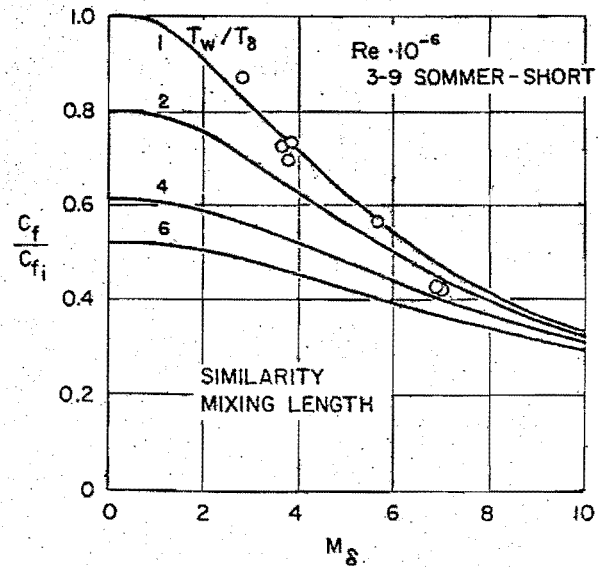

FIG. 14. Effect of heat transfer and Mach Number on mean skin friction coefficient for a body in free flight in a wind tunnel at Reynolds Numbers of approximately 10^7.

turbulent layer, one arrives at the formula[1, 4]

$$s = Pr_T\left[1 + 5\sqrt{\frac{c_f}{2}}\left\{\frac{1}{5K}(1 - Pr_T) \times \left[\frac{\pi^2}{6} + \frac{3}{2}(1 - Pr_T)\right] + \left(\frac{Pr_L}{Pr_T} - 1\right) + \ln\left[1 + \frac{5}{6}\left(\frac{Pr_L}{Pr_T} - 1\right)\right]\right\}\right] \quad (9)$$

for $0.7 \leqq Pr_T \leqq 1$. This formula reduces to the von Kármán formula[5] when it is assumed that $Pr_T = 1$. Also for $Pr_L = Pr_T = 1$, then $s = 1$, which gives the well-known Reynolds analogy formula—viz., $c_H = c_f/2$.

Eq. (9) is presented as the solid line in Fig. 15, upon substitution of the turbulent Prandtl Number 0.86 [determined from Eq. (6)] and a typical laminar Prandtl Number 0.71. Also shown in the Figure are the formulation[5] of von Kármán ($Pr_T = 1$) and the estimate of Colburn ($s = Pr_L^{2/3}$). Thus, it is seen numerically (for the particular example chosen where $Pr_L = 0.71$) that, while Colburn's estimate is a good approximation to Eq. (9) with $Pr_T = 0.86$, von Kármán's formulation yields a result significantly higher.

The effect of compressibility on s can also be estimated in the same manner as with r. The results are plotted in Figs. 16 and 17 for a flat plate in free flight and in a wind tunnel, respectively, using the laminar Prandtl Number of Fig. 2.

The Stanton Number can now be computed using $c_{H_\delta} = (1/s)\cdot(c_{f_\delta}/2)$, where s is taken from Fig. 15, and c_{f_δ} is obtained from Eq. (7). Whence the calculated Stanton Number can be compared with heat-transfer data with an eye to determine what mixing-length law should best be used.

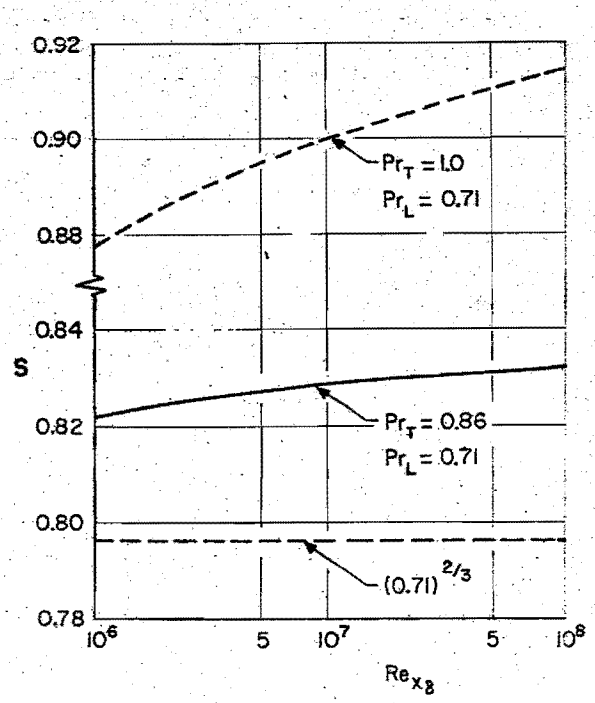

FIG. 15. Reynolds analogy factor for a turbulent boundary layer on a flat plate in air as a function of Reynolds Number ($M_\delta = 0$).

Heat-transfer data obtained at M.I.T.[12] for supersonic Mach Numbers of 2.0, 2.5, and 3.0 are plotted vs. Reynolds Number in Figs. 18, 19, and 20, respectively. Theoretical curves using $s = 0.825$ from Fig. 17 and the similarity law for mixing length [$f(n) = n$] seem to fit the data well. When these data, as well as other data, are plotted vs. Mach Number as in Fig. 21, an apparent favoring of data toward the similarity law is observable.

A discussion of heat transfer would not be complete without a comparison of the results for both laminar and turbulent flow. Fig. 22 gives the Stanton Number for an insulated flat plate in free flight. The laminar-flow curves are obtained from Fig. 6, and the turbulent-flow curves are from Eqs. (4) and (7) assuming $s = 0.825$ and $f(n) = n$. It is significant to note that the turbulent heat transfer is of the order of 10 times the laminar heat transfer.

An apparent difficulty in computing heat transfer is that the rate depends also upon the surface temperature often desired in the first place. Therefore, a tedious iteration process, discouraging to the engineer, must be resorted to. For engineering purposes, it is then convenient to have the Stanton Number as a function of Reynolds Number, Mach Number, and wall-to-free-stream temperature ratio in the form of a nomograph. This has been done in Fig. 23 using $s = 0.825$ and in Eq. (7) with $f(n) = n$. Thus, not only is the basic equation solved for a given wall temperature, but the Stanton Number can be quickly adjusted for changing conditions.

It is pointed out that the local and average values of the skin-friction coefficient are also determined in the nomograph of Fig. 23. Since these are based on the similarity law [$f(n) = n$] in Eqs. (7) and (8), the performance engineer should proceed with caution in the light of the spread of data in Fig. 13. For drag calculation, it would appear safer to use the linear mixing-length assumption.

Application to Cones—The turbulent heat transfer on a flat plate will equal that on a cone in axial flow for the same local Mach Number and wall-to-local-free-stream temperature ratio, provided the heat-transfer coefficient on the plate is computed for a Reynolds Number of one half that on the cone.

BLUNT BODIES

Laminar Flow

The above results for flat plates represented the results for a boundary layer with constant external velocity. The solution for laminar flow was found to be of the form $c_{H_\delta}\sqrt{Re_{x_\delta}} = f_1(M_\delta, T_w/T_\delta, Pr_\delta)$, whence

$$\left.\begin{aligned} q_{w_{plate}} &= c_{H_\delta}\rho_\delta u_\delta c_p(T_r - T_w) \\ &= \frac{f_1}{\sqrt{\frac{\rho_\delta u_\delta x}{\mu_\delta}}}\cdot\rho_\delta u_\delta c_p(T_r - T_w) \end{aligned}\right\} \quad (10)$$

In fact, for incompressible flow,

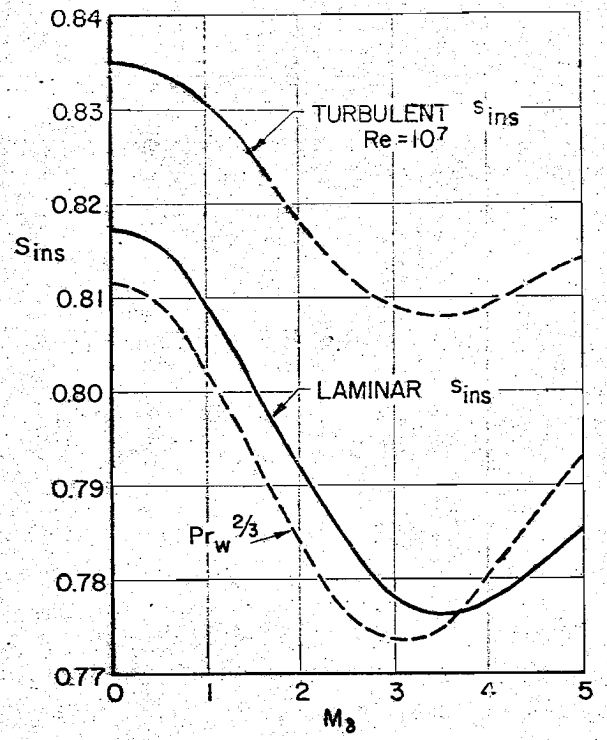

FIG. 16. Reynolds analogy factor for a turbulent boundary layer on a plate in free flight in air.

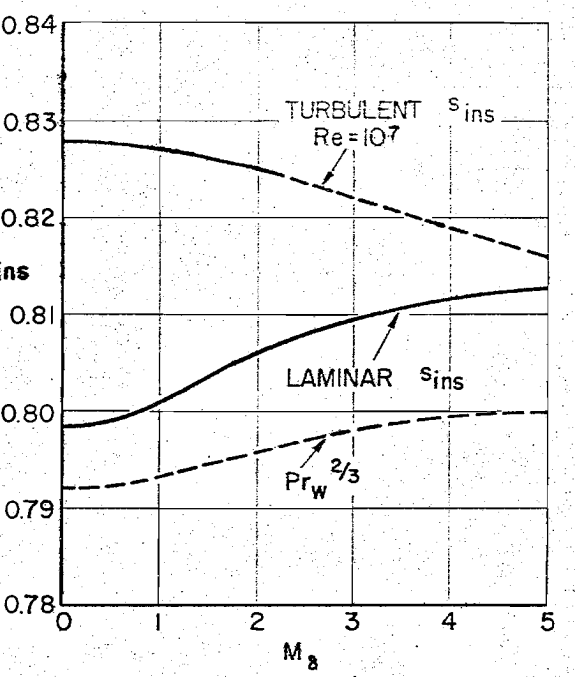

FIG. 17. Reynolds analogy factor for a turbulent boundary layer on a flat plate in air in a wind tunnel.

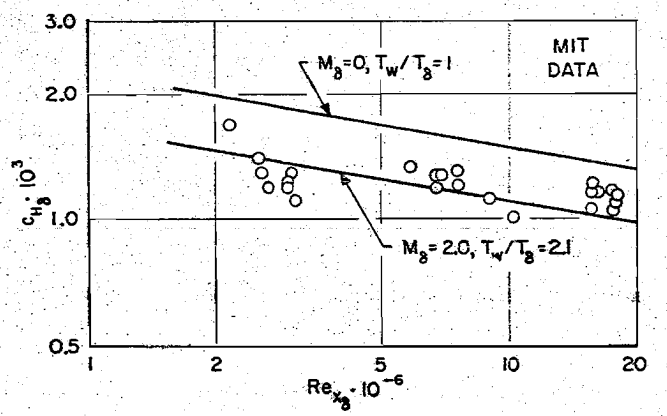

FIG. 18. Local heat-transfer coefficient for a turbulent boundary layer on a heated flat plate ($M_\delta = 2.0$ and $T_w/T_\delta = 2.1$).

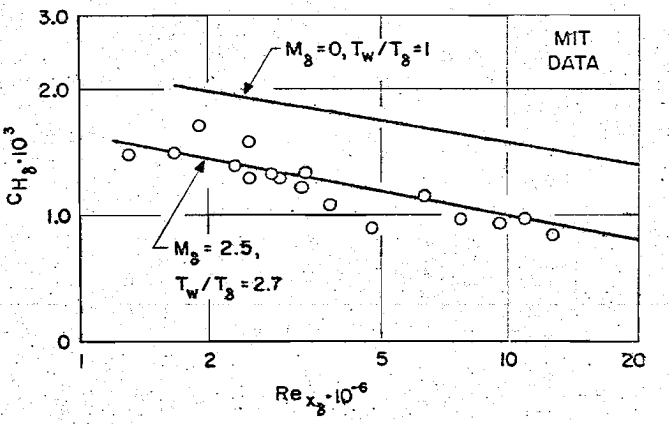

FIG. 19. Local heat-transfer coefficient for a turbulent boundary layer on a heated flat plate ($M_\delta = 2.5$ and $T_w/T_\delta = 2.7$).

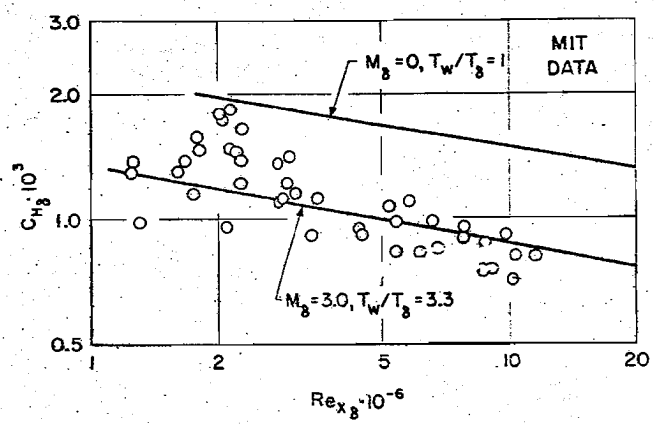

FIG. 20. Local heat-transfer coefficient for a turbulent boundary layer on a heated flat plate ($M_\delta = 3.0$ and $T_w/T_\delta = 3.3$).

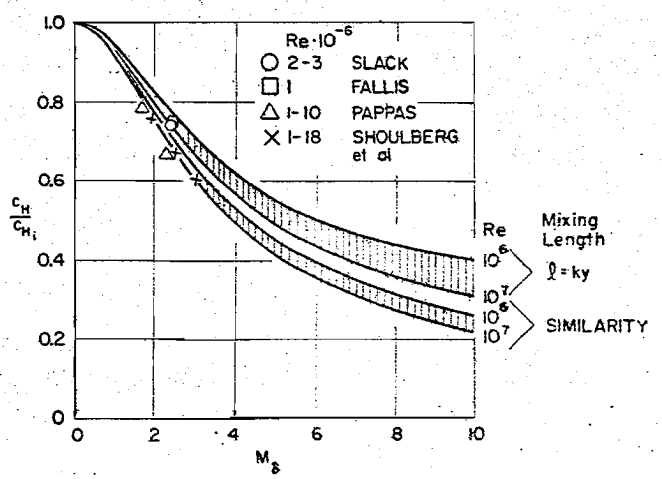

FIG. 21. Comparison of theory and experiment on local heat-transfer coefficient for turbulent boundary layers on near-insulated flat plates.

$$f_1 = c_{H_\delta}\sqrt{Re_{x_\delta}} = 0.332Pr^{-2/3} \qquad (11)$$

in which $Re_{x_\delta} = \rho_\delta u_\delta x/\mu_\delta$. It thus follows that as the leading edge of the plate is approached—i.e., $x \to 0$—the heat-transfer rate becomes exceedingly large. This is a consequence of assuming the boundary layer thin in the first place, an assumption which is not true near the leading edge. However, regardless of the accuracy of the theory, it is evident that the heat-transfer rate would be greatest at the leading edge of a plate or at the point of a cone. Now it is known that the heating rate at the stagnation point is finite. Hence, it appears proper to blunt leading edges or noses in order to relieve the heat-transfer rate at those locations.

In the stagnation regions of cylinders and spheres, the heat-transfer problem can be solved exactly for incompressible flow. However, with high-speed flow, the problem is not amenable to exact solution. Nevertheless, approximate calculations can be made when it is assumed that the flow behind the bow shock wave is incompressible.

The formula for the laminar heat-transfer rate in an incompressible stagnation region is again found to be of the form

$$q_{w_{stag}} = \frac{f_2}{\sqrt{\dfrac{\rho_\delta u_\delta x}{\mu_\delta}}} \cdot \rho_\delta u_\delta c_p(T_r - T_w) \qquad (12)$$

in which x is measured along the surface from the stagnation point, and where f_2 depends also upon the forebody shape. For cylinders,[13]

$$f_2 = c_{H_\delta}\sqrt{Re_{x_\delta}} = 0.570\,Pr^{-0.6} \qquad (13)$$

and for spheres,[14]

$$f_2 = 0.763Pr^{-0.6} \qquad (14)$$

Of course, for incompressible flow, $\rho_\delta = \rho_\infty$, $\mu_\delta = \mu_\infty$, and $T_r = T_\delta = T_\infty$. Now, unlike the flat plate where the velocity u_δ was constant along the outer edge of the boundary layer, in the stagnation region u_δ varies with x along the surface. In fact, Eq. (12) with Eqs. (13) and (14) were derived using $u_\delta = \beta x$, where β is a constant. It turns out that for incompressible flow $\beta = 4u_\infty/D$ for cylinders and $3u_\infty/D$ for spheres, where the D's are the respective diameters, and u_∞ is the velocity of the undisturbed stream.

For supersonic flow whereby a shock wave stands in front of the body and forms a region of subsonic flow around the stagnation point, it is still found,[15] from measurement of pressure and calculation of velocity, that $u_\delta = \beta x$, where β is then a function only of the undisturbed Mach Number M_∞ before the shock wave. Hence, since ρ_δ and μ_δ are relatively constant in the subsonic region behind the shock, $u_\delta = \beta x$ can be used in Eq. (12) with either Eq. (13) or (14), for both subsonic and supersonic flow. Thus

$$\left.\begin{aligned} q_{w_{stag}} &= \frac{f_2}{\sqrt{\dfrac{\rho_\delta \beta x^2}{\mu_\delta}}} \cdot \rho_\delta \cdot \beta x \cdot c_p(T_r - T_w) \\ &= f_2\sqrt{\beta \rho_\delta \mu_\delta}\, c_p(T_r - T_w) \end{aligned}\right\} \qquad (15)$$

from which it is generally concluded that in subsonic as well as in supersonic flow, the heat-transfer rate is a constant independent of x in the immediate neighborhood of the stagnation point. As stated above, for incompressible flow—i.e., $M_\infty = 0$, $\beta = 4u_\infty/D$ for the cylindrical edges of airfoils and $3u_\infty/D$ for the tangent spheres of axisymmetric noses. However, with supersonic flow, a practical solution for β can be obtained when the Newtonian flow is assumed, whence

$$\left.\begin{aligned} \beta &= \frac{u_\infty}{D}\left\{\frac{8\,[(\gamma-1)M_\infty^2 + 2]}{(\gamma+1)M_\infty^2} \cdot \right. \\ &\qquad \left. \left[1 + \frac{\gamma-1}{2}\cdot\frac{(\gamma-1)M_\infty^2 + 2}{2\gamma M_\infty^2 - (\gamma-1)}\right]^{-[1/(\gamma-1)]}\right\}^{1/2} \\ &= \frac{u_\infty}{D} f(M_\infty, \gamma) \end{aligned}\right\} \qquad (16)$$

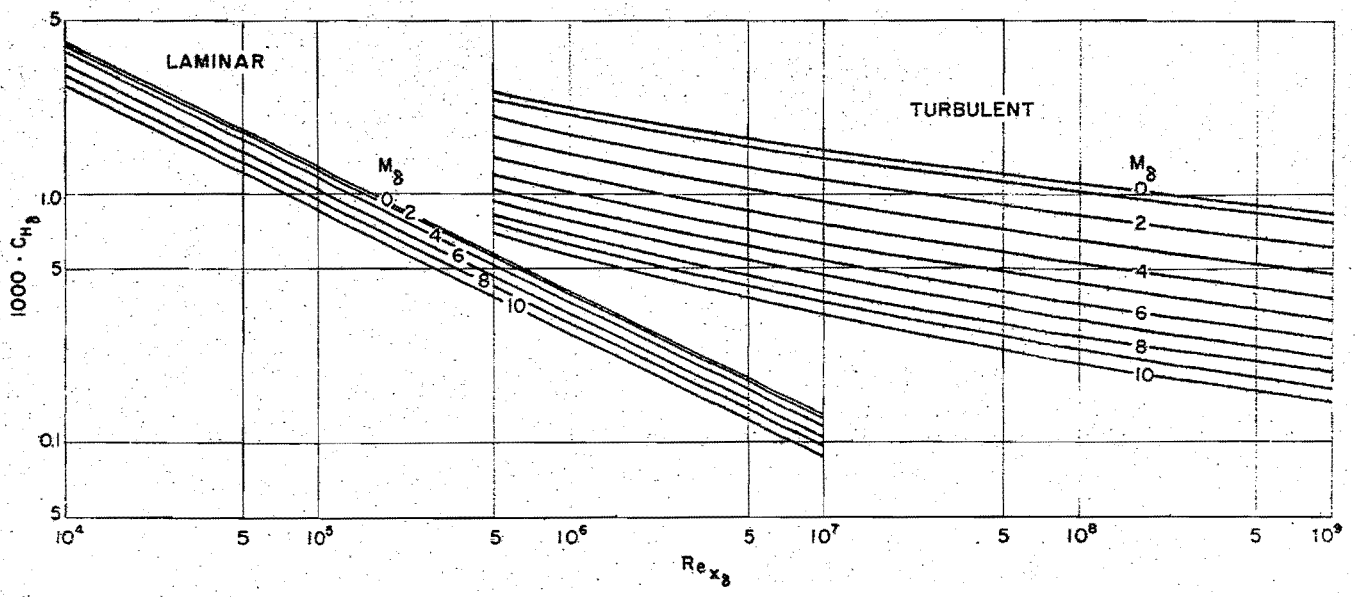

FIG. 22. Heat-transfer coefficient as a function of Reynolds Number and Mach Number for an insulated flat plate in free flight.

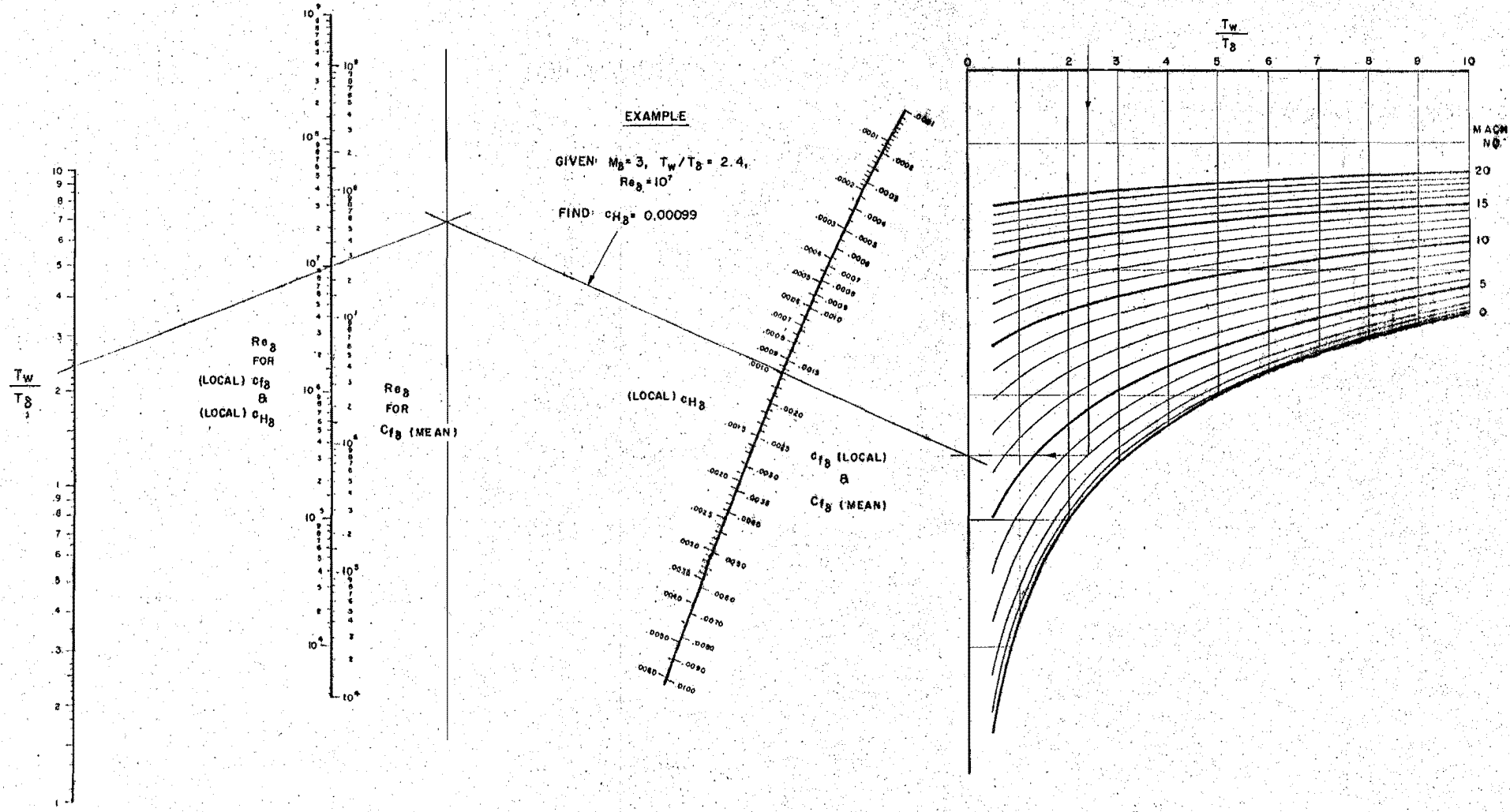

FIG. 23. Nomograph for coefficients of friction and heat transfer of a turbulent boundary layer on a flat plate for air.

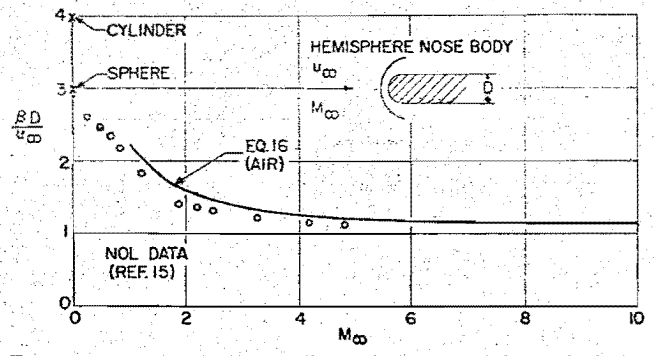

FIG. 24. Local velocity gradient at the stagnation point of a hemisphere-cylinder combination.

in which u_∞ is the velocity ahead of the shock wave.

It is seen from Eq. (15) that the calculation of the heating rate at the stagnation point depends upon the experimental verification of f_2 and β. The validity of Eq. (16) is seen in Fig. 24 where experimental values of β at the stagnation point of a hemispherical nose are plotted. A check on f_2 ($c_{H_\delta}\sqrt{Re_{x_\delta}}$) is obtained in Fig. 25 which shows experimental heat-transfer data[16] around a hemispherical nose at $M_\infty = 1.97$. In spite of the scatter of the data, it appears that Eq. (14) correlates roughly with experiment in the vicinity of the stagnation point. Also plotted in Fig. 25 is a theoretical curve showing how $c_{H_\delta}\sqrt{Re_{x_\delta}}$ decreases as x increases, according to Stine and Wanlass.

As far as aerodynamic heating is concerned, it follows from Eqs. (15) and (16) that $q_{wstag} \sim 1/D^{1/2}$. Hence, by increasing the diameter of tangent cylinder or sphere, one can decrease the heat-transfer rate at the stagnation point.

Since in supersonic flow the temperature will begin to decrease at an increasing rate away from the stagnation region, ρ_δ and μ_δ will likewise decrease, and consequently, according to Eq. (15), q_{wstag} will also begin to fall away from its constant value near the stagnation point. Consequently, the heat transfer is a maximum at the stagnation point so long as laminar flow is assumed.

Turbulent Flow

The above discussion had to do with laminar flow. Indeed, it is expected that the flow at the stagnation point will be laminar, owing to the low Reynolds Numbers there. However, it is possible for the flow to become unstable and eventually turbulent with increasing distance from the stagnation region. This possibility brings to mind the Prandtl-Eiffel experiments. It is recalled that Eiffel's drag data, obtained by dropping spheres from the Eiffel tower, showed the well-known drag-drop for critical sphere Reynolds Numbers above about 300,000. On the other hand, Prandtl's wind-tunnel data did not show a drop. Prandtl explained the phenomenon on the assumption that the boundary layers on Eiffel's spheres became turbulent before separation, whereas his (Prandtl's) boundary layers remained laminar. To prove this, Prandtl induced transition by means of a wire trip, whereupon his drag coefficients agreed with Eiffel's. In the present discussion, however, drag is of no concern but, rather, the increase in heat transfer incurred by transition.

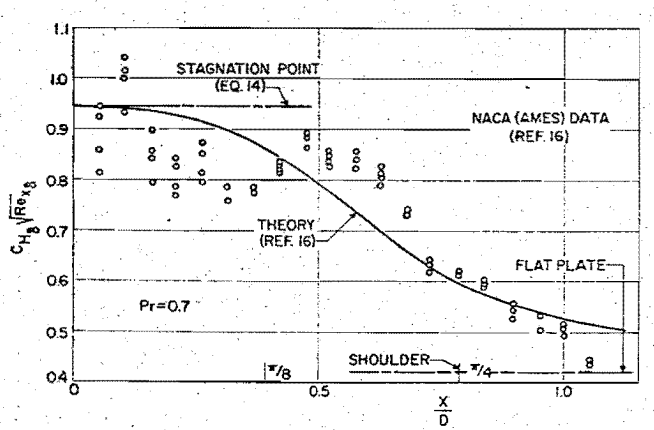

FIG. 25. Local heat-transfer data for a hemispherical nose ($M_\infty = 1.97$).

A theoretical calculation for a turbulent boundary layer can be made when it is assumed that the velocity profile remains similar in the region of the stagnation point. It is also assumed that the flow is fully turbulent in spite of the low Reynolds Numbers there; furthermore, that the turbulence is generated in the boundary layer near the wall, being produced by either roughness or external disturbances which are amplified as they enter the boundary-layer region.

For incompressible flow in the neighborhood of the stagnation point, the heat-transfer rate is then found to be given by[17]

$$q_{wstag} = \frac{f_3}{\left(\frac{\rho_\delta u_\delta x}{\mu_\delta}\right)^{1/5}} \cdot \rho_\delta u_\delta c_p (T_r - T_w) \qquad (17)$$

in which for cylinders

$$f_3 = c_{H_\delta}(Re_{x_\delta})^{1/5} = 0.040 Pr^{-(2/3)} \qquad (18)$$

and for spheres

$$f_3 = 0.042 Pr^{-(2/3)} \qquad (19)$$

It will be recalled that the flat-plate result, assuming a power law for velocity profile, is also of the form

$$q_{wplate} = \frac{f_4}{\left(\frac{\rho_\delta u_\delta x}{\mu_\delta}\right)^{1/5}} \cdot \rho_\delta u_\delta c_p (T_r - T_w) \qquad (20)$$

where

$$f_4 = 0.030 Pr^{-(2/3)} \qquad (21)$$

Thus, as with laminar flow, the forms of the equations are the same for flat plates or for stagnation regions. (For the stagnation region, $u_\delta = \beta x$, again.) Also, as with laminar flow, the incompressible-flow results of Eqs. (17–19) will be used for supersonic flow as well, provided the proper value of β is inserted. Thus, for incompressible flow, $\beta = 4u_\infty/D$ for cylinders and $3\ u_\infty/D$ for spheres, whereas for supersonic flow $\beta = (u_\infty/D)f(M_\infty, \gamma)$.

Substitution of $u_\delta = \beta x$ into Eq. (17) gives

$$q_{w_{stag}} = f_3 \beta^{4/5} \rho_\delta^{4/5} \mu_\delta^{1/5} x^{3/5} c_p (T_r - T_w) \quad (22)$$

Hence, it follows that the turbulent heat-transfer rate increases with distance from the stagnation point. However, with supersonic flow, ρ_δ and μ_δ would gradually decrease so that the turbulent heating rate would eventually begin to fall, thus yielding a maximum some place along the surface. Again, the reader is reminded that the turbulent heating rate given by Eq. (22) could prevail only after the flow has become turbulent.

General

A direct indication of the heating rate in the neighborhood of a stagnation point is presented when the equations [Eqs. (15) and (22)] are put in the following form (say for spheres):

$$q_{w_{stag}} = \frac{0.763}{Pr^{0.6}} \left(\frac{\beta D}{u_\infty}\right)^{1/2} \left(\frac{\mu_\infty}{\rho_\infty u_\infty D}\right)^{1/2} \left(\frac{\rho_\delta}{\rho_\infty}\right)^{1/2} \times \left(\frac{\mu_\delta}{u_\infty}\right)^{1/2} \rho_\infty u_\infty c_p (T_r - T_w) \quad (23)$$

for laminar flow, and

$$q_{w_{stag}} = \frac{0.042}{Pr^{2/3}} \left(\frac{\beta D}{u_\infty}\right)^{4/5} \left(\frac{\mu_\infty}{\rho_\infty u_\infty D}\right)^{1/5} \left(\frac{\rho_\delta}{\rho_\infty}\right)^{4/5} \times \left(\frac{\mu_\delta}{u_\infty}\right)^{1/5} \left(\frac{x}{D}\right)^{3/5} \rho_\infty u_\infty c_p (T_r - T_w) \quad (24)$$

for turbulent flow. Hence writing

$$q_{w_{stag}} = c_{H_\infty} \rho_\infty u_\infty c_p (T_r - T_w) \quad (25)$$

then

$$c_{H_{\infty stag}} = 0.763 \left(\frac{\beta D}{u_\infty}\right)^{1/2} \left(\frac{\mu_\infty}{\rho_\infty u_\infty D}\right)^{1/2} \left(\frac{\rho_\delta}{\rho_\infty}\right)^{1/2} \times \left(\frac{\mu_\delta}{\mu_\infty}\right)^{1/2} Pr^{-0.6} \quad (26)$$

for laminar flow, and

$$c_{H_{\infty stag}} = 0.042 \left(\frac{\beta D}{u_\infty}\right)^{4/5} \left(\frac{\mu_\infty}{\rho_\infty u_\infty D}\right)^{1/5} \left(\frac{\rho_\delta}{\rho_\infty}\right)^{4/5} \times \left(\frac{\mu_\delta}{\mu_\infty}\right)^{1/5} \left(\frac{x}{D}\right)^{3/5} Pr^{-(2/3)} \quad (27)$$

for turbulent flow.

As stagnation point solutions, Eqs. (26) and (27) are plotted in Figs. 26–28 as asymptotes at $x/D = 0$ for $M_\infty = 3$, $Pr = 0.7$, and $Re_{D_\infty} = 10^5, 10^6$, and 10^7. The value of $\beta D/u_\infty = 1.3$ is taken from Fig. 24, and the ratios ρ_δ/ρ_∞ and μ_δ/μ_∞ are computed from stagnation conditions behind a normal shock.

Since the form of the heat-transfer equations is the same for the stagnation point where $u_\delta = \beta x$ as for a flat plate where u_δ = constant [cf. Eqs. (10) and (12), and (17) and (20)], it appears that a reasonable approximation of the heating rate over the entire face of a blunt body may be gained by substituting the local value of β into Eqs. (26) and (27) and also by allowing the coefficient f to change with β as well as with geometry. For the laminar case, the value of f was taken from the Stine and Wanlass curve of Fig. 25—i.e., $f_2 = c_{H_\delta}\sqrt{Re_{x_\delta}}$. For the turbulent case, f was assumed to change linearly with β, the effect of geometry being negligible—i.e., changing only from $0.040\ Pr^{-2/3}$ to $0.042\ Pr^{-2/3}$ in going from cylinders to spheres. This type of calculation is carried out in Figs. 26–28 for a sphere for both laminar and turbulent flow—i.e., using Eqs. (26) and (27), respectively. The ratios ρ_δ/ρ_∞, μ_δ/μ_∞, as well as β, are computed from Newtonian pressure calculations and isentropic expansion from the stagnation point. Apparently, from Figs. 26–28, the maximum heat transfer would occur at about the 40-deg. angle if turbulence should set in, with the maximum turbulent rate increasing relative to the maximum laminar rate with increasing Reynolds Number.

It should also be pointed out[20] that the turbulent shear stress increases as $x^{(8/5)}$ compared to the laminar increase as x. Thus the shear will also be large at the maximum heating region at about 40-deg. angle. This is important from the aerodynamic-erosion standpoint.

Rough Walls

The above discussion had to do only with smooth walls. When the walls are rough, however, the roughness would have an influence not only on transition but also upon turbulent flow itself. The effect of roughness on transition will be illustrated in the next sections. However, the effect on local turbulent skin friction (and therefore heat transfer) is indicated by the following formula for flat plates:

$$\frac{0.242}{A c_{f_\delta}^{1/2} (T_w/T_\delta)^{1/2}} (\sin^{-1}\alpha + \sin^{-1}\beta) = 1.40 + \log_{10}\left(\frac{x}{\epsilon} c_{f_\delta}^{1/2}\right) \quad (28)$$

where ϵ is the plate roughness, and x is the distance from the plate leading edge. It is assumed in the derivation of Eq. (28) that the roughness protuberances are large enough to disrupt the viscous sublayer but not high enough to reach the sonic line. As with skin friction, the heating rates for rough plates should be significantly greater than for smooth plates.

Sweat and Film Cooling

Even if the boundary layer was laminar at the stagnation point, it appears from Figs. 26–28 that the heating rate could still be excessive at extremely high speeds. Sweat or film cooling are means of insulation that are worthy of development. They would be particularly useful to shield the surface in the event of turbulent flow as is also seen in Figs. 26–28. In the latter connection, it should be pointed out that blowing into the boundary layer is a destabilizing agent and therefore should be applied with this in mind.

Boundary-Layer Control and Transition

Now that the extreme cases of laminar and turbulent heat transfer have been discussed with some detail, it is

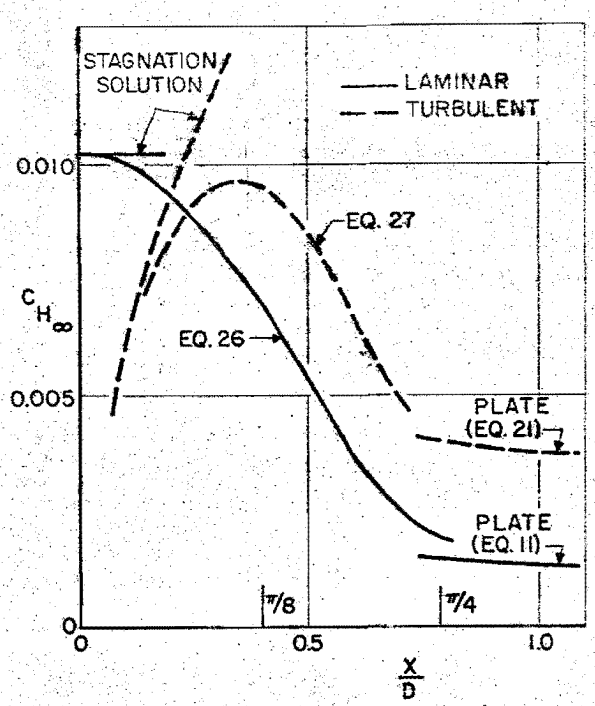

FIG. 26. Heat transfer on the face of a sphere in air ($M_\infty = 3$ and $Re_{D_\infty} = 10^5$).

necessary to examine the important problem of whether or not a boundary layer will be laminar or turbulent. This is the problem of transition. The answer to this question could make or break an overall high-speed-aircraft design because the aerodynamic heating rates for turbulent flow can be 5 to 10 times greater than for laminar flow. While transition is important to the design of such systems as the cruising winged supersonic aircraft, it is critical to the design of the hypersonic glide and ballistic rockets.

It is definitely known that low-speed laminar boundary layers with constant external velocity (pressure) are unstable at relatively low Reynolds Numbers of the order of 100,000 and that turbulence usually sets in at a Reynolds Number of about 3,000,000. High-speed boundary layers on insulated surfaces—i.e., no heat transfer—do not fair much better. However, falling external pressure is a good stabilizing agent for high-speed as well as low-speed flows, as in the case of the laminar flow airfoil which was purposely designed to delay transition by increasing the percentage of chord over which the pressure could fall. In fact, the word "favorable" has been applied to negative pressure gradients along the flow because such gradients tend to hold the boundary layer stable. Ordinarily the pressure gradients on high-speed aircraft wings and bodies are small owing to the flat or slender shapes necessary to decrease wave drag. However, at the noses of bodies and at the leading edges of wings where the heat-transfer rates are expected to be greatest, such as for glide and ballistic-type missiles, the falling pressure will be most welcome. The falling pressure works toward stabilization by filling out the velocity profile—i.e., by increasing the velocity near the surface so that the fluid cannot fold over on itself so easily.

Stabilization by Cooling

Another effective method of boundary-layer control is to cool the laminar boundary layer at the surface. This process is automatic under transient conditions of ascent (boosting) or descent (re-entry). However, for cruising aircraft, some forced method of heat absorption, such as by fuel circulation within the aircraft, must be resorted to. Cooling promotes stabilization by filling out both the density and velocity profiles—i.e., increasing the momentum nearer the surface so that, as with the falling pressure gradient, the fluid cannot fold over on itself so readily. Of course, the opposite effect of encouraging transition would result from heating or from an adverse (positive) pressure gradient.

Theoretical estimates can be made of the cooling rate required to stabilize laminar boundary layers at supersonic speeds. As with incompressible flow where Rayleigh and Tollmien showed that a criterion for instability was that the velocity profile have a reversal—i.e., $\partial^2 u/\partial y^2 = 0$ anywhere in the boundary layer—the criterion for compressible flow[18, 19] is that the gradient of the angular momentum be zero somewhere in the outer part of the layer where

$$\frac{u}{u_\delta} \geqq 1 - \frac{1}{M_\delta}$$

i.e.,
$$\frac{\partial}{\partial y}\left(\rho \frac{\partial u}{\partial y}\right)_{u/u_\delta \geqq 1-1/M_\delta} = 0$$

This is the so-called inviscid solution which is arrived at upon consideration of only the inertial and pressure forces to the neglect of the viscous forces. For the incompressible case with constant external velocity (the Blasius case), the boundary layer is always in impending instability, according to the inviscid solution, because at the wall the curvature of the velocity profile is always zero. For incompressible flow near the stagnation point, where the pressure is favorable, the inviscid criterion indicates stability. For supersonic flow with constant external velocity, the inviscid criterion indicates instability when the flow is insulated—that is, when there is no heat transfer. It is then found that, as the boundary layer is cooled, the layer becomes more and more stable until at a given heat-transfer rate the boundary layer is completely stable. The wall-to-free-stream temperature ratio below which complete stability is possible is shown in Fig. 29. In that Figure, three sets of curves are drawn, depending upon the Prandtl Number and viscosity law (which determine the shape of the density and velocity profiles) prevailing under the condition of motion chosen.[20] It is seen that a limiting Mach Number occurs in each case. A more exact (and complicated) analysis can be carried out which takes into consideration the viscous forces. For incompressible flow with any external pressure variation, it is found that inclusion of the viscous forces in the analysis predicts stability at sufficiently low Reynolds Number so that there is a minimum critical Reynolds Number below which all disturbances damp out. Thus, a Blasius layer can really be either stable or unstable, depending upon the speed—that is, it is not always in a condition of neutral

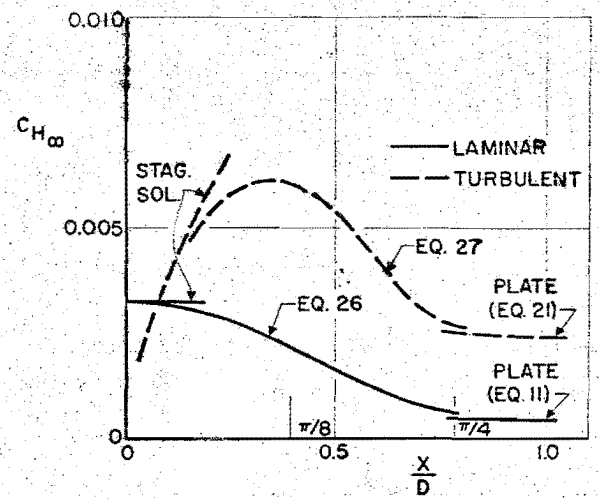

FIG. 27. Heat transfer on the face of a sphere in air ($M_\infty = 3$ and $Re_{D_\infty} = 10^6$).

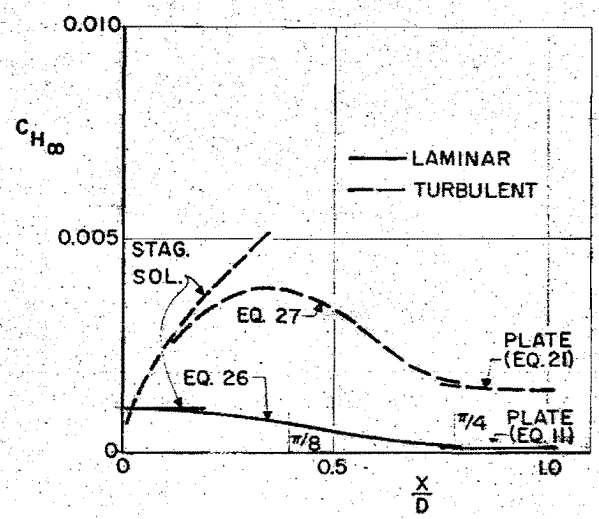

FIG. 28. Heat transfer on the face of a sphere in air ($M_\infty = 3$ and $Re_{D_\infty} = 10^7$).

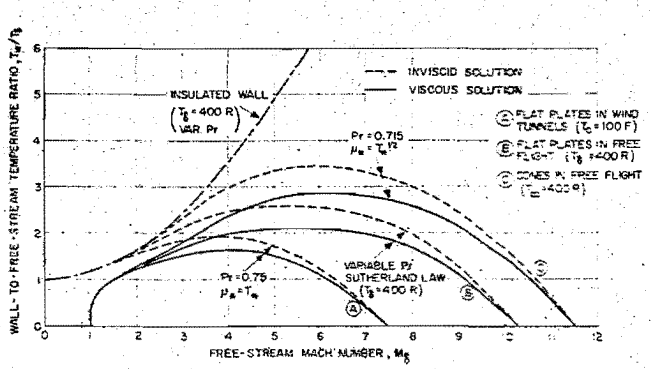

FIG. 29. Cooling required for complete stabilization of the laminar boundary layer for air.

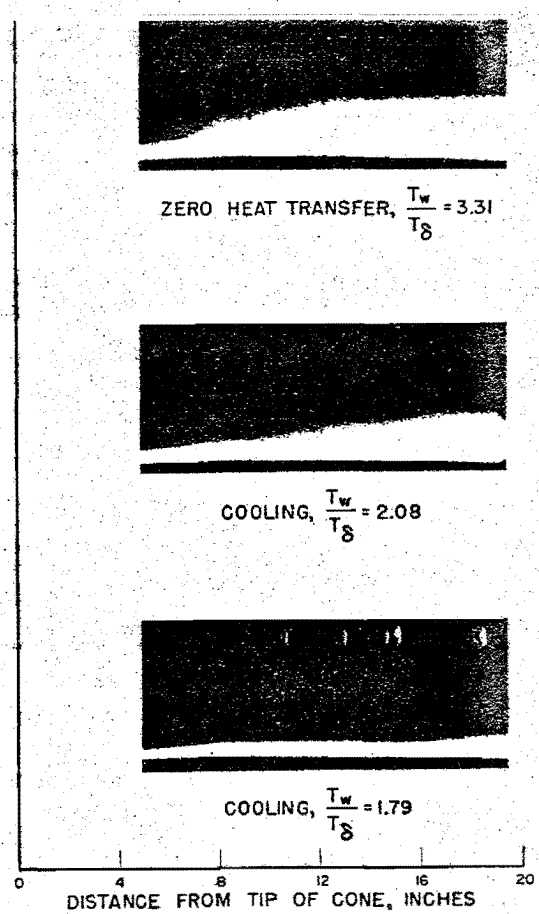

FIG. 30. Magnified schlieren photographs showing delay of transition by surface cooling ($M_\delta = 3.65$ and Re_δ/inch $= 0.50 \cdot 10^6$).

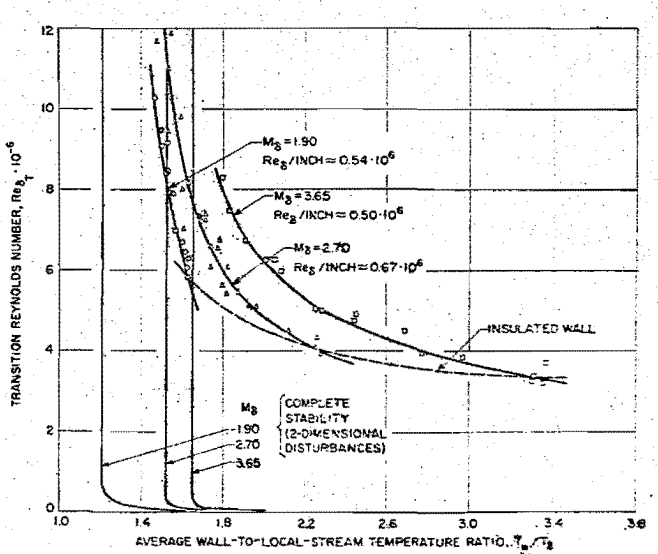

FIG. 31. Effect of surface cooling on transition Reynolds Number for several local Mach Numbers on a smooth 10-deg. cone (0.4 per cent supply turbulence).

stability as indicated by the inviscid solution. In spite of a favorable pressure gradient such as near the stagnation point, a boundary layer is expected to be unstable at a sufficiently high Reynolds Number—although at a greater Reynolds Number than for a Blasius layer owing to the added stabilizing effect of the falling pressure. Finally, for compressible flow, the inclusion of the viscous effects requires a greater cooling rate to stabilize the flow. In fact, it is only in supersonic flow that the boundary layer can be completely stabilized. The viscous solution for two-dimensional disturbances[20] is also shown in Fig. 29.

It is important to notice in Fig. 29 that the cooling rates required to stabilize completely the boundary layer are within practical reach, certainly under transient conditions during which the wall-to-free-stream temperature ratio remains low. Boosting trajectories should penetrate the stability loop from the left, whereas reentry trajectories should enter it from the right.

Experiments have verified the theoretical prediction that cooling the boundary layer delays transition. In a current research program[21] conducted by North American Aviation, a 20-in., 10-deg.-apex-angle cone is cooled internally by precooling gaseous nitrogen so that temperature ratios well below the stability loops of Fig. 29 are obtained. Transition is then observed by means of magnified schlieren technique. Fig. 30 shows photographs of the boundary layer magnified 20 times normal to the flow. The testing was carried out at the Jet Propulsion Laboratory 12-in. Wind Tunnel. The local Mach Number was 3.65, and the Reynolds Number per inch was $0.50 \cdot 10^6$. The top picture shows transition with no cooling; the next two show the successive delay of transition with increasing cooling. Fig. 31 gives transition data obtained from such photographs for local Mach Numbers 1.90, 2.70, and 3.56. In Figs. 30 and 31 the cone was smooth and the turbulence was low.

Figs. 30 and 31 indicate that transition can be delayed by cooling when the surface is smooth and the tunnel turbulence low. However, for engineering purposes, it is necessary to determine whether transition can still be delayed by cooling in the presence of surface roughness and free-stream turbulence. Although the answer to this question is now classified, it can at least be said that the effects of both roughness and turbulence in promoting transition decreases as the Mach Number increases. This is well observed in Figs. 32 and 33 where the ratio of the actual transition Reynolds Number $Re_{\delta T}$ to the smooth-body low supply-chamber turbulence (0.4 per cent) Reynolds Number Re_{δ_0} is plotted vs. intensity of turbulence in the tunnel supply chamber $(u'/u)_0$ and relative roughness (wire height k to displacement thickness δ_k^*), respectively. Only the data for zero heat transfer are shown. The wires were set at 3 in. from the cone vertex. Also shown in Fig. 33 is the low-speed correlation developed by Dryden.[22]

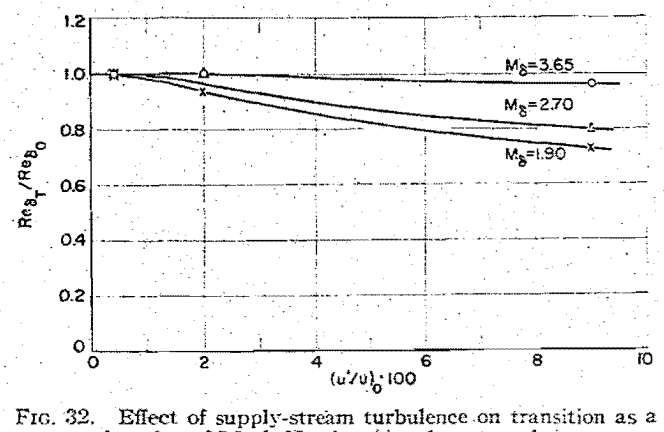

FIG. 32. Effect of supply-stream turbulence on transition as a function of Mach Number (zero heat transfer).

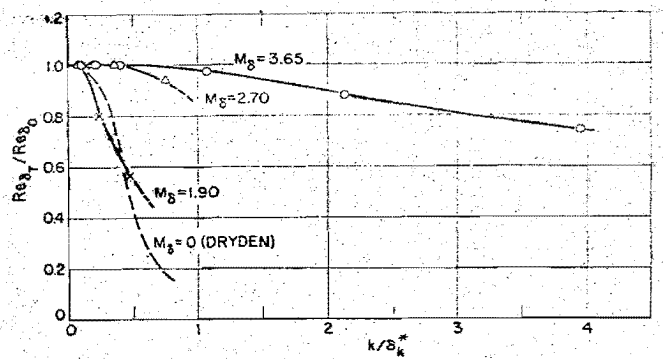

FIG. 33. Effect of roughness on transition as a function of Mach Number (zero heat transfer).

Free-flight data obtained by Fischer and Norris,[23] Sternberg,[24] and Snodgrass[25] also seem to support the theory for smooth surfaces.

Effect on Performance and Design of Winged High-Speed Aircraft

The delay of boundary-layer transition not only decreases the aerodynamic-heating rates considerably but also increases the performance of winged high-speed air vehicles. It is spectacular how many benefits accrue. Aside from the myriad of high-temperature problems (such as with fuel, oil, rubber, electronics) that are alleviated, the structural weights will decrease, and perhaps even stiffer structures could be used. And, of course, for a given range and speed, the quantity of fuel would be less. There would, however, be plumbing problems because undoubtedly the fuel or coolant would have to be circulated within the missile and perhaps through annular surface structure.

An example of the effect of delay of transition on performance is easily calculated. A futuristic commercial air liner designed to fly from coast to coast (say 3,000 miles) at a supersonic Mach Number of perhaps 3 could very well have a zero-lift drag coefficient composed of 50 per cent pressure drag and 50 per cent turbulent friction drag. If the boundary layer could be stabilized by cooling such that considerable laminar flow prevailed over the airplane surface, the skin-friction drag might be reduced by as much as 50 per cent, which would reduce the C_{D_0} by 25 per cent. If other factors remain constant, the range of the airplane would vary proportionally to the square root of the ratio of C_{D_0} with turbulent flow to that with laminar flow. In this illustration, the range would increase about 15 per cent—or 450 miles on the assumed transcontinental flight.

Areas of Future Research

In looking over the vast amount of recent effort to understand the mechanism of aerodynamic heating, one quickly concludes that, although many advances have been made, there is still a lot to be learned before the engineer can be confident in his design. Most of the available knowledge concerns the extreme cases of laminar and turbulent flows with zero or linear pressure gradients. Also, some understanding is evident in the control of transition. Certain areas of research in aerodynamic heating which must be explored further are:

(1) Effects of surface roughness and free-stream turbulence on the control of transition by cooling at supersonic flow for flat plates with cylindrical leading edges and for cones with spherical noses.

(2) Study of (1) for hypersonic flow with realistic temperature behind the bow wave.

(3) More definite data on turbulent heat transfer on flat plates.

(4) Effect of roughness on turbulent heat transfer at ordinary supersonic flow.

(5) Stability of boundary layers near the stagnation point.

(6) Viscous flow solution at leading edges of plates and points of cones.

(7) Heat transfer in separation areas such as before control surfaces and in wakes.

References

[1] van Driest, E. R., *On the Boundary Layer with Variable Prandtl Number*, 1954 Jahrbuch der Wissenschaftlichen Gesellschaft für Luftfahrt e.V. (WGL), pp. 66–75; Friedr. Vieweg & Sohn, Verlag, Braunschweig.

[2] Eber, G. R., *Recent Investigation of Temperature Recovery and Heat Transmission on Cones and Cylinders in Axial Flow in the N.O.L. Aeroballistics Wind Tunnel*, Journal of the Aeronautical Sciences, Vol. 19, No. 1, pp. 1–6, 14, January, 1952.

[3] Shoulberg, R. H., Hill, J. A. F., and Rivas, M. A., Jr., *An Experimental Determination of Flat Plate Recovery Factors for Mach Numbers Between 1.90 and 3.14*, Wind Tunnel Rep. 36, Naval Supersonic Laboratory, Massachusetts Institute of Technology, May, 1952.

[4] van Driest, E. R., *The Turbulent Boundary Layer with Variable Prandtl Number*, 50 Jahre Grenzschichtforschung, pp. 257–271; Friedr. Vieweg & Sohn, Verlag, Braunschweig.

[5] von Kármán, Th., *The Analogy Between Fluid Friction and Heat Transfer*, Trans. ASME, Vol. 61, No. 11, November, 1939.

[6] des Clers, B., and Sternberg, J., *On Boundary-Layer Temperature Recovery Factors*, Journal of the Aeronautical Sciences, Vol. 19, No. 9, pp. 645, 646, September, 1952.

[7] Stine, H. A., and Scherrer, R., *Experimental Investigation of the Turbulent Boundary Layer Temperature Recovery Factor on Bodies of Revolution at Mach Numbers from 2.0 to 3.8*, NACA TN 3020, October, 1953.

[8] Coles, D., *Measurements of Turbulent Friction on a Smooth Flat Plate in Supersonic Flow*, Journal of the Aeronautical Sciences, Vol. 21, No. 7, pp. 433–438, July, 1954.

[9] Korkegi, R. H., *Transition Studies and Skin-Friction Measurements on an Insulated Flat Plate at a Mach Number of 5.8*, Journal of the Aeronautical Sciences, Vol. 23, No. 2, pp. 97–107, 192, February, 1956.

[10] Chapman, D. R., and Kester, R. H., *Measurements of Turbulent Skin Friction on Cylinders in Axial Flow at Subsonic and Supersonic Velocities*, Journal of the Aeronautical Sciences, Vol. 20, No. 7, pp. 441–448, July, 1953.

[11] Sommer, S. C., and Short, B. J., *Free-Flight Measurements of Turbulent-Boundary-Layer Skin Friction in the Presence of Severe Aerodynamic Heating at Mach Numbers From 2.8 to 7.0*, NACA TN 3391, March, 1955.

[12] Shoulberg, R. H., *et al*, *An Experimental Investigation of Flat Plate Heat Transfer Coefficients at Mach Numbers of 2, 2.5, and 3 for a Surface Temperature to Stream Total Temperature Ratio of 1.18*, Wind Tunnel Rep. 39, Naval Supersonic Laboratory, Massachusetts Institute of Technology, June, 1953.

[13] Goldstein, S., *Modern Developments in Fluid Dynamics*, 1st Ed., Vol. 2, p. 631; Oxford University Press, London, 1938.

[14] Sibulkin, M., *Heat Transfer Near the Forward Stagnation Point of a Body of Revolution*, Journal of the Aeronautical Sciences, Vol. 19, No. 8, pp. 570, 571, August, 1952.

[15] Korobkin, I., *Laminar Heat-Transfer Characteristics of a Hemisphere For Mach Number Range, 1.9 to 4.9*, 1955 Heat Transfer and Fluid Mechanics Institute, June 23–25, 1955.

[16] Stine, H. A., and Wanlass, K., *Theoretical and Experimental Investigation of Aerodynamic-Heating and Isothermal Heat-Transfer Parameters on a Hemispherical Nose With Laminar Boundary Layer at Supersonic Mach Numbers*, NACA TN 3344, December, 1954.

[17] van Driest, E. R., *On Skin Friction and Heat Transfer Near the Stagnation Point*, AI-2267, North American Aviation, Inc., March 1, 1956.

[18] Lees, L., and Lin, C. C., *Investigation of the Stability of the Laminar Boundary Layer in a Compressible Fluid*, NACA TN 1115, September, 1946.

[19] Lees, L., *The Stability of the Laminar Boundary Layer in a Compressible Fluid*, NACA TR 876, 1947.

[20] van Driest, E. R., *Calculation of the Stability of the Laminar Boundary Layer in a Compressible Fluid on a Flat Plate with Heat Transfer*, Journal of the Aeronautical Sciences, Vol. 19, No. 12, pp. 801–813, December, 1952. (Fig. 30 also contains results of later calculations.)

[21] van Driest, E. R., and Boison, J. Christopher, *Research on Stability and Transition of the Laminar Boundary Layer*, OSR-TN-55-465, September 1, 1955 (Confidential). (This research was supported by the United States Air Force, through the Office of Scientific Research at the Air Research and Development Command.)

[22] Dryden, H. L., *Review of Published Data on the Effect of Roughness on Transition from Laminar to Turbulent Flow*, Journal of the Aeronautical Sciences, Vol. 20, No. 7, pp. 477–482, July, 1953.

[23] Fischer, W. W., and Norris, R. H., *Supersonic Convective Heat-Transfer Correlation from Skin-Temperature Measurements on a V-2 Rocket in Flight*, Trans. ASME, Vol. 71, No. 5, pp. 457–467, July, 1949.

[24] Sternberg, J., *A Free-Flight Investigation of the Possibility of High Reynolds Number Supersonic Laminar Boundary Layers* Journal of the Aeronautical Sciences, Vol. 19, No. 11, pp. 721–733, November, 1952.

[25] Snodgrass, R. B., *Flight Measurements of Aerodynamic Heating and Boundary-Layer Transition on the Viking 10 Nose Cone*, Jet Propulsion, Vol. 25, No. 12, pp. 701–706, December, 1955.

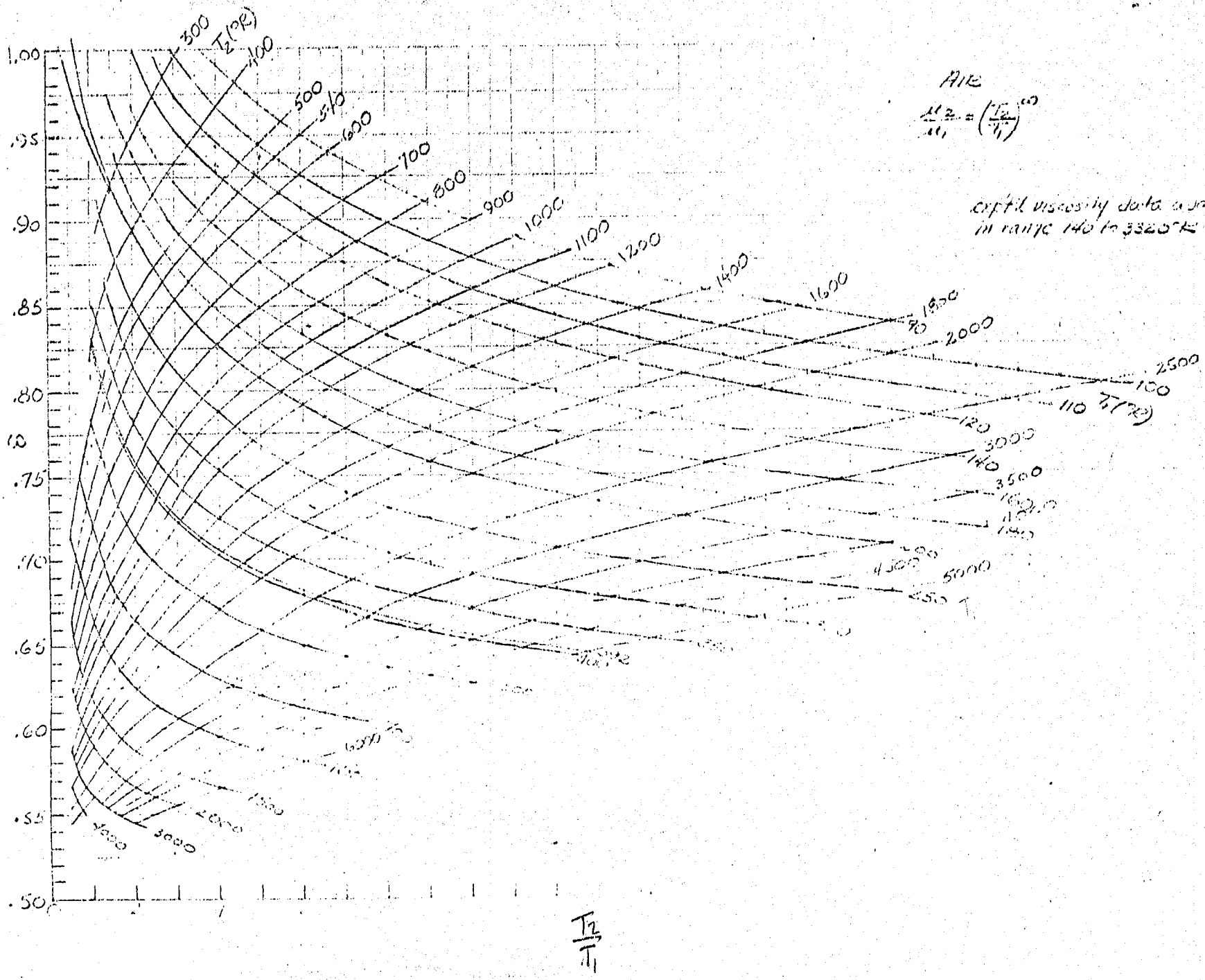

Air

$\frac{\mu_2}{\mu_1} = \left(\frac{T_2}{T_1}\right)^{.76}$

exptl viscosity data available in range 140 to 3320°R

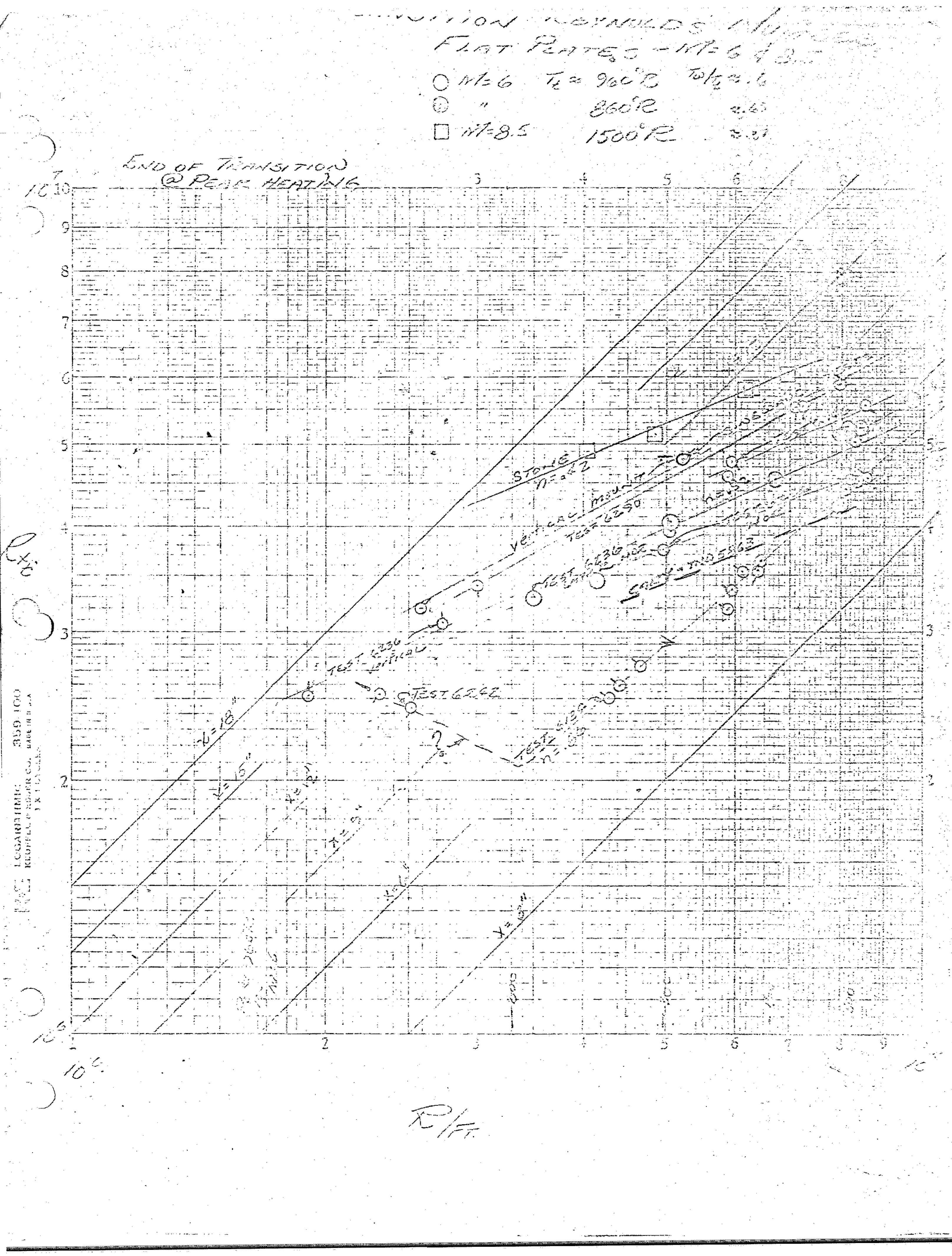
FLAT PLATES - M= 6 & 8.5
○ M=6 Tt = 960°R
" 860°R
□ M=8.5 1500°R
END OF TRANSITION @ PEAK HEATING
STONE
VERTICAL MOUNT
TEST 6250
TEST 6236 VERTICAL
TEST 6242
TEST 6236
SALLY - MOD 5563
x=18"
x=15"
x=12"
x=9"
x=6"
x=3"
R/FT
Rxt
LOGARITHMIC 359-100
KEUFFEL & ESSER CO.

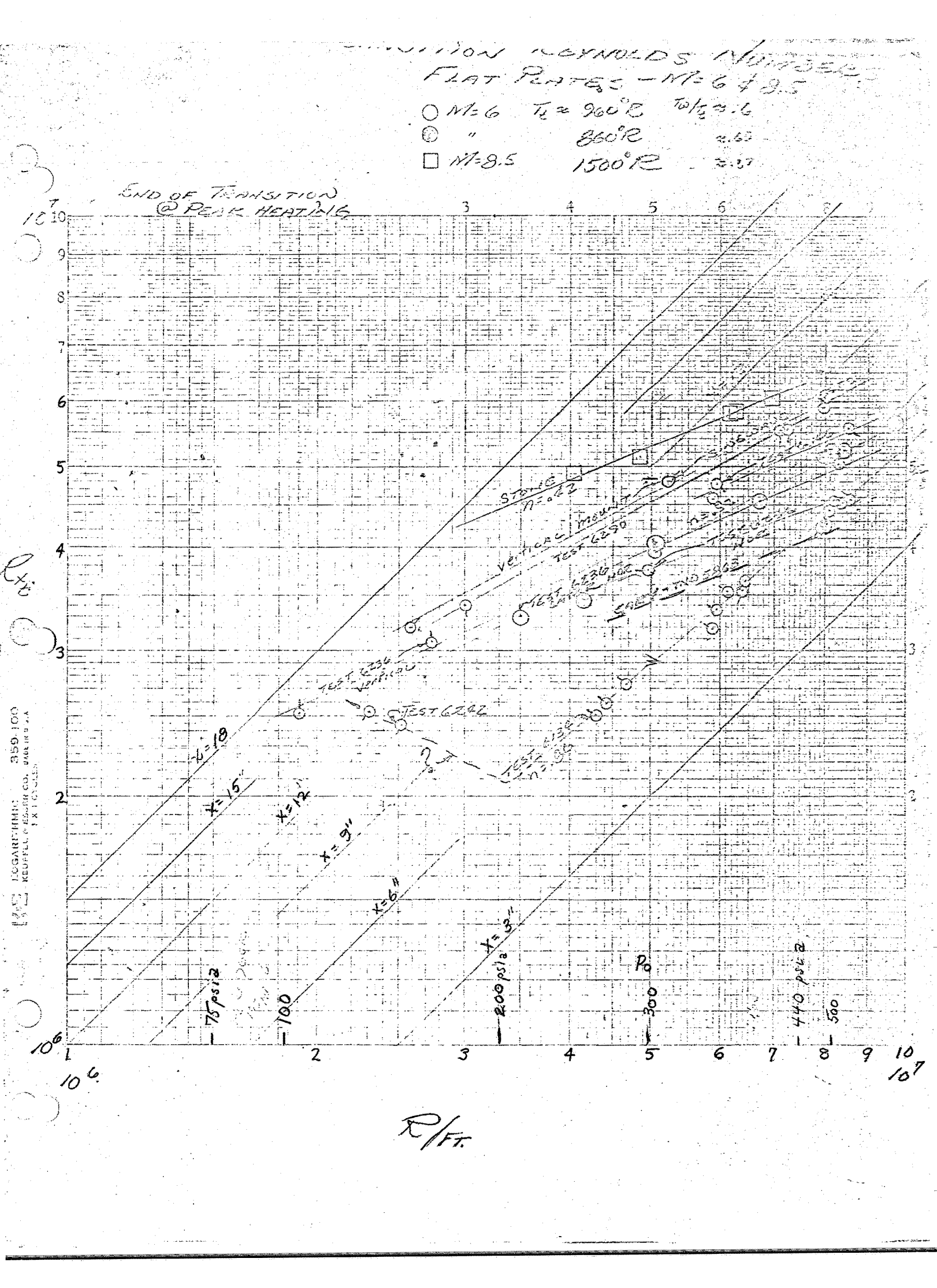
TRANSITION REYNOLDS NUMBER
FLAT PLATE - M = 6 & 8.5
○ M = 6 T_t = 960°R T_w/T_t = 1.6
◎ " 860°R 1.65
□ M = 8.5 1500°R 1.37
END OF TRANSITION @ PEAK HEATING
STATIC
n = 0.22
VERTICAL MEAN
TEST 6250
TEST 6236 VERTICAL
TEST 6242
TEST 6236 HOR.
x = 18"
x = 15"
x = 12"
x = 9"
x = 6"
x = 3"
75 psia
100
200 psia
300
440 psia
500
P_o
R_x
R/Ft.

MEASUREMENTS OF LAMINAR SKIN FRICTION IN SUPERSONIC CONE FLOW

By W. S. Bradfield, Department of Aeronautical Engineering, University of Minnesota*

Abstract

Measurements of laminar skin friction on a 15° cone at freestream Mach number 3.47 are reported. The momentum loss technique was applied to velocity profiles obtained at Reynolds numbers ranging from 486,000 to 2,000,000. The Hantzsche and Wendt transformation from cone to plate flow was applied to the results. The transformed coefficients show agreement with the theory of Chapman and Rubesin.

Notation

p_o = Stagnation pressure of potential flow.

p_o' = Local stagnation pressure sensed by total tube within the boundary layer.

u = Local velocity within the boundary layer.

u_1 = Potential flow velocity at outer surface of boundary layer.

x = Distance measured from the cone tip along a generatrix of the cone.

y = Distance normal to the cone surface.

C_f = Local skin friction coefficient for cone flow.

C_f = Local skin friction coefficient for plate flow.

C_F = Average skin friction coefficient for cone flow.

$\bar{C}_F$ = Average skin friction coefficient for plate flow.

M_1 = Mach number in potential flow at outer surface of boundary layer.

R_x = Reynolds number based on conditions at outer surface of boundary layer.

δ^* = Displacement thickness.

---

*The research reported in this paper has been sponsored by the Air Research and Development Command USAF under Contract No. AF 33 (038) 12918.

$\bar{\eta} = y\sqrt{\frac{u_1}{\nu_1 x}}$ Dimensionless variable for plate flow.

θ = Momentum thickness.

ν_1 = Kinematic viscosity at outer surface of boundary layer.

Introduction

The investigation which is discussed in what follows was carried out at freestream Mach number 3.47 in an intermittent tunnel. Total pressure profiles, were recorded in the boundary layer on a 15° cone at various distances from the nose and velocity profiles, displacement thicknesses and momentum thicknesses were calculated. Skin friction coefficients were determined and were compared with the theory. The variation of the distance from the nose of the cone combined with variation of stagnation conditions provided a Reynolds number range from 486,000 to 1,909,000. The purpose of the present paper is to present a comparison of the experimental results obtained with existing theory, and to discuss the technique employed.

Description of Apparatus and Techniques

The wind tunnel used in this investigation is a 6" x 6" asymmetric blow down channel operated during this series of tests at Mach number 3.47. A photograph of the channel is shown as Fig. 1. The model shown installed is a typical 15° conical model of the type used throughout the investigation. The flow inclination at the tip of the model (as measured after completion of the current investigation) was less than 1° in pitch and in yaw. The potential flow Mach number behind the nose shock along the outer edge of the boundary layer was 3.1 as measured by total pressure tube and the distribution of the Mach number along the outer edge of the laminar boundary layer is shown in Fig. 2.

The primary piece of equipment used in the investigation is a conical model of the type shown in Fig. 1. A small pitot tube (Ref. 1) was attached to the model for test purposes as shown in Fig. 3. The pitot tube dimensions were approximately 3 mils by 15 mils outside dimensions with an orifice opening of approximately 1 mil in height. A photomicrograph of a typical pitot tube is shown as Fig. 4.

Inasmuch as the tunnel operation is of intermittent type, it became expedient to utilize the pump up time between runs for adjusting and measuring the probe positions within the boundary layer with tunnel windows removed. Use of this technique permitted the simplest kind of probe adjustment to be used throughout the investigation.

Figure 5 shows the experimental setup employed for determination of probe location relative to the model surface. Precautions were taken through use of a long focus, low magnification microscope during running to make certain that the probe did not change its position relative to the surface.

Figure 6 is a shadowgraph showing a probe immersed in the boundary layer on the cone. Figure 7 shows the total pressure profile for Reynolds number 1,909,000, the largest Reynolds number for which laminar flow was observed.

Data Reduction

The total pressure data was reduced to velocity profile information through application of the isoenergetic assumption (Ref. 2, 3, 4). That is to say, it was assumed that the net energy transferred across stream lines of the boundary layer was zero. It was further assumed that the variation in static pressure normal to the cone surface within the boundary layer was negligible. It was assumed that the effect of heat transfer from the model surface to the boundary layer (due to the difference between stream equilibrium temperature and model wall temperature) had negligible effect on skin friction coefficients.

A velocity profile computed by this procedure is shown as Fig. 8. For the purpose of comparison, a profile calculated (Ref. 5) for plate flow at the same Mach number and Reynolds number is shown.

In order to effect a direct comparison of existing plate flow theory to the experimental results, the transformation of Hantzsche and Wendt (Ref. 6) was applied. A transformed velocity profile for Reynolds number 1,909,000 is plotted as Fig. 9. The comparison of the velocity profile with theoretical results (Ref. 5, 7) is reasonable; however, the departure of the experimental results from the theoretical results increases systematically as the surface is approached. This characteristic was also exhibited in the other profiles obtained in the laminar boundary layer.

The velocity profiles together with the density profiles obtained by the method just described were used to compute displacement thickness and momentum thickness at each station investigated. The variation of dimensionless momentum thickness versus distance along the conical ray is shown in Fig. 10. The function

$$\theta/x = \frac{0.370}{\sqrt{R_x}} \qquad (1)$$

obtained from the results of (Ref. 7) is shown for comparison.

The momentum integral relation for conical compressible flow (Ref. 8) was applied to the experimental points. The functional dependence of momentum thickness on Reynolds number is

$$\theta/x = 0.664\ R_x^{-0.542} \qquad (2)$$

by least squares from the data of Fig. 10. From the momentum integral (with help from Eq. 2) the local skin friction coefficient in terms of momentum thickness becomes

$$C_f = 2.92\ \theta/x \qquad (3)$$

and, by definition, the average skin friction coefficient for the cone is

$$C_F = \frac{\int_0^L C_f(x)x\,dx}{L^2/2} \qquad (4)$$

Using the results plotted as Fig. 10, Eq. 3 was evaluated. The result was then transformed to equivalent plate flow conditions through use of the Hantzsche-Wendt transformation to plate flow (Ref. 6)

$$C_f = \sqrt{3}\ \bar{C}_f \qquad (5)$$

The transformed coefficients are shown as Fig. 11.

The function $C_f(R_x)$ having been obtained, average values of skin friction coefficient were calculated in accordance with Eq. 4 and plotted as in Fig. 12. The transformation to plate flow (Ref. 6)

$$C_F = \frac{2}{3}\sqrt{3}\ \bar{C}_F \qquad (6)$$

was applied and agreement of the transformed results with flat plate theory is indicated.

Conclusion

The results of this investigation indicate that the analysis of compressible laminar boundary layer flow over a flat plate may be applied to conical flow at about Mach number 3 through use of the Hantzsche-Wendt geometrical transformation. The result obtained should be extended over a wider range of Mach number before any more general conclusions are drawn.

It appears that the use of small pitot tubes in thin boundary layers will produce satisfactory results. However, there is a systematic divergence of the experimental results

from the theoretical results for velocity profiles which must be explained.

References

(1) Bradfield, W. S. and Yale, G. E., "Small Pitot Tubes with Fast Pressure Response Time," Readers' Forum, Journal of Aeronautical Sciences, 18, No. 10, 697-698, (October 1951).

(2) Wilson, R. E., Young, E. C., and Thompson, M. J., "Second Interim Report on Experimentally Determined Turbulent Boundary Layer Characteristics at Supersonic Speeds." Contract Nord - 9195, University of Texas, (January 1949).

(3) Kuethe, A. M. and Schetzer, J. D., Foundations of Aerodynamics, John Wiley and Sons, Incorporated, New York, 299-300, (1950).

(4) Goldstein, S., Modern Development in Fluid Dynamics, Oxford U. Press, London, II, 610-612 and 627-628, (1938).

(5) Emmons and Brainerd, "Temperature Effects in a Laminar Compressible Fluid Boundary Layer Along a Flat Plate." Journal of Applied Mechanics, (August 1941).

(6) Hantzsche, W. and Wendt, H., "The Laminar Boundary Layer on a Cone in a Supersonic Air Stream at Zero Angle of Attack." Translation N. RAT-6, Douglas, Santa Monica.

(7) Chapman, D. R. and Rubesin, M. W., "Temperature and Velocity Profiles in the Compressible Laminar Boundary Layer with Arbitrary Distribution of Surface Temperature." Journal of Aeronautical Sciences, 16, (September 1949).

(8) Bradfield, W. S., "Momentum Integral Relation for Compressible Conical Flow and Transformation of Results to Plate Flow." University of Minnesota, Department of Aeronautical Engineering, Engineering Memorandum 3, (July 1951).

Fig. 1. - Mach number 3.47 channel with 15-deg. conical model (side door raised).
Fig. 2. - Mach number distribution at outer edge of boundary layer, as measured by total pressure tube.
Fig. 3. - Momentum loss cone with Pitot tube attached.
Fig. 4. - Photomicrograph of Pitot tube.
Fig. 5. - Equipment used for total pressure probe adjustment.
Fig. 6. - Shadowgraph of cone at Mach number 3.47 with total pressure tube installed.
Fig. 7. - Total pressure ratio versus distance from cone surface
Fig. 8. - Comparison of velocity ratio measured in cone flow to that computed for plate flow.
Fig. 9. - Velocity profile in the laminar boundary layer on a 15-deg. cone compared with plate flow theory.

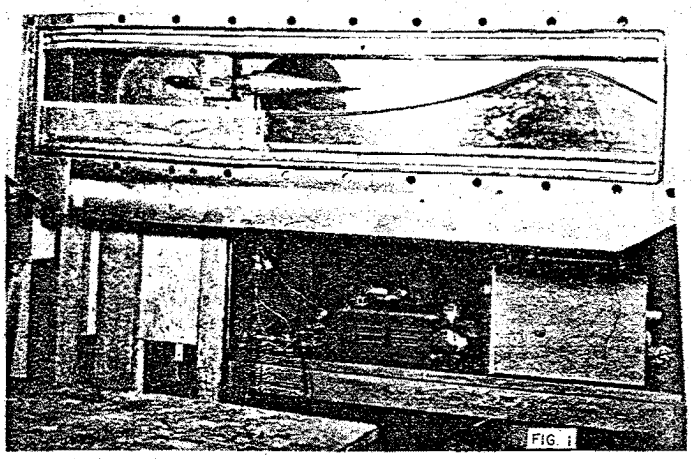
FIG. 1

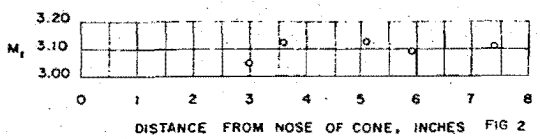

FIG 2

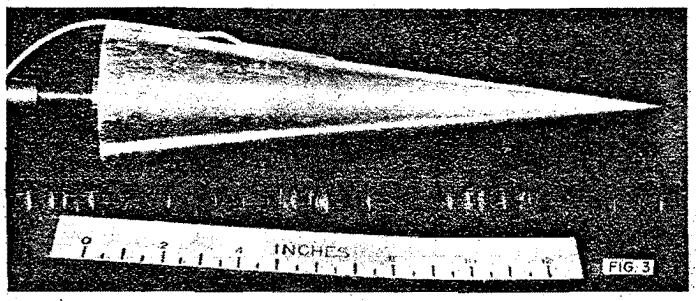

FIG. 3

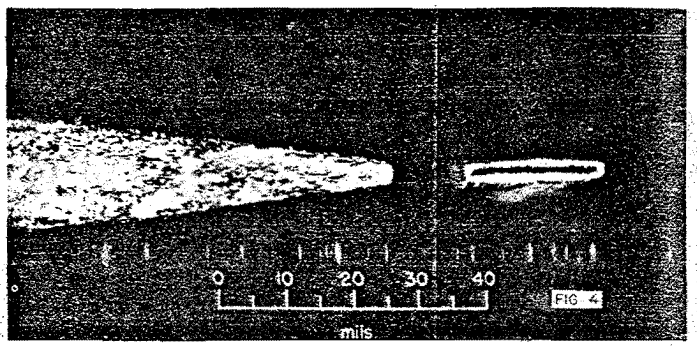

FIG. 4

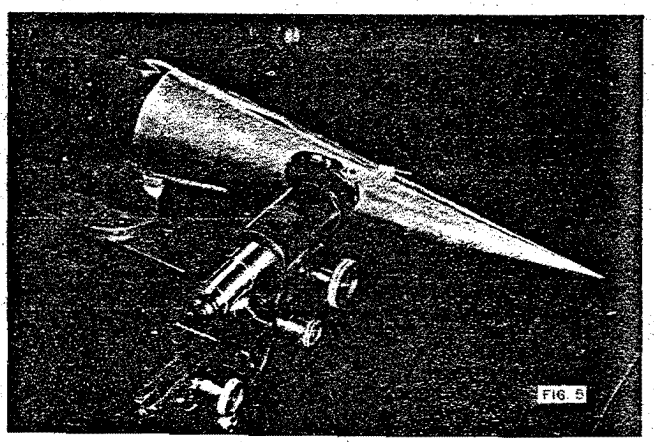
FIG. 5

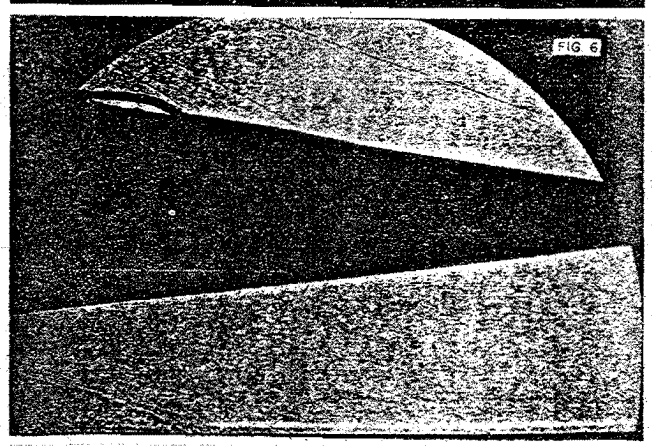
FIG. 6

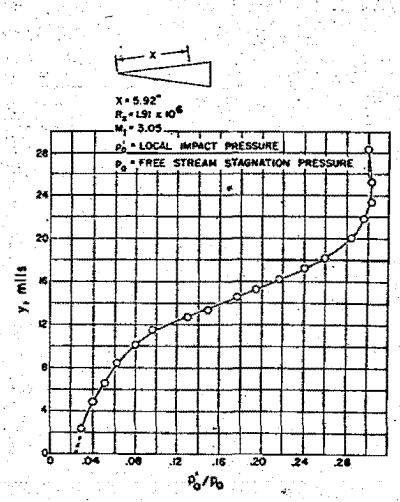

FIGURE 7

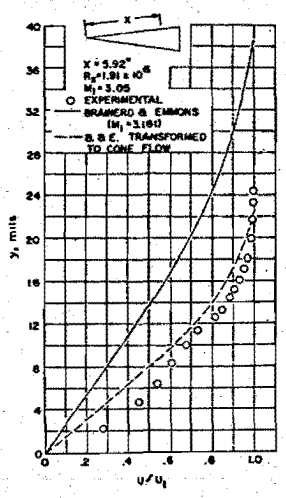

FIGURE 8

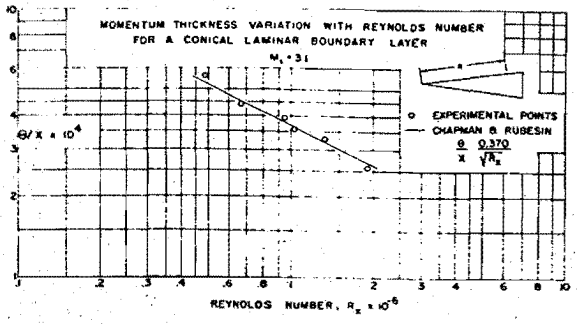

FIGURE 10

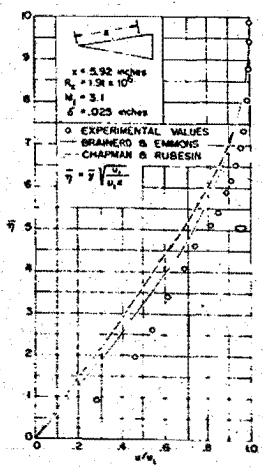

FIGURE 9

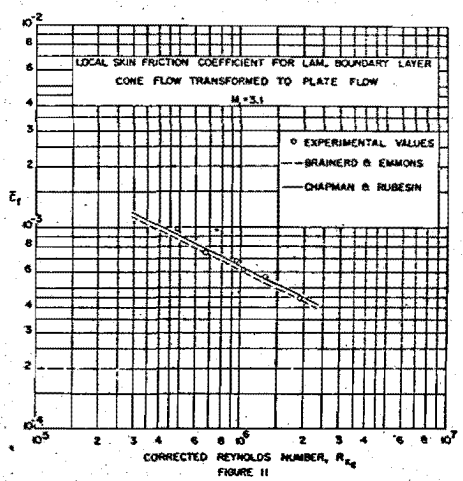

FIGURE 11

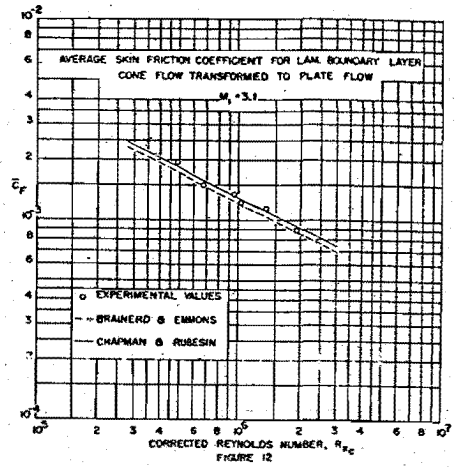

FIGURE 12